1976

Calorimetry of 4-aminopyridine

Alan Everett Van Til
Iowa State University

Calorimetry of 4-aminopyridine

by

Alan Everett Van Til

A Dissertation Submitted to the
Graduate Faculty in Partial Fulfillment of
The Requirements for the Degree of
DOCTOR OF PHILOSOPHY

Department: Chemistry
Major: Analytical Chemistry

Approved:

Signature was redacted for privacy.

In Charge of Major Work

Signature was redacted for privacy.

For the Major Department

Signature was redacted for privacy.

For the Graduate College

Iowa State University
Ames, Iowa

1976

TABLE OF CONTENTS

LIST OF FIGURES

LIST OF TABLES

I. INTRODUCTION

In principle, differential methods in instrumental chemical analysis provide a means of reducing background sources of noise in experimental designs. Desirable in the use of differential techniques is linearity of sensor sensitivity, system stability, and equivalent sensor sensitivity in each part of the system.

Although standard in solid state calorimetric methods, such as DTA and DSC, differential methods are rarely used in solution calorimetry. The exceptions are calorimeters using thermopiles such as Tian-Calvet microcalorimeters. The developments of semiconductor electronics has given us a thermally sensitive resistor, called a thermistor, which has a temperature sensitivity equivalent to that of a thermopile. Thermopiles have the disadvantages of large size and high cost. Operational amplifiers are now sufficiently sophisticated to fulfill the need for ultra-stable power supplies and high gain bridge amplifiers in differential thermometry. Material research on thermal and mechanical properties of insulating materials has provided criteria for selecting the appropriate design to minimize heat transfer between the calorimeter system and its environment. Hydrodynamic studies in chemical process design have yielded accurate descriptions of mass transport under stirred conditions.

It was the purpose of this work to apply developments from each area cited above to the design, construction, and use of a differential solution calorimeter for thermometric titrimetry.

II. LITERATURE REVIEW

A. Thermometric Titrimetry

The equipment, techniques and applications of thermometric titrimetry received detailed examination in the monographs by Tyrrell and Beezer (1) and Bark and Bark (2). Reviews by Jordan (3) and Carr (4) are limited to analytical applications and the mathematical procedures used in obtaining thermodynamic parameters from thermometric titrations. Very sophisticated methods have been derived for mathematical treatment of experimental data by Christensen and co-workers (5).

B. Studies of 4-Aminopyridine

In a nonexhaustive listing of publications abstracted by Chemical Abstracts, more than 280 entries for 4-aminopyridine were found for the period 1923-1974.

An inexpensive and convenient synthesis of 4-aminopyridine and its derivatives was developed by Ochai (6) and independently by den Hartog and Overhoff (7). The procedure utilizes the oxidation of pyridine to pyridine-1-oxide with H_2O_2, nitration with HNO_3 at 128 deg C, and reduction with Fe or Sn in acidic media. Other synthetic methods used which provide satisfactory yields of 4-aminopyridine are the Curtius reaction (8) and use of $SOCl_2$ with pyridine to form 1-(4-pyridyl) pyridinium chloride which when treated at room temperature with ammonia and phenol yields 4-aminopyridine (9).

The dissociation constant of the monoprotonated form of 4-aminopyridine has been determined in aqueous solutions using UV spectrophotometry (10, 11, 12, 13), electrochemistry (14, 15), and calorimetry (16). The dissociation constant of monoprotonated 4-aminopyridine was determined in a 50% methanol-water mixture by Paabo and co-workers (17).

The dissociation constant of the diprotonated form of 4-aminopyridine was determined in H_2SO_4 media (12, 18, 19, 20). From these determinations, the dissociation constant, pK_{a2}, can be given as 9.15 ± 0.05 in aqueous media and 8.520 in a 50% methanol-water mixture at 25 deg C. The dissociation constant, pK_{a1}, is -6.3 ± 0.2 at 25 deg C. The heat of neutralization at infinite dilution, ΔH_N°, has been determined electrochemically (14, 15) and thermometrically (16). The value of ΔH_N° is -11.28 ± 0.04 kcal/mole at 25 deg C as calculated by averaging the best determinations (15, 16) together.

Extensive NMR studies of 4-aminopyridine in DMSO (21, 22, 23), and in H_2O-H_2SO_4 mixtures (24, 25) showed that the ring N is protonated first followed by the exocyclic amino N. The deprotonation rate of monoprotonated 4-aminopyridine was determined by Delpuech and Serratrice (26) who used NMR to measure the coalescence of the pyridine α-protons. The deprotonation rate constant, k, of 3.44×10^2 $M^{-1}s^{-1}$ was shown to be independent of salt concentration in a

$CF_3COOH/H_2O/HClO_4$ solution. The unprotonated form of 4-aminopyridine was shown to have a symmetrical A_2X_2 NMR spectra in DMSO (21) and CCl_4(27).

A fluorescence study (28) showed that charge transfer from the exocyclic N to the ring N occurs on excitation of 4-aminopyridine in acidic media. The weak fluorescence of 4-aminopyridine makes fluorometry unsuitable as an analytical method for this compound.

Extensive mammalian toxicity studies as summarized in the review by Schafer and co-workers (29) proceeded from the proposed use of 4-aminopyridine as a bird repellent for field corn. The pharmacological action of 4-aminopyridine in mammalian systems is similar to adrenalin (30, 31, 32, 33, 34).

Electrochemical studies of 4-aminopyridine are limited to polarography (35, 36). An electrochemical method for synthesizing 4-picoline using a Pb electrode and 20% H_2SO_4 (aq) as the supporting electrolyte was described by Emmert and Dorn (37). The Ag complex (38) was studied potentiometrically and Cu (39) and Rh (40) complexes were examined polarigraphically to determine their formation constants.

Complexes including 4-aminopyridine as one of several ligands have been synthesized for most of the transition elements including V (41, 42, 43), Cr (44), Fe (45, 46, 47, 48), Co (46, 49, 50, 51, 52, 53, 54, 55, 56), Ni (57, 58, 59, 60, 61), Cu (39, 59, 62, 63, 64, 65, 66), Zn (61, 67, 68, 69),

Zr (70, 71), Nb (72), Mo (73), Rh (40, 51, 74), Pd (75), Ag (38, 76), Cd (75, 76, 77, 78, 79), Re (80), Ir (51), Pt (81, 82, 83), and Hg (78). Especially strong complexes are formed with I_2 (84, 85, 86) and of lesser strength with Sn (87) and Tl (88). A charge transfer complex between 4-aminopyridine and 1,3,5-trinitrobenzene was prepared by Waclawek and Hurwic (89).

Proposed as an acidimetric standard in 1955 by Van Hall and Stone (90) since it can be readily purified, 4-aminopyridine was also shown in a high precision coulometric determination of the Faraday to be obtainable in 100.000 percent purity (91).

III. THEORY OF CALORIMETRIC MEASUREMENTS

A. Steady-State Sensitivity of Electronic Bridge Circuit

1. Temperature sensitivity of NTC and PTC thermistors

The theoretical sensitivity of 6.6×10^{-9} deg C/nA for a proposed temperature sensor utilizing a MOS transistor with pyroelectric material on the gate has not yet been realized (92). Existing circuits are continually being revised to increase sensitivity and linearity of response. Linde and co-workers (93) initiated modern thermometric titrimetry in 1953 by employing a thermistor with a negative temperature coefficient (NTC) as one arm of a dc Wheatstone bridge. Since that time, increased thermistor bridge sensitivity has been achieved in various ways including use of two or more NTC thermistors in parallel as one arm of the bridge (94, 95, 96). Electronic amplification has been reported for dc (97, 98) and ac bridges (99, 100). The ac bridges use sine wave voltages although square wave voltage has been proposed (101). Detection limits of 5 - 10 μdeg C have been reported for several instruments (100).

A nonlinear response is observed in the bridge offset potential because of the parallel arrangement of bridge resistances and the nature of the semiconductor material in the thermistor. Numerical methods have been applied for linearization of bridge output (102, 103); their use is

tedious and requires electronic computational facilities. Analog linearization has been achieved by the use of resistors for thermistor-shunting networks with some sacrifice of sensitivity (104, 105).

Steady-state response of thermistors has been rigorously treated by Buhl (106) using the assumption that the wall temperature of the thermistor outer surface is equal to the bulk gas temperature. This approach ignors any influence of a thermal boundary layer, that is, the surface thermal resistance is assumed to be zero. Transient thermistor response including response times and problems of undershoot and overshoot are generally ignored in analytical applications. Hence, application is limited to slow reactions or when transient response is to be ignored. Results of research described in this thesis are evidence that critical damping of the measurement system is easily achieved when those circuit and experimental parameters affecting transient response are identified and properly adjusted.

The construction and operation of dc thermistor circuits are simple. The basic circuit of Vanderborgh and Spall (107) was modified to achieve theoretical output and an improvement in linearity of temperature response. A schematic of the circuit is shown in Figure III.1. Improvements achieved include elimination of loading of the bridge power supply by use of operational amplifiers as ideal current sources and incorporation of negative temperature coefficient (NTC)

thermistors with positive temperature coefficient (PTC) thermistors for an increase of bridge sensitivity by a factor of 5X over the straight NTC circuits. This NTC-PTC hybrid circuit is intended primarily for single cell calorimetry. The description of the steady-state behavior of the thermistor network, the effect of the thermistor dissipation constant on transient response, and the effect of various solution parameters on the temperature sensitivity and response time is given below.

The semiconductor equation for a NTC thermistor is given by Equation A.1 (104, 108, 109).

$$R_t = Z_t \exp\{\beta_t / T_t\} \qquad [A.1]$$

where t = thermistor

R_t = resistance of thermistor at its geometric center (Ω)

Z_t = pre-exponential term in thermistor resistance functions (Ω)

β_t = material coefficient of thermistor with negative temperature coefficient (deg K)

T_t = thermistor temperature at the geometric center (deg K)

Equation A.1 is frequently written in the form

$$\ln R_t = z_t + \beta_t / T_t \qquad [A.2]$$

where $z_t = \ln Z_t$. Equation A.2 can be differentiated with respect to T_t to yield

$$\frac{1}{R_t}\frac{dR_t}{dT_t} = -\frac{\beta_t}{T_t^2} + \frac{1}{T_t}\frac{d\beta_t}{dT_t} + \frac{1}{Z_t}\frac{dZ_t}{dT_t} \qquad [A.3]$$

The quantity $(1/R_t)(dR_t/dT_t)$ is called the temperature coefficient of resistance of the thermistor. The value of $(1/T_t)(d\beta_t/dT_t) + (1/Z_t)(dZ_t/dT_t) << -\beta_t/T_t^2$ and is frequently ignored. Thus

$$\frac{1}{R_t}\frac{dR_t}{dT_t} \simeq -\frac{\beta_t}{T_t^2} \qquad [A.4]$$

Equation A.1 is known as the zero power equation and applies only in the case of negligible electrical power dissipation by the thermistor. Buhl (106) has considered steady-state thermistor response in the case of appreciable power dissipation.

The output potential of operational amplifier OA-3 in Figure III.1 is related to the resistance of thermistors in positions t_1 and t_2 (R_1 and R_2) by Equation A.5.

$$e_{o,3} = -\left(\frac{R_f}{R_1}\right) e_- - \left(\frac{R_f}{R_2}\right) e_+ \qquad [A.5]$$

where

$e_{o,3}$ = output voltage of Operational Amplifier 3 in Figure III.1 (V)

e_+, e_- = positive and negative voltages applied to thermistors t_2 and t_1, respectively (V)

Figure III.1. Circuit diagram of thermistor bridge

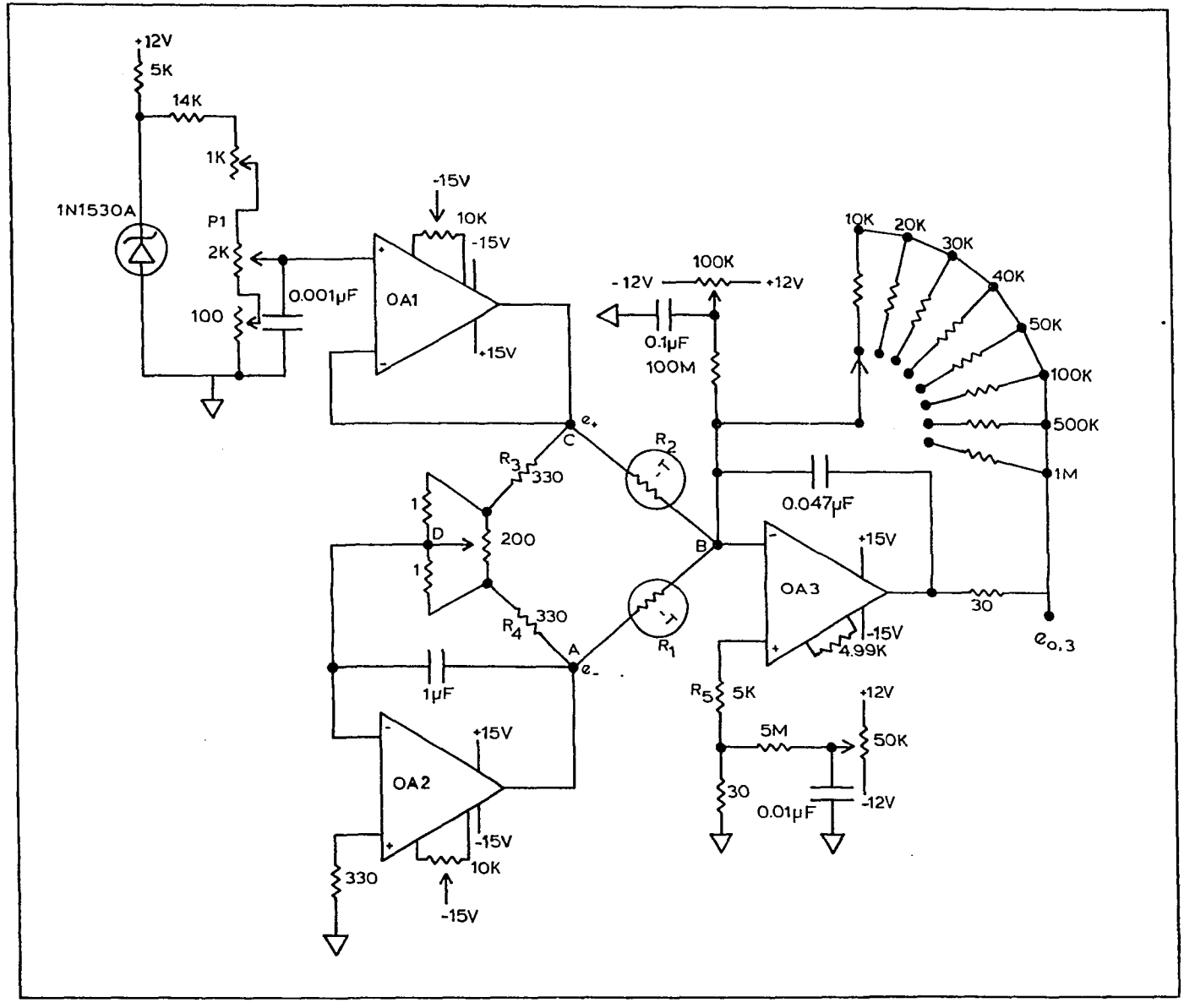
+12V
5K
14K
1K
P1
2K
100
1N1530A
0.001μF
OA1
-15V
10K
-15V
+15V
-12V
100K
+12V
0.1μF
100M
10K
20K
30K
40K
50K
100K
500K
1M
C
e+
R3
330
R2
1
D
200
1
B
0.047μF
+15V
OA3
30
-15V
4.99K
R4
330
A
e-
R1
1μF
eo.3
R5
5K
5M
+12V
50K
30
0.01μF
-12V
OA2
+15V
-15V
10K
330
-15V

R_f = feedback resistance of operational amplifier 3 in Figure III.1 (Ω)

Under conditions of negligible power dissipation, equations A.1 and A.5 are combined and differentiated to yield the temperature response of the circuit.

$$\frac{de_{o,3}}{dT} = -\frac{R_f e_-}{R_1}\left(\frac{\beta_1}{T_1^2} - \frac{1}{T_1}\frac{d\beta_1}{dT_1} - \frac{1}{Z_1}\frac{dZ_1}{dT_1}\right) - \frac{R_f e_+}{R_2}\left(\frac{\beta_2}{T_2^2} - \frac{1}{T_2}\frac{d\beta_2}{dT_2} - \frac{1}{Z_2}\frac{dZ_2}{dT_2}\right) \qquad [A.6]$$

For NTC thermistors, $d\beta/dT$ is positive and the term $(1/T)(d\beta/dT)$ tends to decrease the sensitivity of $e_{o,3}$ with increased temperature. However, dR_t/dT_t is negative and the sign of $de_{o,3}/dT$ is positive.

For $T_1 = T_2 = T$ and $e_+ = -e_- = e$, the equation resulting when $\beta_1 \neq \beta_2$ may be written

$$\frac{de_{o,3}}{dT} = \frac{R_f e}{T^2}\left[\frac{\beta_1}{R_1} - \frac{\beta_2}{R_2}\right] + \frac{R_f e}{T}\left[\frac{1}{R_2}\frac{d\beta_2}{dT} - \frac{1}{R_1}\frac{d\beta_1}{dT}\right] + R_f e\left[\frac{1}{R_2 Z_2}\frac{dZ_2}{dT} - \frac{1}{R_1 Z_1}\frac{dZ_1}{dT}\right] \qquad [A.7]$$

Equation A.7 is of the form of a quadratic equation which describes a parabola.

The properties and applications of PTC thermistors were reviewed by Andrich (110). Methods of manufacturing PTC

thermistors were described by Sauer and Fisher (111). A plot of ln R_t for a PTC thermistor vs. T_t closely resembles the sigmoidal curves familiar for potentiometric titrations. Over a restricted temperature interval (~5 deg C), the slope of the plot is large and the zero-power resistance is given by Equation A.8 (112).

$$R_t = Z_t \exp\{\alpha_t T_t\} \qquad [A.8]$$

where,

α_t = material coefficient of thermistor with positive temperature coefficient (1/deg K).

Differentiation of Equation A.8 yields

$$\frac{1}{R_t}\frac{dR_t}{dT_t} = \alpha_t + T_t\frac{d\alpha_t}{dT_t} + \frac{1}{Z_t}\frac{dZ_t}{dT_t} \qquad [A.9]$$

The value of $\alpha_t >> T_t\frac{d\alpha_t}{dT_t} + \frac{1}{Z_t}\frac{dZ_t}{dT_t}$. Thus, $\frac{1}{R_t}\frac{dR_t}{dT_t} \simeq \alpha_t$ [A.10]

The value of the material coefficient for a PTC thermistor, α_t, can be more than 10X that for a NTC thermistor, β_t. The sensitivity of temperature sensing circuits made with PTC thermistors is, therefore, greater than that for NTC circuits; so also is the nonlinearity.

The combination of a NTC and a PTC thermistor in the circuit of Figure III.1 can result in a highly sensitive device for single cell thermometry which can be linearized by adjustment of e_- relative to e_+. Combining Equations A.4, A.5, and A.10 and differentiating

$$\frac{de_{o,3}}{dT_t} = -\frac{R_f e_-}{R_{NTC}}\left(\frac{\beta_t}{T^2}\right) + \frac{R_f e_+ \alpha_t}{R_{PTC}} \qquad [A.11]$$

Repeating the differentiation and setting the result equal to zero specifies the equality required for linear response.

$$\frac{R_f e_-}{R_{NTC}}\left(\frac{2\beta_t}{T_t^3} - \frac{\beta_t^2}{T_t^4}\right) = \frac{R_f e_+ \alpha_t^2}{R_{PTC}} \qquad [A.12]$$

For typical operating parameters ($\beta \simeq 4000$ and $T = 300$ deg K)

$$\frac{\beta_t^2}{T_t^4} >> \frac{2\beta_t}{T_t^3}$$

and linearity is achieved if

$$-\frac{e_-}{e_+} = \frac{\dfrac{\alpha_t^2}{R_{PTC}}}{\dfrac{\beta^2}{R_{NTC}T^4}} = \frac{\dfrac{1}{R_{PTC}^3}\left(\dfrac{dR_{PTC}}{dT}\right)^2}{\dfrac{1}{R_{NTC}^3}\left(\dfrac{dR_{NTC}}{dT}\right)^2} \qquad [A.13]$$

Typically, linearity results if $-e_-/e_+ \simeq 16$. Linearity may also be achieved with use of series NTC thermistors with the PTC thermistor such that $\sum_{i=1}^{n} \beta_i = \alpha_t$. Such a circuit also has greater sensitivity than the single NTC thermistor with the PTC thermistor.

2. Approximation to an ideal voltage source for a resistive bridge circuit

Implicit in the development of Equation A.5 is the requirement that ideal voltage sources are used to supply t_1 and t_2 with prescribed voltages independent of the currents in each thermistor. An ideal voltage source does not exist but can only be approximated in the real world.

A Wheatstone bridge in first order theory is considered to be simply two voltage dividers connected together. This implies that only two corners of the bridge have controlled potentials. The bridge output is simply the difference between the floating potentials at the remaining corners of the bridge.

In several attempts (113) to achieve better bridge characteristics, an operational amplifier was used as a bridge amplifier with the inverting input connected to one corner of the bridge maintaining the potential of that corner at virtual ground. This bridge amplifier then operates as a current to voltage transducer. This procedure was used in the research described here and a schematic diagram of the circuit is shown in Figure III.1. Increasingly complex transfer functions result when attempts are made to control the potential of the remaining bridge corner using the same operational amplifier described above.

Besides control of corner potentials, three problems remain for the design of bridge circuits in resistance thermometry and approximate solutions to these will be given below. First, as shown by Equation A.13, a means must be provided for adjusting the driving voltages of the thermal sensors so their sensitivities are equivalent. Second, the changing resistance of a thermal sensor changes the power drain placed upon any emf source over a considerable range and the emf source should have low internal resistance. Third, the absolute driving potential of the thermal transducer should be adjustable to allow compensation for aging effects and experimental conditions.

The impossibility of using a galvanic cell directly or with a resistive network to fulfill all of these requirements is obvious. Some of the problems cited above can be solved using transistorized voltage supplies except that they can introduce a new problem; if e_- and e_+ do not track each other very closely, the relative sensitivities of t_1 and t_2 will not remain constant and considerable error results. Operational amplifiers were chosen for their simplicity of use and inherent stability. Through the use of simple resistive networks together with operational amplifiers, simple transfer functions are obtained showing the approximation to an ideal voltage source.

Analysis of the bridge shown in Figure III.1 in qualitative terms shows all corner potentials are well defined.

Points B and D are at virtual ground potential and points A and C can be varied independently to adjust the relative and absolute sensitivities of the thermistors. The values of R_3 and R_4 effectively determine the bridge current when they are much smaller than R_1 and R_2. They serve also as current limiting resistors when R_1 and R_2 become small. The bridge voltage is determined solely by potentiometer, P_1. The problem of voltage tracking by e_- of e_+ is decreased since amplifier OA-2 serves to invert the output of OA-1.

One of the most important characteristics of an operational amplifier is that its output impedance changes negligibly through its entire ± 10 volts output range. Provided that correct current and voltage offset biasing is achieved, and operational amplifiers with very large voltage gain and low noise are selected, the absolute bridge voltage stability is determined by the zener reference diode as the primary voltage standard.

The use of multi-stage voltage regulation together with a temperature compensated zener reference diode provides an absolute voltage stability of a few parts per 100,000. The relative stability of e_- versus e_+ depends on the relative frequency response of the amplifiers plus random noises of all the electronic components, passive as well as active. Judicious choice of amplifiers and passive components provides ppm-level stability of the total bridge circuit. The work

needed to accomplish ppm-level stability for a thermistor bridge is not simply a desirable feature but an absolute necessity. The temperature coefficient of resistance (TCR) of a NTC thermistor is ∿400 ohms/deg C at 25 deg C. To resolve 40 μdeg C, which represents 0.016 ohms using a 10-K thermistor, a relative resistance change, $\Delta R/R_t$, of 1.6 ppm must be measured. Hence, stability in the fullest sense of the word is required for resistance thermometry.

Mathematical analysis of a bridge circuit leading to a quantitative description is easiest done using Thevenin's theorem. The current in thermistor t_1 is independent of the current in t_2 since OA-3 maintains the potential at point B at virtual ground. Circuit analysis will be applied to the top half of the bridge since the primary reference potential used is e_+. Figure III.2 illustrates how the analysis is carried through. Considering e_+ to be the source potential, e_s, reduction of the circuit problem is illustrated.

The Thevenin voltage, V_{th}, is equal to the source potential, e_s, and the Thevenin resistance, R_{th}, is equal to the parallel combination of R_2 and R_3.

$$R_{th} = \frac{R_2 R_3}{(R_2 + R_3)} \qquad [A.14]$$

The potential difference between a and b is kept very small by the action of OA-2 and OA-3. The input impedances of OA-2 and OA-3 are considered to be many times R_{th}. Hence, the

Figure III.2. Thevenin equivalent circuit of thermistor bridge

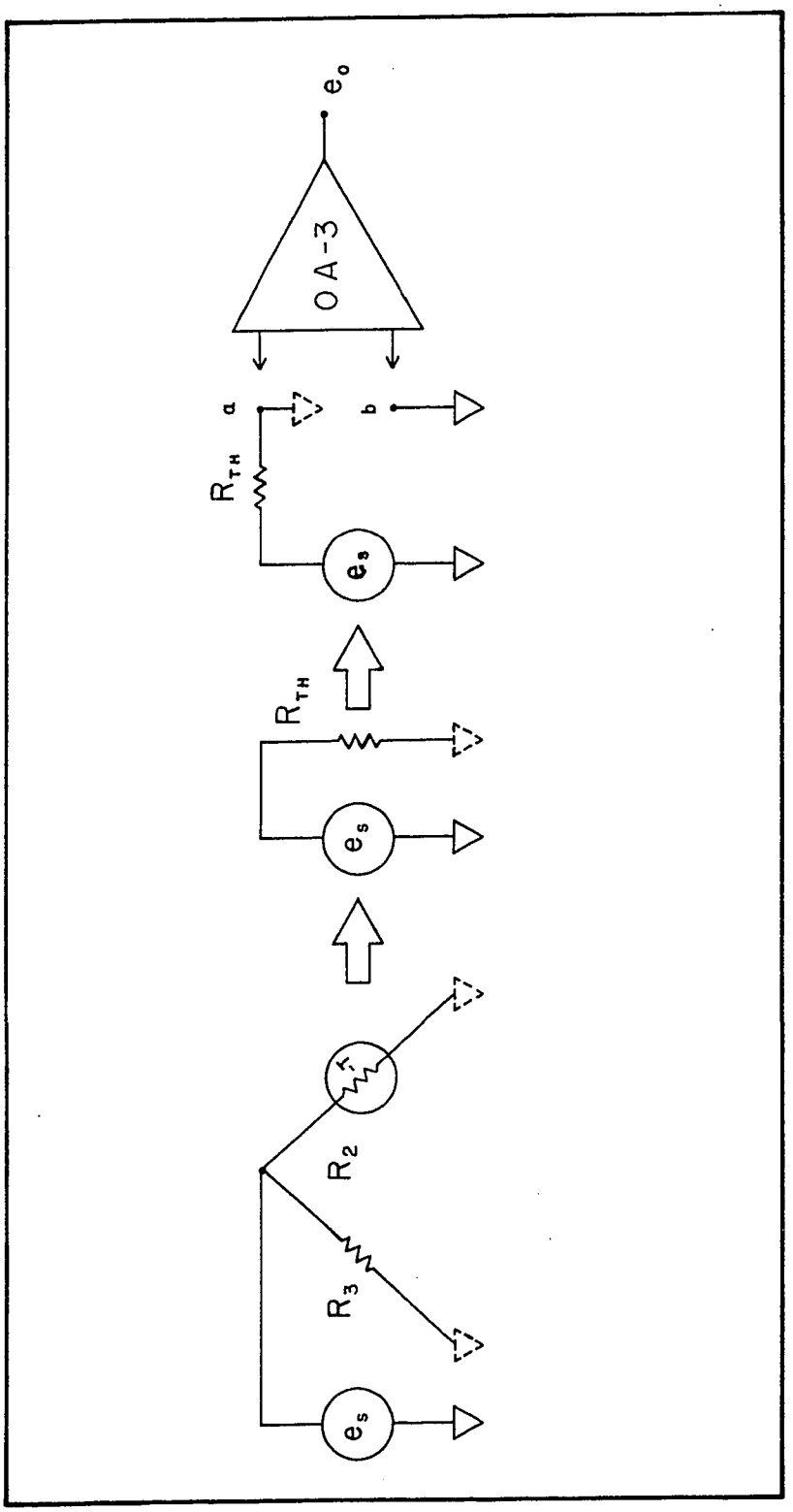
e_o
OA-3
a
b
R_{TH}
e_s
R_{TH}
e_s
R_1
R_2
R_3
e_s

load resistance, R_{a-b}, is much larger than R_{th}, and the current, I_{a-b}, is very small since V_{a-b} is very small. What is of interest now is the change in current in R_{th} when the temperatures of R_2 and R_3 are changed. Since the potential difference, V_{a-b}, is negligible relative to e_s, I_{a-b} must change and this is reflected in e_o considered here to be the sum of changes in $e_{o,2}$ of OA-2 and $e_{o,3}$ of OA-3. The resistor, R_3, and thermistor, R_2, are in different temperature environments and the value of dR_{th} must be expressed as

$$dR_{th} = \left(\frac{\partial R_{th}}{\partial T_t}\right)_{T_a} dT_t + \left(\frac{\partial R_{th}}{\partial T_a}\right)_{T_t} dT_a \qquad [A.15]$$

where

T_a = ambient temperature of bridge amplifier enclosure (deg C)

T_t = thermistor temperature at geometric center (deg K)

Using Equation A.14, we may determine that

$$\left(\frac{\partial R_{th}}{\partial T_t}\right)_{T_a} = \left(\frac{R_3^2}{(R_2 + R_3)^2}\right) \frac{dR_2}{dT_t} \qquad [A.16]$$

and

$$\left(\frac{\partial R_{th}}{\partial T_a}\right)_{T_t} = \left(\frac{R_2^2}{(R_2 + R_3)^2}\right) \frac{dR_3}{dT_a} \qquad [A.17]$$

From Equation A.3 together with Equations A.15, A.16, and A.17, and ignoring $d\beta_t/dT_t$, we obtain

$$dR_{th} = -\left[\frac{R_2 R_3^2 \beta}{(R_2 + R_3)^2 T_t^2}\right] dT_t + \left[\frac{R^2 \alpha_3}{(R_2 + R_3)^2}\right] dT_a \qquad [A.18]$$

where

α_3 = temperature coefficient of resistance of bridge resistor (ohm/deg C)

Also,

$$dI_{th} = \frac{R_{th} dV_{th} - V_{th} dR_{th}}{R_{th}^2} \qquad [A.19]$$

Substitution of Equation A.18 into Equation A.19 yields

$$dI_{th} = \left[\frac{1}{R_{th}}\right] dV_{th} + \left[\frac{\beta V_{th}}{R_2 T_t^2}\right] dT_t - \left[\frac{\alpha_3 V_{th}}{R_3^2}\right] dT_a \qquad [A.20]$$

which upon substitution of $e_+ = V_{th}$ and rearrangement yields

$$dI_{th} = \left[\frac{\beta e_+}{R_2 T_t^2}\right] dT_t + \left[\frac{1}{R_{th}}\right] de_+ - \left[\frac{\alpha_3 e_+}{R_3^2}\right] dT_a \qquad [A.21]$$

Equation A.21 is recognized to be the sum of the desired signal, as represented by the first term, plus noise contributions. Electronic noise is recognized to be composed of all frequencies, thus de_+ and dT_a include both long term (drift) and short term contributions. Systematic changes in e_+ are also reflected in e_-, effectively cancelling them in the output of OA-3. Changes in the potential of OA-2 are not

discriminated against making relative bridge stability dependent on the stabilities of OA-2 and OA-3.

The term de_+ is small and the result of random events if a nearly ideal voltage source is used for e_+. Causes for deviations from ideality in operational amplifiers have been treated adequately elsewhere (114, 115). Voltage offset and current offset corrections are necessary in real operational amplifiers to obtain zero output voltage for zero input. Drift in these offsets is the source of long term noise whereas "popcorn", "flicker", "Johnson", and "shot" noises dominate short term noise measurements.

The parameter, de_+, then is a combination of short term and long term noises, which can be expressed as

$$de_+ = e_n + \Delta e_{os} \qquad [A.22]$$

where e_n = short term electronic noise which is random in nature (volt)

Δe_{os} = long term electronic drift of amplifier offsets (volt)

Source resistance is known to affect very strongly the noise contribution from current offset. Since offset current at each input of an operational amplifier tends to be equal, use of equal impedances from each amplifier input to ground reduces the offset current contribution. The effective input impedance to the inverting input of OA-3, point B of the bridge circuit, is the parallel combination of R_1, R_2, and

the feedback resistance R_f. The resistance, R_5, connected to the noninverting input of OA-3 is chosen to equal the effective input impedance connected to point B. The drift contribution is now the differential current offset between the two inputs rather than the current offset of one input. This technique is also used to reduce the current offset drift of OA-2. Zener diodes have low resistances, generally well below 100 ohms, and impedance compensation of OA-1 is unnecessary.

Strata (114) has given methods of calculating e_{os} from test measurements both for absolute values of offset currents and voltages plus changes in these in these parameters. The offset expression for a noninverting amplifier such as OA-1 is given by

$$\Delta e_{os} = de_{os} \qquad [A.23]$$

whereas by comparison when amplifiers are used in a differential input mode such as OA-2 and OA-3,

$$\Delta e_{os} = de_{os} \left(\frac{R_f + R_i}{R_i} \right) + R_i(i_{os}^- - i_{os}^+) \qquad [A.24]$$

where R_i is the input resistance at the inverting input of the operational amplifier. Examination of Equations A.23 and A.24 reveal that for the present bridge circuit, offset errors are contributed mainly by OA-2 and OA-3. Resistors R_3 and R_4 are equal in resistance meaning that OA-2 will

contribute twice as much drift as OA-1 since for the value of R_3 used in this research, the second term in Equation A.24 is negligible. The parameter de_{os} has been given by Strata (114) as

$$de_{os} = \left[\frac{de_{os}}{dT_a}\right] dT_a + \left[\frac{de_{os}}{dV^+}\right] dV^+ + \left[\frac{de_{os}}{dV^-}\right] dV^- + \left[\frac{de_{os}}{dt}\right] dt \qquad [A.25]$$

where V^+, V^- are positive and negative supply voltages of the operational amplifier. A similar relation is used for calculation of di_{os}. It should be evident after study of Equations A.20 and A.25 that temperature control of the bridge circuit enclosure and supply voltage regulations are the prime factors in minimizing bridge potential drift.

B. Dynamic Models for Heat Transfer

1. Thermistor probes in fully turbulent flows

For small changes of temperature of an NTC thermistor through which $d\beta_t/dT_t$ can be ignored, the zero power operation (Equation A.1) can be described

$$R_b = R_t \exp\{\beta_t \left[\frac{T_t - T_b}{T_t^2}\right]\} \qquad [B.1]$$

where T_b is the bulk solution temperature (deg K) and R_b is the value of R_t when $T_t = T_b$. Equation B.1 is valuable for beginning a consideration of the response of R_t when the bulk media surrounding the thermistor is heated at a rate γ_b and $T_t \neq T_b$. For small γ_b, $(T_b - T_t)/T_t^2 \simeq 0$ and the exponential term of Equation B.2 can be accurately given by the first two members of an Euler series expansion. Thus,

$$R_b = R_t \left[1 + \beta_t \left(\frac{T_t - T_b}{T_t^2}\right)\right] \qquad [B.2]$$

Rearranging Equation B.2,

$$\Delta R_{b-t} = R_b - R_t \qquad [B.3]$$

$$= \frac{R_t \beta_t}{T_t^2}(T_t - T_b)$$

Combining Equations A.4 and B.3,

$$\Delta R_{b-t} = \frac{-dR_t}{dT_t}(T_t - T_b) \qquad [B.4]$$

Carslaw and Jaeger (116) solved the problem of heat transfer between a sphere and the surrounding media. For the case of heat transfer from an electrically heated spherical thermistor to the surrounding media at zero initial temperature,

$$T_t' - T_b' = \frac{P_t}{8\pi r_t \lambda_t}\{1 + \frac{2\lambda_t}{h_t r_t} - \frac{12h_t}{\lambda_t}$$

$$\sum_{n=1}^{\infty} \frac{\exp(-\alpha_n^2 D_t t)}{\alpha_n[r_t^2\alpha_n^2 + r_t h(r_t h - 1)]\sin r_t\alpha_n}\} \qquad [B.5]$$

where

P_t = electrical power applied to thermistor (cal/sec)

r_t = radius of thermistor bead (cm)

λ_t = thermal conductivity of thermistor material (cal/cm-sec-deg C)

h_t = convective heat transfer coefficient of thermistor bead (cal/cm^2-sec-deg C)

α_n = roots of the transcendental equation

$$r_t\,\alpha_n \cot r_t\,\alpha_n + r_t\,h - 1 = 0$$

$h = h_t/\lambda_{eq}$ (1/cm)

D_t = thermal diffusivity of thermistor material (cm^2/sec)

t = time (sec)

For the case of external heating of a spherical thermistor at zero initial temperature by the bulk media,

$$T_t'' - T_b'' = \frac{-\gamma_b r_t^2}{6D_t}\{1 + \frac{2\lambda_t}{h_t r_t} - \frac{12h_t}{\lambda_t}$$

$$\sum_{n=1}^{\infty} \frac{\exp(-\alpha_n^2 D_t t)}{\alpha_n[r_t^2\alpha_n^2 + r_t h(r_t h - 1)]\sin r_t\alpha_n}\} \qquad [B.6]$$

The treatment of the heat transfer between a thermistor bead and the surrounding media assumes it to be a perfect

sphere. The actual thermistor configuration used in this research resulted from mounting a thermistor bead with epoxy into the end of a Teflon cylinder having a diameter slightly greater than the diameter of the thermistor as shown in Figure III.3.

The time independent portions of Equations B.5 and B.6 yield temperature differences across the thermistor bead material and thermal boundary layer when no extraneous material covers the thermistor. Correction factors must be applied to account for stem conduction and the surface film of epoxy. Initially, consider only the epoxy film. The second term of Equations B.5 and B.6 ($2\lambda_t/h_t r_t$) is multiplied by a factor to yield the average temperature difference across the epoxy film plus the thermal boundary layer. From Fourier's law, dimensional analysis and geometrical considerations, the inner conductivity, λ_i, can be derived to replace λ_t in the second term by Equation B.7

$$\lambda_i = 2\lambda_t \left(\frac{r_t \lambda_e + x_e \lambda_t}{r_t \lambda_e} \right) \qquad [B.7]$$

where

λ_e = thermal conductivity of epoxy (cal/cm-sec-deg C)

x_e = thickness of epoxy film on thermistor (cm)

The equivalent conductivity, λ_{eq}, substituted for λ_t in the time dependent terms of Equations B.5 and B.6 can be shown to be

$$\lambda_{eq} = 0.5\lambda_t\left(\frac{r_t\lambda_e}{r_t\lambda_e + x_e\lambda_t}\right) \qquad [B.8]$$

The superposition principle commonly used for linear systems and in many problems of heat conduction is applied. Accordingly, the difference $T_t - T_b$ is assumed given by a linear combination of Equations B.5 and B.6. The prime and double prime designations in Equation B.9 assist in

$$T_t - T_b = (T_t' + T_t'') - (T_b' + T_b'') \qquad [B.9]$$

recognizing the equation (B.5 or B.6) used to calculate the designated term.

So that the solution of Equation B.4 is made more tractable, only the time-independent parts of Equations B.5 and B.6 are considered here. Simple calculations show that the second terms of Equations B.5 and B.6 control thermistor response. Hence, Equation B.7 may be written as

$$T_t - T_b = \left(\frac{3P_t - 4\pi r_t^3 c_t\gamma_b}{12\pi r_t\lambda_t}\right)\left(\frac{\lambda_i}{h_t r_t}\right)$$

where

c_t = volume heat capacity of thermistor material (cal/cm^3-deg C)

γ_b = heating rate of bulk solution (deg C/sec)

The time-independent parts of Equations B.5 and B.6 contain terms common to the thermistor dissipation constant,

δ_t, and the thermistor time constant, τ_t.

$$\delta_t = \frac{\delta_o \delta_b}{\delta_o + \delta_b} = 8\pi r_t \lambda_t \left[\frac{h_t r_t}{h_t r_t + 2\lambda_i} \right]$$

where

δ_b = dissipation constant of epoxy plus stem and boundary layer (cal/sec-deg C)

δ_o = dissipation constant of thermistor bead (cal/sec-deg C)

$$\tau_t = \tau_o + \tau_b = \frac{r_t^2}{6D_t} \left[\frac{h_t r_t + 2\lambda_i}{h_t r_t} \right] \qquad [B.12]$$

where

τ_b = time constant of epoxy plus stem and boundary layer (sec)

τ_o = time constant of thermistor bead (sec)

For rates of bulk fluid stirring which approach zero, $h_t r_t \to \lambda_b$, and

$$\delta_t \to 8\pi r_t \lambda_t \left[\frac{\lambda_b}{\lambda_b + 2\lambda_i} \right] \qquad [B.13]$$

$$\tau_t \to \frac{r_t^2}{6D_t} \left[\frac{\lambda_b + 2\lambda_i}{\lambda_b} \right] \qquad [B.14]$$

where

λ_b = thermal conductivity of bulk solution (cal/cm-sec-deg C)

For high rates of stirring, $h_t r_t >> 2\lambda_i$, and

$$\delta_t \rightarrow 8\pi r_t \lambda_t \qquad [B.15]$$

$$\tau_t \rightarrow \frac{r_t^2}{6D_t} \qquad [B.16]$$

The nonlinear dependence of δ_t on h_t as given by Equation B.11 was demonstrated by Rasmussen (117).

Substitution of the time independent parts of Equation B.5 and B.6 into Equation B.9 and combining the result with Equation B.4 yields

$$\frac{\Delta R_{t-b}}{dR_t/dT_i} = \frac{P_t}{8\pi r_t \lambda_t}\left(1 + \frac{2\lambda_i}{h_t r_t}\right) - \frac{\gamma_b r_t^2}{6D_t}\left(1 + \frac{2\lambda_i}{h_t r_t}\right) \qquad [B.17]$$

Since $D_t = \lambda_t / c_t$,

$$\frac{-dR_t}{dT_t} = \frac{\lambda_t \Delta R_{b-t}}{\left[\frac{P_t}{8\pi r_t}\left(1 + \frac{2\lambda_i}{h_t r_t}\right) - \frac{\gamma_b r_t^2 c_t}{6}\left(1 + \frac{2\lambda_i}{h_t r_t}\right)\right]} \qquad [B.18]$$

Hence, the temperature coefficient of resistance for the thermistor, $dR_t/R_t dT_t$, is directly related to its thermal conductivity, λ_t, as discussed by Kudryavtsev, et al. (118).

Combining Equations B.11, B.12 and B.17 yields

$$\tau_t = \left(\frac{P_t}{\delta_t} + \frac{\Delta R_{b-t}}{dR_t/dT_t}\right)\frac{1}{\gamma_b} \qquad [B.19]$$

Using the definition $P_t = C_t \gamma_t$,

where

C_t = heat capacity of thermistor (cal/deg C)

γ_t = heating rate of thermistor by electrical power (deg C/sec)

$$\tau_t = \frac{C_t \gamma_t}{\delta_t \gamma_b} + \frac{\Delta R_{b-t}}{dR_t/dT_t}\left(\frac{1}{\gamma_b}\right) \qquad [B.20]$$

In the limit where $\gamma_b \to \infty$, Equation B.20 becomes

$$\tau_t = \frac{C_t}{\delta_t}\frac{\gamma_t}{\gamma_b} \qquad [B.21]$$

If $\gamma_t = \gamma_b$

$$\tau_t = \frac{C_t}{\delta_t} \qquad [B.22]$$

This equality is experimentally valid only if the thermistor is suspended by its leads such that the thermistor surface is uniformly accessible.

Equation B.19 can also be written

$$\tau_t = \frac{\Delta R_{b-t}}{dR_t/dT_i}\left(\frac{1}{\gamma_b - \gamma_t}\right) \qquad [B.23]$$

Because dR_t/dT_t is negative for a NTC thermistor, $\Delta R_{b-t}/(\gamma_b - \gamma_t)$ is negative. Increasing P_t will decrease the effect of γ_b on τ_t and the slope of a plot of τ_t vs. $1/\gamma_b$ will decrease.

The convective heat transfer coefficient, h_t, in Equation B.18 is part of the Nusselt number, Nu

$$Nu = \frac{h_t \, r_t}{\lambda_b} \qquad [B.24]$$

For a stirred media, Nu is related to the Prandtl, Pr, and Reynolds, Re, numbers by equations of the general form

$$Nu = Re^b Pr^c \qquad [B.25]$$

where a, b, and c are constants and Re and Pr are defined

$$Re = \frac{U \, r}{\nu_b}$$

$$Pr = \frac{\nu_b}{D_b}$$

where

ν_b = kinematic viscosity of bulk solution (cm^2/sec)

D_b = thermal diffusity of bulk solution (cm^2/sec)

A sphere is a poorly streamlined body and separation of boundary layer flow occurs for Re > 50. For the stirred systems of interest in calorimetry ($10^3 < Re < 10^4$), the bulk fluid is fully turbulent and the hydrodynamic boundary layer around the thermistor is laminar with separation. Kutateladze (119) determined that for a sphere, the diameter Nusselt number is

$$Nu_d \simeq 2 + 0.35 \, Re^{0.58} \, Pr^{0.36} \qquad [B.26]$$

The radius Nusselt number is

$$Nu_r = 1.00 + 0.175\ Re^{0.58}\ Pr^{0.36} \qquad [B.27]$$

Murdock et al. (120) showed that

$$h_t r_t = (N_s r_t)^{0.6} \qquad [B.28]$$

where N_s is the rotation speed of the bulk media stirrer in units of rev/min. Rice et al. (121) determined that the fluid velocity, U, at a distance r from the axis of stirrer rotation and in the plane of the stirrer is given by

$$U(r) = \frac{2\pi r_s^2 N_s}{60\ r} \qquad [B.29]$$

where

r_s = radius of stirrer disk (cm)

Equation B.29 is valid for distances up to half way from the outer edge of the stirrer to the cell wall. Combining Equations B.21-B.28

$$\frac{h_t r_t}{\lambda_b} = 0.50 + 0.0875 \left(\frac{r_s^2 \omega_s 2 r_t}{r\ \nu_b}\right)^{0.58} \left(\frac{\nu_b c_b}{\lambda_b}\right)^{0.36} \qquad [B.30]$$

where

ω_s = angular velocity of stirrer (rad/sec)

c_b = mass heat capacity of bulk solution (cal/g-deg C)

The coefficient of the second term in Equation B.29 was calculated for direct exposure of one-half the thermistor surface to the solution. When $\omega_s = 0$,

$$h_t r_t = 0.50\lambda_b$$

and from Equation B.13,

$$\delta_t = 4\pi r_t \lambda_t \left[\frac{\lambda_b}{0.5\lambda_b + 2\lambda_i}\right] \qquad [B.31]$$

Application of a thermistor to determine values of the thermal conductivity of the bulk fluid was performed by Papadopoulos (122).

The Pai power series for calculating the velocity distribution in a pipe can also be applied to calculation of Re for use in Equation B.27 (123).

$$\frac{U(r)}{U_{max}} = 1 + a_1\left(\frac{r}{r_c}\right)^2 + a_2\left(\frac{r}{r_c}\right)^{2m} \qquad [B.32]$$

where

r_c = radius of calorimeter cell (cm)

In Equation B.32:

$$U_{max} = \omega_s r_s$$

$$a_1 = \frac{n - m}{m - 1}$$

$$a_2 = \frac{1 - n}{m - 1}$$

$$m = -0.617 + 8.21 \times 10^{-3} (Re_{max})^{0.786}$$

$$n = 0.585 + 3.17 \times 10^{-3} (Re_{max})^{0.833}$$

and $$Re_{max} = \frac{\omega_s r_s^2 r_c}{\nu_b}$$

The values of $U(r)/U_{max}$ calculated from Equations B.29 and B.32 are different. The lack of agreement occurs because of the calculation of the cell velocity profile in the plane of the stirrer (Equation B.32) versus that outside the plane of the stirrer (Equation B.29). Equation B.33 should be used when the thermistor is in the plane of the stirrer.

$$Re_t = \frac{U(r)\ r_s \omega_s 2r_t}{U_{max}\quad \nu_b} \qquad [B.33]$$

Rewriting Equation B.3 as

$$\frac{\Delta R_{b-t}}{R_t(T_t - T_b)} = \frac{\beta_t}{T_t^2} \qquad [B.34]$$

and substituting into Equation A.6 yields

$$\frac{de_{o,3}}{dT} = -\left[\frac{R_f e_-}{R_1^2}\ \frac{\Delta R_{b-t,1}}{(T_1 - T_b)}\right] - \frac{R_f e_+}{R_2^2}\left[\frac{\Delta R_{b-t,2}}{(T_2 - T_b)}\right] \qquad [B.35]$$

Combining Equations B.10 and B.35 and writing only the half of the equation corresponding to R_1

$$\frac{de_{o,3}}{dT} = -\frac{R_f e_-}{R_1^2}\left[\frac{12\pi r_{t,1}\lambda_t \Delta R_{b-t,1}}{(3P_{t,1} - 4\pi r_{t,1}^3 c_t \gamma_b)}\left[\frac{h_{t,1} r_{t,1}}{\lambda_{t,1}}\right]\right] + \cdots [B.36]$$

Combining Equations B.30 and B.36

$$\frac{de_o}{dT} = -\frac{R_f e_-}{R_1^2} \quad . \qquad [B.37]$$

$$\frac{r_{t,1}\lambda_t \Delta R_{b-t,1}(18.8\lambda_{b,1} + 3.30\lambda_{b,1})\left[\frac{r_{s,1}^2 \omega_{s,1} 2r_{t,1}}{r_1 \nu_b}\right]^{0.58}\left[\frac{\nu_b c_b}{\lambda_b}\right]^{0.36}}{\lambda_{i,}\,(3P_{t,1} - 4\pi r_{t,1}{}^3 c_t \gamma_b)}$$

Examination of Equation B.37 reveals that de_o/dT gains decreased dependency on γ_b as P_t increases. This fact is important in thermokinetic studies since uniform response to change of solution temperature is needed when the rate of the chemical reaction is time dependent.

When $\gamma_b = 0$ and $\omega_s = 0$, Equation B.37 reduces to

$$\frac{de_o}{dT} = -\frac{R_f e_-}{R_1^2}\left[\frac{6.28 r_{t,1}\lambda_t \Delta R_{b-t,1}\lambda_{b,1}}{\lambda_{i,1}\, P_{t,1}}\right] + \cdots \qquad [B.38]$$

Implicit in the derivation of Equation B.26 was the assumption that thermal conduction of the thermistor support is negligible. Dutt and Stickney (124) demonstrated that conduction errors are only negligible if the thermal sensor is mounted on a support of low thermal conductivity. Contact resistance between the thermistor and mount is also important. Since no perfect insulator exists, a stem correction was applied to Equation B.7. Without stem correction, the tip solution predicts excessive tip temperature and time constants (125).

For the thermistor probe design used in this research, correction was made only for the exposed portion of Teflon

tubing in which the head was mounted. Correction applied to Equation B.7 yields

$$\lambda_i = \frac{2\lambda_t^2}{\lambda_e}\left(\frac{h_s r_{st}}{\lambda_s}\right)\left(\frac{r_t\lambda_e + x_e\lambda_t}{r_t\lambda_s + x_{ts}\lambda_t}\right) \qquad [B.39]$$

where

h_s = convective heat transfer coefficient of thermistor stem (cal/cm^2-sec-deg C)

r_{st} = radius of thermistor stem (cm)

λ_s = equivalent thermal conductivity of thermistor stem (cal/cm-sec-deg C)

x_{ts} = length of thermistor stem (cm)

The parameter, λ_s, in Equation B.39 is calculated from

$$\lambda_s = \frac{\lambda_e A_e + \lambda_w A_{tw}}{A_{ts}}$$

where

A_e = cross sectional area of epoxy filling plus Teflon tubing in thermistor mounting (cm^2)

A_{ts} = total cross sectional area of thermistor stem (cm^2)

A_{tw} = cross sectional area of thermistor lead wires (cm^2)

λ_w = thermal conductivity of thermistor lead wires (cal/cm-sec-deg C)

The heat transfer coefficient, h_s, in Equation B.39 is calculated from

$$Nu_d = 0.478\ Re^{0.5}\ Pr^{0.3}$$

as described by Scadron and Warshawsky (126) for cylinders in a crossflow.

An area correction must also be applied to the time dependent portions of Equation B.6. The exponential term is multiplied by the reciprocal of the fractional area of the thermistor exposed to the solution (2 for our case). The equivalent conductivity, λ_{eq}, corrected for stem conduction is given by

$$\lambda_{eq} = 0.5 \left| \lambda_t \left(\frac{r_t \lambda_e}{r_t \lambda_e + x_e \lambda_t} \right) + \lambda_t \left(\frac{r_t r_s h_s}{r_t \lambda_s + x_{ts} \lambda_t} \right) \right| \qquad [B.40]$$

Equations B.39 and B.40 are derived in Appendix B.

The signal strength of the bridge circuit shown in Figure III.1 is now completely described. The signal-to-noise ratio, S/N, which is perhaps the most important parameter of any circuit, cannot be calculated yet. From the basic equations given above, all of the relations needed to describe S/N will now be derived.

Noise is a distortion or disruption of the desired signal in either a random or systematic manner. Removal of systematic noises is generally straightforward, involving nothing more than careful experimental design and execution. Reduction of random noise in an experiment is much more difficult. Ultimate noise levels are determined by the number of physical variables studied and quantization errors caused by the

particle-like behaviour of energy transmission at the microscopic level in nature. Energy transmission on a macroscopic scale is a continuous function but at the microscopic level it is discontinuous and governed by distribution laws governing random events.

In thermistors, this is readily seen in consideration of the term β_t used in Equation B.1. β_t is given by

$$\beta_t = - \frac{E_g}{2 k_B}$$

where E_g = gap energy of semiconductor (eV)

k_B = Boltzmann constant

The parameter β_t then describes the energy which individual charge carriers need to move from the valence band into the conduction band. A fundamental constant of quantum quantum processes, k_B, completes the description of β_t. Distribution of electrons in n-type semiconductors such as NTC thermistors is thus described using the band theory with a multiplicity of energy levels in each band and varying probability that each is populated primarily as a function of temperature as given in Equation A.3.

Noises can be divided into two categories, correlated and uncorrelated. Correlated noises are those having the same frequency and phase even though they differ in amplitude. For example, the bridge output was designed so that e_- tracks e_+ (reduction of systematic fluctuations in de_o/dT) and

correspondingly noise in e_- as seen by OA-3 is correlated with noise in e_+. The temperature in each Dewar cell of the calorimeter is independent and fluctuations in bulk solution temperatures of the two cells are uncorrelated noises.

The first term of Equation A.5 will be used in the initial development of a noise strength equation. Equations A.4 and B.4 when rearranged and used in the first term of Equation A.5 yield

$$e_o = - \frac{R_f \beta_t e_-}{T_t^2} \frac{(T_t - T_b)}{R_{b-t}} \qquad [B.41]$$

To simplify nomenclature, Equation B.41 is rewritten as

$$e_o = - \frac{R_f \beta_1 e_-}{T_1^2} \frac{\Delta T_1}{\Delta R_1}$$

which in turn can be written as

$$\frac{e_o}{R_f} = i_1 = - \frac{\beta_1 e_-}{T_1^2} \frac{\Delta T_1}{\Delta R_1} \qquad [B.42]$$

Equation B.42 allows consideration of the noises produced by the driving voltage and thermistor apart from the amplifier noise of OA-3.

The random noise $\sigma_{i_1}^2$ can now be written as

$$\sigma_{i_1}^2 = \left(\frac{e_- \Delta T_1}{T_1^2 \Delta R_1}\right)^2 \sigma_{\beta_1}^2 + \left(\frac{\beta_1 \Delta T_1}{T_1^2 \Delta R_1}\right)^2 \sigma_{e_-}^2 + \left(\frac{\beta_1 e_-}{T_1^2 \Delta R_1}\right)^2 \sigma_{\Delta T_1}^2 +$$

$$\left(\frac{\beta_1 e_- \Delta T_1}{T_1^2 \Delta R_1}\right)^2 \sigma_{\Delta R_1}^2 + \left(\frac{-2\beta_1 e_- \Delta T_1}{T_1^3 \Delta R_1}\right)^2 \sigma_{T_1}^2 \qquad [B.43]$$

Before further substitutions, Equation B.43 needs to be expressed in familiar variables. That is, σ_{e_-} is already known and $\sigma_{\Delta T_1}$ can be readily calculated from Equation B.10, but σ_{β_1} and $\sigma_{\Delta R_1}$ are not calculable separately. The value of σ_{T_1} is certainly a desired parameter when experimentally determined values of σ_{i_1} are known.

The parameters σ_{β_1} and $\sigma_{\Delta R_1}$ are derived from Equations A.3 and B.3, respectively, using simplifying assumptions.

$$\sigma^2_{\beta_1} = \left(\frac{T_1}{R_1}\right)^2 \sigma^2_{R_1} + \left(\frac{\beta_1}{T_1}\right)^2 \sigma^2_{T_1} \qquad [B.44]$$

and

$$\sigma^2_{R_1} = \left(\frac{-R_1\beta_1}{T_1{}^2}\right)^2 \sigma^2_{T_1} \qquad [B.45]$$

$$\sigma^2_{\Delta R_1} = \left(\frac{\Delta R_1}{R_1}\right)^2 \sigma^2_{R_1} + \left(\frac{\Delta R_1}{\beta_1}\right)^2 \sigma^2_{\beta_1} + \left(\frac{-2\Delta R_1}{T_1}\right)^2 \sigma^2_{T_1} + \left(\frac{\Delta R_1}{\Delta T_1}\right)^2 \sigma^2_{\Delta T_1} \qquad [B.46]$$

Substitution of Equation B.45 into B.44 and B.44 plus B.45 into B.46 yields

$$\sigma^2_{\beta_1} = 2\left(\frac{\beta_1}{T_1}\right)^2 \sigma^2_{T_1} \qquad [B.47]$$

and

$$\sigma^2_{\Delta R_1} = \left(\frac{\Delta R_1}{\Delta T_1}\right)^2 \sigma^2_{\Delta T_1} + \left[\left(\frac{\beta_1 \Delta R_1}{T_1{}^2}\right)^2 + 6\left(\frac{\Delta R_1}{T_1}\right)^2\right] \sigma^2_{T_1} \qquad [B.48]$$

Use of Equations B.47 and B.48 in B.43 yields

$$\sigma_i^2 = \left(\frac{\beta_1 \Delta T_1}{T_1^2 \Delta R_1}\right)^2 \sigma_{e_-}^2 + 2\left(\frac{\beta_1 e_-}{T_1^2 \Delta R_1}\right)^2 \sigma_{\Delta T_1}^2 + \left| 12\left(\frac{\beta_1 e_- \Delta T_1}{T_1^3 R_1}\right)^2 + \left(\frac{\beta_1^2 e_- \Delta T_1}{T_1^4 \Delta R_1}\right)^2 \right| \sigma_{T_1}^2 \qquad [B.49]$$

Evaluation of Equation B.49 is seen to be very dependent on a knowledge of ΔT_1. Through the entire treatment, Equations B.3 - B.49, ΔT_1 is treated as a dynamic variable and ΔR_1 as a steady state variable. The logic of this assumption is clear since R_1 is controlled by T_1 and not vice versa. That is to say that although in reality R_1 changes, the change is seen in dR_1 as T_1 changes. Accordingly, the transient portion of ΔT_1 is considered to operate on the ratio $\Delta T_1/\Delta R_1$ even though no separate transient term is discussed for R_1. In the development of Equation B.10, little was said about the relative magnitude of each term in Equations B.5 and B.6. The first term of these equations describes the temperature difference between the wall of the thermistor and the geometric center of the thermistor. The second term defines the temperature drop from the thermistor wall to the bulk solution temperature.

As noted earlier, calculation shows that the second term is much larger than the first, generally 30 times larger. The thermal gradient across the thermal boundary layer, which is on the order of 10^{-4} cm, then is much larger than the

thermal gradient within the thermistor. The time constant τ_o in Equation B.12 is also approximately 30 times smaller than τ_b. Before turning to the case where noises in e_-, ΔT_1 and T_1 are completely random, let us consider the case where e_- or T_1 change instantaneously to a new value, the situation of Equations B.5 and B.6. Knowing the relative size of terms in Equations B.5 and B.6 and using the series approximations for the trignometric functions represented in the transient portions of each equation it can be shown that when $r_t << 1$

$$\Delta T_1 = \left[\frac{e_-^2}{4\pi r_1 \lambda_t R_1} - \frac{r_1^2 c_t \gamma_b}{3\lambda_t}\right] \cdot \left[\frac{\lambda_{i,1}}{h_1 r_1} - \frac{2\lambda_{eq,1}^2}{h_1^2 r_1} \exp\left(\frac{-3h_1 D_t t}{\lambda_{eq} r_1}\right)\right] \qquad [B.50]$$

The structure of Equation B.50 is characteristic of equations defining systems such as RC or RL circuits. Noise models for such circuits have already been derived and tested (115), placing the present analysis on a firmer theoretical foundation.

Since ΔT_1 is essentially controlled by the properties of the thermal boundary layer, variations of h_t must be calculated. Random errors in ΔT_1 are considered ultimately with respect to time assuming that the mean value of T_1 is constant. The assumption of constant temperature leads to the assumption of constant properties for the bulk solution

parameters such as c_b, λ_b, ν_b and thermistor properties c_t, λ_i, λ_{eq} and r_t.

Setting $\rho_t = h_t r_t$ as defined by Equation B.30, σ_{ρ_t} is then governed by σ_{ω_s} using assumption stated above.

$$\sigma^2_{\rho_1} = \left[\left(\frac{0.0508}{\omega_s}\right)\left(\frac{U(r) r_s \omega_s 2 r_1}{U_{max}\ \nu_b}\right)\left(\frac{\nu_b c_b}{\lambda_b}\right)^{0.36} \lambda_b\right]^2 \cdot \sigma^2_{\omega_s} \qquad [B.51]$$

With Equations B.49 and B.50 in hand, it can be shown that

$$\begin{aligned}\sigma^2_{\Delta T_1} \approx\ & \left\{\frac{e_-}{2\pi r_1 \lambda_t R_1}\left[\frac{\lambda_{i,1}}{\rho_1} - 2\frac{2\lambda^2_{eq,1}}{\rho_1^2}\exp\left(\frac{-3\rho_1 D_t t}{\lambda_{eq,1}\ r_1^2}\right)\right]\right\}^2 \sigma^2_{e_-} \\ & + \left\{\frac{r_1^2 c_1}{3\lambda_t}\left[\frac{\lambda_{i,1}}{\rho_1} - \frac{2\lambda^2_{eq,1}}{\rho_1^2}\exp\left(\frac{-3\rho_1 D_t t}{\lambda_{eq,1}\ r_1^2}\right)\right]\right\}^2 \sigma^2_{\gamma_{b,1}} \\ & + \left\{\left[\frac{e_-^2}{4\pi r_1 \lambda_t R_1} - \frac{r_1^2 c_t \gamma_{b,1}}{3\lambda_t}\right]\left[\frac{-\lambda_{i,1}}{\rho_1^2} + \frac{4\lambda^2_{eq,1}}{\rho_1^3}\cdot\right.\right. \\ & \left.\left.\exp\left(\frac{-3\rho_1 D_t t}{\lambda_{eq,1}\ r_1^2}\right) + \frac{6\lambda_{eq,1}\ D_t t}{r_1^2}\exp\left(\frac{-3\rho_1 D_t t}{\lambda_{eq,1}\ r_1^2}\right)\right]\right\}^2 \cdot \\ & \sigma^2_{\rho_1} \qquad [B.52]\end{aligned}$$

Damping of fluctuations in e_-, ΔT_1, and T_1 sensed by the thermistor is evident from Equations B.50 and B.52. Noises in e_- and γ_b are not correlated making cross-products in Equation B.52 zero. Ignoring the damping effect, the steady-state current noise at the input of OA-3 from the sources

considered so far can be shown to be given by an equation of the form

$$\sigma_{i_1}^2 = a_1 + b_1 e_-^2 + c_1 e_-^4 + d_1 e_-^6 \qquad [B.53]$$

Equation B.53 is similar to the thermistor noise equation derived semiempirically by Bowers and Carr (127) and of identical form if σ_{e_-} is assumed to equal zero.

In fully expanded form, $\sigma_{i_1}^2$ is given by

$$\sigma_{i_1}^2 = \left\{\left(\frac{\beta_1\tau_1\gamma_{b,1}}{T_1^2\Delta R_1}\right)^2\sigma_{e_-}^2\right\} + \left\{2\left(\frac{\beta_1\tau_1}{T_1^2\Delta R_1}\right)^2\sigma_{\gamma_{b,1}}^2 + 2\left(\frac{\beta_1\tau_1\gamma_{b,1}}{\rho_1 T_1^2\Delta R_1}\right)^2\sigma_{\rho_1}^2 + \left[12\left(\frac{\beta_1\tau_1\gamma_{b,1}}{T_1^3\Delta R_1}\right) + \left(\frac{\beta_1\tau_1\gamma_{b,1}}{T_1^4\Delta R_1}\right)^2\right]\sigma_{T_1}^2\right\}e_-^2 +$$

$$\left\{0.513\left(\frac{\beta_1\tau_1}{r_1^3 c_t T_1^2 R_1\Delta R_1 J}\right)^2\sigma_{e_-}^2\right\}e_-^4 +$$

$$\left\{0.114\left(\frac{\beta_1\tau_1}{r_1^3 c_t\rho_1 T_1^2 R_1\Delta R_1 J}\right)^2\sigma_{\rho_1}^2 + \left[0.685\left(\frac{\beta_1\tau_1}{r_1^3 c_t T_1^3 R_1\Delta R_1 J}\right)^2 + 0.0571\left(\frac{\beta_1^2\tau_1}{r_1^3 c_t T_1^4 R_1\Delta R_1 J}\right)^2\right]\sigma_{T_1}^2\right\}e_-^6 \qquad [B.54]$$

The dependence of σ_{i_1} on σ_{e_-} and noises in the thermal boundary layer is neatly divided in Equation B.54 indicating that the coefficients a_1 and c_1 are constants and coefficients b_1 and d_1 are variables in Equation B.53.

Actual noise sources are completely random rather than approximating the power surge in a RC system seen when a switch to a battery is turned on.

The frequency dependence of noise must also be accounted for in revision of Equation B.54. A finite number of sampling points in noise analysis predicate the use of standard deviation rather than variance in Equation B.54. The root-mean-squared (rms) value of the noise wave is equal to the standard deviation of the noise wave. Motchenbacher and Fitchen (115) showed that for a RC or RL circuit, the noise voltage, e_n, at a particular frequency, f, is determined from the rms noise voltage, e_{rms}, by the relationship

$$e_n^2(f) = \left(\frac{1}{1 + \omega^2\tau^2}\right) e_{rms}^2 \qquad [B.55]$$

where ω is the angular frequency of the noise in radians/sec. Noise in e_- is affected by the thermistor body, thermal boundary layer and correlation between the thermistor thermal boundary layer and the bulk solution. Effects of random noises in the heat transfer coefficient, h_t, on S_{i_1} as given in S_{ρ_1} are considered to be controlled by the time constants of the thermal boundary layer and the thermistor body. Random fluctuations of the bulk solution temperature involve the preceding time constants and the time constant of mixing, τ_m.

Hence,

$$S^2_{e_-}(f) = \left(\frac{1}{1 + \omega^2\tau_o^2}\right)\left(\frac{1}{1 + \omega^2\tau_b^2}\right)\left(\frac{1}{1 + \tau_t^2/\tau_m^2}\right) e_{-,rms} \qquad [B.56]$$

$$S^2_{\rho_1}(f) = \left(\frac{1}{1 + \omega^2\tau_o^2}\right)\left(\frac{1}{1 + \omega^2\tau_b^2}\right) \rho^2_{1,rms} \qquad [B.57]$$

$$S^2_{\gamma_{b,1}}(f) = \left(\frac{1}{1 + \omega^2\tau^2}\right)\left(\frac{1}{1 + \omega^2\tau_b^2}\right)\left(\frac{1}{1 + \tau_t^2/\tau_m^2}\right) \cdot \gamma^2_{b,1,rms} \qquad [B.58]$$

$$S^2_{T_1}(f) = \left(\frac{1}{1 + \omega^2\tau_t^2}\right)\left(\frac{1}{1 + \omega^2\tau_m^2}\right) T^2_{1,rms} \qquad [B.59]$$

Substitution of Equations B.56 - B.59 into Equation B.54 followed by multiplication throughout by df and addition of the Johnson noise to the right side yields

$$i^2_{1,n}df = \left\{\left(\frac{\beta_1\tau_1\gamma_{b,1}}{T_1\Delta R_1}\right)^2\left(\frac{1}{1 + \omega^2\tau^2_{o,1}}\right)\left(\frac{1}{1 + \omega^2\tau^2_{b,1}}\right) \cdot \left(\frac{1}{1 + \tau_t^2/\tau_m^2}\right) e^2_{-,rms}\, df + \left(\frac{4k_BT_1}{R_1}\right) \cdot \left(\frac{1}{1 + \omega^2\tau_{o,1}}\right) df\right\} + \left\{2\left(\frac{\beta_1\tau_1}{T_1{}^2\Delta R_1}\right)^2 \cdot \left(\frac{1}{1 + \omega^2\tau^2_{o,1}}\right)\left(\frac{1}{1 + \omega^3\tau^2_{b,1}}\right)\left(\frac{1}{1 + \tau_1^2/\tau_m^2}\right) \cdot \gamma^2_{b,1,rms}\, df + 2\left(\frac{\beta_1\tau_1\gamma_{b,1}}{\rho_1T_1{}^2\Delta R_1}\right)^2\left(\frac{1}{1 + \omega^2\tau^2_{o,1}}\right) \cdot$$

$$\left(\frac{1}{1+\omega^2\tau_{b,1}}\right)\rho_{1,rms}^2\,df +$$

$$\left[12\left(\frac{\beta_1\tau_1\gamma_{b,1}}{T_1^3\Delta R_1}\right)^2+\left(\frac{\beta_1^2\tau_1\gamma_{b,1}}{T_1^4\Delta R_1}\right)^2\right]\cdot$$

$$\left(\frac{1}{1+\omega^2\tau_1^2}\right)\left(\frac{1}{1+\omega^2\tau_m^2}\right)T_{1,rms}^2\,df\}\,e_-^2 +$$

$$\{0.513\left(\frac{\beta_1\tau_1}{r_1^3c_tT_1^2R_1\Delta R_1J}\right)^2\left(\frac{1}{1+\omega^2\tau_{o,1}^2}\right)\cdot$$

$$\left(\frac{1}{1+\omega^2\tau_{b,1}^2}\right)\left(\frac{1}{1+\tau_1^2/\tau_m^2}\right)e_{-,rms}\,df\}\,e_-^4 +$$

$$\{0.114\left(\frac{\beta_1\tau_1}{r_1^3c_t\rho_1T_1^2R_1\Delta R_1J}\right)^2\left(\frac{1}{1+\omega^2\tau_{o,1}^2}\right)\cdot$$

$$\left(\frac{1}{1+\omega^2\tau_{b,1}^2}\right)\rho_{1,rms}^2 + \left[0.685\left(\frac{\beta_1\tau_1}{r_1^3c_tT_1^3R_1\Delta R_1J}\right)^2+\right.$$

$$\left.0.0571\left(\frac{\beta_1^2\tau_1}{r_1^3c_tT_1^4R_1\Delta R_1J}\right)^2\right]\left(\frac{1}{1+\omega^2\tau_1^2}\right)\cdot$$

$$\left(\frac{1}{1+\omega^2\tau_m^2}\right)T_{1,rms}^2\,df\}\,e_-^6 \qquad [B.60]$$

The parameter ω is equal to $2\pi f$. Integration of equations exemplified by Equations B.57 - B.59 is difficult for the usual range in f of zero to infinity. As discussed earlier, $\tau_b >> \tau_o$ and when the Reynolds number is greater than 2×10^4,

later work will show that $\tau_t >> \tau_m$. These relations then lead to the approximation

$$(1 + \omega^2\tau_o^2)(1 + \omega^2\tau_b^2) \simeq \omega^2\tau_b^2\left[\omega^2\tau_o^2 + \frac{(\tau_b^2 + \tau_o^2)}{\tau_b^2}\right]$$

which in turn can be shown to be in a form readily integrated using standard tables.

$$\int_{f_1}^{f_2} \frac{df}{(1 + \omega^2\tau_o^2)(1 + \omega^2\tau_b^2)} \simeq \frac{1}{16\pi 4\tau_b^2\tau_o^2} \int_{f_1}^{f_2} \frac{df}{f^2(f^2 + \frac{1}{4\pi^2\tau_o^2})} \qquad [B.61]$$

Equation B.61 when integrated reads as

$$16\pi^4\tau_b^2\tau_o^2 \int_{f_1}^{f_2} \frac{df}{f^2(f^2 + \frac{1}{4\pi^2\tau_o^2})} = \frac{1}{4\pi^2\tau_b^2}\left(\frac{1}{f_1} - \frac{1}{f_2}\right) + \frac{\tau_o}{2\pi\tau_b^2}\left[\arctan(2\pi\tau_o f_1) - \arctan(2\pi\tau_o f_2)\right] \qquad [B.62]$$

Making use of extrapolation beyond the range where the initial approximation $\omega^2\tau^2 >> 1$ is valid, that is, making $f_1 \to 0$, Equation B.62 reduces to

$$\frac{1}{16\pi^4\tau_b^2\tau_o^2} \int_{f_1}^{f_2} \frac{df}{f^2(f^2 + \frac{1}{4\pi^2\tau_o^2})} \simeq \left(\frac{1}{4\pi^2\tau_b^2}\right)\frac{1}{f_1} - \frac{\tau_o}{2\pi\tau_b^2} \arctan(2\pi\tau_o f_2) \qquad [B.63]$$

Equation B.63 then shows the usual 1/f dependence of noise for all electronic devices. Equation B.63 suggests that the use of a notch filter with $f_1 > 1$ Hz and $f_2 < 10$ Hz would greatly reduce noises due to thermal boundary layer fluctuations and bulk solution temperature fluctuations. The use of a simple single pole RC filter in the feedback path of OA-3 is seen to do little in reducing contributions of coefficients b_1 and d_1 of Equation B.53. Increase of the time constant, $R_f C_f$, for OA-3 will reduce the bandwidth, Δf, and consequentially the contributions of coefficients a_1 and c_1 of Equation B.53. The arc tan term of Equation B.63 for the usual f_2 of 0.5 to 20 Hz is only about 2% of the first term when $f_1 = 0.01$ Hz. The choice of $f_1 = 0.01$ Hz is obviously an arbitrary one, but is a standard used in operational amplifier noise specifications.

The preceding discussion of the random noise characteristics of Equation B.60 integrated with respect to frequency simplifies the expression of the total input noise, $I_{1,n}$ of OA-3 contributed by thermistor t_1.

$$I_{1,n}\Big|_{f_1}^{f_2} = \sqrt{\int_{f_1}^{f_2} i_{1,n}^2 \, df} =$$

$$\left[\left(\frac{\beta_1 \tau_1 \gamma_{b,1} e_{-,rms}}{T_1^2 \Delta R_1}\right)^2 \left(\frac{1}{1 + \tau_1^2/\tau_m^2}\right) \cdot \right.$$

$$\left. \left[\frac{1}{4\pi^2 \tau_{b,1}^2 f_1} - \frac{\tau_{o,1}}{2\pi \tau_{b,1}^2} \arctan(2\pi \tau_{o,1} f_2)\right] + \right.$$

$$[0.636(\frac{k_B T_1}{R_1})][\arctan(2\pi\tau_{o,1} f_2)]\} +$$

$$\{\left(\frac{\beta_1 \tau_1 \gamma_{b,1,rms}}{T_1^2 \Delta R_1}\right)^2 \left(\frac{1}{1 + \tau_1^2/\tau_m^2}\right)\left[\frac{1}{2\pi^2 \tau_{b,1} f_1} -$$

$$\frac{\tau_{o,1}}{\pi\tau_{b,1}^2} \arctan(2\pi\tau_{o,1} f_2)\right] +$$

$$\left(\frac{\beta_1 \tau_1 \gamma_{b,1} \rho_{1,rms}}{\rho_1 T_1^2 \Delta R_1}\right)^2 \left[\frac{1}{2\pi^2 \tau_{b,1}^2 f_1} - \frac{\tau_{o,1}}{\pi\tau_{b,1}^2} \cdot\right.$$

$$\left.\arctan(2\pi\tau_{o,1} f_2)\right] +$$

$$\left[12\left(\frac{\beta_1 \tau_1 \gamma_{b,1}}{T_1^3 \Delta R_1}\right)^2 + \left(\frac{\beta_1^2 \tau_1 \gamma_{b,1}}{T_1^4 \Delta R_1}\right)^2\right] \cdot \left[\frac{1}{4\pi^2 \tau_1^2 f_1} -\right.$$

$$\left.\frac{\tau_m}{2\pi\tau_1^2} \arctan(2\pi\tau_m f_2)\right] T_{1,rms}^2\} e_-^2 +$$

$$\{0.513\left(\frac{\beta_1 \pi_1 e_{-,rms}}{r_1^3 c_t T_1^2 R_1 \Delta R_1 J}\right)^2 \left(\frac{1}{1 + \tau_1^2/\tau_m^2}\right) \cdot$$

$$\left[\frac{1}{4\pi^2 \tau_{b,1}^2 f_1} - \frac{\tau_{o,1}}{2\pi\tau_{b,1}^2} \arctan(2\pi\tau_{o,1} f_2)\right]\} \cdot$$

$$e_-^4 +$$

$$\{0.0182\left(\frac{\beta_1 \tau_1 \rho_{1,rms}}{r_1^3 c_t \rho_1 T_1^3 R_1 \Delta R_1 J}\right)^2 \left[\frac{1}{2\pi^2 \tau_{b,1}^2 f_1} -\right.$$

$$\left.\frac{\tau_{o,1}}{\tau_{b,1}^2} \arctan(2\pi\tau_{o,1} f_2)\right] +$$

$$\left[0.109\left(\frac{\beta_1\tau_1}{r_1^3 c_t T_1^3 R_1 \Delta R_1 J}\right)^2 + 0.0909\left(\frac{\beta_1^2\tau_1}{r_1^3 c_t T_1^4 R_1 \Delta R_1 J}\right)^2\right] \cdot \left[\frac{1}{2\pi\tau_1^2 f_1} - \frac{\tau_m}{\tau_1^2} \text{ arc tan } (2\pi\tau_m f_2)\right] \cdot T_{1,rms}^2\} \; e_-^6\Big]^{1/2} \qquad [B.64]$$

The value of $e_{-,rms}$ in Equation B.64 must also be calculated separately from manufacturers data for the frequency range under consideration.

The total circuit noise is measured at the output of OA-3 and is given by Equation B.65 with C being the correlation coefficient between $I_{1,n}$ and $I_{2,n}$, noises of thermistors t_1 and t_2.

$$I_{o,n}^2 = I_{1,n}^2 + 2\ C\ I_{1,n}\ I_{2,n} + I_{2,n}^2 + I_{a,n}^2 \qquad [B.65]$$

The total noise contribution of OA-3 itself is given in the form of a noise corrent, $I_{a,n}^2$. The cross-product term, $2C\ I_{1,n}\ I_{2,n}$, is only nonzero for noises that are correlated, those of e_- and e_+. Hence, coefficients b_1 and d_1 are assumed to equal zero in calculation of $I_{1,n}$ as used in the cross-product term of Equation B.65. As noted earlier, noises in e_+ only are completely discriminated against when circuit gains

are equal for changes in R_1 and R_2. The value of the correlation coefficient, C, is -0.5 rather than -1 which would be true if noises in e_- also were discriminated against.

Calculation of a theoretical S/N ratio is now possible and comparisons with experimental results can be made for variations in circuit parameters and sampling time employed in noise measurements. Shot noise in the thermistors was not incorporated into the present model of thermistor noise since thermistors $\leq$ 10 K only were considered with currents $\leq$ 100 μA flowing in them. Noise contributions from the zener reference diode can be straight-forwardly added to the present model since the zener mechanism exhibits primarily shot noise (115).

2. Temperature response of the stirred fluid in a cylindrical calorimeter during electrical heating

Traditionally, calorimeters have been divided into adiabatic and isothermal (isoperibol) types with the distinction being related to the manner of temperature control of the environment of the calorimeter. The preferred method for maintaining a uniform temperature environment around the calorimeter involves the so-called submarine technique in which the calorimeter cell is submerged in a tank containing a thermostated liquid with mechanical stirring. A second method used only for isothermal calorimetry employs a thick insulating jacket, usually of a plastic foam, around the cell. White (128), in his classic text on calorimetry, treated in

detail many other aspects of solution calorimetry. A recent review of Churney et al. (129) further defined the requirements of solution calorimetry. In these references, transient behavior and the dynamics of the change in bulk solution temperature during and immediately after the main period of heating are ignored. Ignorance of the response dynamics can lead to erroneous application of solution calorimetry especially in the study of reaction kinetics. A calorimeter is described below which is sufficiently compact for use in a fume hood, is operable with readily available temperature controllers, and is sufficiently stable to permit 2 - 6 part-per-thousand precision for measurement of total energy change in the range of 5 - 15 cal. A theoretical examination of the dynamic response of the solution bulk temperature to electrical heating is given using linear methods to obtain a useful mathematical solution.

Solution calorimetry is a diversified area of research and standardization of equipment design has not yet been attained (130). This results, no doubt, from differing requirements and opinions of the workers involved. Sunner and Wadsö (131) discussed the general requirements of isoperibol calorimeters. Christensen et al. (132) elaborated on these requirements and a commercial unit was constructed according to their design (133). Both groups of workers decided early that a submarine isoperibol calorimeter is best

suited for solution calorimetry of short duration (< 1 hr). Sunner and Wadsö came to the correct conclusion that the design of the calorimeter lid has a great affect on the dynamic calorimetric behavior. Christensen et al. (134) apparently also experienced difficulty in obtaining a uniform temperature field above the solution as witnessed by the lid modification proposed. Two factors are of special importance in lid design: the means for attaining a uniform temperature field across the lid and the method by which mounting probes can be suspended into the calorimeter vessel so that heat conduction along the probes is minimized. If materials with low thermal conductivity are used for the entire calorimeter lid, large radial temperature gradients can develop even when the lid is submerged with the cell in a constant temperature bath. The quantity of heat flowing into or out of the solution in the cell via the probes depends on the type of material in contact with the solution and the total submerged area. The volume of the submerged portions of the probes will also affect the dynamic response of the solution temperature because of interference with convective heat transport in the solution. A very low heat-loss modulus was reported by Christensen et al. (132) which undoubtedly resulted from their use of Teflon tubing around probes into the solution and their efforts to miniaturize the probes.

Two requirements are suggested for the design of solution calorimeters in addition to the five given by Sunner and

Wadsö in Reference 131. 1) Mixing of the solution in the calorimeter should be uniformly turbulent throughout the bulk. 2) Bulk solution evaporation and uptake of gases from the vapor space above the solution should be minimized.

Popular stirring devices are propellers, magnetic stirring bars, and vibrating rods. Problems common to the first two types are vortex formation and spraying of the solution onto the calorimeter walls and lid at high stirring speeds. Highly volatile or toxic materials must be handled in a completely closed system for which magnetic stirring is the only option. Stirring by a smooth rotating disk has not been discussed although it was apparently used by Johansson (135). Experience shows that a rotating disc provides rapid solution stirring, and a uniform flow pattern around a thermistor placed just below the plane of the disc. Positioning the disc at a depth of 3/4 l_b provides adequate stirring with no vortex formation, minimal gas uptake, and no spraying. It is a common misconception that a great amount of visible surface disruption is indicative of rapid solution mixing. The movement of a large volume of fluid is not equivalent, however, to efficient mixing. Needed is uniform turbulent flow such that eddies are small and, hence, thermal and mass diffusion can be effective for eliminating spatial discontinuities in temperature and concentration. As expected, a compromise must be reached between efficient stirring and the maximum heat of stirring which can be tolerated.

Concurrent with mixing is the interaction of the bulk solution in the calorimeter cell with the vapor space above the solution. White (128) stressed that the calorimeter lid should be slightly warmer than the solution in the calorimeter cell to eliminate condensation of solvent vapors. Minimization of the volume of vapor space is also important especially for highly volatile solvents. The elimination of CO_2 absorption by the solution has long been recognized as a difficult problem. Frequently, excess base is added to decrease the effect when pH change is not critical. Electroanalytical studies with a rotating disc electrode showed that exclusion of O_2 is more difficult in cylindrical cells with flat bottoms rather than spherical cells (136). This can be understood from a study of the fluid-flow patterns in the two cell shapes and the consequential degree of disruption of the solution surface. Cells used in this work had round bottoms.

Theoretical consideration proceeds form the work of Polaczek and Lisicki (137). Their key simplifying assumption was the combining of heat capacity and heat transfer characteristics of the probes with those of the cell wall. In practice, the surface area of the probes in contact with the bulk solution may nearly equal the area of the cell wall but the heat capacity of the probes cannot be determined independent of the cell wall in the single apparatus. In this work, the separate heat transfer coefficients of the probes

and wall are used with the combined heat capacity to calculate the cell wall time constant. A second new consideration here is that the time constant of mixing, τ_m, is the value determined according to Brodkey (138) at r, the distance from the cell's vertical axis to the electrical heater. The bulk solution temperature, T_b, is usually considered to be uniform throughout the solution except in the boundary layer of the electrical heater. The boundary layer temperature, T_{bl}, is equal to T_b before heating but is greater than T_b during heating. The third new consideration is a correction for spatial inhomogeneity of T_b within the calorimeter cell. This yields the 'excess' temperature in the region of the temperature sensor.

The time response of the bulk solution temperature can be derived from the heat flux balances given by Equation B.66

$$h_h A_h (T_h - T_{bl}) = C_w \frac{dT_w}{dt} + C_b \frac{dT_b}{dt} + C_b \frac{d(T_{bl} - T_b)}{dt} \qquad [B.66]$$

where

h_h = heat transfer coefficient of cylindrically shaped electrical heater (cal/cm^2-sec-deg C)

A_h = surface area of electrical heater (cm^2)

T_h = temperature of electrical heater (deg K)

T_{bl} = temperature of bulk solution at the interface of the bulk solution and electrical heater boundary layer (deg K)

C_w = heat capacity of calorimeter wall (cal/deg C)

T_w = temperature of calorimeter wall (deg K)

C_b = heat capacity of bulk solution (cal/deg C)

The combined heat capacities of the cell wall and stems is C_w and

$$C_w \frac{dT_w}{dt} = h_w A_w (T_b - T_w) \qquad [B.67]$$

where

h_w = heat transfer coefficient of calorimeter wall (cal/cm^2-sec-deg C)

A_w = surface area of calorimeter wall in contact with bulk solution (cm^2)

A wall time constant is defined as

$$\tau_w = \frac{C_w}{h_w A_w} \text{ with } Z_1 = \frac{1}{\tau_w} \qquad [B.68]$$

Consideration of heat flux at the heater yields

$$\frac{dQ_h}{dt} = P_h = h_h A_h (T_h - T_{b1}) + C_h \frac{dT_h}{dt} \qquad [B.69]$$

where

Q_h = heat supplied electrically to the calorimeter (cal)

P_h = electrical energy supplied for heating per unit time (cal/sec)

C_h = heat capacity of electrical heater (cal/deg C)

A heater time constant is defined as

$$\tau_h = \frac{C_h}{h_h A_h} \text{ with } Z_2 = \frac{1}{\tau_h} \qquad [B.70]$$

The temperature difference $T_{bl} - T_b$ is expressed in terms of the time constant for mixing

$$T_{bl} - T_b = \tau_m \frac{dT_b}{dt} = \tau_m \gamma_b \qquad [B.71]$$

with $Z_3 = \frac{1}{\tau_m}$

The solution of Equation B.66 for T_b and dT_b/dt can be obtained several ways. The method chosen here is the use of the Laplacian operator technique which involves three steps:

1. Transformation according to specific rules of the original integrodifferential equations.
2. Solution of the algebraic equations for the desired variable, and
3. Inverse transformation of the desired unknown variable back into the domain of the original equations.

Combinations of the Laplacian transforms of Equations B.66, B.67, and B.69 yields Equation B.72

$$\left[\frac{h_h A_h}{C_h s + h_h A_h}\right] [sQ_h(s) - Q_h(o)] + \left[\frac{h_h A_h C_h}{C_h s + h_h A_h}\right] T_h(o)$$

$$+ h_h A_h \left[\frac{h_h A_h}{C_h s + h_h A_h} - 1\right] T_{bl}(s) = C_b[sT_b(s) - T_b(o)]$$

$$+ \left[\frac{C_w h_w A_w s}{C_w s + h_w A_w}\right] T_b(s) + C_w \left[\frac{C_w s}{C_w s + h_w A_w} - 1\right] T_w(o)$$

$$+ C_b \tau_m [s^2 T_b(s) - sT_b(o) - T_b'(o)] \qquad [B.72]$$

An initial approximation is made that the $T_{b1}(s)$ term is negligible.

Solving Equation B.72 for $T_b(s)$ yields Equation B.73.

$$T_b(s) = \frac{Z_2Z_3}{C_b}\left[\frac{(s + Z_1)}{s(s + Z_2)(s^2 + (Z_1 + Z_3)s + Z_1Z_3(1 + C_w/C_b))}\right] \cdot$$

$$[sQ_h(s) - Q_h(o)] + \left[\frac{(s^2 + (Z_1 + Z_3)s + Z_1Z_3}{s(s^2 + (Z_1 + Z_3)s + Z_1Z_3(1 + C_w/C_b))}\right] T_b(o)$$

$$+ \frac{C_wZ_1Z_3}{C_b}\left[\frac{1}{s(s^2 + (Z_1 + Z_3)s + Z_1Z_3(1 + C_w/C_b))}\right] T_w(o)$$

$$+ \left[\frac{(s + Z_1)}{s(s^2 + (Z_1 + Z_3)s + Z_1Z_3(1 + C_w/C_b))}\right] T_b'(o)$$

$$+ \frac{C_hZ_2Z_3}{C_b}\left[\frac{(Z_1 + s)}{s(Z_2 + s)(s^2 + (Z_1 + Z_3)s + Z_1Z_3(1 + C_w/C_b))}\right] T_h(o) \qquad [B.73]$$

The total generated heat is

$$Q_h = P_ht \qquad [B.74]$$

and the Laplacian transform of Q_h is

$$Q_h(s) = P_h/s^2 \qquad [B.75]$$

The solution for T_b *versus* time can now be given. The solution of dT_b/dt *versus* time is given in Appendix C.

3. An approximate solution to the calorimeter equations

a. Main period The initial conditions for the main period of heating are

$$t = 0: \quad Q_h = 0$$
$$T_h = T_b = T_{b1} = 0$$
$$dT_b/dt = 0$$
$$T_w > T_b$$
$$0 < t < t_{co}: \quad Q_h = P_h t$$
$$T_h > T_{b1} > T_b$$
$$T_w \neq T_b$$

At t = o, the values of T_b for the two solutions in the differential calorimetric system are equal. For all values t > o, the equality of T_b values no longer exists. The heat of stirring, γ_{str}, and electrical heating of the solution by the thermistor, γ_{th}, are compensated for by use of a differential system. The remaining heat source is γ_{bkg} which results because $T_w > T_b$. Differences in heat exchange by the calorimeter's cells with the environment are compensated by use of trickle heaters initially adjusted when t < o.

From the initial conditions, Equation B.73 is written

$$T_b(s) = \frac{Z_2 Z_3}{C_b}\left[\frac{(s + Z_1)}{s^2\{(s + Z_2)(s^2 + (Z_1 + Z_3)s + Z_1 Z_3(1 + C_w/C_b))\}}\right] P_h$$
$$+ \frac{Z_1 Z_3 C_w}{C_b}\left[\frac{1}{s\{s^2 + (Z_1 + Z_3)s + Z_1 Z_3(1 + C_w/C_b)\}}\right] T_w(o) \qquad [B.76]$$

The denominators of the coefficients of P_h and $T_w(o)$ are characteristic of a second-order differential equation $\{s^2 + (Z_1 + Z_3)s + Z_1Z_3(1 + C_w/C_b)\}$ typically encountered for RLC circuits. The roots of the equation are

$$s = -\left(\frac{Z_1 + Z_3}{2}\right) \pm \left[\left(\frac{Z_1 + Z_3}{2}\right)^2 - Z_1Z_3(1 + C_w/C_b)\right]^{1/2} \qquad [B.77]$$

Depending on the values of Z_1, Z_3, and C_w/C_b, the roots may be real or complex. Three cases result with three corresponding expressions for Equation B.77.

Case I: The condition of underdamping exists when

$$\left(\frac{Z_1 + Z_3}{2}\right)^2 < Z_1Z_3(1 + C_w/C_b) \qquad [B.78]$$

The coefficient of P_h can be factored as

$$\frac{K_1}{s} + \frac{K_2}{(s + Z_2)} + \frac{K_3}{(s + \alpha + \beta j)} + \frac{K_4}{(s + \alpha - \beta j)} \qquad [B.79]$$

where $j = \sqrt{-1}$

$$\alpha = \frac{Z_1 + Z_3}{2}$$

$$\beta = \left[Z_1Z_3(1 + C_w/C_b) - \left(\frac{Z_1 + Z_3}{2}\right)^2\right]^{1/2}$$

The parameter, α, is the damping coefficient, whose inverse is the calorimeter system's time constant

$$\tau_{sys} = \frac{1}{\alpha} \qquad [B.80]$$

which can be recognized as the harmonic mean of the time constant of mixing and calorimeter wall time constant

$$\tau_{sys} = \left(\frac{\frac{1}{\tau_w} + \frac{1}{\tau_m}}{2}\right)^{-1} \qquad [B.81]$$

β is the damped natural frequency of the calorimeter system. Derivation of equation constants K_1-K_5 is shown in detail below. However, derivations of subsequent constants will not be shown due to their length and repetitious nature. Solving for K_1, let $s \to o$ after multiplying Equation B.79 by s throughout. Hence,

$$K_1 = \frac{1}{C_b + C_w} \qquad [B.82]$$

Equation B.79 is multiplied throughout by $(s + Z_2)$ letting $s \to -Z_2$. Hence,

$$K_2 = \frac{Z_3(Z_1 - Z_2)}{C_b Z_2[Z_2^2 - Z_2(Z_1 + Z_3)] + Z_1 Z_3(C_b + C_w)} \qquad [B.83]$$

solving for K_3 with $s \to -\alpha-\beta j$

$$K_3 = \frac{Z_2 Z_3}{C_b} \frac{(s + Z_1)}{s^2(s + Z_2)(s + \alpha-\beta j)} \Bigg|_{s \to -\alpha-\beta_j}$$

$$= \frac{Z_2 Z_3(Z_1 - \alpha-\beta j)}{C_b(-\alpha-\beta j)^2(Z_2-\alpha-\beta j)(-2\beta j)} \qquad [B.84]$$

multiplying numerator and denominator by $\alpha-\beta j$, knowing that

$$(\alpha + \beta j)(\alpha - \beta j) = \alpha^2 - \beta^2 j^2$$

$$= Z_1 Z_3 (1 + C_w/C_b)$$

$$K_3 = \frac{Z_2 C_b}{Z_1(C_b + C_w)} \frac{(Z_1 - \alpha - \beta j)(\alpha - \beta j)}{(Z_2 - \alpha - \beta j)(-2\beta j)(\alpha + \beta j)} \qquad [B.85]$$

Now the numerator and denominator of Equation B.85 is multiplied by $(Z_2 - \alpha + \beta j)(\alpha - \beta j)j$ knowing that

$$(Z_2 - \alpha - \beta j)(Z_2 - \alpha + \beta j) = Z_2^2 - 2Z_2\alpha + Z_1 Z_3 (1 + C_w/C_b)$$

and

$$(Z_1 - \alpha - \beta j)(Z_2 - \alpha + \beta j) = Z_1 Z_2 - (Z_1 + Z_2)\alpha + Z_1 Z_3 (1 + C_w/C_b) + (Z_1 - Z_2)\beta j$$

Thus,

$$K_3 = \frac{Z_2(Z_1 Z_2 - (Z_1 + Z_2)\alpha + Z_1 Z_3 (1 + C_w/C_b) + (Z_1 - Z_2)\beta j)(\alpha j + \beta)(\alpha - \beta j)}{2Z_1 Z_3 (C_b + C_w)^2 (Z_2^2 - Z_2(Z_1 + Z_3) + Z_1 Z_3 (1 + C_w/C_b))\beta} \qquad [B.86]$$

Equation B.86 is greatly simplified by setting

$$\phi = Z_1 Z_2 - (Z_1 + Z_2)\alpha + Z_1 Z_3 (1 + C_w/C_b)$$

$$\psi = 2Z_1 [Z_2^2 - Z_2(Z_1 + Z_2) + Z_1 Z_3 (1 + C_w/C_b)]\beta$$

Expanding the resulting equation in the numerator and regrouping yields

$$K_3 = \frac{Z_2 C_b}{Z_1 Z_3 \psi (C_b + C_w)^2} \{\beta[2\alpha\phi + (\beta^2 - \alpha^2)(Z_1 - Z_2)] + [\alpha^2\phi + 2\alpha\beta^2(Z_1 - Z_2) - \beta^2\phi]j\} \quad [B.87]$$

which is of the form

$$K_3 = a + bj$$

where

$$a_1 = \frac{Z_2 C_b \beta[2\alpha\phi + (\beta^2 - \alpha^2)(Z_1 - Z_2)]}{Z_1 Z_3 \psi (C_b + C_w)^2} \quad [B.88]$$

$$b_1 = \frac{Z_2 C_b [\alpha^2 \phi + 2\alpha \beta^2 (Z_1 - Z_2) - \beta^2 \phi]}{Z_1 Z_3 \psi (C_b + C_w)^2} \quad [B.89]$$

The form a+bj through the use of the Euler relationship

$$e^{\pm j\theta} = \cos \theta \pm j \sin \theta$$

can be used to reduce K_4 to the final working form needed.

Since,

$$a + bj = r(\cos \theta + j \sin \theta)$$

where

$$r_1 = [(a_1)^2 + (b_1)^2]^{1/2} \quad [B.90]$$

and $$\sin \theta_1 = b_1/r_1$$

hence $$\theta_1 = \text{arc sin } \{b_1/r_1\}$$

which leads to the expression

$$K_3 = r_1 \exp\{j\theta_1\} \qquad [B.91]$$

Complex roots always occur in conjugate pairs, hence,

$$K_4 = r_1 \exp\{-j\theta_1\} \qquad [B.92]$$

The coefficient of the $T_w(o)$ term in Equation B.76 is factored as

$$\frac{K_5}{s} + \frac{K_6}{s + \alpha + \beta j} + \frac{K_7}{s + \alpha - \beta j} \qquad [B.93]$$

It can be shown that

$$K_5 = \frac{C_w}{C_b + C_w} \qquad [B.94]$$

$$K_6 = r_2 \exp\{j\theta_2\} \qquad [B.95]$$

$$K_7 = r_2 \exp\{-j\theta_2\} \qquad [B.96]$$

where $r_2 = [(a_2)^2 + (b_2)^2]^{1/2}$

$$a_2 = \frac{-C_w}{2(C_b + C_w)}$$

$$b_2 = \frac{-\alpha C_w}{2\beta(C_b + C_w)}$$

$$\theta_2 = \text{arc sin } (b_2/r_2)$$

Finally, Equation B.76 for $T_b(s)$ becomes

$$T_b(s) = \left[\frac{1}{s^2}\left(\frac{1}{C_b+C_w}\right)\right.$$

$$+ \left(\frac{1}{s+Z_2}\right)\left(\frac{Z_3(Z_1-Z_2)}{Z_2[C_b(Z_2^2-(Z_1+Z_3)Z_2+Z_1Z_3(1+C_w/C_b))]}\right.$$

$$\left.\left. + \frac{r_1\exp\{j\theta_2\}}{(s+\alpha+\beta j)} + \frac{r_1\exp\{-j\theta_2\}}{(s+\alpha-\beta j)}\right] P_h\right.$$

$$\left. + \left[\frac{r_2\exp\{j\theta_2\}}{(s+\alpha+\beta j)} + \frac{r_2\exp\{-j\theta_2\}}{(s+\alpha-\beta j)}\right] T_w(o)\right. \qquad [B.97]$$

The inverse transform of Equation B.97 is

$$T_b(t) = \frac{P_h t}{(C_b + C_w)} + \frac{P_h Z_3(Z_1 - Z_2)\exp\{-Z_2 t\}}{Z_2[(Z_2^2 - Z_2(Z_1 + Z_3))C_b + Z_1Z_3(C_b + C_w)]}$$

$$+ P_h r_1[\exp\{j\theta_1\}\exp\{-(\alpha + \beta j)t\} + \exp\{-j\theta_1\}\exp\{-(\alpha-\beta j)t\}]$$

$$+ \left[T_b(o) + \tau_w\left(\frac{dT_b}{dt}\right)_{t=o}\right]\left[r_2(\exp\{j\theta_2\}\exp\{-(\alpha + \beta j)t\}\right.$$

$$\left. + \exp\{-j\theta_2\}\exp\{-(\alpha + \beta j)t\})\right] \qquad [B.98]$$

The value dT_b/dt at t=o in Equation B.98 is the background heating rate, γ_{bkg}.

Evaluating the exponential terms in j,

$$T_b(t) = P_h\left[\frac{t}{(C_b + C_w)} + \frac{Z_3(Z_1 - Z_2)\exp\{-Z_2 t\}}{Z_2[(Z_2^2 - Z_2(Z_1 + Z_3))C_b + Z_1 Z_3(C_b + C_w)]}\right.$$

$$\left. + 2\, r_1 \exp\{-\alpha\, t\}\cos\{\beta t - \theta_1\}\right]$$

$$+ \frac{2\gamma_{bkg}\, r_2 \exp\{-\alpha\, t\}\cos\{\beta t - \theta_2\}}{Z_1} \qquad [B.99]$$

Case II: The condition for critical damping is

$$\left(\frac{Z_1 + Z_3}{2}\right)^2 = Z_1 Z_3(1 + C_w/C_b) \qquad [B.100]$$

and a single root for s in the second-order differential equation is obtained. Equation B.76 can be written

$$T_b(s) = \frac{Z_2 Z_3}{C_b}\left[\frac{(s + Z_1)}{s^2(s + Z_2)(s + \alpha)^2}\right]P_h$$

$$+ \frac{Z_1 Z_3 C_w}{C_b}\left[\frac{1}{s(s + \alpha)^2}\right]T_w(o) \qquad [B.101]$$

The coefficient of P_h in Equation B.76 is factored as

$$\frac{K_8}{s^2} + \frac{K_9}{s + Z_2} + \frac{K_{10}}{(s + \alpha)^2} + \frac{K_{11}}{(s + \alpha)} \qquad [B.102]$$

where $K_8 = \dfrac{Z_1 Z_3}{C_b \alpha^2}$ [B.103]

$$K_9 = \frac{Z_3(Z_2 - Z_1)}{C_b Z_2(\alpha - Z_2)^2} \qquad [B.104]$$

$$K_{10} = \frac{Z_2 Z_3(Z_1 - \alpha)}{C_b \alpha^2(Z_2 - \alpha)} \qquad [B.105]$$

$$K_{11} = \frac{Z_2 Z_3}{C_b}\left[\frac{\alpha^2(Z_2 - \alpha) - (Z_1 - \alpha)(3\alpha^2 - 2\alpha Z_2)}{\alpha^4(Z_2 - \alpha)^2}\right] \qquad [B.106]$$

The coefficient of $T_w(o)$ in Equation B.76 is factored as

$$\frac{K_{12}}{s} + \frac{K_{13}}{(s + \alpha)^2} + \frac{K_{14}}{(s + \alpha)} \qquad [B.107]$$

where $K_{12} = \frac{Z_1 Z_3 C_w}{C_b \alpha^2}$ [B.108]

$$K_{13} = \frac{-Z_1 Z_3 C_w}{C_b \alpha} \qquad [B.109]$$

$$K_{14} = \frac{-Z_1 Z_3 C_w}{C_b \alpha^2} \qquad [B.110]$$

The inverse transform of Equation B.76 for the critically damped system is

$$T_b(t) = \frac{P_h}{C_b}\left[\frac{Z_1 Z_3 t}{\alpha^2} + \frac{Z_3(Z_2 - Z_1)\exp\{-Z_2 t\}}{Z_2(\alpha - Z_2)^2} + \frac{Z_2 Z_3(Z_1 - \alpha)\, t \exp\{-\alpha t\}}{\alpha^2(Z_2 - \alpha)}\right]$$

$$+ \frac{\gamma_{bkg}}{C_b}\left[\frac{Z_3 C_w}{\alpha^2} - \frac{Z_3 C_w t \exp\{-\alpha t\}}{\alpha}\right.$$

$$\left. - \frac{Z_3 C_w \exp\{-\alpha t\}}{\alpha^2}\right] \qquad [B.111]$$

Case III: The case of an overdamped systems occurs when

$$\left(\frac{Z_1 + Z_3}{2}\right)^2 > Z_1 Z_3 (1 + C_w/C_b) \qquad [B.112]$$

The coefficient of P_h is factored as

$$\frac{K_{15}}{s^2} + \frac{K_{16}}{(s + Z_2)} + \frac{K_{17}}{(s + \alpha + \sigma)} + \frac{K_{18}}{(s + \alpha - \sigma)} \qquad [B.113]$$

The constants are evaluated

$$K_{15} = \frac{Z_1 Z_3}{C_b(\alpha + \sigma)(\alpha - \sigma)} \qquad [B.114]$$

$$K_{16} = \frac{Z_3(Z_1 - Z_2)}{C_b Z_2(\alpha + \sigma - Z_2)(\alpha - \sigma - Z_2)} \qquad [B.115]$$

$$K_{17} = \frac{-Z_2 Z_3(Z_1 - \alpha - \sigma)}{2C_b\sigma(\alpha + \sigma)^2(Z_2 - \alpha - \sigma)} \qquad [B.116]$$

$$K_{18} = \frac{Z_2 Z_3(Z_1 - \alpha + \sigma)}{2C_b\sigma(\sigma - \alpha)^2(Z_2 - \alpha + \sigma)} \qquad [B.117]$$

where $\sigma = \left[\left(\frac{Z_1 + Z_3}{2}\right)^2 - Z_1 Z_3 (1 + C_w/C_b)\right]^{1/2}$

The coefficient of the $T_w(o)$ term is factored

$$\frac{K_{19}}{s} + \frac{K_{20}}{(s + \alpha + \sigma)} + \frac{K_{21}}{(s + \alpha - \sigma)} \qquad [B.118]$$

where $K_{19} = \frac{Z_1 Z_3 C_w}{C_b(\alpha + \sigma)(\alpha - \sigma)}$ [B.119]

$$K_{20} = \frac{Z_1 Z_3 C_w}{2C_b\sigma(\alpha - \sigma)} \qquad [B.120]$$

$$K_{21} = \frac{Z_1 Z_3 C_w}{2C_b\sigma(\sigma - \alpha)} \qquad [B.121]$$

The inverse transform of Equation B.76 is

$$T_b(t) = \frac{P_h}{C_b}\left[\frac{Z_1 Z_3 t}{(\alpha + \sigma)(\alpha - \sigma)} + \frac{Z_3(Z_1 - Z_2)\exp\{-Z_2 t\}}{Z_2(\alpha + \sigma - Z_2)(\alpha - \sigma - Z_2)}\right.$$

$$- \frac{Z_2 Z_3(Z_1 - \alpha - \sigma)\exp\{-(\alpha + \sigma)t\}}{2\sigma(\alpha + \sigma)^2(Z_2 - \alpha - \sigma)}$$

$$\left. + \frac{Z_2 Z_3(Z_1 - \alpha + \sigma)\exp\{-(\alpha - \sigma)t\}}{2\sigma(\sigma - \alpha)^2(Z_2 - \alpha + \sigma)}\right]$$

$$+ \frac{\gamma_{bkg}}{C_b}\left[\frac{Z_3 C_w}{(\alpha + \sigma)(\alpha - \sigma)} + \frac{Z_3 C_w \exp\{-(\alpha + \sigma)t\}}{2\sigma(\alpha - \sigma)}\right.$$

$$\left. + \frac{Z_3 C_w \exp\{-(\alpha - \sigma)t\}}{2\sigma(\sigma - \alpha)}\right] \qquad [B.122]$$

b. Anterior period The anterior period begins at the time in the main period for power cut off, $t = t_{co}$. Time at cut off is designated $t = o$ for mathematical consideration of the anterior period. The general equation applies with the

recognition that $dQ_h/dt = 0$ when $t > o$

$$T_b(s) = \left[\frac{(s^2 + (Z_1 + Z_3)s + Z_1Z_3)}{s(s^2 + (Z_1 + Z_3)s + Z_1Z_3(1 + C_w/C_b))}\right]T_b(o)$$

$$+ \frac{C_wZ_1Z_3}{C_b}\left[\frac{1}{s(s^2 + (Z_1 + Z_3)s + Z_1Z_3(1 + C_w/C_b))}\right]T_w(o)$$

$$+ \left[\frac{(s + Z_1)}{s(s^2 + (Z_1 + Z_3)s + Z_1Z_3(1 + C_w/C_b))}\right]T_b'(o) + \frac{C_hZ_1Z_3}{C_b} \cdot$$

$$\left[\frac{(Z_1 + s)}{s(Z_2 + s)(s^2 + (Z_1 + Z_3)s + Z_1Z_3(1 + C_w/C_b))}\right]T_b(o) \qquad [B.123]$$

The denominator of each term contains the second-order differential equation considered above as a function of the system damping.

Case I: When the system is in an underdamped condition the coefficient of $T_h(o)$ can be written as

$$\frac{L_1}{s} + \frac{L_2}{s + Z_2} + \frac{L_3}{s + \alpha + \beta j} + \frac{L_4}{s + \alpha - \beta j} \qquad [B.124]$$

where $L_1 = \dfrac{C_h}{C_b + C_w}$ [B.125]

$$L_2 = \frac{C_hZ_3(Z_2 - Z_1)}{C_b(Z_2^2 - Z_2(Z_1 + Z_3) + Z_1Z_3(1 + C_w/C_b))} \qquad [B.126]$$

$$L_3 = \frac{-C_hr_1 \exp\{j\theta_1\}}{C_b + C_w} \qquad [B.127]$$

$$L_4 = \frac{-C_h r_1 \exp\{-j\theta_1\}}{C_b + C_w} \qquad [B.128]$$

and α, β, r_1, and θ_1 were defined previously.

The coefficient of the $T_b(o)$ term can be written as

$$\frac{L_5}{s} + \frac{L_6}{s + \alpha + \beta j} + \frac{L_7}{s + \alpha - \beta j} \qquad [B.129]$$

It can be shown that

$$L_5 = \frac{C_b}{C_b + C_w} \qquad [B.130]$$

$$L_6 = r_3 \exp\{j\theta_3\} \qquad [B.131]$$

$$L_7 = r_3 \exp\{-j\theta_3\} \qquad [B.132]$$

$$r_3 = [(a_3)^2 + (b_3)^2]^{1/2} \qquad [B.133]$$

where $a_3 = \dfrac{-C_b[Z_1 Z_3 - \alpha^2 - \beta^2]}{2Z_1 Z_3 (C_b + C_w)}$

$$b_3 = \frac{-C_b[2\alpha\beta^2 + \alpha^3 - \alpha\beta^2 - (\alpha^2 + \beta^2)(Z_1 + Z_3) + \alpha Z_1 Z_3]}{2Z_1 Z_3 \beta (C_b + C_w)}$$

$$\theta_3 = \text{arc sin}\{b_3/r_3\}$$

The coefficient of the $T_w(o)$ term can be written as

$$\frac{L_8}{s} + \frac{L_9}{s + \alpha + \beta j} + \frac{L_{10}}{s + \alpha - \beta j} \qquad [B.134]$$

It can be shown that

$$L_8 = \frac{C_w}{C_b + C_w} \qquad [B.135]$$

$$L_9 = r_4 \exp\{j\theta_4\} \qquad [B.136]$$

$$L_{10} = r_4 \exp\{-j\theta_4\} \qquad [B.137]$$

where $r_4 = [(a_4)^2 + (b_4)^2]^{1/2}$

$$a_4 = \frac{-C_w}{2(C_b + C_w)}$$

$$b_4 = \frac{-\alpha\, C_w}{2(C_b + C_w)\beta}$$

$$\theta_4 = \text{arc sin}\{b_4/r_4\}$$

The coefficient of the $T_b'(o)$ term can be written as

$$\frac{L_{11}}{s} + \frac{L_{12}}{s + \alpha + \beta j} + \frac{L_{13}}{s + \alpha - \beta j} \qquad [B.138]$$

It can be shown that

$$L_{11} = \frac{C_b}{Z_3(C_b + C_w)} \qquad [B.139]$$

$$L_{12} = -r_5 \exp\{j\theta_5\} \qquad [B.140]$$

$$L_{13} = -r_5 \exp\{-j\theta_5\} \qquad [B.141]$$

where $r_5 = [(a_5)^2 + (b_5)^2]^{1/2}$

$$a_5 = \frac{C_b}{2Z_3(C_b + C_w)}$$

$$b_5 = \frac{C_b(\alpha Z_1 - \alpha^2 - \beta^2)}{2Z_1 Z_3 \beta (C_b + C_w)}$$

$$\theta_5 = \text{arc sin}\{b_5/r_5\}$$

Equation B.123 now becomes

$$T_b(s) = \left[\left(\frac{C_b}{C_b + C_w}\right)\left(\frac{1}{s}\right) + \frac{r_3 \exp\{j\theta_3\}}{(s + \alpha + \beta j)} + \frac{r_3 \exp\{-j\theta_3\}}{(s + \alpha - \beta j)}\right] T_b(o)$$

$$+ \left[\left(\frac{C_w}{C_b + C_w}\right)\left(\frac{1}{s}\right) + \frac{r_4 \exp\{j\theta_4\}}{(s + \alpha + \beta j)} + \frac{r_4 \exp\{-j\theta_4\}}{(s + \alpha - \beta j)}\right] T_w(o)$$

$$+ \left[\left(\frac{C_b}{Z_3(C_b + C_w)}\right)\left(\frac{1}{s}\right) - \frac{r_5 \exp\{j\theta_5\}}{(s + \alpha + \beta j)} - \frac{r_5 \exp\{-j\theta_5\}}{(s + \alpha - \beta j)}\right] T_b'(o)$$

$$+ \left[\left(\frac{C_h}{C_b + C_w}\right)\left(\frac{1}{s}\right)\right.$$

$$\left. - \frac{C_h Z_3(Z_1 - Z_2)}{C_b(Z_2^2 - Z_2(Z_1 + Z_3) + Z_1 Z_3(1 + C_w/C_b))(s + Z_2)}\right.$$

$$\left. - \frac{C_h r_2 \exp\{j\theta_2\}}{(C_b + C_w)(s + \alpha + \beta j)} - \frac{C_h r_2 \exp\{-j\theta_2\}}{(C_b + C_w)(s + \alpha - \beta j)}\right] T_h(o)$$

[B.142]

The initial conditions for the anterior period correspond to the conditions at $t = t_{co}$ for the main period. Provided the main period is of sufficient length the heater is at a steady-state temperature

$$\left(\frac{dT_h}{dt}\right)_{t = t_{co}} \simeq T_h'(o) \simeq 0$$

Hence from Equations B.69 and B.71

$$T_h(o) = \frac{P_h}{h_h A_h} + T_{bl}(o) = \frac{P_h}{h_h A_h} + \frac{P_h t_{co}}{C_b + C_w} + \tau_m \gamma_b$$

The value of $T_b(o)$ for the anterior period is determined by P_h, t_{co}, and the heat capacity terms, C_b and C_w

$$T_b(o) = \frac{P_h t_{co}}{C_b + C_w} \qquad [B.143]$$

It follows that

$$T_b'(o) = \frac{P_h}{C_b + C_w} \qquad [B.144]$$

Inequality of $T_w'(o)$ and $T_b'(o)$ must be accounted for because at $t = t_{co}$ $t_w(o) \neq T_b(o)$. The background correction term is called γ_{bkg} and

$$\frac{dT_w(o)}{dt} = \frac{dT_b(o)}{dt} - \gamma_{bkg}$$

$$= \frac{P_h}{C_b + C_w} - \gamma_{bkg} \qquad [B.145]$$

From Equation B.67

$$\frac{1}{Z_1}\left(\frac{dT_w(o)}{dt}\right) = T_b(o) - T_w(o) \qquad [B.146]$$

and

$$T_w(o) = T_b(o) - \frac{1}{Z_1}\left(\frac{dT_w(o)}{dt}\right)$$

$$= \frac{P_h t_{co}}{C_b + C_w} - \frac{1}{Z_1}\left(\frac{P_h}{C_b + C_w} - \gamma_{bkg}\right) \qquad [B.147]$$

The inverse transform of Equation B.142 is

$$T_b(t) = \left[\left(\frac{C_b}{C_b + C_w}\right) + 2r_3 \exp\{-\alpha t\} \cos\{\beta t - \theta_3\}\right]\left[\frac{P_h t_{co}}{C_b + C_w}\right]$$

$$+ \left[\left(\frac{C_w}{C_b + C_w}\right) + 2r_4 \exp\{-\alpha t\} \cos\{\beta t - \theta_4\}\right]\left[\frac{P_h t_{co}}{C_b + C_w} - \right.$$

$$\left. \frac{P_h}{Z_1(C_b + C_w)} + \frac{\gamma_{bkg}}{Z_1}\right]$$

$$+ \left[\frac{C_b}{Z_3(C_b + C_w)} - 2r_5 \exp\{-\alpha t\} \cos\{\beta t - \theta_5\}\right]\left[\frac{P_h}{C_b + C_w}\right]$$

$$+ \left[\left(\frac{C_h}{C_b + C_w}\right) + \frac{C_h Z_3(Z_2 - Z_1) \exp\{-Z_2 t\}}{C_b(Z_2^2 - Z_2(Z_1 + Z_3) + Z_1 Z_3(1 + C_w/C_b))}\right.$$

$$\left. - \frac{2C_h r_2 \exp\{-\alpha t\} \cos\{\beta t - \theta_2\}}{(C_b + C_w)}\right]\left[\frac{P_h}{h_h A_h} + \frac{P_h t_{co}}{C_b + C_w} + \tau_m \gamma_b\right]$$

[B.148]

Case II: For critical system damping,

$$\left(\frac{Z_1 + Z_3}{2}\right)^2 = Z_1 Z_3(1 + C_w/C_b) \qquad [B.149]$$

and Equation B.123 is written

$$T_b(s) = \left[\frac{(s + Z_1)(s + Z_3)}{s(s + \alpha)^2}\right] T_b(o)$$
$$+ \frac{Z_1 Z_3 C_w}{C_b}\left[\frac{1}{s(s + \alpha)^2}\right] T_w(o)$$
$$+ \frac{(s + Z_1)}{s(s + \alpha)^2} T_b'(o) + \frac{Z_2 Z_3 C_h}{C_b}\left[\frac{(s + Z_1)}{s(s + Z_2)(s + \alpha)^2}\right] T_h(o)$$

[B.150]

The coefficient of $T_h(o)$ can be factored as

$$\frac{L_{14}}{s} + \frac{L_{15}}{s + Z_2} + \frac{L_{16}}{(s + \alpha)^2} + \frac{L_{17}}{s + \alpha} \qquad [B.151]$$

where $L_{14} = \dfrac{Z_1 Z_3 C_h}{\alpha^2 C_b}$ [B.152]

$$L_{15} = \frac{Z_3(Z_2 - Z_1)C_h}{(\alpha - Z_2)^2 C_b} \qquad [B.153]$$

$$L_{16} = \frac{Z_2 Z_3(Z_1 - \alpha(C_h}{\alpha(\alpha - Z_2)C_b} \qquad [B.154]$$

$$L_{17} = \frac{Z_2 Z_3 C_h}{C_b}\left[\frac{\alpha(\alpha - Z_2) - (Z_1 - \alpha)(Z_2 - 2\alpha)}{\alpha^2(Z_2 - \alpha)^2}\right] \qquad [B.155]$$

The coefficient of $T_b(o)$ can be written as

$$\frac{L_{18}}{s} + \frac{L_{19}}{(s + \alpha)^2} + \frac{L_{20}}{(s + \alpha)} \qquad [B.156]$$

where $L_{18} = \dfrac{Z_1 Z_3}{\alpha^2}$ [B.157]

$$L_{19} = \frac{-(Z_1 - \alpha)(Z_3 - \alpha)}{\alpha} \qquad [B.158]$$

$$L_{20} - \frac{\alpha(Z_1 + Z_3 - 2\alpha) - (Z_1 - \alpha)(Z_3 - \alpha)}{\alpha^2} \qquad [B.159]$$

The coefficient of the $T_b'(o)$ term can be written

$$\frac{L_{21}}{s} + \frac{L_{22}}{(s + \alpha)^2} + \frac{L_{23}}{(s + \alpha)} \qquad [B.160]$$

where $L_{21} = \frac{Z_1}{\alpha^2}$ [B.161]

$$L_{22} = \frac{(\alpha - Z_1)}{\alpha} \qquad [B.162]$$

$$L_{23} = \frac{-Z_1}{\alpha^2} \qquad [B.163]$$

The coefficient of $T_w(o)$ can be written

$$\frac{L_{24}}{s} + \frac{L_{25}}{(s + \alpha)^2} + \frac{L_{26}}{(s + \alpha)} \qquad [B.164]$$

where $L_{24} = \frac{Z_1 Z_3 C_w}{\alpha^2 C_b}$ [B.165]

$$L_{25} = \frac{-Z_1 Z_3 C_w}{\alpha C_b} \qquad [B.166]$$

$$L_{26} = \frac{Z_1 Z_3 C_w}{\alpha^2 C_b} \qquad [B.167]$$

Equation B.123 can now be written

$$T_b(s) = + \left[\frac{\alpha(Z_1 + Z_3 - 2\alpha) - (Z_1 - \alpha)(Z_3 - \alpha)}{\alpha^2(s + \alpha)}\right] T_b(o)$$

$$+\left[\frac{Z_1Z_3C_w}{\alpha^2C_bs}-\frac{Z_1Z_3C_w}{\alpha C_b(s+\alpha)^2}+\frac{Z_1Z_3C_w}{\alpha^2C_b(s+\alpha)}\right]T_w(o)$$

$$+\left[\frac{Z_1}{\alpha^2s}+\frac{(\alpha-Z_1)}{\alpha(s+\alpha)^2}-\frac{Z_1}{\alpha^2(s+\alpha)}\right]T_b'(o)$$

$$+\left[\frac{Z_1Z_3C_h}{\alpha^2C_bs}+\frac{Z_3(Z_2-Z_1)C_h}{(\alpha-Z_2)^2C_b(s+Z_2)}+\frac{Z_2Z_3(Z_1-\alpha)C_h}{\alpha(\alpha-Z_2)C_b(s+\alpha)^2}\right.$$

$$\left.+\frac{C_hZ_2Z_3}{C_b(s+\alpha)}\left\{\frac{\alpha(\alpha-Z_2)-(Z_1-\alpha)(Z_2-2\alpha)}{\alpha^2(Z_2-\alpha)^2}\right\}\right]T_h(o) \quad [B.168]$$

Taking the inverse transform of Equation B.168

$$T_b(t)=\left[\frac{Z_1Z_3}{\alpha^2}-\frac{(Z_1-\alpha)(Z_3-\alpha)t\ \exp\{-\alpha t\}}{\alpha}\right.$$

$$\left.+\left\{\frac{\alpha(Z_1+Z_3-2\alpha)-(Z_1-\alpha)(Z_3-\alpha)}{\alpha^2}\right\}\exp\{-\alpha t\}\right]\left[\frac{P_ht_{co}}{C_b+C_w}\right]$$

$$+\left[\frac{Z_1Z_3C_w}{\alpha^2C_b}-\frac{Z_1Z_3tC_w\ \exp\{-\alpha t\}}{\alpha C_b}\right.$$

$$\left.+\frac{Z_1Z_3C_w\ \exp\{-\alpha t\}}{\alpha^2C_b}\right]\left[\frac{P_ht_{co}}{C_b+C_w}-\frac{P_h}{Z_1(C_b+C_w)}+\frac{\gamma_{bkg}}{Z_1}\right]$$

$$+\left[\frac{Z_1}{\alpha^2}+\frac{(\alpha-Z_1)t\ \exp\{-\alpha t\}}{\alpha}-\frac{Z_1\ \exp\{-\alpha t\}}{\alpha^2}\right]\left[\frac{P_h}{C_b+C_w}\right]$$

$$+\left[\frac{Z_1Z_3C_h}{\alpha^2C_b}+\frac{Z_3(Z_2-Z_1)C_h\ \exp\{-Z_2t\}}{(\alpha-Z_2)^2C_b}\right.$$

$$+\frac{Z_2Z_3(Z_1-\alpha)C_ht\ \exp\{-\alpha t\}}{\alpha(\alpha-Z_2)C_b}$$

$$\left.+C_hZ_2Z_3\left\{\frac{(\alpha^2-\alpha Z_2)-(Z_1-\alpha)(Z_2-2\alpha)}{\alpha^2(Z_2-\alpha)^2C_b}\right\}\exp\{-\alpha t\}\right]$$

$$\left[\frac{P_h}{h_h A_h} + \frac{P_h t_{co}}{C_b + C_w}\,\tau_m \gamma_b\right] \qquad [B.169]$$

Case III: For the case of over damping the coefficient of $T_h(o)$ can be written

$$\frac{L_{27}}{s} + \frac{L_{28}}{(s + Z_2)} + \frac{L_{29}}{(s + \alpha + \sigma)} + \frac{L_{30}}{(s + \alpha - \sigma)} \qquad [B.170]$$

where $L_{27} = \dfrac{Z_1 Z_3 C_h}{(\alpha + \sigma)(\alpha - \sigma) C_b}$ [B.171]

$$L_{28} = \frac{Z_3(Z_2 - Z_1)C_h}{(\alpha + \sigma - Z_2)(\alpha - \sigma - Z_2)C_b} \qquad [B.172]$$

$$L_{29} = \frac{C_h\, Z_2 Z_3 (Z_1 - \alpha - \sigma)}{C_b\, 2\sigma(\alpha + \sigma)(Z_2 - \alpha - \sigma)} \qquad [B.173]$$

$$L_{30} = \frac{-C_h\, Z_2 Z_3 (Z_1 - \alpha + \sigma)}{2C_b \sigma(\alpha - \sigma)(Z_2 - \alpha + \sigma)} \qquad [B.174]$$

The coefficient of $T_b(o)$ can be written as

$$\frac{L_{31}}{s} + \frac{L_{32}}{(s + \alpha + \sigma)} + \frac{L_{33}}{(s + \alpha - \sigma)} \qquad [B.175]$$

where $L_{31} = \dfrac{Z_1 Z_3}{(\alpha + \sigma)(\alpha - \sigma)}$ [B.176]

$$L_{32} = \frac{(Z_1 - \alpha - \sigma)(Z_3 - \alpha - \sigma)}{2\sigma(\alpha + \sigma)} \qquad [B.177]$$

$$L_{33} = \frac{(Z_1 - \alpha + \sigma)(Z_3 - \alpha + \sigma)}{2\sigma(\sigma - \alpha)} \qquad [B.178]$$

The coefficient of $T_b(o)$ can be written

$$\frac{L_{34}}{s} + \frac{L_{35}}{s + \alpha + \sigma} + \frac{L_{36}}{s + \alpha - \sigma} \qquad [B.179]$$

where $L_{34} = \dfrac{Z_1}{(\alpha + \sigma)(\alpha - \sigma)}$ [B.180]

$$L_{35} = \frac{Z_1 - \alpha - \sigma}{2\sigma(\alpha + \sigma)} \qquad [B.181]$$

$$L_{36} = \frac{Z_1 - \alpha + \sigma}{2\sigma(\sigma - \alpha)} \qquad [B.182]$$

The coefficient of $T_w(o)$ can be written

$$\frac{L_{37}}{s} + \frac{L_{38}}{s + \alpha + \sigma} + \frac{L_{39}}{s + \alpha - \sigma} \qquad [B.183]$$

where $L_{37} = \dfrac{Z_1 Z_3 C_w}{(\alpha + \sigma)(\alpha - \sigma)C_b}$ [B.184]

$$L_{38} = \frac{Z_1 Z_3 C_w}{2\sigma(\alpha + \sigma)C_b} \qquad [B.185]$$

$$L_{39} = \frac{Z_1 Z_3 C_w}{2\sigma(\sigma - \alpha)C_b} \qquad [B.186]$$

Equation B.123 is now written

$$T_b(s) = \left[\frac{Z_1 Z_3}{s(\alpha + \sigma)(\alpha - \sigma)} + \frac{(Z_1 - \alpha - \sigma)(Z_3 - \alpha - \sigma)}{2\sigma(\alpha + \sigma)(s + \alpha + \sigma)} + \frac{(Z_1 - \alpha + \sigma)(Z_3 - \alpha + \sigma)}{2\sigma(\sigma - \alpha)(s + \alpha - \sigma)}\right] T_b(o) + \left[\frac{Z_1 Z_3 C_w}{s(\alpha + \sigma)(\alpha - \sigma)C_b} +\right.$$

$$\frac{Z_1 Z_3 C_w}{2\sigma C_b(\alpha+\sigma)(s+\alpha+\sigma)} + \frac{Z_1 Z_3 C_w}{2\sigma C_b(\sigma-\alpha)(s+\alpha-\sigma)}\Bigg] T_w(o)$$

$$+ \left[\frac{Z_1}{2(\alpha+\sigma)(\alpha-\sigma)} + \frac{Z_1-\alpha-\sigma}{2\sigma(\alpha+\sigma)(s+\alpha+\sigma)} + \right.$$

$$\left.\frac{Z_1-\alpha+\sigma}{2\sigma(\sigma-\alpha)(s+\alpha-\sigma)}\right] T_b'(o) + \left[\frac{Z_1 Z_3 C_h}{2(\alpha+\sigma)(\alpha-\sigma)C_b} + \right.$$

$$\frac{C_h Z_3(Z_2-Z_1)}{C_b(\alpha+\sigma-Z_2)(\alpha-\sigma-Z_2)(s+Z_2)}$$

$$+ \frac{C_h Z_2 Z_3(Z_1-\alpha-\sigma)}{2C_b\sigma(\alpha+\sigma)(Z_2-\alpha-\sigma)(s+\alpha+\sigma)} -$$

$$\left.\frac{C_h Z_2 Z_3(Z_1-\alpha+\sigma)}{2C_b\sigma(\alpha-\sigma)(Z_2-\alpha+\sigma)(s+\alpha-\sigma)}\right] T_h(o) \qquad [B.187]$$

The inverse transform of equation B.187 is

$$T_b(t) = \left[\frac{Z_1 Z_3}{(\alpha+\sigma)(\alpha-\sigma)} + \frac{(Z_1-\alpha-\sigma)(Z_3-\alpha-\sigma)\exp\{-(\alpha+\sigma)t\}}{2\sigma(\alpha+\sigma)}\right.$$

$$\left. + \frac{(Z_1-\alpha+\sigma)(Z_3-\alpha+\sigma)\exp\{-(\alpha-\sigma)t\}}{2\sigma(\sigma-\alpha)}\right]\left[\frac{P_h t_{co}}{C_b+C_w}\right]$$

$$+ \left[\frac{Z_1 Z_3 C_h}{(\alpha+\sigma)(\alpha-\sigma)C_b} + \frac{Z_3(Z_2-Z_1)C_h \exp\{-Z_2 t\}}{(\alpha+\sigma-Z_2)(\alpha-\sigma-Z_2)C_b}\right.$$

$$+ \frac{Z_2 Z_3(Z_1-\alpha-\sigma)C_h \exp\{-(\alpha+\sigma)t\}}{2\sigma(\alpha+\sigma)(Z_2-\alpha-\sigma)C_b}$$

$$\left. - \frac{Z_2 Z_3(Z_1-\alpha+\sigma)C_h \exp\{-(\alpha-\sigma)t\}}{2\sigma(\alpha-\sigma)(Z_2-\alpha+\sigma)C_b}\right]\left[\frac{P_h}{h_h A_h} + \frac{P_h t_{co}}{C_b+C_w}\tau_m\gamma_b\right]$$

$$+\left[\frac{Z_1 Z_3 C_w}{(\alpha+\sigma)(\alpha-\sigma)C_b}+\frac{Z_1 Z_3 C_w \exp\{-(\alpha+\sigma)t\}}{2\sigma(\alpha+\sigma)C_b}\right.$$

$$\left.+\frac{Z_1 Z_3 C_w \exp\{-(\alpha-\sigma)t\}}{2\sigma(\sigma-\alpha)C_b}\right]\left[\frac{P_h t_{co}}{C_b+C_w}-\frac{P_h}{Z_1(C_b+C_w)}+\frac{\gamma_{bkg}}{Z_1}\right]$$

$$+\left[\frac{Z_1}{(\alpha+\sigma)(\alpha-\sigma)}+\frac{(Z_1-\alpha-\sigma)\exp\{-(\alpha+\sigma)t\}}{2\sigma(\alpha+\sigma)}\right.$$

$$\left.+\frac{(Z_1-\alpha+\sigma)\exp\{-(\alpha-\sigma)t\}}{2\sigma(\sigma-\alpha)}\right]\left[\frac{P_h}{C_b+C_w}\right] \qquad [B.188]$$

c. Implementation of calculations Values of the time constants τ_h, τ_w, τ_m must be accurately computed to account for the various mechanisms of heat conduction and convection occurring at the heater, disc stirrer, and cell wall. The geometry of the heater is cylindrical with a hemispherical tip. Terms in preceding equations for τ_h

$$Z_2 = 1/\tau_h = h_h A_h / C_h$$

which do not account for differing heat transport rates over the surface of the heater are replaced by

$$Z_2 = \frac{h_h A_h}{C_h}\left[\frac{\lambda_h}{h_{hs} r_h}\right] \qquad [B.189]$$

where

λ_h = thermal conductivity of electrical heater (cal/cm-sec-deg C)

h_{hs} = heat transfer coefficient of heater stem (cal/cm^2-sec-deg C)

r_h = radius of electrical heater (cm)

The value of h_{hs} is calculated by the equation of Scadron and Warshawsky (139) given below.

$$h_{hs} = 0.239\left[\left(\frac{U(r)}{U_{max}}\right)\frac{\omega_s\, r_s\, 2r_h}{\nu_b}\right]^{0.50}\left[\frac{\nu_b\, c_b}{\lambda_b}\right]^{0.30}\left[\frac{\lambda_b}{r_h}\right] \qquad [B.190]$$

The value of C_h was calculated assuming the metal film resistor to be essentially Al_2O_3 (140). Thus,

$$C_h = m_r c_r + m_{Cu} c_{Cu} \qquad [B.191]$$

where

m_r = mass of electrical heater resistive element (g)

c_r = mass heat capacity of resistive element (cal/g-deg C)

m_{Cu} = mass of copper sheath of electrical heater resistive element (g)

c_{Cu} = mass heat capacity of copper metal (cal/g-deg C)

The equivalent thermal conductivity of the electrical heater is given by

$$\lambda_h = \lambda_r\left[\frac{\lambda_{Cu}\lambda_e}{\lambda_{Cu}\lambda_e + x_{Cu}/r_h\lambda_e\lambda_r + x_{e,h}/r_h\lambda_{Cu}\lambda_r}\right]$$

where

λ_r = thermal conductivity of metal film resistor (cal/cm-sec-deg C)

λ_{Cu} = thermal conductivity of copper metal (cal/cm-sec-deg C)

x_{Cu} = thickness of copper tubing surrounding metal film resistor (cm)

$x_{e,h}$ = thickness of epoxy coating an electrical heater (cm)

Heat gain by stem conduction of the probes is computed with the cell wall conduction

$$\tau_w = C_w(1/h_w A_w + 1/h_{stem} A_{stem}) \qquad [B.192]$$

where

h_{stem} = heat transfer coefficient of heater, thermistor, mounting tubes, etc. (cal/cm^2-sec-deg C)

A_{stem} = area of mounting tubes in contact with bulk solution (cm^2)

All solution probes are considered to be of equal size and composition and to be positioned at identical distances from the center of the cell. The calculation of h_{stem} must account for stirring effects of the rotating shaft and the disc of the stirrer. This is done by using weighting factors

$$h_{stem} = \left[\frac{r_{sh}}{r_{sh} + r_s}\right]^{2/3} h_{stem,shaft} + \left[\frac{r_{sh}}{r_{sh} + r_s}\right]^{2/3} h_{stem,disc} \qquad [B.193]$$

where

r_{sh} = radius of stirrer shaft (cm)

r_s = radius of stirring disc (cm)

The values of $h_{stem,shaft}$ and $h_{stem,disc}$ are calculated by the equation of Žukauskas (141) given here for $h_{stem,shaft}$.

$$h_{stem,shaft} = 0.135\left[\left(\frac{U(r)}{U_{max}}\right)\frac{\omega_s r_{sh} 2r_{stem}}{\nu_b}\right]^{0.63}\left[\frac{\nu_b c_b}{\lambda_b}\right]^{0.36}\left[\frac{\lambda_b}{r_{stem}}\right] \quad [B.194]$$

where

r_{stem} is the average radius of mounting tubes (cm)

Equation B.194 is particularly suited for cylinders with diameters greater than 0.25-in. whereas the equation of Scadron and Warshawsky (139) is applicable to cylinders of smaller diameter. The value of h_w is calculated from the equation of Nagata, et al. (142) for an unbaffled vessel containing a cooling coil

$$h_w = 0.128\left[\frac{0.637\ r_s^2 \omega_s}{\nu_b}\right]^{0.667}\left[\frac{\nu_b c_b}{\lambda_b}\right]^{0.33}\left[\frac{r_s}{r_c}\right]^{-0.25}\left[\frac{l_1}{l_2}\right]^{0.15}\left[\frac{x_s}{2r_c}\right]^{0.15}\left[\frac{\lambda_b l_2}{r_c^2}\right] \quad [B.195]$$

where

r_c = radius of calorimeter cell (cm)

l_1 = height of stirrer disc above the bottom of the calorimeter (cm)

l_2 = depth of immersion of stirrer disc in bulk solution (cm)

x_s = thickness of stirrer disc (cm)

Efficient solution mixing in the cell results from uniform turbulent flow. The time constant of mixing, τ_m, used for derivations described here was defined specifically in terms

of the rate of heat transport across the thermal boundary layer of the heater (see Equation B.71). The surfaces of the rotating disc and, to a lesser extent, the shaft provide the stirring. Stirring by the disc results when fluid is pumped from the fluid bulk in an axial direction to the surface of the disc from whence it flows radially over the surfaces of the probes. Stirring by the shaft also results from radial and angular fluid flow. The net value of τ_m is taken to be the harmonic mean of individual time constants computed for stirring by the disc and by the shaft.

$$\tau_m = \left[\frac{1/\tau_{m,disc} + 1/\tau_{m,shaft}}{2} \right]^{-1} \qquad [B.196]$$

The values of $\tau_{m,disc}$ and $\tau_{m,shaft}$ were calculated from the fluid velocity at the position of the heater by application of equations derived for turbulent mixing in pipe flow described by Brodkey (138). The choice of analogy between mixing at the heater and that for pipe flow was made of necessity since rigorous treatment of turbulent mixing according to the literature has been accomplished only for pipe flow. The radial fluid velocity at the rim of the disc is corrected by the Pai power series to give the velocity at the position of the electrical heater. The radical assumption is then made that this velocity is analogous to the main-stream velocity of the pipe flow treated by Brodkey. The value of τ_m weakly reflects variation of the Schmidt number.

Although the Schmidt number for 0.01 M electrolyte solutions is more than 3X that for water (1000 vs. 300), τ_m differs by only about 10%.

A spatial temperature function was derived to describe inhomogeneities of the bulk solution temperature which were disregarded in the initial discussion. The electrical heater is sufficiently small compared to the total volume of the calorimeter to be considered a point source of heat. Depending on the location of the temperature sensor relative to the electrical heater, the temperature sensor may be in an 'excess' temperature region or 'deficient' temperature region. The coordinate origin for the calorimeter was taken as the intersection of the calorimeter longitudinal axis with the bottom of the disc stirrer. Considering ε to be the angle between the center point of the electrical heater and the longitudinal axis of the calorimeter and χ to be the angle between the electrical heater and the temperature sensor, it can be shown that there is a temperature difference function of the following form.

$$T_{b,t} - T_{b,ave} = 3.14\ \gamma_{b,ave}\ t\left(\frac{l_2}{r_c}\right)\left(\frac{\tau_m}{\tau_h}\right)\cos(\sigma_s\chi)\sin(\sigma_s\varepsilon) \quad [B.197]$$

where l_2/r_c is considered to be the cell asymmetry factor and σ_s the shielding parameter which describes the shielding of the temperature sensor by the stirrer and is given by

$$\sigma_s = \frac{U_s(r)}{U_{sh}(r)}\ \frac{r_s^{\ 2/3}}{(r\ r_c)^{1/3}} \quad [B.198]$$

$U_s(r)$ = radial velocity of bulk fluid at distance r due only to stirrer disc (cm/sec)

$U_{sh}(r)$ = radial velocity of bulk fluid at distance r due only to stirrer shaft (cm/sec)

C. Pseudo-Isothermal Calorimetry

1. Requirements for a differential operation

A calorimeter is defined in general terms as an instrument used to measure energy changes of a system through changes in the internal temperature. The energy changes within the calorimeter are best determined by comparison to a standard which is electrical work converted to heat over the same temperature range. Ideally, then, any environmental interactions with the calorimeter are eliminated.

Traditionally, calorimetry was divided according to experimental conditions employed to reduce instrumental artifacts. If study for the system required long term stability (>4 hours) or a large temperature excursion was expected (>0.5 deg C), adiabatic conditions were specified. That is, heat transfer between the calorimeter and environment was made as small as possible. An adiabatic calorimeter requires a large bath of mechanically stirred fluid and complex temperature regulation equipment to maintain a uniform temperature field around the calorimeter. Concurrent is the requirement that the calorimeter must be totally submerged and

the technique is referred to as 'submarine calorimetry'. The foremost proponent of adiabatic calorimetry in this country during the early part of the present century was T. W. Richards as noted by Kopperl and Parascandola (143).

The requirement of greater sensitivity in calorimetry led to the use by Gucker, et al. (144) of the twin calorimeter originally proposed by Joule, together with thermopiles to test the predictions of the Debye-Hückel theory of electrolytic solutions. As an example of the usefulness of adiabatic solution microcalorimeters, we can cite the work of Spedding and co-workers in their examination of the behavior of rare earths at both low and high concentrations in aqueous media as reviewed by Mohs (145).

When experimental conditions were not as stringent, isothermal calorimetry was preferred so long as heat loss to the calorimeter environment could be made reproducible from experiment to experiment (146). True isothermal calorimetry requires that the jacket temperature, T_j, as well as the calorimeter's internal temperature, T_i, must be constant throughout the experiment. This requirement can only be met using the Bunsen ice calorimeter or the recently developed semiconductor devices utilizing the Peltier effect. The efficiency of Peltier devices are presently low making work with high solution heating rates difficult. When T_j is kept constant, but T_i varies, the term isoperibol is used for the calorimeter instead of isothermal to denote that the operation

is pseudo-isothermal. The primary advantage of isoperibol calorimetry is the simplicity of calorimeter operation.

In a recent review, Churney et al. (129) showed that adiabatic and isothermal calorimetry yield data of equivalent precision when the change in state is completed rapidly. Since thermometric titrimetry is normally carried out over a period of a few hundred seconds, isoperibol calorimeters are used exclusively for thermal titrations.

Accurate cancellation of temperature sensor response to solution heating by processes other than the one of interest is difficult. These processes include heating from stirring, γ_{str}, Joule heating from the electrically powered temperature sensor, γ_{sen}, and background heating, γ_{bkg}, when the environment temperature, T_w, is greater than the bulk solution temperature, T_b. The heat of stirring can be reduced by using a smaller stirrer operating at a lower rotational velocity; however, solution thermal homogeneity requires a high degree of turbulence with uniform eddy size, a condition proceeding from large stirrers turning rapidly. The Joule heating is very small ($\gamma_{str} \sim \gamma_{bkg} \sim 1000\ \gamma_{sen}$) and usually can be ignored except for very small calorimeters with less than 5-ml capacity. The background heating rate is generally reduced by using evacuated containers and materials with low thermal conductivity for the calorimeter walls.

Peltier devices, when operated along with an electrical heater driven by pulsating current (147, 148, 149, 150) can be used to cancel all solution heating effects or, if used alone (151), background effects. Alternately, twin calorimeters can be used with trickle heaters to achieve a nearly zero baseline. In this study, twin calorimeters in an isothermal environment were used in pseudo-isothermal calorimetric studies. The reference calorimeter was heated electrically at nearly the same rate as the reaction calorimeter.

The internal energy of a system, ΔU, is defined by the first law of thermodynamics as

$$\Delta U = dq - dw \qquad [C.1]$$

or the difference between the heat absorbed by the system and the work done by the system. Either through the use of a true adiabatic calorimeter or by effective cancellation of environmental-calorimeter heat exchange, $dq \sim 0$ and $U = - dw$. Knowing $U = f(T, V, n)$ where T is the system temperature, V, the system's volume and n, the number of moles involved, dU may be written as

$$dU = \left(\frac{\partial U}{\partial T}\right)_{V,n} dT + \left(\frac{\partial U}{\partial V}\right)_{T,n} dV + \left(\frac{\partial U}{\partial n}\right)_{V,T} dn \qquad [C.2]$$

Equation C.2 is given in terms of the intensive variable, T, and the extensive variables V and n of the macroscopic

state of a chemical system. The third term ultimately leads to insights about the microscopic processes in dilute solutions, notably the square root dependence of physically measurable parameters on the concentration predicted from electrostatics.

If there is an increase in energy of the system which is not allowed to escape, this energy is converted to heat and PV work. This is expressed mathematically as

$$\Delta U = \Delta H - \Delta(PV) \qquad [C.3]$$

where ΔH is the enthalpy, the difference in heat content between two states of the system. This must not be confused with heat capacity, dq/dT.

Systems where liquids and solids only are studied permit a simplification in that $\Delta(PV) \sim o$ and thus, at constant pressure,

$$dH = \left(\frac{\partial H}{\partial T}\right)_{P,n} dT + \left(\frac{\partial H}{\partial n}\right)_{T,P} dn \qquad [C.4]$$

The importance of the second term of Equation C.4 will be shown later in plots of experimental data at concentrations $<10^{-2}$ M.

In summary, the requirements for operation of a differential isoperibol calorimeter for pseudo-isothermal calorimetry can now be listed.

1. The heat loss modulus, k, of each calorimeter cell should be small, $<10^{-2}$ min^{-1} is desirable, and nearly equal for the two cells.
2. The thermal environment of the calorimetry cells should be identical around each cell.
3. Temperature sensors in the two cells should be nearly equivalent in sensitivity.
4. The mass of bulk solution in each cell should be nearly equal.
5. The heat of stirring and sensor Joule heating should be nearly equal in each calorimeter cell.
6. Evaporation of bulk solution in each cell should be nearly equal in each cell.
7. Surface areas in contact with the bulk solution of the calorimeter wall and solution probes should be nearly equal.
8. Vapor volumes of each cell should be as small as possible and equal.
9. Cell covers should fit reasonably tight, but pressure above bulk solution must be atmospheric so that $\Delta(PV) = 0$.
10. The addition of titrant must be equal to each cell.

2. Magnitude of errors

Starting from Ohm's law, the current in the standard resistor, R_{std}, used in this work can be given as

$$I_{std} = \frac{E_{std}}{R_{std}} \qquad [C.5]$$

The electrically produced heat, over an infinitesimal period of time, in the calorimeter reference cell is

$$dq_e = \frac{E_1 \, I_{std}}{J} \, dt \qquad [C.6]$$

assuming I_{std} and E_1 are constant. J is the Joule mechanical equivalent of heat (4.184 joules/cal). The determination of the heat capacity ratio, c_2/c_1, is necessary since, as can be readily shown,

$$\Delta H_r = \left(\frac{\Delta q_{e,1}}{c_{r1} m_{r1}}\right)\left(\frac{c_2}{c_1}\right) \qquad [C.7]$$

assuming that $\Delta T_1 = \Delta T_2$. In Equation C.7,

ΔH_r = heat of reaction/mole of limiting reactant (cal/mole)

Δq_e = electrical energy transferred into the reference cell of the calorimeter (cal)

c_{r1} = concentration of limiting reactant (mole/g)

m_{r1} = mass of limiting reactant (g)

c_2 = heat capacity of reaction cell (cal/deg C)

c_1 = heat capacity of reference cell (cal/deg C)

Using electrical energy to heat both calorimeter cells simultaneously by connecting the calibration heaters in series with the standard resistance,

$$\Delta q'_{e,1} = \frac{E'_1 I_{std} t}{J} = c_1 \Delta T'_1 \qquad [C.8a]$$

and

$$\Delta q'_{e,2} = \frac{E'_2 I_{std} t}{J} = c_2 \Delta T'_2 \qquad [C.8b]$$

Dividing C.8b by C.8a yields

$$\frac{c_2}{c_1} = \frac{E'_2 \, T'_1}{E'_1 \, T'_2} \qquad [C.9]$$

The prime notation is used to indicate that values of E_1 and E_2 measured in a heat capacity determination are not necessarily the same as those measured during a thermal titration since the measurements are taken at different times in an experiment. The primes do not denote derivatives of E_1 and E_2.

Since a constant current supply is always used to supply current to the calibration heaters, the assumption is made here that $E_1 = E'_1$ for simplicity of discussion of subsequent derivations. Substitution of Equation C.9 into Equation C.7 followed by use of the integrated form of Equation C.6 yields

$$\Delta H_r = \left(\frac{E_{std} E'_2 t}{R_{std} J}\right)\left(\frac{1}{c_{r1} m_{r1}}\right)\left(\frac{\Delta T'_1}{\Delta T'_2}\right) \qquad [C.10]$$

As is well-known in calorimetry, errors in temperature measurement are usually most significant in establishing the error in ΔH_r. Standard methods of error analysis for

estimating the standard deviation of the molar heat of reaction, $S_{\Delta H_r}$, yields

$$S^2_{\Delta H_r} = \left(\frac{\Delta H_r}{E_2'}\right)^2 S^2_{E_2'} + \left(\frac{\Delta H_r}{I_{std}}\right)^2 S^2_{I_{std}} + \left(\frac{\Delta H_r}{t}\right)^2 S^2_t + \left(\frac{\Delta H_r}{\Delta T_1'}\right)^2 S^2_{\Delta T_1'} + \left(\frac{\Delta H_r}{\Delta T_2'}\right)^2 S^2_{\Delta T_2'} + \left(\frac{\Delta H_r}{J}\right)^2 S^2_J + \left(\frac{\Delta H_r}{m_r}\right)^2 S^2_{m_r} + \left(\frac{\Delta H_r}{c_r}\right)^2 S^2_{c_r} \qquad [C.11]$$

The value, S_J, equals zero by definition since J is a defined constant. The variables in Equation C.11 are grouped together into five primary quantities measured: energy, time, temperature, mass and concentration in a calorimetry experiment. Increases in E_2', I_{std}, t, ΔT_1, ΔT_2, m_r, and c_r result in a decrease of $S_{\Delta H_r}$ assuming that H_r is nearly constant over the concentration range studied.

Approximate values of the parameters in Equation C.11 for this study were substituted in Equation C.11 for a ΔH_r of 10 kcal/mole and an experimental reaction energy of 10 calories to calculate $S_{\Delta H_r}$.

$$S^2_{\Delta H_r} = \left(\frac{1\text{x}10^4}{1.5}\right)^2 (2\text{x}10^{-4})^2 + \left(\frac{1\text{x}10^4}{5\text{x}10^{-2}}\right)^2 (2\text{x}10^{-6})^2 +$$

$$\left(\frac{1x10^4}{6x10^2}\right)^2 (1.5x10^{-5})^2 + 4\left(\frac{1x10^4}{4x10^{-1}}\right)^2 (4.5x10^{-5})^2 +$$
$$\left(\frac{1x10^4}{5}\right)^2 (1x10^{-4})^2 + \left(\frac{1x10^4}{2x10^{-4}}\right)^2 (1x10^{-7})^2$$

which reduces to

$$S^2_{\Delta H_r} = 1.8 + 0.2 + 6.3 \times 10^{-8} + 4.6 + 4 \times 10^{-2} + 25$$

and $S_{\Delta H_r} = 5.6$

The relative error, δ, equals 5.6 parts per 10,000. In the ratio method used in this study, only m_r and t vary as ΔH_r is studied versus the number of moles of the limiting reactant. The development of Equation C.11 assumes zero error in determining that the final baseline is equal to the initial baseline before titration.

A more realistic determination of error in the ratios

$$\left(\frac{\Delta T_1'}{\Delta T_2'}\right)\left(\frac{\Delta T_2}{\Delta T_1}\right)$$

now can be made using the thermistor circuit equations developed earlier. Recall that

$$e_{o,3} = -\frac{R_f}{R_1} e_- - \frac{R_f}{R_2} e_+$$

and $\frac{1}{R_t}\frac{dR_t}{dT_t} \simeq -\frac{\beta_t}{T_t^2}$ for small temperature ranges, which should

be written as $\frac{1}{R_t}\frac{\Delta R_t}{\Delta T_t} \simeq -\frac{\beta_t}{T_t^2}$ for other than infinitesimal temperature changes. The calorimeter cells are heated simultaneously at certain times in experiments. In determination of the heat capacity ratio, the difference, $T_1 - T_2$ is always less than 2.5 mdeg C for experimental conditions used in this work.

The cell temperatures are also very closely matched at the beginning and end of the thermometric titration of the reactive species. This permits a considerable number of simplifications to be made provided that the thermistors are also closely matched in resistance and sensitivity. Hence, since $T_1 - T_2$ is small, $R_1 \sim R_2$, $e_+ = -e_- = e$, and $dR_1/dT_1 \sim dR_2/dT_2$, the following relation can be written

$$e_{o,3} = \left(\frac{R_2 - R_1}{R_1 R_2}\right) R_f e = \left(\frac{\Delta R}{R^2}\right) R_f e \qquad [C.12]$$

where $R = \sqrt{R_1 R_2}$

Using the sensitivity equation in Equation C.12,

$$e_{o,3} = -\left(\frac{\beta \Delta T}{T^2}\right)\left(\frac{R_f}{R}\right) e$$

$$= -\left[\frac{\beta(T_2 - T_1)}{T^2}\right]\left(\frac{R_f}{R}\right) e \qquad [C.13]$$

where $T = \sqrt{T_1 T_2}$ in deg K and $\beta = \sqrt{\beta_1 \beta_2}$ in deg K

The temperature range for the total calorimetry experiment, heat capacity ratios and titration, is ∿0.5 deg C; therefore, sensitivity of the thermistor circuit can be considered constant.

Before turn-on of cell calibration heaters in series,

$$e_{o,3,i} = - \left[\frac{\beta(T'_{2,i} - T'_{1,i})}{T'^{2}_{i}}\right]\left(\frac{R_f}{R}\right) e \qquad [C.14]$$

After turn-off,

$$e_{o,3,f} = - \left[\frac{\beta(T'_{2,f} - T'_{1,f})}{T'^{2}_{f}}\right]\left(\frac{R_f}{R}\right) e \qquad [C.15]$$

$T_f - T_i \leq 0.05$ deg C which permits statement of the equalities

$$T'^{2}_{i} = T'^{2}_{f} = T'^{2}$$

Subtracting Equation C.14 from C.15,

$$e_{o,3,f} - e_{o,3,i} = [(T'_{2,i} - T'_{2,f}) + (T'_{1,f} - T'_{1,i})]\left(\frac{R_f\beta}{RT'^{2}}\right) e \qquad [C.16]$$

Dividing through by $T'_{2,f} - T'_{2,i}$, after rearrangement

$$\frac{T'_{1,f} - T'_{1,i}}{T'_{2,f} - T'_{2,i}} = \left(\frac{RT'^{2}}{R_f\beta}\right)\left(\frac{e_{o,3,f} - e_{o,3,i}}{e}\right) \cdot \left(\frac{1}{T'_{2,f} - T'_{2,i}}\right) + 1 \qquad [C.17]$$

or

$$\frac{\Delta T_1'}{\Delta T_2'} = 1 + \frac{RT'^2\ \Delta e_{o,3}}{R_f \beta\ e\ \Delta T_2'} \qquad [C.18]$$

Similarly,

$$\frac{\Delta T_2}{\Delta T_1} = 1 - \frac{RT^2\ \Delta e_{o,3}}{R_f \beta\ e\ \Delta T_1} \qquad [C.19]$$

The value of $\Delta T_1'/\Delta T_2'$ in Equation C.18 and $\Delta T_2/\Delta T_1$ in Equation C.19 differ from unity because of any mismatch of cell heat capacities (calorimeter + contents) and operator judgment, respectively. The parameters R_f, β, and e can be considered constant over the temperature range used, ~0.5 deg C, R decreases much faster than T^2 increases (4 pph/deg C versus 4 ppt) making $\Delta T_1'/\Delta T_2' \rightarrow 1$ as the temperature increases provided solution effects are negligible.

The requirement that the second terms in Equations C.18 and C.19 be as small as possible is soon realized not only from the assumptions made in the derivation but also in numerical evaluation. R and T are calculated using the average values of R_1, R_2, T_1, and T_2 for the experimental temperature change in each cell upon electrical heating. $\Delta T_2'$ is determined using a separate electrical heating trial on calorimeter cell #2 only following the heat capacity ratio heating. Using the circuit sensitivity and electrical heating of cell #2 only, the ratio $\Delta T_2/\Delta q_{e,2}$ can be calculated and also from a subsequent ratio, $\Delta T_2'$. The numerical value of ΔT_1

can be calculated in like manner with a check made through monitoring the reference cell of the calorimeter with a Hg thermometer.

The evaluation of the standard deviation terms

$$\left(\frac{\Delta H_r}{\eta}\right)^2 S_\eta^2 + \left(\frac{\Delta H_r}{\eta}\right)^2 S_\zeta^2$$

according to the error analysis given in Equation C.11 can be made with the equalities $\eta = T_1'/T_2'$ and $\zeta = T_2/T_1$.

The room temperature, T_a, is considered to be constant, leading to the assumption that $S_{R_f} = 0$. The terms $(\eta/2T)$, (η/R), and (η/β) are also seen by inspection to be negligible knowing that $\eta \sim 1.01$ in this study. Using approximate values of the parameters defining η,

$$\eta = \frac{(1x10^4)(8.88x10^4)(2x10^{-3})}{(1x10^6)(3.56x10^3)(5\ 10^{-2})} + 1$$

$$\eta = 9.9x10^{-3} + 1 = 1.0099$$

and

$$S_\eta^2 = \left(\frac{\eta}{\Delta e_o}\right)^2 S_{e_o}^2 + \left(\frac{\eta}{e}\right)^2 S_e^2 + \left(\frac{\eta}{\Delta T_2'}\right)^2 S_{\Delta T_2'}^2$$

$$= \left(\frac{9.9x10^{-3}}{2x10^{-3}}\right)^2 (1.8x10^{-4})^2$$

$$+ \left(\frac{9.9x10^{-3}}{1}\right)^2 (2x10^{-5})^2 + \left(\frac{9.9x10^{-3}}{5x10^{-2}}\right) (2x10^{-3})^2$$

which reduces to

$$S_\eta^2 = 7.9x10^{-7} + 3.9x10^{-14} + 1.6x10^{-7}$$

$$S_{\eta} = 9.7 \times 10^{-4}$$

whence

$$\left(\frac{\Delta H_r}{\eta}\right)^2 S_{\eta}^2 = 97$$

For simplicity, ζ will be considered to be the complement of η or 0.99020 and $S_{\eta}^2 = S_{\zeta}^2$.

Finally, using

$$2\left(\frac{\Delta H_r}{\eta}\right)^2 S_{\eta}^2 \text{ in place of } \left(\frac{\Delta H_r}{\Delta T_1'}\right)^2 S_{\Delta T_1'}^2 + \left(\frac{\Delta H_r}{\Delta T_2'}\right)^2 S_{\Delta T_2'}^2$$

$S_{\Delta H_r} = 15$ and $\delta = 1.5$ ppt, a reasonable result. The error in ΔH_r indeed proceeds primarily from η and ζ making measurements of these quantities critical for high quality work in differential calorimetry. It is increasingly difficult to estimate a priori ΔH_r for very dilute solutions $<10^{-3}$ m since dependence of ΔH_r on η_r is not initially well-known. Errors of 2 - 4% in heater turn-off times based on initial estimations of ΔH_r from determinations at higher concentrations and initial slopes are generally considered satisfactory for differential calorimetry.

IV. INSTRUMENTATION

A. Thermistor Detector

The NTC bead thermistor probes were Type 44031 from Yellow Springs Instrument Co. They were chosen because of low manufacturing tolerances (10,000 Ω ± 0.5%) and excellent long term stability (152). The PTC thermistors were Positemp[1] Type 713T15 from Pennsylvania Electronics Technology, Inc., and were nominally 10,000 Ω at 25 deg C. The thermistors were mounted as shown in Figure IV.1. The thermistor beads were pushed flush against the end of a 1-in length of 0.125-in o.d. Teflon tubing. With the thermistor leads set parallel and equidistant from the tubing wall, the tubing was filled with epoxy resin, Type A-270, from Armstrong Products Co., Warsaw, IN.

Leads to the thermistor were silver soldered to Belden AWG #32 plastic coated stranded wire. The leads were twisted together and threaded through 0.125-in o.d. Teflon tubing which was inserted in the braided shielding wire from a RG-59/U coaxial cable. This assembly was slipped into a 6-in length of 8-mm Pyrex tubing. With the thermistor projecting 0.5-in beyond the end of the Pyrex tubing, the space between the Teflon and Pyrex was filled with A-270 epoxy

---

[1]Registered Trademark of Pennsylvania Electronics Technology.

Figure IV.1. Thermistor probe

A. Tygon tubing

B. Thermistor lead wires (copper)

C. Pyrex tube (probe)

D. Tygon tubing

E. Teflon tubing

F. Epoxy

G. Thermistor lead wires (platinum)

H. Thermistor bead

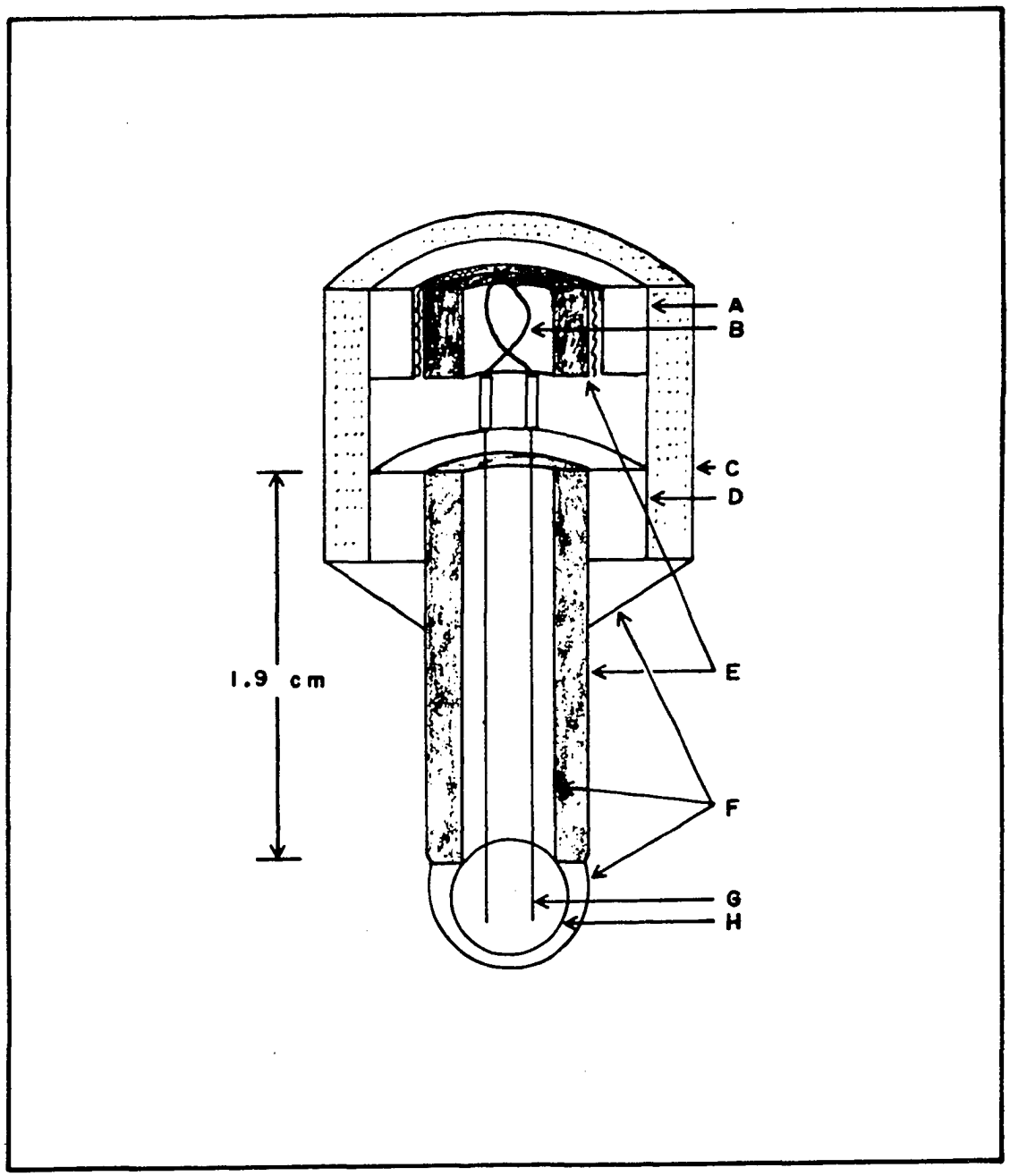
A
B
C
D
E
F
G
H
1.9 cm

resin. Thus, the thermistor bead was provided with a mechanically rigid mounting with low thermal conductivity. Effective electrostatic shielding was provided to within 0.65-in of the thermistor bead by the braided wire sheath. A common junction box mounted on the calorimeter head was used for all connections between the amplifier circuit and thermistor leads. The sheath of each thermistor cable was soldered to a common ground and heat sink in the common junction box. A hybrid NTC-PTC thermistor probe was constructed in a similar manner to that described above.

B. Electronic Circuitry

1. Two-thermistor differential bridge

The amplifier circuit is shown schematically in Figure III.1. The amplifier circuits were constructed following the usual precautions of electrostatic shielding by means of a Faraday cage. Considerable attention was devoted to thermal shielding of critical components. Baffles and heat sinking techniques were used to reduce the possibility of rapidly changing thermal gradients within the amplifier enclosure. Coaxial cables, 30-in in length, used to connect OA-1 and OA-2 to t_2 and t_1 were placed within an additional braided wire sheath to give protection from electrostatic pick-up.

All resistors used were 1% carbofilm or metal film types except R_3 and R_4, which are 0.1% wire wound resistors. Capacitors were polystyrene or mylar types.

Several mini-DIP 741C operational amplifiers were tested for character and two with very low noise characteristics were selected for use as OA-1 and OA-2. Amplifier OA-3 was an Analog Devices 147C FET operational amplifier. After six months of successful operation of the circuit in Figure III.1, the long term stability was improved by substituting Analog Devices 504J amplifiers for OA-1 and OA-2. This circuit was also constructed on a printed circuit board to decrease stray capacitances found for point-to-point wiring. This modification is referred to as Circuit B.

2. Voltage regulation

Three stages of voltage regulation were used to supply ± 15 VDC. A conventional line voltage regulator, Applied Research Laboratories, Glendale, CA, was used as the first stage followed by a Wanlass CVR-120 regulator, Allied Electronics, Chicago, IL. The third stage was an Analog Devices Model 902 dual op-amp power supply. The fourth stage, ± 12 VDC, shown in Figure IV.2, employed a 723C voltage regulator operated as a series regulator to provide + 12 VDC and a 741C amplifier to provide - 12 VDC.

C. Differential Isoperibol Calorimetry

1. Design

A photograph of a new compact design for an isoperibol calorimeter of the submarine type with variable heat shields

Figure IV.2. Voltage regulation circuit

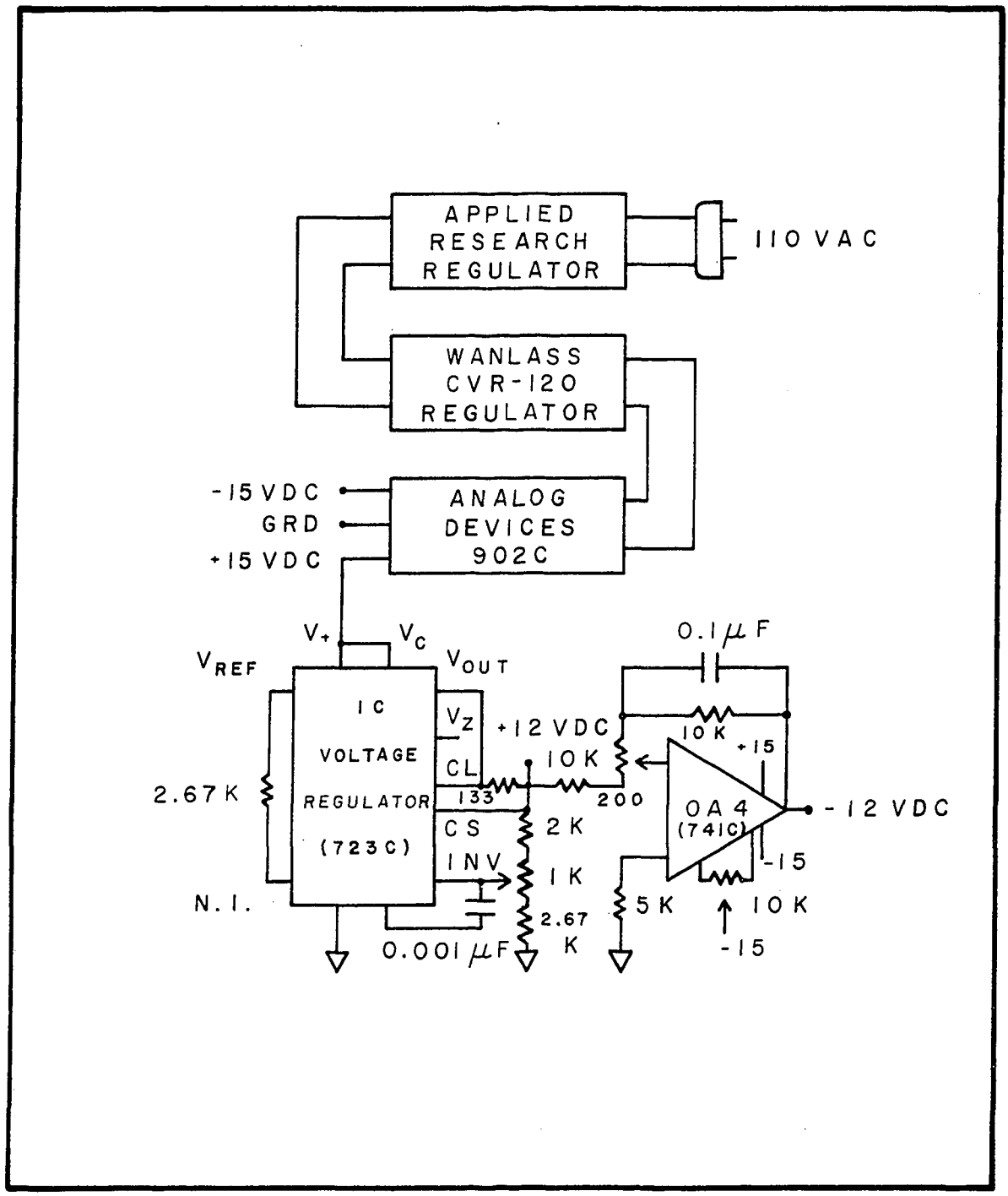
APPLIED RESEARCH REGULATOR
110 VAC
WANLASS CVR-120 REGULATOR
-15 VDC
GRD
+15 VDC
ANALOG DEVICES 902C
V+
VC
VREF
VOUT
IC VOLTAGE REGULATOR (723C)
VZ
CL
CS
INV
N.I.
2.67 K
133
200
2 K
1 K
2.67 K
0.001 μF
+12 VDC
10 K
0.1 μF
10 K
+15
OA 4 (741C)
-12 VDC
-15
5 K
10 K
-15

above and around the Dewar cells is shown in Figure IV.3. A photograph of the calorimeter is shown in Figure IV.4. The design avoids the disadvantage of leaky seals which commonly plague completely submerged calorimeters by utilizing a lid with its own system of enclosed chambers for circulation of a thermostated liquid. The temperature of the lid could be maintained at a temperature independent of the Dewar cells by use of a separate thermostatic bath and circulation pump. The cell was unique in that no gaskets, flanges, or other parts needed to be reassembled each time the calorimeter was used. Instead, the calorimeter cells were raised or lowered on a laboratory jack and could be moved to one side to facilitate addition of solution by pipeting or removal by aspiration. All manipulations including cleaning were accomplished quickly with minimal chance for component damage.

2. Construction

A detailed scale drawing of the calorimeter head is given in Figure IV.5. A massive aluminum block with channels cut into it for the flow of thermostating fluid provided a large heat sink above and well beyond the edges of the calorimeter vessels. A thin coat of Dow Corning Silicone sealant prevented any problems with leakage when the large aluminum discs and main aluminum plate were bolted together. The calorimeter Dewar tops were ground flat so that application

Figure IV.3. Photograph of calorimeter

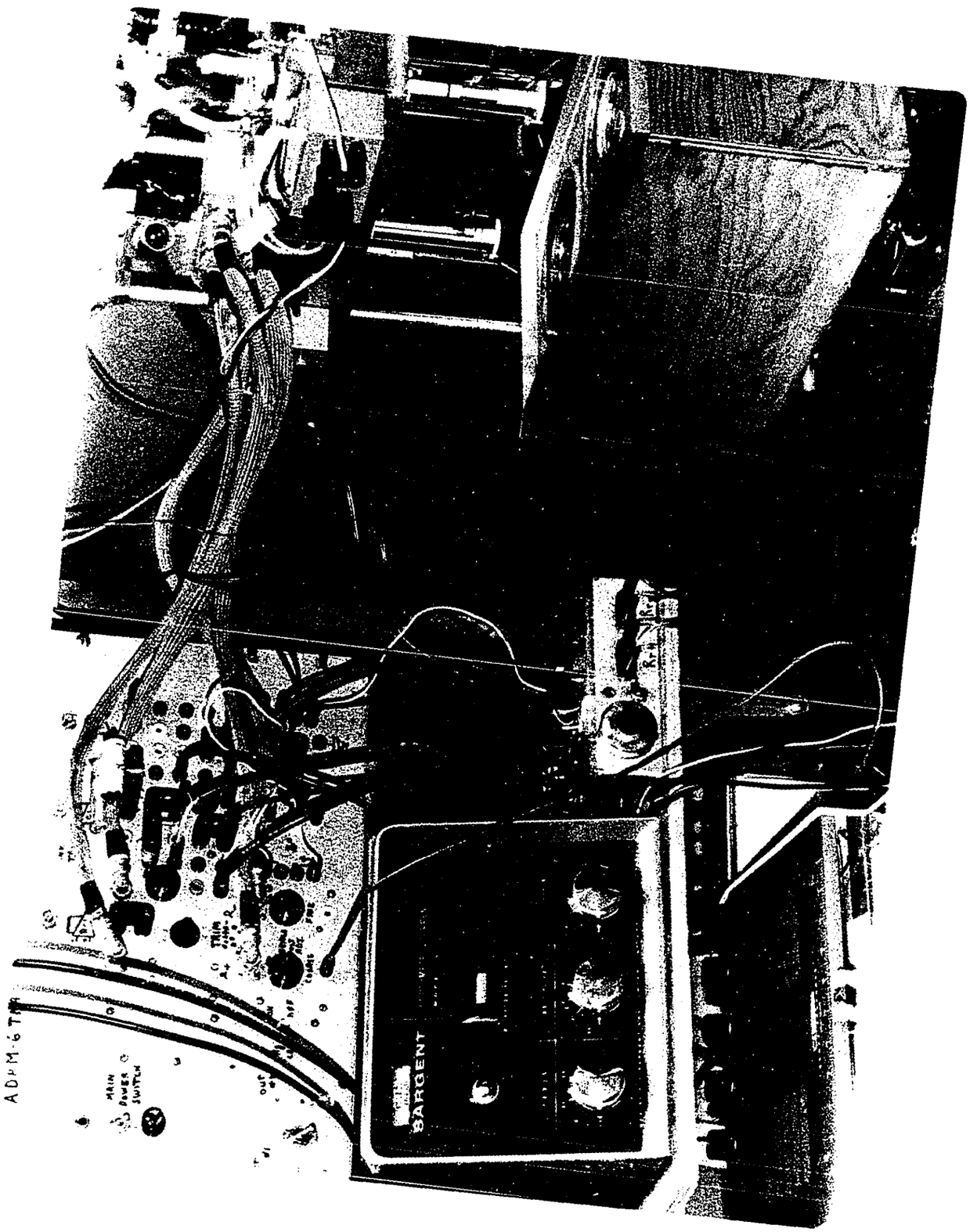
SARGENT
MAIN POWER SWITCH

Figure IV.4. Photograph of calorimeter probes

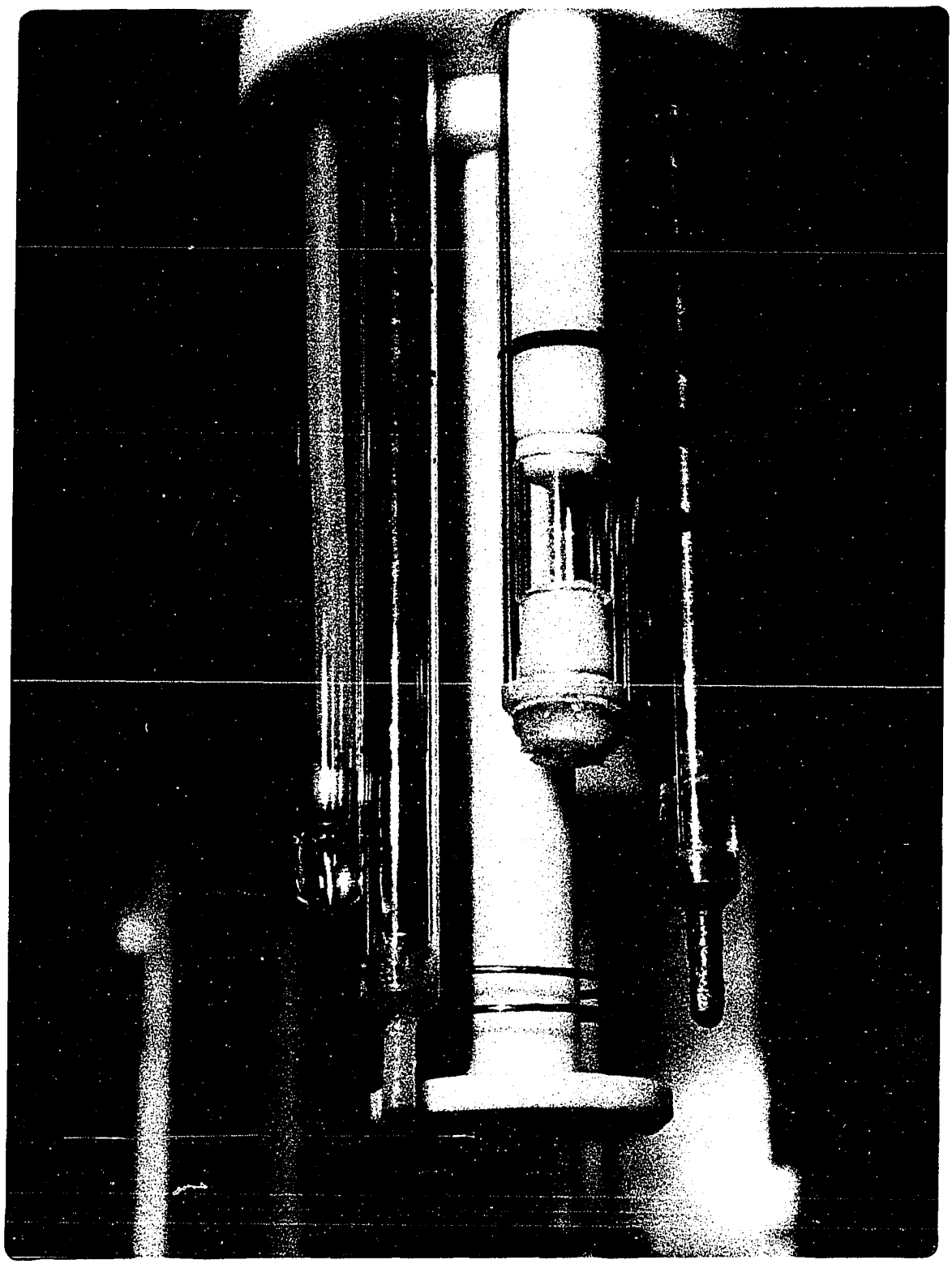

Figure IV.5. Diagram of calorimeter head

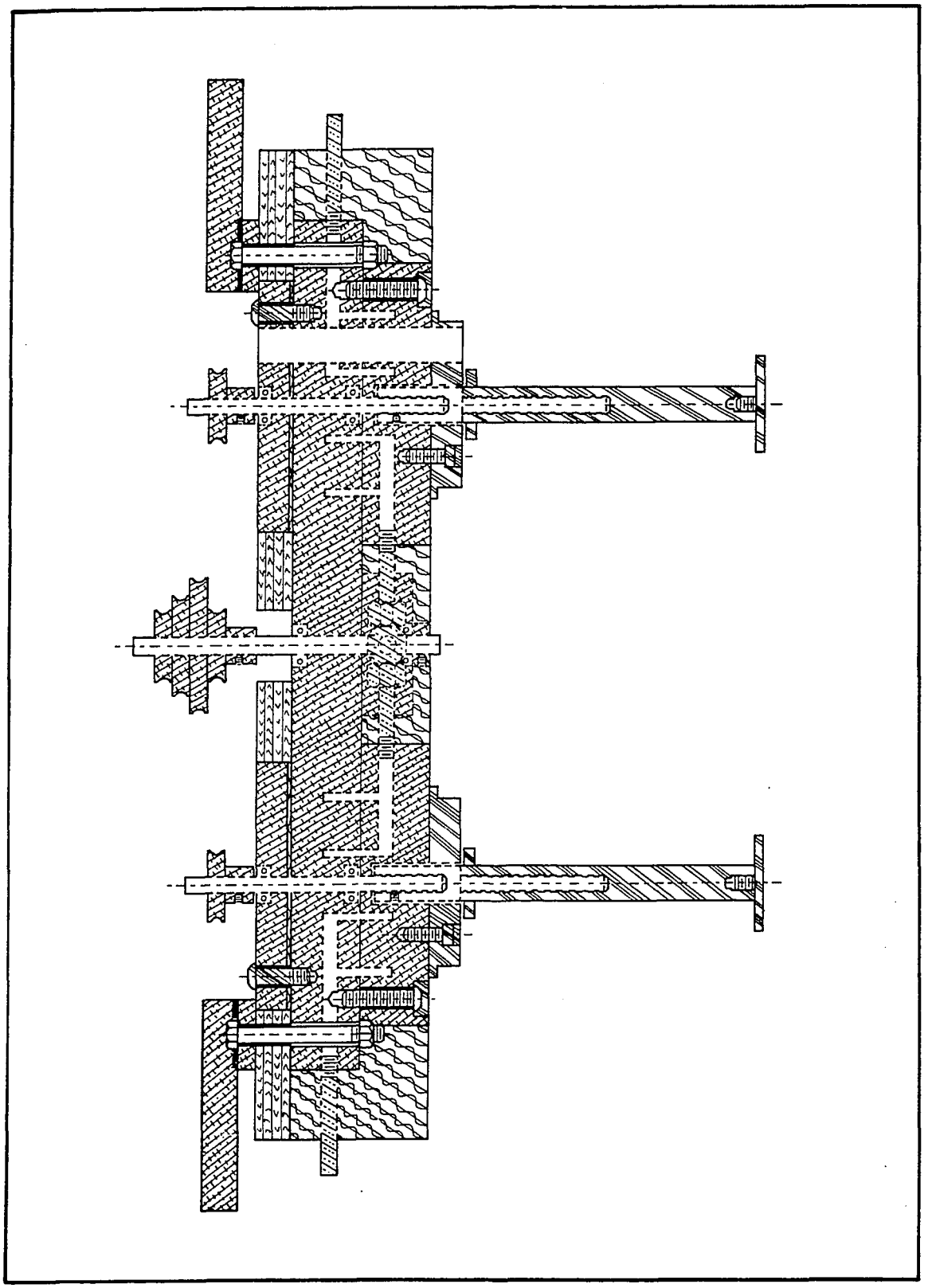

of small amounts of sealant grease to the Teflon calorimeter covers provided a nearly vapor proof seal.

Careful inspection of Figure IV.5 reveals that the upper bearings of the calorimeter stirrers were mounted in aluminum blocks thermally separated from the main mounting block. Tygon tubing surrounded the four bolts used to suspend the calorimeter head from the mounting frame. The head was covered by a 1-in thick layer of Styrofoam on the sides and bottom. The aluminum disks projecting below the block were not covered by Styrofoam on their bottom surfaces, but were covered with epoxy. The top of the block was covered by 0.5-in thick plywood and the outside edges were enclosed by 0.25-in thick plywood. When the calorimeter box was raised into position, there were a series of interlocking seals at the calorimeter box-calorimeter head interface.

The bulk solution stirrers were driven by a common pulley with bearings mounted in the main head block. Step pulleys were used on the stirrer shafts and on the drive motor, a T-line stirrer, Model #105, Talboys Engineering Corp., Emerson, NJ. The calorimeter Dewars, Aladdin's No. 020A, a 10-oz wide mouth vacuum bottle replacement filler, manufactured by Aladdin Industries, Inc., Nashville, TE, were mounted in 4-l polyethylene bottles cut equal in height.

The Dewars were set on rubber rings and plastic base plates supplied by the manufacturer. A 24-ft coil of 0.25-in

copper tubing for circulation of thermostated fluid were set on a cork ring trimmed to fit the bottom of the polyethylene bottle. There was approximately 0.5-in clearance on each side of the coil. The Dewars were held in place by Plexiglas rings enclosing the top of the polyethylene bottles. Mineral oil was used as the heat transfer media between the coil and Dewar filling the polyethylene bottle up to the covers.

Thermostating water (25.00 ± 0.01 deg C) from a Forma Temp. Jr. bath and circulator (Model No. 2095-2) flowed to the appropriate titrant injection thermostat and corresponding Dewar cell thermostat. The water streams were rejoined after leaving the calorimeter thermostat and flowed back to the main temperature control bath. The polyethylene bottles were set in Plastic foam and held in place by a Plexiglas plate setting on projections in the enclosing plywood box.

A titrant injection system was constructed so that all parts in contact with the titrant were either Pyrex or Teflon. The titrant reservoir was a 250-ml Pyrex aspirator bottle at ambient temperature joined to a three-way stopcock. The titrant was protected from evaporation by a bubbler tube. Two other three-way stopcocks were joined to the first in the form of an H with the legs of the H joined to 2.000-ml micrometer syringes, Type #7844 Cole Parmer Instrument Co., Chicago, IL. The arms of the H were connected to the titrant injection thermostats by Teflon tubings 0.063-in i.d., Type

#T125063, Chromatronic Inc., Berkeley, CA, plus appropriate fittings. The titrator syringes were mounted according to the design of Ebell (153) using a RMS shaded pole AC motor, 10 rpm, reversible, variable speed, 225 in-oz torque at 10 rpm, Type BG5P19K, plus control box. This unit was purchased from Allied Radio Corp., Chicago, IL. The motor and syringes were connected using three 2-in diameter, 48-teeth Boston gears set in line with the motor in the center. The motor and syringe holders were mounted on 0.25-in aluminum plate throughout with the entire syringe unit set vertically and attached by screws to 0.5-in aluminum rods. The flow rate could be manually adjusted from 0-1 ml/min. An electrical brake in the motor control box permitted exact shutoff of titrant at any point.

The titrant thermostats were made to resemble distillation condensers. The internal volume of the thermostats was approximately 10-ml or 5 times the volume of titrant injected any time. The reference cell titrant thermostat had a small opening in its midpoint where a 100KΩ NTC thermistor was mounted as part of a second thermistor bridge. The titrant thermostats were wrapped with layers of glass wool for a total thickness of 0.5-in followed by plastic tape for insulation.

The titrant was injected into the calorimeter Dewar cells through 6-mm o.d., 0.5-mm i.d. Pyrex capillaries tapered sharply at the injection point.

A detailed listing of materials used in construction of the calorimeter is given in Table IV.1. Area and volume specifications of the calorimeter cell and mounting probes are given in Table IV.2.

Table IV.1. Listing of materials used in calorimeter

Description	Material		Quantity
Calorimeter head	Aluminum		3760 g
Top bearing holder	Aluminum		194.5 g
Calorimeter cell lid cover	Teflon		67.0 g
Heat exchange fluid	Mineral oil		1700 ml
Calorimeter cell	Glass	Cell 1	173.7 g
		Cell 2	170.5 g

The electrical heating elements were constructed similar to the manner of Stern et al. (154) with several changes. Copper tubing was used instead of the Ag foil suggested in the original design. More importantly, metal film resistors having a far lower temperature coefficient of resistance and

Table IV.2. Area and volume specifications of calorimeter

Description	Material	Cell	Area/Volume	
Total calorimeter channel volume	Water		40	ml
Cell vapor volume	Air + vapor	1	59.5	ml
		2	49.4	ml
Cell surface area exposed to bulk solution	Glass		227	cm^2
Cell surface area exposed to vapor	Glass		37.2	cm^2
Mounting probe surface area exposed to vapor	Glass + Teflon		75.9	cm^2
Mounting probe surface area exposed to bulk solution	Glass	1	181	cm^2
		2	169	cm^2
Bulk solution electrical grounds	Pyrex, Pt, Hg, Cu, and polyethylene		18.1	cm^2
Titrant injection capillaries	Pyrex		9.1	cm^2
Bulk solution stirrers	Teflon		48.6	cm^2
Cell thermistors	Pyrex, Teflon, and epoxy		22.2	cm^2
Titrant thermistor, t_4	Pyrex, Teflon, and epoxy	1	24.1	cm^2

Table IV.2. (Continued)

Description	Material	Cell	Area/Volume
Hg reference thermometer	Glass and Hg	1	25.3 cm^2
Solid injector	Pyrex, Teflon, and silicone rubber	2	23.8 cm^2
Heat capacity balancing tube	Pyrex and Hg	2	13.2 cm^2
Trickle heaters	Pyrex, Cu, and epoxy		14.2 cm^2
Calibration heaters	Pyrex, Cu, and epoxy		19.4 cm^2

otherwise far superior to carbon resistors (140) were used as the resistance elements. The resistors used were TRW CEA-T9 RN553 30R1F, 30.1 ± 1%, 1/10 W, 200 VDC with a TCR of ± 25 ppm purchased from Allied Electronics Corp., Chicago, IL.

Actual resistances were determined by the Physics Instrument Services of Iowa State University. The current leads used were AWG #20 stranded copper vinyl covered wire noninductively twisted together. The current leads were placed within RG-59/U coaxial cable from which the center

conductor and polyethylene core insulation were removed. Measurement of the IR potential across the heaters was made at the instrument panel. The electrical leads to the heaters were shorter than 24 inches and IR drop in the leads was negligible. An aluminum box was used to mount all sockets for both calorimeter heaters and a standard resistance.

The standard resistance used is one of the metal film resistors cited earlier, which had a convenient value of 30.300 Ω. The standard resistance was mounted in an aluminum heat sink and coated with silicone heat transfer compound. All connections made to resistors, sockets, and banana jacks were silver soldered.

The trickle heater supply was built after the design of Stern and co-workers (154) adding an additional regulation step to improve stability.

The solid sample holder was made using a 16-mm long piece of 10-mm o.d. Pyrex tubing with a loose fitting Teflon plug for each end. A silicone rubber disc sealed the sample holder within a 13-mm o.d. Pyrex tube having a Teflon plunger fitted with a rubber O-ring.

The bulk solution was electrically grounded by a AWG #20 Pt wire spiral sealed into a 8-mm o.d. Pyrex tube. Electrical contact was made using a small drop of Hg into which the inner conductor of RG-59/U coaxial cable projected.

A Hg-filled NMR tube was placed in the reaction cell of the calorimeter to offset the heat capacity of the Hg bomb calorimeter thermometer in the reference cell of the calorimeter.

V. STEADY STATE AND DYNAMIC BEHAVIOR OF THERMISTORS

A. Experimental

1. Temperature sensitivity of NTC and PTC thermistors

Calibration of the bridge and amplifiers was made by substituting decade resistance boxes adjustable to ± 1 Ω for t_1 and t_2. Circuit parameters were $R_f = 1.0016 \times 10^6$ Ω and $e_+ = -e_- = 0.50000$ V to insure high sensitivity and a zero power approximation. The decade resistance boxes were calibrated by Physics Instrument Services of Iowa State University. NTC thermistor resistances were measured at approximately three-degree intervals in the range 0 - 48°C. Solution temperatures were read from a partial immersion Hg thermometer to ± 0.01°C. The Hg thermometer was calibrated at four points maintaining a stem temperature of 25.0 ± 0.5°C. The four points were: the ice point, 0.000°C; the NaCl - Na_2SO_4 - H_2O eutectic, 17.878°C (103); the Na_2SO_4 - H_2O eutectic, 32.383°C (103); and the freezing point of sublimed phenol, 40.85°C (155). The last reference point was given the least significance because of the difficulty of obtaining phenol which is free of cresols. Solution temperatures were measured by the Hg thermometer at a point 1-in from the thermistor bead.

The temperature control bath used in thermistor resistance measurements was a 10-l plastic tub filled with water and

resting on a magnetic stirrer. Temperature control for the bath involved circulation of water at 1 l/min from a 20-l Sargent thermostated bath controlled to ± 0.01°C through an immersed 50-ft coil of 0.5-in polystyrene tubing.

The isoperibol differential calorimeter used for measurement of circuit sensitivity ($e_{o,3}$ vs. T) consisted of two glass Dewars, matched in size and thermal characteristics, with stirrers and electrical resistance heaters. The stirrers were perforated Teflon disks with 1.27-cm radius and 3.18-mm thickness operating at 800 rev/min. The heaters were 30 Ω metal-film resistors coated with epoxy resin. This calorimeter was also used for thermometric titrations and a complete description was given in Section IV.C.2.

The temperature sensitivity of the thermometric circuit was measured using only one calorimeter cell after replacing one thermistor in the bridge by a 10,088 ± 1 Ω metal-film resistor. This resistor was mounted on a heat sink in the junction box. A 250-ml volume of deionized water in the cell was electrically heated and T_b and the corresponding value of $e_{o,3}$ measured. All potentials were measured with a Corning Digital 112 pH meter in the mV mode or a Leeds and Northrup K-2 potentiometer readable to ± 5 μV. The Corning meter was calibrated with the K-2 potentiometer against an unsaturated Weston cell with a potential of 1.01891 absolute volts at 25°C. The Weston cell was calibrated 2 October 1973 by Ames

Laboratory USAEC at Ames, Iowa, against four parallel Weston cells standardized periodically against a National Bureau of Standards cell.

Solution temperatures for determination of circuit sensitivity were measured with a Parr type 1622, bomb calorimeter thermometer (5E2808) which was calibrated 23 May 1973 by Parr Instrument Co. against a National Bureau of Standards Pt resistance thermometer. The calibration was made with full immersion and stem corrections for partial immersion in this work were made according to the procedure of Swindells (156).

2. Thermistor time constant

Thermistor response to a step change in temperature and the thermal time constant were determined by two methods. Method 1: The thermistor was heated electrically after the manner of Papadopoulos (122) and the return to equilibrium temperature followed. The thermistor was heated electrically as part of a conventional Wheatstone bridge. A 2KΩ 10-turn potentiometer adjusted to yield equal resistances as measured from the center tap to either end was used to form the fixed arms of the bridge. Bridge current for time constant measurements was provided by a 1.346 volt Hg cell in series with a 10KΩ resistor connected to the center tap of the 2KΩ potentiometer. Method 2: The thermistor probe was plunged into a solution at a temperature other than ambient according to the method of Pharo (157). The method of Pharo starts with the

dry thermistor suspended in air at ambient temperature, in this work 27.0 deg C, followed by instant immersion in equilibrated water at temperatures removed from ambient. Plotted temperatures are the final water temperatures measured with a separate calibrated Hg thermometer near the thermistor. All thermal time constant measurements according to Methods 1 and 2 were made using 250-ml deionized water in Dewars equivalent to the calorimeter Dewars. The same rotational speed used in thermistor temperature sensitivity measurements was used in Methods 1 and 2 of thermistor time constant measurement.

A separate study of thermistor time constant dependence on stirrer rotational velocity was made at velocities of 45-207.3 rad/sec with the initial air temperature being 22 deg C and the water temperature 25.5 deg C. A smooth Teflon disc with a thickness of 3.50-mm and a radius of 1.63-cm was used in this study. The recorder chart rate used in Methods 1 and 2 was 12-in/min and a chart scale of either 10 or 25-mV/in was used in these studies. Bridge output was monitored by a Heath EU-20W recorder without damping.

Measurement of time constant vs. heating rate was made with unperforated disk stirrers of different radii at velocities of 45.0-207.3 rad/sec. Rotational velocities were determined by a Sanborn 7701 oscillograph. Controlled heating rates were provided by a Sargent Coulometric Current Source (Model IV) connected to the resistance heater in the cell.

3. Thermistor dissipation constant

Steady-state measurements of thermistor resistance as a function of rotational velocity under low and high power conditions provided data for calculation of the thermistor dissipation constant. Bridge current for high power conditions was supplied by a 77 ampere-hour, 6 volt lead storage battery connected to the center tap of the 2KΩ potentiometer.

4. Thermistor noise

Circuit noise and drift were measured after substitution of 10-KΩ metal-film resistors in positions t_1 and t_2. Other circuit parameters were $e_+ = e_- = 1.00000$ V, $R_f = 1.0016 \times 10^6$ Ω and $C_f = 0.047$ μF. $e_{o,3}$ vs. time was recorded for 33 hr on the Heath recorder at a sensitivity of 1.130 mV/in. The recovery time of the circuit to application of a 100 mV step function to the output of OA-1 was measured with a Hewlett Packard 122A oscilloscope. Circuit transients were recorded on Polaroid Type 107, B&W, ASA 3000 film with a Hewlett Packard Model 196B Oscilloscope Camera attached to the oscilloscope. A sensitivity of 0.1 volt/cm and scan rates of 100 msec/cm or 200 msec/cm were used to record all transient response data.

B. Results and Discussion

1. NTC thermistor material parameters

The value of β_t for thermistor t_1 and t_2 (both NTC) were determined at the standard temperature reference points cited earlier. Plots of β_t vs. T_t were nearly linear and were analyzed by a linear least-squares computer program. The results were:

$$\beta_1 = 3.3816 \pm 0.0373\ T(\text{deg K}) + (2.5506 \pm 0.0111) \times 10^3 \text{ deg K}$$

$$\beta_2 = 3.3378 \pm 0.0426\ T(\text{deg K}) + (2.5634 \pm 0.0127) \times 10^3 \text{ deg K}$$

The uncertainties given are deviations for 95% confidence. At 25.00 deg C,

$$\beta_1 = 3558.8 \pm 1.5 \text{ deg K}$$

$$\beta_2 = 3558.5 \pm 1.7 \text{ deg K}$$

Thermistor resistance data was obtained in the temperature range 24.929 - 25.080 deg C and dR_t/dT_t calculated by Equation A.1. Results are given in Table V.1. Values of Z_t and dZ_t/dT_t at 25.00 deg C were approximated from resistance data obtained at 24.08 deg C and 26.03 deg C. The results are included in Table V.1. The approximate value of dR_t/dT_t from Equation A.4 was used for the remaining work because all temperature intervals were 2 deg C or less.

A strong criticism of differential thermometric titrimetery is the impossibility to date of obtaining identical sensitivities for two thermistors. The origin of this problem can be seen by noting the differences in material parameters

Table V.1. Thermistor material parameters at 25 deg C

Thermistor	R_t	dR_t/dT_t (Eq. A.3) (deg K)	Z_t	dZ_t/dT_t (deg K)	dR_t/dT_t (Eq. A.4) (deg K)
$t_{NTC,1}$	10,001 ± 1Ω	$-3.9582 \times 10^2\Omega$	0.06545Ω	$-7.092 \times 10^4\Omega$	$-4.0035 \times 10^2\Omega$
$t_{NTC,2}$	9,997 ± 1Ω	$-3.9459 \times 10^2\Omega$	0.06565Ω	$-6.969 \times 10^4\Omega$	$-4.0031 \times 10^2\Omega$

for even the closely matched thermistors in Table V.1. An experimental error curve ($e_{o,3}$ vs. T_b) is shown in Figure V.1 for the two thermistors described in Table V.1. The slope of the curve is very small except at temperatures considerably below 25 deg C and, presumably, greater than 45 deg C assuming the parabolic shape for the error curve predicted by Equation A.7. Linear response can be obtained by adjustment of e_+ relative to e_-. Following the procedure similar to that for the NTC-PTC hybrid in Equations A.11-A.13, it can be demonstrated that

$$\frac{e_-}{e_+} = \frac{R_1 \beta_2^2}{R_2 \beta_1^2}$$

The calculated value of e_-/e_+ for linear response in this case is 1.00023 and the experimental value is 1.000185.

2. NTC, PTC, and NTC-PTC circuit temperature sensitivity

Attempts to increase temperature sensitivity of a thermistor bridge circuit have involved choice of thermistors with larger values of R_t because of the associated increase in β_t (158). The signal-to-noise ratio suffers, however, because the thermistor noise is proportional to R_t^2. Sensitivity can be increased by use of larger bridge voltages as shown in Equation A.7. For small temperature changes (< 1 deg C) when $e_- = e_+ = e$

$$\Delta e_{o,3}/\Delta T_b = -(R_f e/R_t)(\beta_t/T_t^2)$$

Figure V.1. Error curve for thermistor t_2 vs t_1

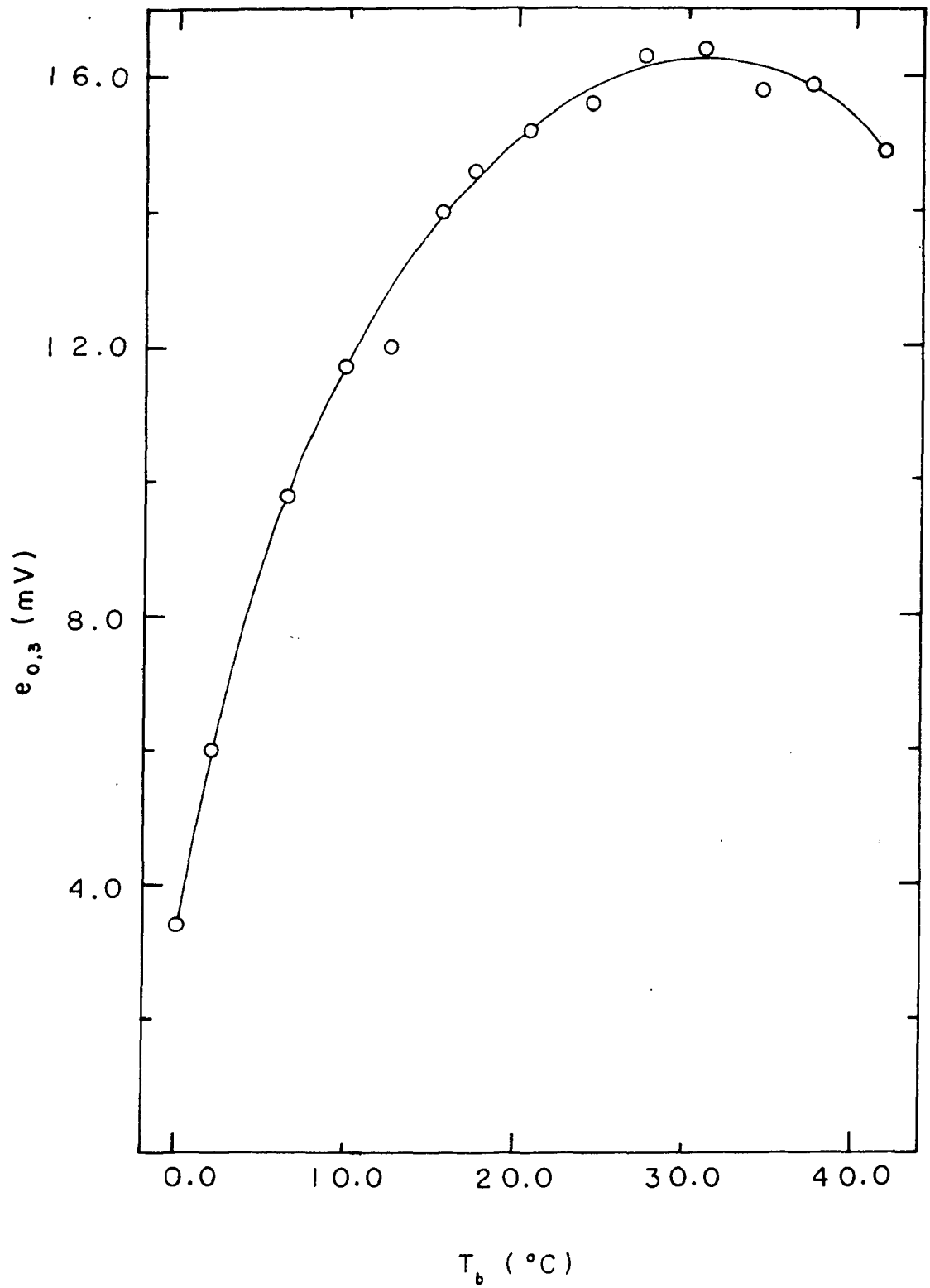
16.0
12.0
8.0
4.0
$e_{0,3}$ (mV)
0.0
10.0
20.0
30.0
40.0
T_b (°C)

Experimental values of $\Delta e_{o,3}/\Delta T_t$ are given in Table V.2 for a NTC thermistor. The results at e = 0.5 V agree with theory to 1 ppt. For bridge voltage > 0.5 V, self-heating of the thermistor was significant and for our rate of stirring, $T_t \neq T_b$. Hence, R_t was less than in the absence of self heating and apparent sensitivity increases. The results in Table V.2 at 1.0 V are in good agreement with theory when correction is made for self-heating.

Table V.2. Sensitivity data for $t_{NTC,1}$

N_s = 540 rev/min			C_f = 0.047 μf		
250 ml H_2O			r_s = 1.27 cm		
Run	Points	e	R_f	ΔT_b	
1	11	0.50000 V	100.04 KΩ	0.497°C	200.3 ± 0.1 mV/°C
2	25	0.50000 V	100.04 KΩ	1.188°C	200.6 ± 0.1 mV/°C
3	20	1.00001 V	1.0016 MΩ	0.490°C	4,005 ± 2 mV/°C
4	40	1.00001 V	1.0016 MΩ	1.102°C	4,027 ± 1 mV/°C

The temperature sensitivity for several thermistor configurations was determined over a 2-degree interval centered at 25 deg C as shown in Figure V.2. The data was fitted to cubic

Figure V.2. Temperature sensitivity of thermistors

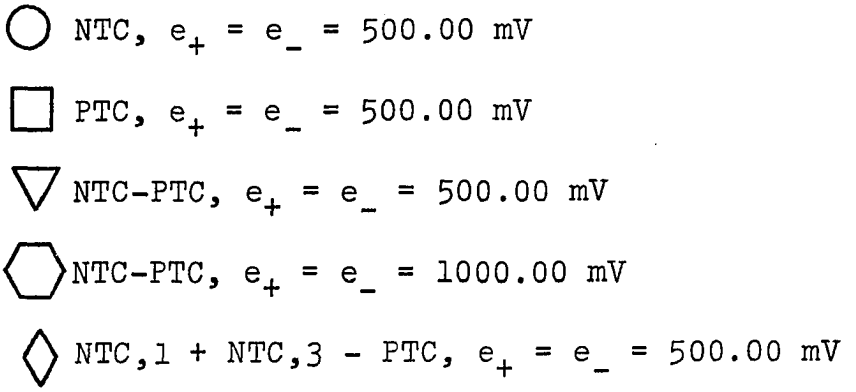

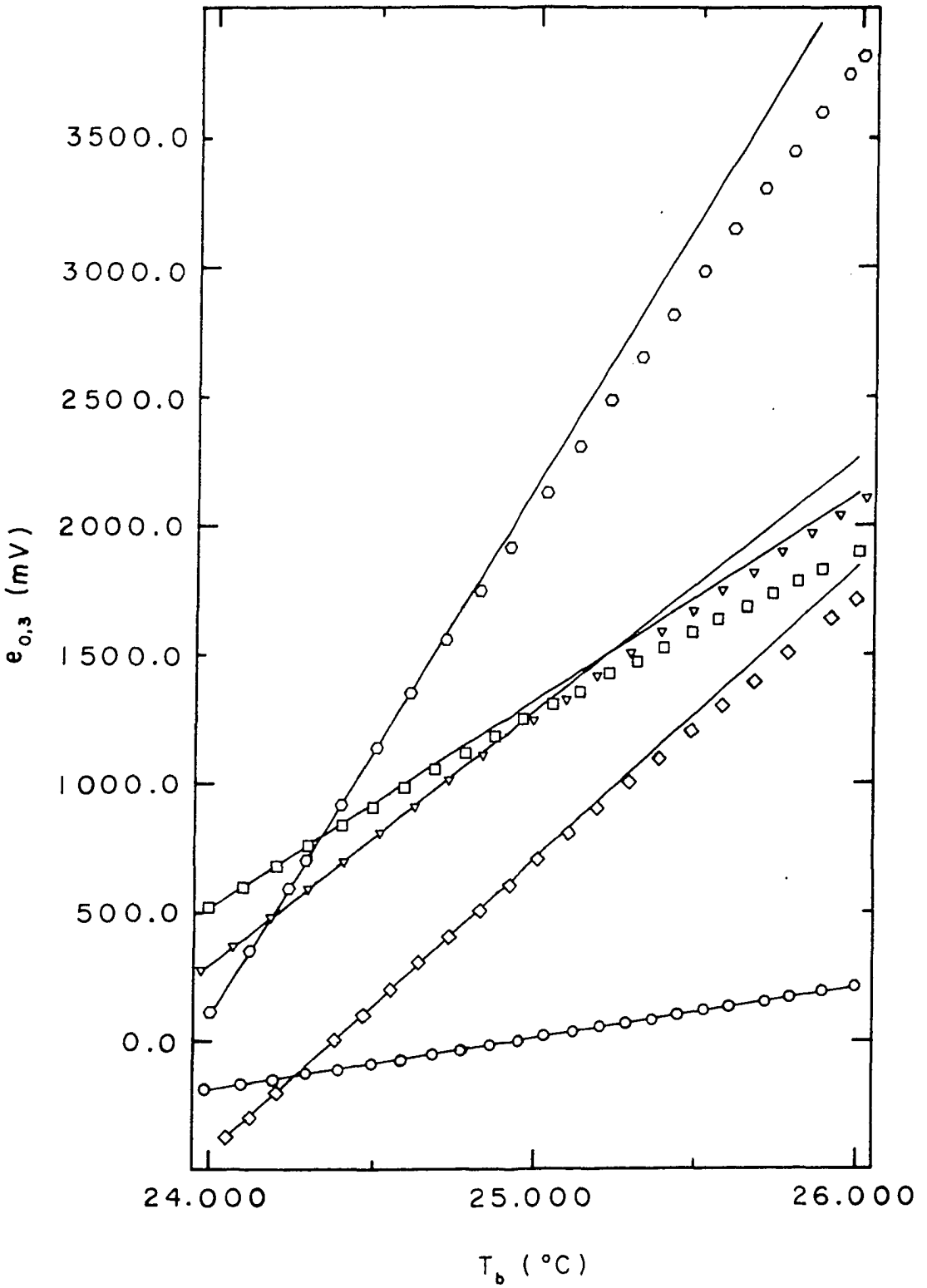
3500.0
3000.0
2500.0
2000.0
1500.0
1000.0
500.0
0.0
$e_{0,3}$ (mV)
24.000
25.000
26.000
T_b (°C)

equations for the purpose of comparing changes in linearity and sensitivity with temperature. The results are summarized in Table V.2.

For a small ΔT, the sensitivity is most easily approximated by the value of the coefficient b in Table V.3. The sensitivity for an NTC-PTC hybrid is much greater than for a single NTC thermistor. A comparison of the sensitivity of the circuit developed in this work with the sensitivities for several dc circuits described in the literature is given in Table V.4. The sensitivity of the new circuit is the greatest of any reported to date and is in agreement with the theoretical prediction by Equation A.7.

3. Theoretical time constants

The calculations indicated by Equations B.11, B.12, B.32 and B.40 were programmed in WATFIV and executed on an IBM 360-5 digital computer at the Iowa State University Computation Center. A listing of the program is given in Appendix D.1. Although exact specifications of thermistor composition are proprietary information, general information is that NTC thermistors are made of Mn_3O_4 and PTC thermistors are of Sr-doped $BaTiO_3$. Properties of these materials are given in Table V.5 with physical dimensions for the thermistor mountings. The calculated and measured time constants (by Method 2) for $t_{NTC,1}$ as a function of N_s with r_s = 1.63 cm are plotted in Figure V.3.

Table V.3. Cubic equation for temperature response (161, 162)

$$e_{o,3}\ (mV) = a + bT + cT^2 + dT^3$$

R_f = 100.04 KΩ N_s = 540 rev/min

C_f = 0.047 μf r_s = 1.27 cm

250.00 ml H_2O

Thermistor	e	a(mV)
$t_{NTC,3}$	0.50000 V	1.68507×10^2
t_{PTC}	0.50000 V	-1.03472×10^5
$t_{NTC,3} - t_{PTC}$	0.50000 V	-5.42410×10^4
$t_{NTC,3} - t_{PTC}$	1.00000 V	-7.92404×10^4
$(t_{NTC,1} + t_{NTC,3}) - t_{PTC}$	0.50000 V	-1.61952×10^4

b(mV/°K)	c(mV/°K^2)	d(mV/°K^3)
-3.36247×10^{2}	1.807513×10^{1}	-1.95253×10^{-1}
9.68844×10^{3}	-2.99636×10^{2}	3.18728
3.46573×10^{3}	-4.65991×10^{1}	-1.29459×10^{-1}
3.10707×10^{3}	6.76171×10^{1}	-2.47241
1.46028×10^{3}	1.56476×10^{2}	-2.81641

Table V.4. Comparison of sensitivity for several dc circuits

Reference	Bridge Voltage	Thermistor Resistance	Thermistor Power	Circuit Amplification	Sensitivity
159	12.000 V	100 KΩ	not given	not given	139.5 mV/deg C
96	2.037 V	5-5 KΩ in parallel	1037 μ watts	100	3875 mV/deg C
160	1.35 V	10 KΩ	1.1 μ watts	not given	417 mV/deg C
this work ($t_{NTC,1}$)	1.00000 V	10 KΩ	100 μ watts	100	4005 mV/deg C

Table V.5. Thermistor data

Mn_3O_4: ρ_t = 4.21 g/cm^3 (163)

λ_t = 1.76 x 10^{-2} cal/cm sec deg C (163)

C_t' = 0.1547 cal/g deg C (163)

C_t'' = 2.70 x 10^{-2} cm^2/sec (calculated)

$BaTiO_3$ (1.5% Sr doped):

ρ_t = 5.03 g/cm^3 (164)

λ_t = 1.37 x 10^{-2} cal/cm sec deg C (164)

C_t' = 0.105 cal/g deg C (165)

D_t = 2.59 x 10^{-2} cm^2/sec (calculated)

Epoxy resin:

λ_e = 5.0 x 10^{-4} cal/cm sec deg C (166)

Dimensions:	$t_{NTC,1}$	$t_{NTC,2}$	$t_{NTC,3}$	t_{PTC}
r_t (x 10^1 cm^{-1})	1.45	1.64	0.85	1.88
x_e (x 10^2 cm^{-1})	6	6	6	12
x_s (cm)	0.7	0.7	1.2	1.2

Figure V.3. Time constant of t_1 as a function of N_s

Calculated

Experimental

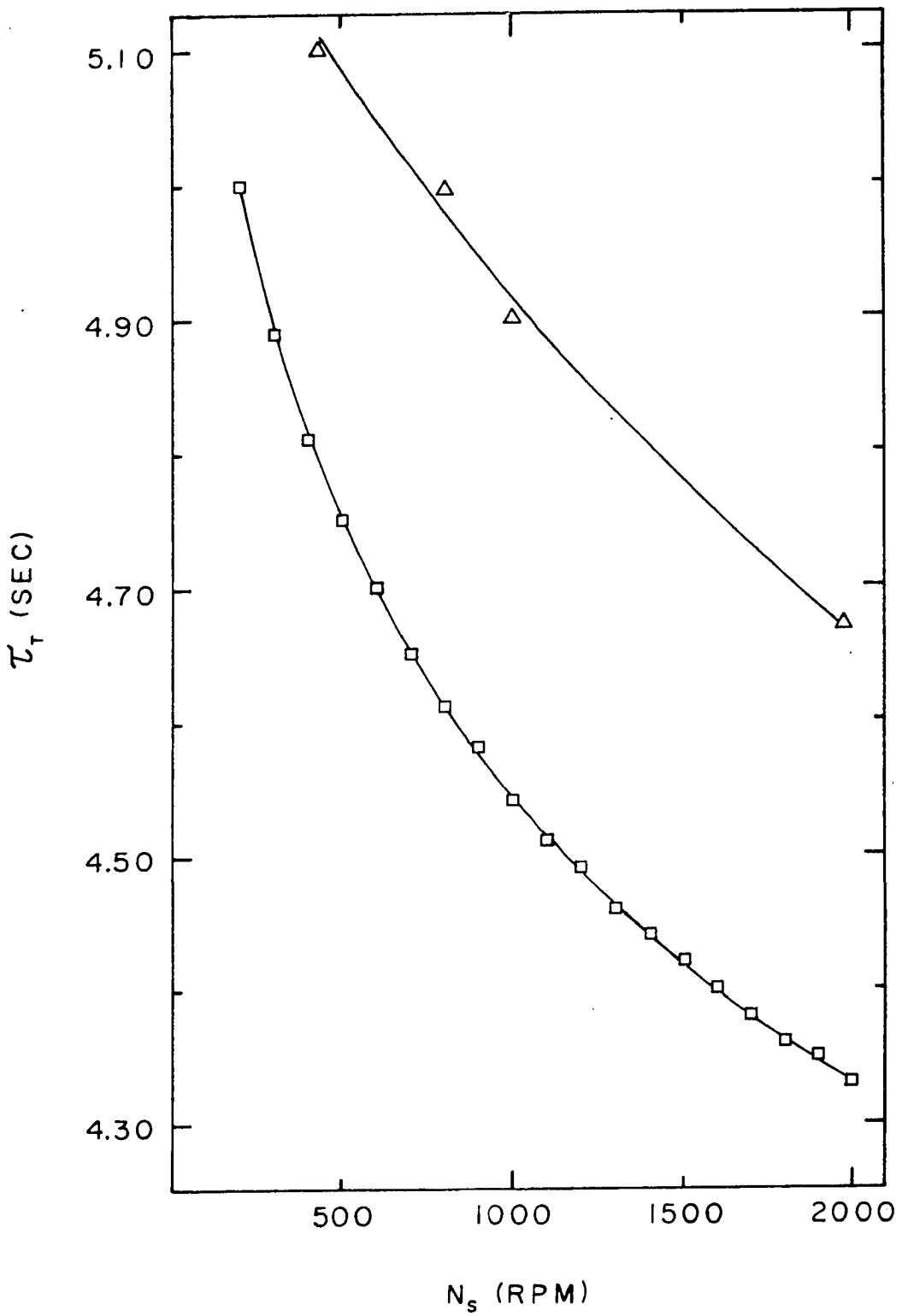
5.10
4.90
4.70
4.50
4.30
τ_r (SEC)
500
1000
1500
2000
N_s (RPM)

From Equations B.11 and B.12, δ_t is proportional to r_t and τ_t is proportional to r_t^2. This has been demonstrated for bead thermistors (161). It is beyond question that an epoxy coating on the thermistor will change both δ_t and τ_t. The usual coating material is glass which has a thermal conductivity about 4x that of most plastics. The effects of various thermistor coatings were experimentally shown by Rogers and Sasiela (162). Experimentally measured values of τ_t for a NTC and PTC thermistor are given in Figure V.4 as a function of temperature. It is interesting that the plots are mirror images of dR_t/dT_t for both thermistors as predicted by Equation B.23.

Careful examinations of Equations B.5 and B.6 reveals that the temperature difference across the thermistor material and across the epoxy plus thermal boundary layers can be calculated. Such calculations show that the predominant difference is across the epoxy plus thermal boundary layer; the ratio of difference is 35:1.

The dependence of τ_t upon γ_b as predicted by Equation B.19 was studied by heating the calorimeter bulk solution at four rates. The experimental results are given in Figure V.5. The values of curve intercepts were those obtained in a study of τ_t $\underline{vs}$ N_s for a step change in the temperature of the fluid surrounding the thermistor. Differences in the intercepts in Figure V.5 as determined by Method 2 in comparison to those from electrical heating experiments is due to the time of

Figure V.4. NTC and PTC thermistor time constants as a function of T

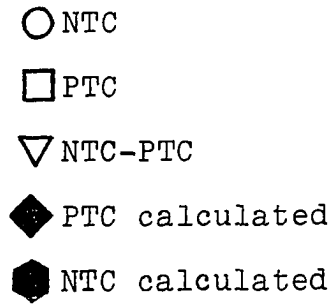

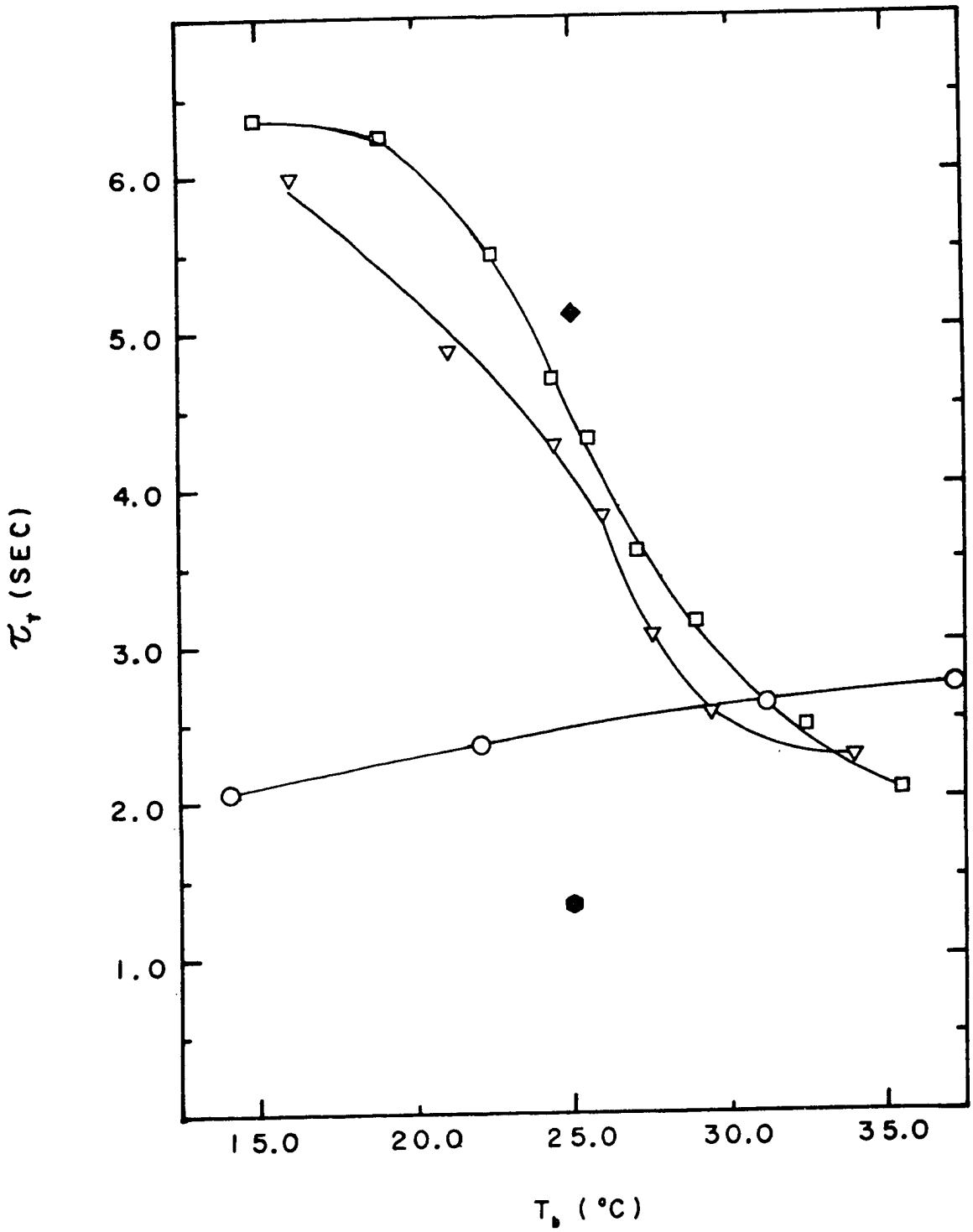
6.0
5.0
4.0
3.0
2.0
1.0
τ_r (SEC)
15.0
20.0
25.0
30.0
35.0
T_b (°C)

Figure V.5. Time constant of t_1 as a function of $1/\gamma_b$

N_s = 430 rev/min and r_s = 1.63 cm

○ electrical heater above the plane of the stirrer

□ electrical heater in the plane of the stirrer

N_s = 1000 rev/min and r_s = 1.63 cm

▽ electrical heater above the plane of the stirrer

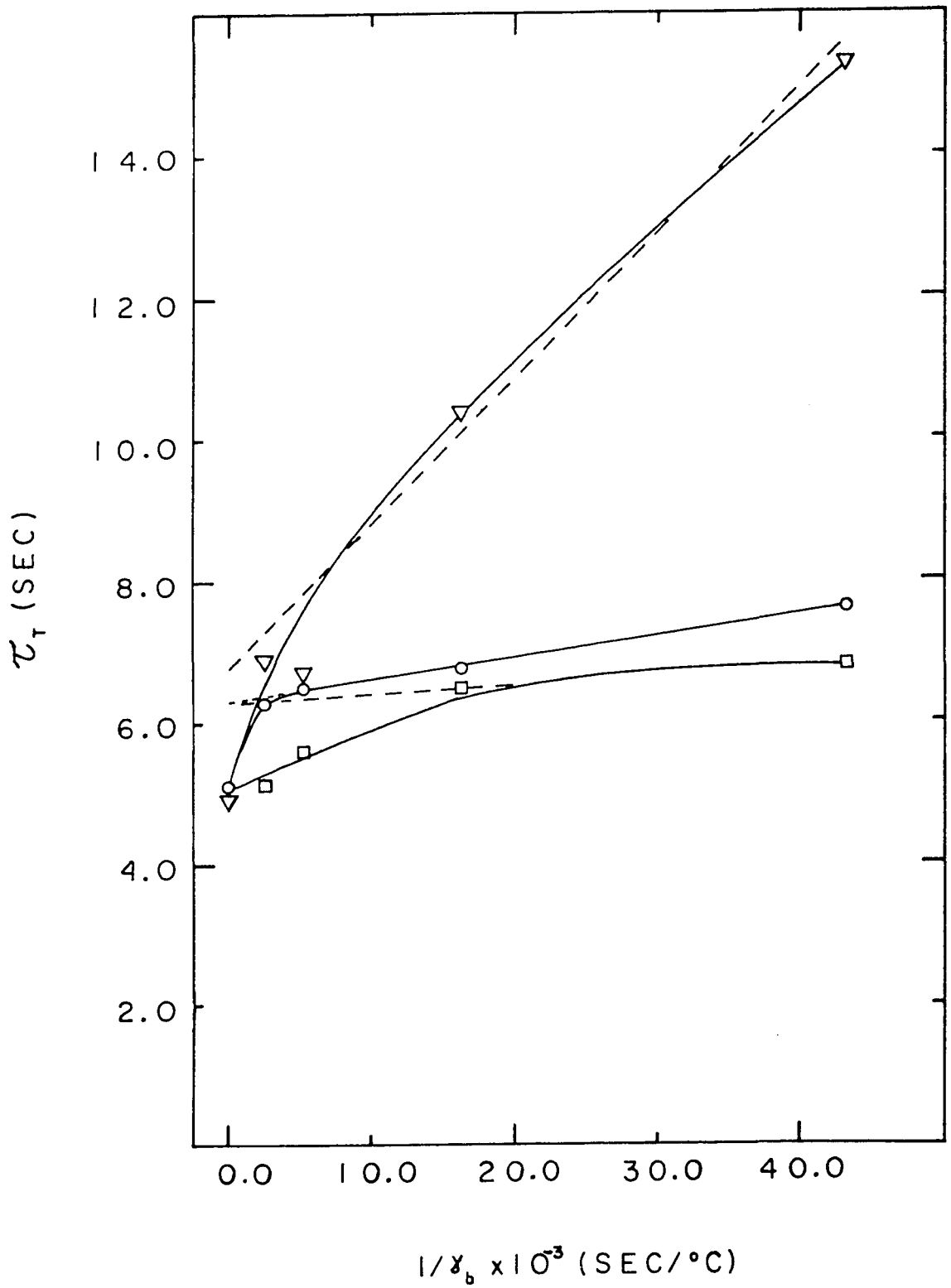
14.0
12.0
10.0
8.0
6.0
4.0
2.0
τ_r (SEC)
0.0
10.0
20.0
30.0
40.0
$1/\gamma_b \times 10^{-3}$ (SEC/°C)

fluid mixing and the time constant of the electrical heater. Although not shown in Figure V.5, the predicted decrease in the slope of τ_t vs $1/\gamma_b$ plot with increase of P_t was verified experimentally. Placement of the electrical heater affects the relationship of τ_t to $1/\gamma_b$ since incomplete mixing leads to underdamping of the system response. Larger values of N_s lead to overdamping which produces increased slope as seen in Figure V.5 for N_s = 1000 rev/min. More will be said concerning heater placement in a later section.

4. Theoretical dissipation constants

The dissipation constant, δ_t, measured for an NTC thermistor as a function of N_s showed no variation for $400 < N_s < 2000$ rev/min with r_s = 1.27 cm. Calculated and measured values of δ_t for a PTC thermistor are plotted in Figure V.5 as a function of N_s. Agreement between experimental and predicted values is good considering many sources of error neglected in the theoretical development of which assumptions regarding stem conduction is major. Illustration of stem effects and thermistor leads is shown clearly in Figure V.6. The ordinate of Figure V.7, $\log(1/(1 - \Delta T/\Delta T_\infty))$, can be readily derived from Equations B.5 and B.6. Region A shows the effect of the high thermal conductivity of the thermistor Cu leads when the thermistor is electrically heated. Region B shows the combination of the thermistor bead material and epoxy coating. Region C shows the effect

Figure V.6. NTC and PTC thermistor dissipation constants as a function of N_s

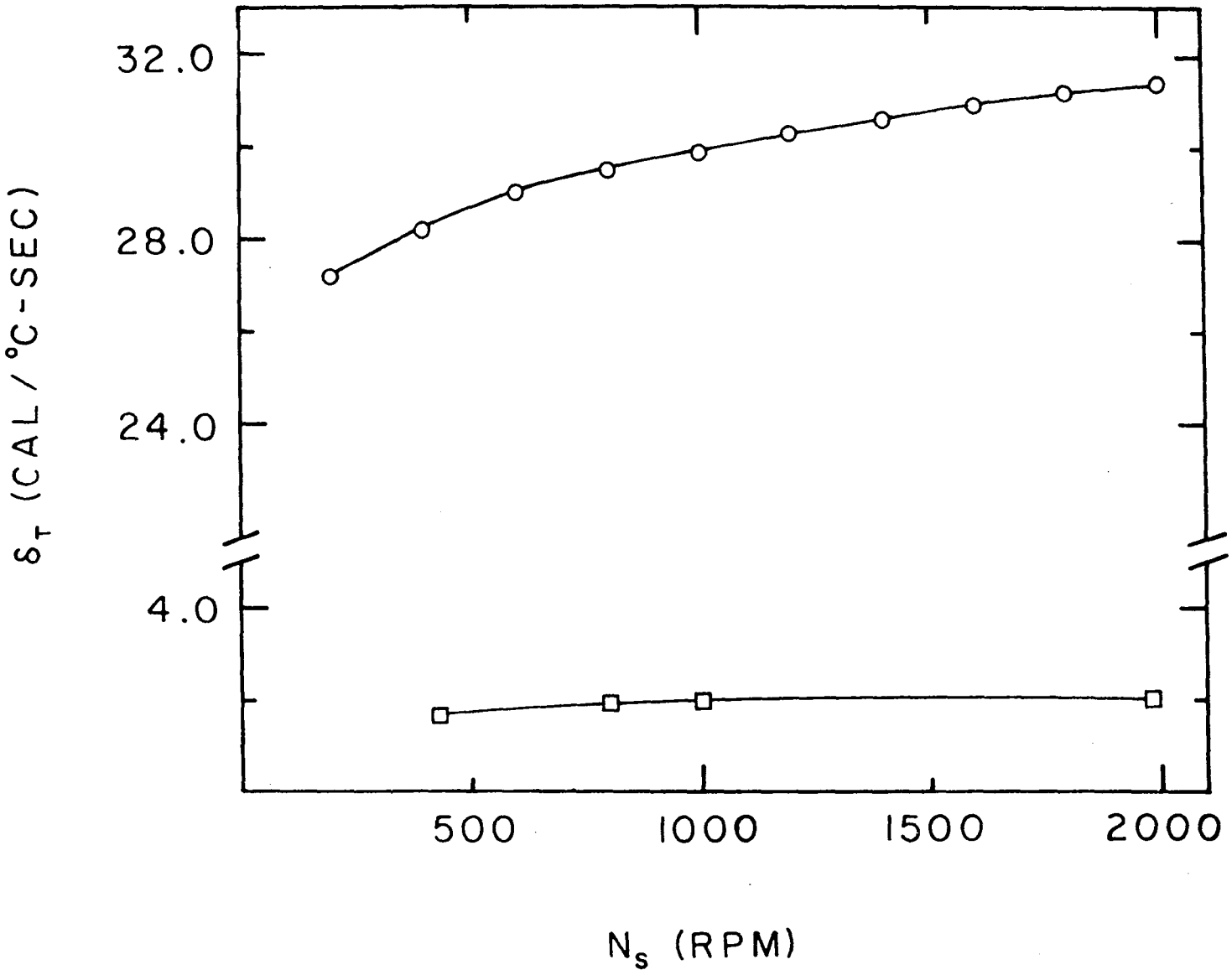
32.0
28.0
24.0
4.0
δ_T (CAL / °C-SEC)
500
1000
1500
2000
N_s (RPM)

Figure V.7. Temperature ratio of thermistor t_1 as a function of time for electrical and environmental heating

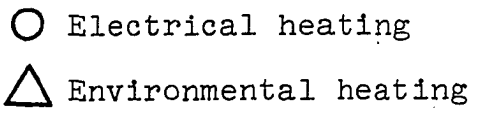

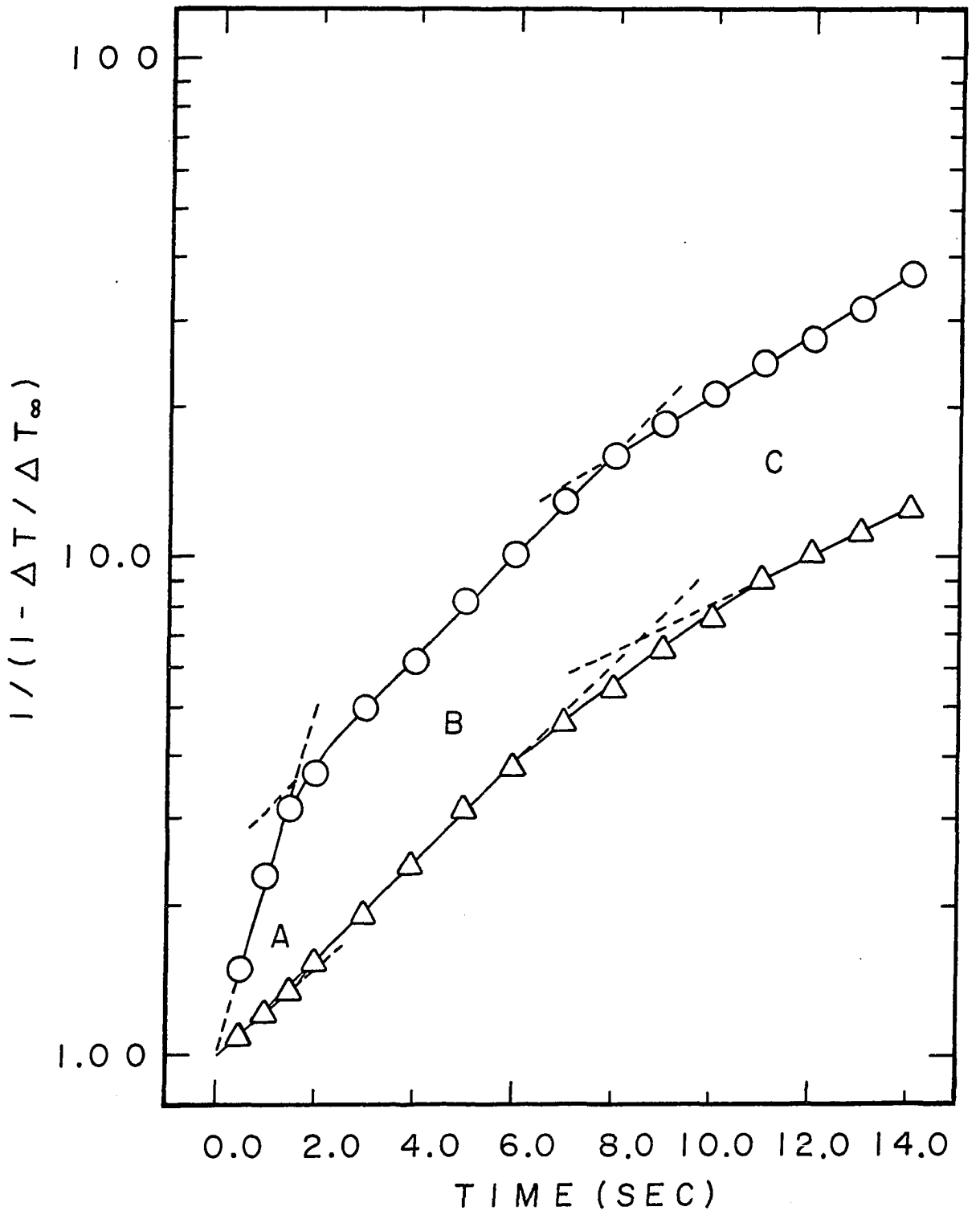
100
10.0
1.00
1/(1-ΔT/ΔT∞)
A
B
C
0.0
2.0
4.0
6.0
8.0
10.0
12.0
14.0
TIME (SEC)

of the thermistor stem, that of heat loss from the thermistor bead.

5. Theoretical thermistor noise

a. Power supply stability The power supply described has required little adjustment over a one-year period of successful operation. Typical stability was determined by measurement of e_+, e_- and $|e_+ - e_-|$ at irregular intervals over a two-week period with at least one measurement per working day. The results fitted by linear least squares are:

$$e_+ = 1{,}000.0 \pm 0.02 \text{ mV} - 0.0025 \pm 0.0021 \text{ mV/day}$$

$$e_- = 1{,}000.2 \pm 0.02 \text{ mV} - 0.0010 \pm 0.0021 \text{ mV/day}$$

$$|e_+ - e_-| = 0.175 \pm 0.007 \text{ mV} + 0.003 \pm 0.001 \text{ mV/day}$$

With the bridge connected and 10-KΩ metal film resistors replacing the thermistors, the peak-to-peak noise and drift over a 24 hr period was 10 ppm for a room temperature constant to ± 1 deg C. Recovery time from a transient voltage applied to the output of OA-1 was 0.3 sec for C_f = 0.047 μF. Circuit B had a peak-to-peak noise of 7 ppm for C_f = 2μF. Distinct advantages of this circuit are the absence of power supply loading and easy adjustment of thermistor bridge sensitivity by adjustment of potentiometer P1 (see Figure III.1).

b. Circuit noise Uncertainty (noise) in the temperature measurement for various thermistors and thermistor combinations is given in Table V.6. The value of ΔT_n was calculated from experimental data by the PARD convention (167)

Table V.6. Thermistor circuit noise

Literature Values:

Reference	Bridge Voltage	Amplifier Damping	ΔT_n
96	2.037 V	3 sec	50 μdeg C
158	12.000 V	not given	30 μdeg C

This work:

r_s = 1.27 cm

N_s = 540 rev/min

C_f = 0.047μF

Thermistor	R_f	R_fC_f	e	ΔT_n
t_{NTC}	100.04 KΩ	0.005 sec	0.50000 V	125 μdeg C
			1.00000 V	125 μdeg C
t_{PTC}	100.04 KΩ	0.005 sec	0.50000 V	94 μdeg C
			1.00000 V	94 μdeg C
$t_{NTC,3} - t_{PTC}$	100.04 KΩ	0.005 sec	0.50000 V	50 μdeg C
			1.00000 V	60 μdeg C
$(t_{NTC,1} + t_{NTC,3}) - t_{PTC}$	100.04 KΩ	0.005 sec	0.50000 V	43 μdeg C
$t_{NTC,1}$	1.0016 MΩ	0.05 sec	1.00000 V	25 μdeg C

and represents the uncertainty in T_b for an isothermal solution as determined from the mean of $e_{o,3}$ over a 5 min recording period. It is interesting to note the successive decrease in ΔT_n as the number of thermistors in the circuit is increased. Thermistors are generally accused of being noisy. The predominent sources of noise determined in this research are stray electrostatic and electromagnetic pickup by the lead wires; the precaution of double-shielding had a noticeable benefit to decrease ΔT_n. Maximum noise levels determined by recording $e_{o,3}$ for a 1 hr period are about 3x the values in Table V.6 which is in agreement with the observation of LaForce, et al. (99).

Calculations using parameters listed were used in the numerical evaluation of Equation B.64 for circuit A:

T_1 = 298 deg K, ΔR_1 = 3.2 Ω, N_s = 600 rev/min,

$\rho_1 = h_1 r_1 = 2.13 \times 10^{-2}$ cal/cm-sec-deg C,

$\sigma_{\rho_1} = 5.72 \times 10^{-7}$ cal/cm-sec-deg C assuming σ_{ω_s} = 5 ppt,

τ_1 = 5.0 sec, $\tau_{b.1}$ = 4.8 sec, $\tau_{o,1}$ = 0.199 sec,

τ_m = 1.08 sec, f_1 = 0.01 Hz, f_2 = 20 Hz,

arc $\tan(2\pi\tau_m f_2)$ = 1.57, arc $\tan(2\pi\tau_o f_2)$ = 1.53.

The value of $e_{-,rms}$ was calculated from the noise spectrum plot given by Motchenbacher and Fitchen (115) for the 741C operational amplifier. For frequencies <1000 Hz, the noise spectrum plot shows that e_n of the amplifier is predominantly 1/f in character. By extrapolation for frequencies <10 Hz,

$e_{-,rms}$ was calculated to equal 6.4×10^{-7} volt/$\sqrt{Hz}$ for 0.01 to 20 Hz. Values must be assumed for $\gamma_{b,1,rms}$ and $T_{1,rms}$ since quantitative theory is still lacking. Hence, the assumptions of $\gamma_{b,1,rms} = 1.3 \times 10^{-9}$ deg C/sec and $T_{1,rms} = 1 \times 10^{-6}$ deg C although reasonable are only best estimates of these parameters at this time.

The numerical evaluation of Equation B.64 yields:

$$I_{1,n} = [\{(2.50 \times 10^{-25})(0.0482)(0.110 - 0.002) + (2.62 \times 10^{-25})(1.53)\} + \{(6.63 \times 10^{-21})(0.0482)(0.220 - 0.004) + (4.78 \times 10^{-22})(0.220 - 0.004) + (8.96 \times 10^{-17} + 1.06 \times 10^{-15})(0.101 - 0.006) \cdot (1 \times 10^{-12})\} e_-^2 + \{(2.50 \times 10^{-19})(0.0482)(0.110 - 0.002)\} e_-^4 + \{(1.76 \times 10^{-22})(0.691 - 0.013) + (1.46 \times 10^{-12} + 1.74 \times 10^{-10})(0.637 - 0.068) \cdot (1 \times 10^{-12})\} e_-^6]^{\frac{1}{2}}$$

$$I_{1,n} = [4.02 \times 10^{-25} + 1.74 \times 10^{-22} e_-^2 + 1.36 \times 10^{-21} e_-^4 + 2.19 \times 10^{-22} e_-^6]^{\frac{1}{2}}$$

In this work, $e_- = 1.00000$ volt except where noted and accordingly, $I_{1,n} = 4.19 \times 10^{-11}$ amp. I_f equals I_{in} for OA-3 and $e_{o,n} = 4.19 \times 10^{-5}$ volt (rms). The definition that p-p noise is 6.6 times rms noise was used although a standard

definition seems to be lacking (115, 127). Hence, $e_{o,n}$ (p-p) = 0.28 mV for thermistor t_1 from the theory developed in Section III.B.1. Calculation of the total thermometric circuit noise proceeds from Equations B.64 and B.65 assuming that both thermistors t_1 and t_2 contribute equally to the total circuit output. Using the measured value of amplifier noise for OA-3 of 3.03×10^{-11} amp (rms), Equation B.65 yields $I_{o,n} = 5.5 \times 10^{-11}$ amp (rms) and $e_{o,n}$ (p-p) = 0.37 mV which corresponds to a temperature noise of 92 μdeg C. Comparison to the measured value cited earlier of 75 μdeg is excellent considering the assumptions made in the theoretical treatment and difficulty of experimental measurement of circuit noises. The theoretical S/N equals approximately 110 for a temperature change of 0.01 deg C when the temperature change occurs over a time span of 100 seconds.

Theoretical noise calculations for Circuit B using the same procedure as above for N_s = 1000 rev/min and r_s = 1.63 cm yields:

$$I_{1,n} = [4.04 \times 10^{-25} + 9.36 \times 10^{-22}\ e_-^2 + 3.22 \times 10^{-22}\ e_-^4 + 2.26 \times 10^{-22}\ e_-^6]^{\frac{1}{2}}$$

and $T_{o,n}$ (p-p) = 97 μdeg C. The measured value of 90 μdeg C was in closer agreement with the theoretically derived value presumably because of a more closely defined value of e_n for OA-1 and OA-2 in Circuit B. The larger size of $T_{o,n}$ for Circuit B was due to the increase in N_s and r_s which increased

the turbulence around the thermistor bead. The factor of 3 found by LaForce and confirmed in this work is readily seen in Equation B.64, since when the lower frequency f_1 changes by a decade, $I_{1,n}$ changes by 3.16. The present study confirmed the conclusion of Bowers and Carr (127) that the temperature noise of thermistors is on the order of 5-15 μdeg (rms) for DC systems. However, two new conclusions proceeded from this work, namely, the use of several NTC thermistors in a NTC-PTC hybrid thermistor probe reduced the size of $T_{o,n}$ (Table V.6), and concurrently, the S/N also increased for such probes, since the temperature sensitivity increased. The S/N for the hybrid combination of two NTC thermistors and one PTC thermistor was approximately 235 (calculated as above) or twice that of a NTC thermistor alone.

VI. STEADY-STATE AND DYNAMIC BEHAVIOR OF AN ELECTRICALLY HEATED FLUID CALORIMETER

A. Introduction

The design and application of calorimeters has too frequently been approached in an empirical manner. Evaluation was then only possible after construction of the entire calorimeter. This approach is expensive and time consuming and progress is slow. The theoretical model of the temperature response of the stirred fluid in a cylindrical calorimeter during electrical heating was derived in Section III.B.2. This section describes some new techniques which were developed for this dissertation which should enable workers to calculate certain parameters before construction of a calorimeter.

B. Experimental

1. Heat loss moduli

Since no method is described in the literature for selection of matched Dewar cells on the basis of thermal characteristics for use in differential calorimetry, a simple procedure was devised based on measurement of the cell heat-loss modulus. Each of ten Dewar flasks was filled with 250-ml of deionized water at ambient temperature (23 - 25 deg C) and a Beckman thermometer centered in a #12 rubber stopper was placed in the water. After equilibration for 20 - 30 min, the Dewar was placed in a heated mineral-oil bath (39 - 41 deg C).

The temperature of the Dewar contents was measured a 1-min intervals for 30 min. The water was not stirred during the procedure. The heat-loss moduli for the cells were calculated from the heating curve by the method of Gunn (168).

The effect of stirring and the calorimeter head on the heating curve was determined as described above. A single Dewar flask was selected with $k = 1.2 \times 10^{-3}$ min^{-1}. The thermometer was inserted in the head through a port vacated by removal of a thermistor probe.

The overall heat-loss modulus of the reference cell for the assembled differential calorimeter was determined by two methods. Method A: The procedure of Swietoslawski (169) with temperature measurements made over a total time of 4.5×10^{4} sec. Method B: The procedure of Gunn (168) as part of a determination of $\underline{C}_{w}$.

2. Heat capacity of reference cell

Heat capacities of the calorimeter cells were determined by electrical heating with current from a Sargent Coulometric Current Source (Model IV). Two methods were used to determine the combined heat capacities of the bulk solution and reference cell of the calorimeter. Method A: The bulk solution was heated electrically at a rate of $\sim 6.722 \times 10^{-2}$ cal/sec and the temperature of the bulk solution was measured with the bomb calorimeter thermometer cited earlier. Approximately 375 calories were used to heat the reference

cell. Method B: The heat capacities of the reference cell and reaction cell of the calorimeter were determined individually before and after thermometric titrations of NaOH by $HClO_4$. A heating rate of $\sim 1.679 \times 10^{-2}$ cal/sec applied for 450 sec yielded ~7.555 calories. Temperatures were measured with the calibrated thermistor circuit described in Section V.B.2. The output of OA-3 was amplified by a current to voltage converter, OA-4, with a gain of 10.000. The output potential of OA-4, $e_{o,4}$, was measured with a Corning Digital 112 pH meter in the mV mode.

Bulk solvents thermostated at 25.00 ± 0.02 deg C were pipetted by a specially designed 250-ml Pyrex pipet with a drain time of 90 sec. A total dispensing time of 100 sec was used to achieve a high precision in the volume delivered. The solvent was triply distilled water boiled gently before delivery to a closed container followed by placement in the thermostatic bath. The order of solvent dispensing was as follows: the reference cell, two previously weighed polyethylene bottles, and the reaction cell. The polyethylene bottles were again weighed to determine the mass of water dispensed by the pipet. Typical uncertainties in the mass of solvent delivered are approximately ± 0.014 g (95% confidence for 6 trials). All masses reported here are corrected to vacuum. The total time expired during solvent transfer was approximately 10 min.

3. Time constant of solution mixing

The time constant of mixing, τ_m, for the Dewar cells was estimated from photometric measurements made with a Pyrex cell, matching closely the size and shape of the Dewar cell set in place of the reaction cell. A beam of blue light (dark shade blue-green glass filter) 1-cm in diameter was directed horizontally through the cell with the beam centered 1.5-cm from the longitudinal axis of the cell. The cell contained 250-ml of water with 10 drops of 0.05% phenolphthalein. The output of a Heath 701A photomultiplier detector positioned to receive the transmitted light was recorded vs. time on a Sanborn oscillographic recorder as 0.25-ml of 50% NaOH solution was injected into the stirred solution. The transmittance of the solution was observed to decrease as an exponential function of time. The value of τ_m was taken as the point along the time axis when the change in transmittance was 63.2% of the total change.

4. Time constant of calorimeter system

The time constant of the calorimeter system was studied as a function of γ_b, N_s, P_t, r_s, and placement of the calibration heater relative to the thermistor probe. As is known both from experimental and theoretical work, heating rate and system response are directly related. Therefore, the highest bulk solution heating rate available using the calibration heaters was used to study τ_t as a function of N_s and r_s.

When additional time constants influence the measured value of τ_t, the resulting time constant becomes the system time constant, τ_s. Heating rates were measured by heating the bulk solution of deionized water for intervals of 1 - 3 x 10^3 seconds using the same value of N_s and r_s as used to study τ_s as a function of γ_b and heater placement. Changes of electrical power applied to the thermistors were judged to have a negligible effect on γ_b since C_b was large ($\sim$250 cal/deg C). Temperatures were measured using the bomb calorimeter thermometer cited earlier. Corrections were made for γ_{bkg} which was determined in separate experiments over the same temperature range as used in γ_b studies. Solution heating times used in time constant studies varied from 20 - 100 seconds depending on the heating rate. The validity of data depends on measurements made over a temperature range as small as possible. In this work, all measurements of τ_s were made between 24.7 - 25.3 deg C.

The time constant of the calorimeter system was measured by extrapolation of the straight portion of the ascending temperature-time curve to the baseline. The distance between heater turn-on and the extrapolated intercept was converted into units of time by applying the appropriate calibrated chart rate. To facilitate the extrapolation, recorder chart rates were selected so that the ascending temperature-time curves rose at approximately 45-degrees relative to the time axis.

5. Balance of cell heat capacities

Most parts of the cells for isoperibol calorimeter were specifically designed to be symmetric and to be used in both cells. Three items were unavoidably used in one cell only; the bomb calorimeter thermometer used in the reference cell, the thermistor used as part of a second thermometric bridge used to compare titrant-titrand temperatures located in the reference cell, and the solid sample injector used in the reaction cell. It was judged necessary to include a pseudo-thermometer in the reaction cell for adjusting c_2/c_1. The pseudo-thermometer was made from a NMR tube filled to depth of 4-cm with Hg.

The two cells were filled with equal volumes of triply distilled water and heated simultaneously with the calibration heaters connected in series. Bulk solution temperatures were measured by the calibrated thermistor circuit (see Section V.B.2) with a sensitivity of 4,027 mV/deg C. The differential output, $e_{o,3}$, was recorded vs. time at a calibrated span of 2.805 mV/in in a Heath EU-20W recorder. A chart rate of 0.5 in/min was used for all heat capacity, heat capacity ratio, and thermometric titration measurements. Graphical extrapolation of recorder data was used to evaluate c_2/c_1. The heat capacity ratio of the two cells was adjusted progressively closer to unity by raising or lowering the pseudo-thermometer. Since raising or lowering of the pseudo-thermometer changes

C_W and A_W, the potential placed across the trickle heaters was adjusted to maintain a time invariant baseline before a new heating trial.

6. Experimental procedures

a. Energy measurement Long term stability of the unsaturated Weston cell was essential to energy measurements made in calorimetric studies over the research period. The Weston cell was thermostated for all potential measurements made in this work. The thermostating container used was made from 6-ft of 0.375-in copper tubing wound into a coil within a 1-in thick Styrofoam box. Thermostating water flowing from the calorimeter thermostat back to the main thermostating bath was used to control the Weston cell temperature at 25.00 ± 0.01 deg C. The current was calculated from the IR-drop across a standard resistor determined by a Leeds and Northrup K-2 potentiometer. Potentials across the resistance heaters were measured at the banana-jack connectors by the L & N K-2 potentiometer. Potentials were measured at 100-second intervals throughout this work either across the standard resistance or the calibration heater resistors. Energies were calculated in calories on the basis of the conversion factor 4.184 joules/cal.

b. Time measurement The mechanical counter of the coulometer was used for all time measurements and was calibrated by comparison with the NBS radio time signals from

Fort Collins, Colorado. An initial series of measurements was made to check short term accuracy of the mechanical counter over a one-week interval. The accuracy of the counter was rechecked at monthly intervals thereafter. The error in time measurement was estimated to be due to reset error and reading error for a total error of ± 0.02 sec provided the counter was driven by a precise line frequency.

C. Results and Discussion

1. Characteristics of calorimeter cells

a. Heat loss moduli The heat-loss moduli, k, of ten Dewar cells were determined and the values are in the range 5.6×10^{-4} to 13.1×10^{-4} min^{-1}. Two cells matched within experimental error ($5.6 \pm 0.5 \times 10^{-4}$ min^{-1}) and were used in constructing the differential calorimeter.

The effect of the lid temperature, lid design, and the nature of bulk stirring on the measured heat loss modulus was studied with a single Dewar cell having $k = 1.2 \times 10^{-3}$ min^{-1}. The results are summarized in Figure VI.1. The effect of a heated lid to change the value of k is substantial. The initial slope of the response curve for $T_{lid} = T_b + 16$ deg C was a factor of 1.51 greater than that for $T_{lid} = T_b$. This result is consistent with the conclusion of Sunner and Wadsö (131) that the design and temperature of the calorimeter lid affects the measured value of k. Their conclusion that the

Figure VI.1. Heat loss modulus of calorimeter dewar

r_s = 1.63 cm

○ Rubber stopper, N_s = 0, ambient cell lid temperature;

□ Teflon stopper, N_s = 0, ambient cell lid temperature;

△ Teflon stopper, N_s = 1760 rev/min, ambient cell lid temperature;

⬡ Teflon stopper, N_s = 1760 rev/min, cell lid heated to thermostat temperature;

▽ Teflon stopper, N_s = 0, cell lid heated to thermostat temperature

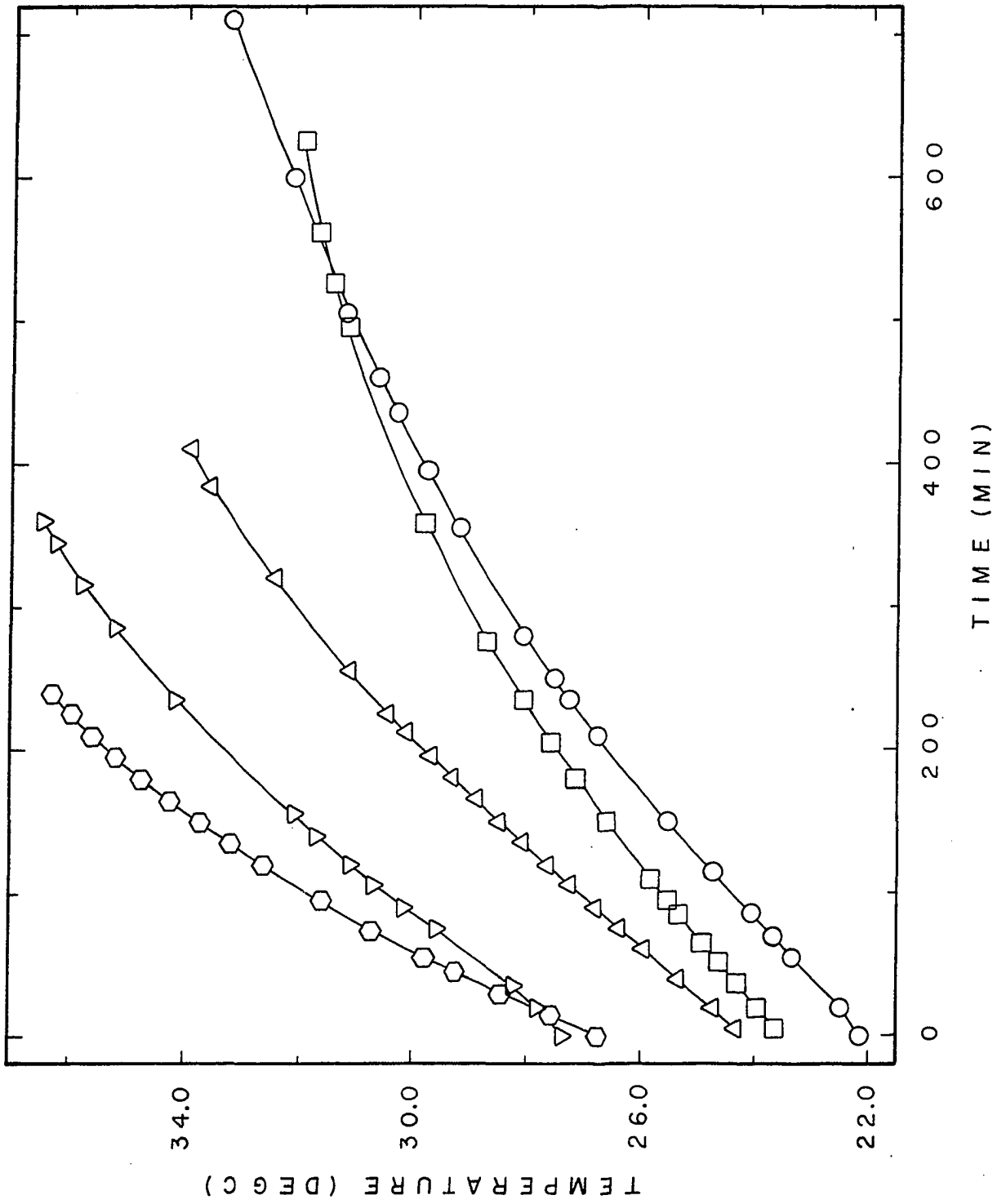
TEMPERATURE (DEG C)
34.0
30.0
26.0
22.0
0
200
400
600
TIME (MIN)

short term (< 2 min) dynamic response is controlled by k is not correct. Results described later show the short term response is primarily determined by mixing conditions. Long term (> 2 min) is greatly affected by k.

Results of calculations of k according to the methods of Swietslawski (A) and Gunn (B) are 2.80×10^{-3} min^{-1} and 2.87×10^{-3} min^{-1}, respectively. The agreement between the two values is excellent considering the differences in the methods employed. These values are in the mid-range of those reported by Tyrrell and Beezer (170) of 1×10^{-3} to 6×10^{-3} min^{-1}.

b. Heat capacities The heat capacity of the bulk solution and reference cell combined as determined in a single experiment with Method A was 282.98 ± 0.56 cal/deg C with 95% confidence. The mean temperature of the single experiment using Method A was 25.118 deg C. The error cited was calculated according to standard methods.

Heat capacities of bulk solutions and the reference cell or reaction cell were also determined according to Method B. This data was obtained from an initial set of seven titrations of NaOH (aq) solutions of varying concentrations with an identical mass of $HClO_4$ (aq). The reference cell in all cases initially contained only triply distilled water of varying mass approximately equal to the sum of triply distilled water and NaOH (aq) added to the reaction cell. The addition of water to the reference cell increased the total measured heat

capacity in direct proportion to the mass of water added. Physical and chemical properties of dilute solutions of highly dissociated electrolytes are proportional to the one-half power of the mass of electrolyte solution. The heat capacity of the reaction cell was also directly proportional to the mass of NaOH (aq) added due to the solvent of NaOH, water.

The total heat capacity of the calorimeter cells before titration was calculated as follows: The reference cell heat capacity,

$$c_1 = c_{o,1} + a\, m_{H_2O}$$

and, the reaction cell heat capacity,

$$c_2 = c_{o,2} + a_1\, m_{NaOH}^{\frac{1}{2}} + a_2\, m_{NaOH}$$

After each thermometric titration, a sufficient amount of acid had been added to both calorimeter cells to bring them to a nearly constant ionic strength for the set of titrations. Hence, the measured heat capacity of the reference cell after titrations was fitted to a linear equation. The pH of the reaction cell did not remain constant. Therefore, the ionic strength term, $m^{\frac{1}{2}}$, is replaced with log m. It is immediately obvious that since log m is undefined when m=0, such an equation is only valid for nonzero values of m. Therefore, several approximations were made. First, the log m term was evaluated for experimental data and the corresponding coefficient a_1 of log m was assumed equal to unity to facilitate linear least squares treatment of the reduced

equation. Second, the reduced equation was assumed to accurately describe c_2 at m=0. A more exact analysis would require the use of a complex nonlinear least squares model; such models require at least twenty data points to be valid. Heat capacities measured with zero addition of NaOH or H_2O were not included in this treatment.

The calculated equations for the heat capacities prior to titration are

$$c_1 = 282.15 \pm 1.30 + 1.2555 \pm 0.1942\ m_{H_2O}$$

$$c_2 = 283.48 + 1.9684\ m_{NaOH}^{\frac{1}{2}} + 0.71643\ m_{NaOH}$$

Heat capacities determined following titration are

$$c_1 = 282.11 \pm 1.60 + 0.79838 \pm 0.19482\ m_{(H_2O + HClO_4)}$$

$$c_2 = 283.67 \pm 1.49 + 0.92318 \pm 0.18059\ m_{(NaOH + HClO_4)}$$

Agreement in values determined for $c_{o,1}$ and $c_{o,2}$ is excellent. A slight decrease of $c_{o,1}$ with temperature occurred since the heat capacity of water decreased faster than the heat capacity of the calorimeter 'wall'. The temperature range of experiments for Method B was 24.7 - 25.3 deg C. The mean temperature of heat capacity determinations before titrations was 24.837 deg C and that of heat capacity determinations after titrations, 25.146 deg C. The relatively large uncertainties cited were due primarily to thermometric circuit noise. The change in $e_{o,3}$ during a heat capacity determination was

$\sim$100 mV and two sets of measurements of $e_{o,3}$ *vs.* time over a 350-second interval were needed to calculate the corrected $\Delta e_{o,3}$ (equivalent to the corrected temperature rise in conventional calorimetry). From the p-p circuit noise cited in Section V.A.5, the relative error contribution from the circuit noise is readily calculated to be $\sim$4 ppt. The trickle heater contributed negligible error to these determinations. A study of the trickle heater stability as measured from the potential drop across the trickle heater of the reference cell over a 4.5-day interval yielded 400.64 ± 0.076 mV + 0.0106 ± 0.0295 mV/day using sixteen measurements.

Agreement between Methods A and B is excellent considering that the temperature change was 1.324 ± 0.002 deg C in Method A and 0.0268 ± 0.0001 deg C in Method B. The average value of heat capacities determined by Method B was used in computer simulations of electrical heating discussed in Section VI.C.3. The ratio of $c_{o,2}/c_{o,1}$ calculated from the averages of data taken before and after thermometric titrations is 1.0051 at 25.00 deg C. The value of C_w was determined by subtraction of C_b (248.85 cal/deg C) as calculated at 25.0 deg C using the average mass of 249.28-g of H_2O added with the calibrated pipet. The calculated value of $C_{w,1}$ is 33.28 cal/deg C and $C_{w,2}$ is 34.72 cal/deg C.

2. Energy and time measurement

The 0.05 multiplier setting of the coulometer was used for the majority of calorimetric studies carried out for this thesis. The average current in the seven experiments discussed above which were made over a one-month period was $4.8358 \pm 0.0002 \times 10^{-2}$ amp. The measured error in the coulometer current represents a relative error of 41-ppm. A similar relative error of 53-ppm was calculated for potentials measured across the calibration heater in the reference cell.

The mechanical counter calibration data was evaluated according to the following equation with a linear least squares computer program:

measured time = correction x actual time + turn-on error.

With 95% confidence, the calculated fit of twelve measurements is

$$t_m = 0.999\ 963 \pm 0.000\ 019\ t_a + 1.55 \pm 0.98 \text{ sec}$$

The response time of the average person is $\sim$0.75-sec which is in good agreement with the calculated turn-on plus turn-off error. The relative error of time measurements is 12-ppm making the total relative error for energy measurements in this work, 0.011-ppt.

3. Implementation of the theoretically derived calorimeter model

The primary difficulty in using the mathematical model for the calorimetric response to electrical heating is that four time constants are required and only τ_m and τ_t can be measured experimentally. Values of τ_h and τ_w must be calculated as described earlier. The theoretical model for the time constant of mixing, described in Section III.B.2 was programmed in WATFIV and executed on an IBM 360-5 digital computer in the Iowa State University Computation Center. A listing of the program is given in Appendix D.2. Experimental and calculated values of τ_m are given in Figure VI.2. The agreement is satisfactory for low rotation speeds but the calculated values are low for high rotational velocities. This error probably results from the assumption that the Pai power series which is used for calculating velocity distribution in a pipe is valid for flow in a closed cylinder.

The theoretical model for the response of the calorimeter bulk temperature, described in Section III.B.3, was programmed in WATFIV and executed on an IBM 360-5 digital computer in the Iowa State University Computation Center. A listing of the program is given in Appendix D.3. Parameter values used in the computer simulation of electrical heating of a calorimeter are given in Table VI.1.

The theoretical output of the bridge circuit as a function of time is shown in Figure VI.3 for an overall circuit gain of

Figure VI.2. Experimental and theoretical time constants of mixing in the calorimeter cells as a function of N_s

Radius (r): A 2.75 cm
B 2.45 cm
C 2.15 cm
D 1.85 cm
E 1.55 cm

Data: + Calculated
x Experimental

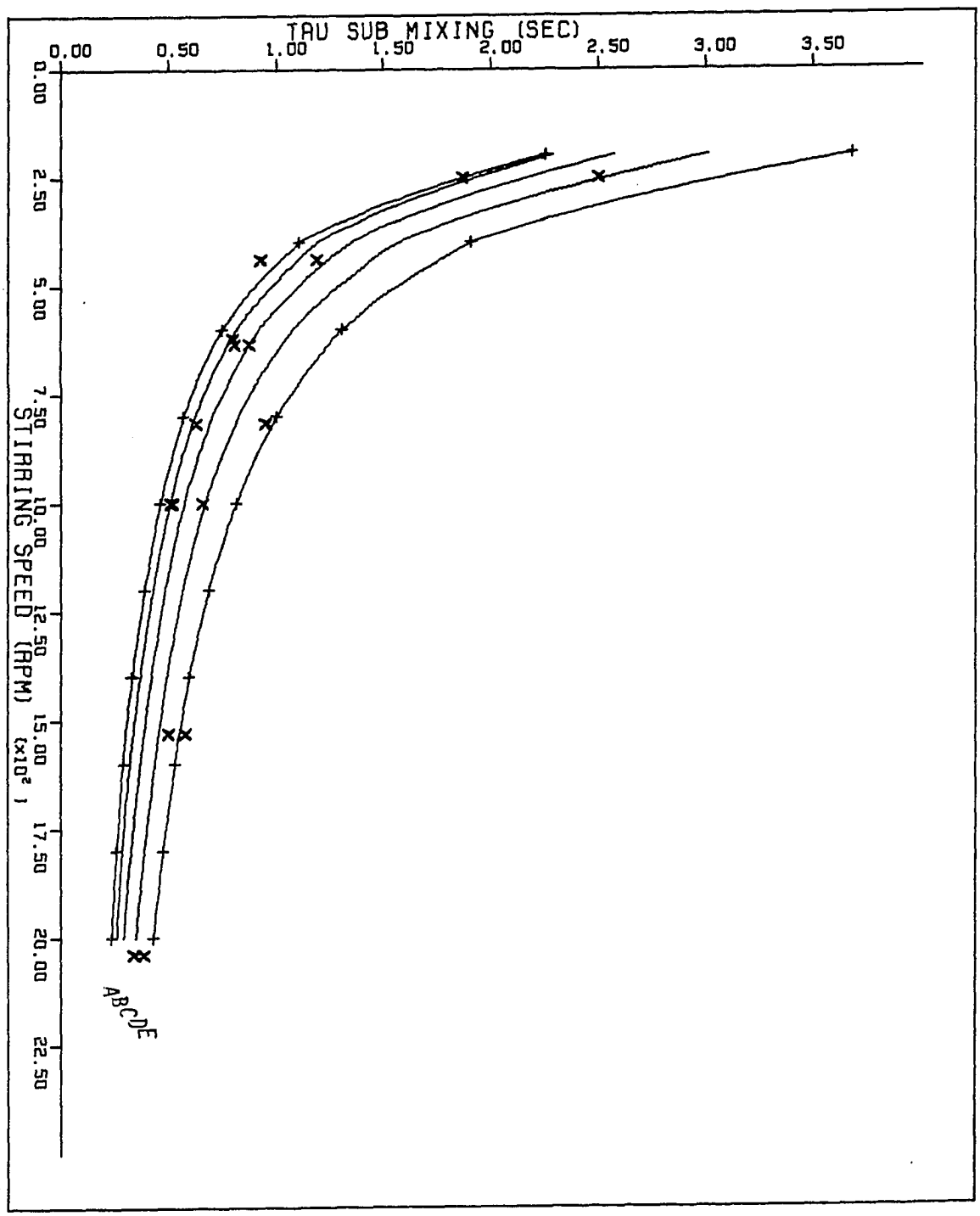
TAU SUB MIXING (SEC)
0.00
0.50
1.00
1.50
2.00
2.50
3.00
3.50
STIRRING SPEED (RPM) (x10²)
0.00
2.50
5.00
7.50
10.00
12.50
15.00
17.50
20.00
22.50
A
B
C
D
E

Table VI.1. Parameter values for computer calculations

A. Reference cell of calorimeter:

r_{sh}	= 0.64 cm	l_1	= 1.6 cm
r_s	= 2.96 cm	l_2	= 10.8 cm
r	= 2.15 cm	ε	= 0.7854 rad
r_{stem}	= 0.40 cm	χ	= 2.0246 rad
A_{stem}	= 181 cm^2	C_b	= 248.8 cal/deg C (H_2O)
A_w	= 227 cm^2	C_w	= 33.3 cal/deg C
x_s	= 0.35 cm	vapor volume	= 59.5 ml

B. Bulk solvent

Parameter	Water, 25°C	Toluene, 25°C
λ_b	1.45 x 10^{-3} cal/cm-sec-deg C (171)	3.22 x 10^{-4} cal/cm-sec-deg C (171)
ν_b	8.937 x 10^{-3} cm^2/sec	6.42 x 10^{-3} cm^2/sec (172)
Pr	6.16	7.11
Sc	297 (173)	257 (174)
c_p	0.998 cal/g-deg C (172)	0.356 cal/g-deg C (175)

C. Electrical

λ_h = 3.9 x 10^{-3} cal/cm-sec-deg C	A_h = 1.2 cm^2
C_h = 7 x 10^{-2} cal/deg C	r_h = 0.12 cm
γ_{bkg} = 1.76 x 10^{-5} deg C/sec (N_s = 1000 rpm, r_s = 1.63 cm)	

Figure VI.3. Theoretical voltage output of the bridge circuit as a function of time

N_s = 400 rev/min

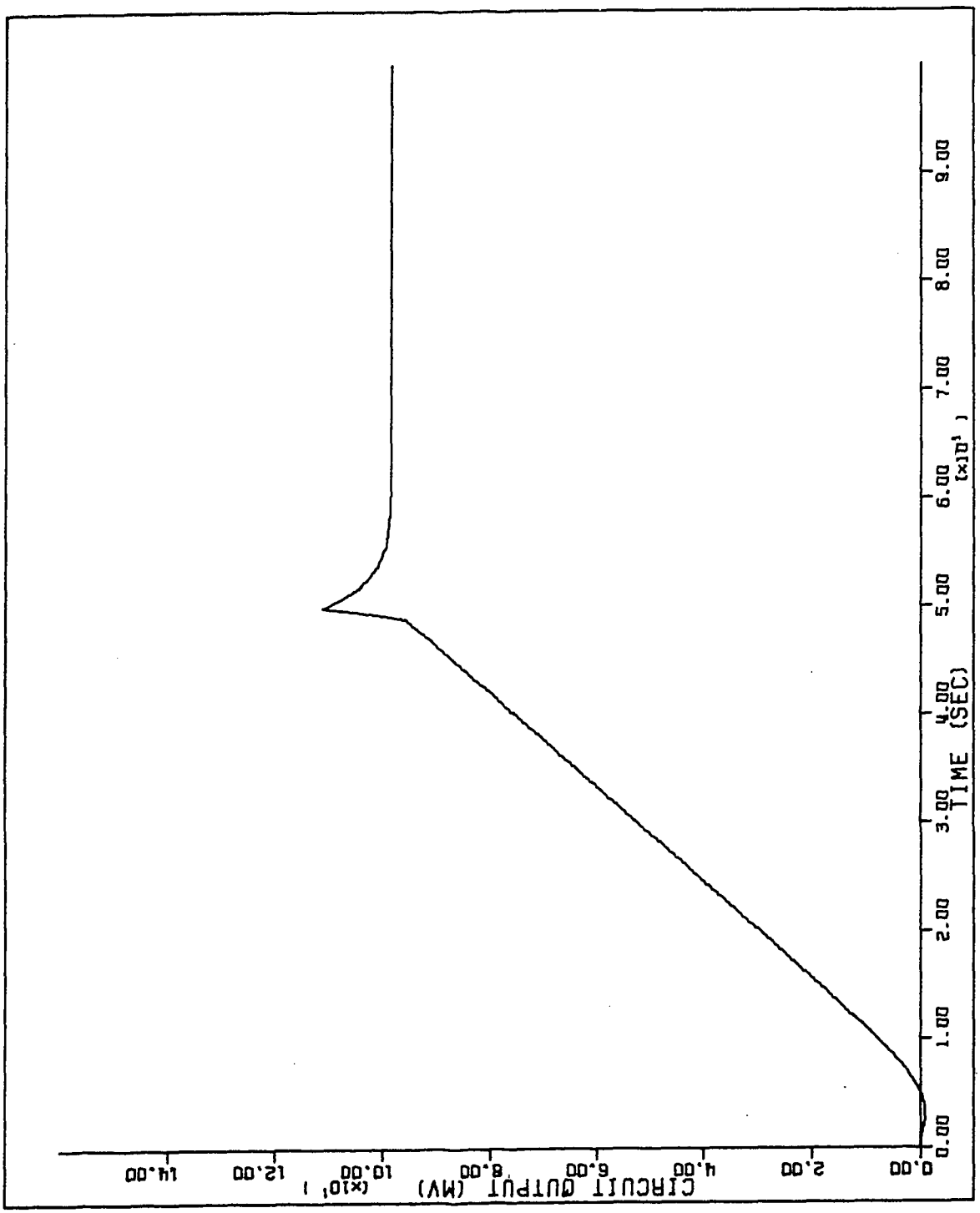
CIRCUIT OUTPUT (MV)
(x10¹)
0.00
2.00
4.00
6.00
8.00
10.00
12.00
14.00
TIME (SEC)
0.00
1.00
2.00
3.00
4.00
5.00
6.00
7.00
8.00
9.00
(x10¹)

100. The mathematical model does not give a completely satisfactory description of the transient regions of the main and anterior periods. The error is small, however, for the steady-state regions of both periods. For example, the experimental time constant is 6.3 sec when $\gamma_b = 4.92 \times 10^{-4}$ deg C/sec, $N_s = 430$ rpm, and $r_s = 1.63$ cm. The value predicted at 400 rpm is 6.6 sec. The predicted change in the circuit output, Δe_o, measured from start to the steady-state region of the anterior period is 98.44 mV. A value of 98.74 mV was observed experimentally for a heating time of 49 seconds.

$T_h > T_b$ during electrical heating and the early portion of the anterior period before a steady-state temperature is reached. The location of the thermistor relative to the heater determines whether the thermistor is in a region of excess temperature ($T_{b,t} > T_{b,ave}$) or a region of deficient temperature ($T_{b,t} < T_{b,ave}$). When the thermistor is in a region of excess temperature, overshoot is observed at the point of heater cutoff, t_{co}. The temperature excess ($T_{b,t} - T_{b,ave}$) is on the order of 7 m deg C for $\gamma_b = 4.92 \times 10^{-4}$ deg C/sec, $N_s = 200$ rpm, and $r_s = 1.63$ cm.

Experimental and theoretical heating curves are given in Figures VI.4 and VI.5 for $r_s = 0.64 - 1.85$ cm. Experimental and theoretical heating curves showing the effect of N_s for a r_s of 1.63 cm are given in Figures VI.6 and VI.7 for $N_s = 400 - 2000$ rpm. The curves illustrate dramatically that

Figure VI.4. Experimental heating curves of reference cell as a function of r_s

$e_+ = 1000.0$ mV

$e_- = 1000.2$ mV

$R_f = 1.0016$ MΩ

$C_f = 0.047$ μfd

Radius (r_s): A 0.64 cm

B 1.27 cm

C 1.85 cm

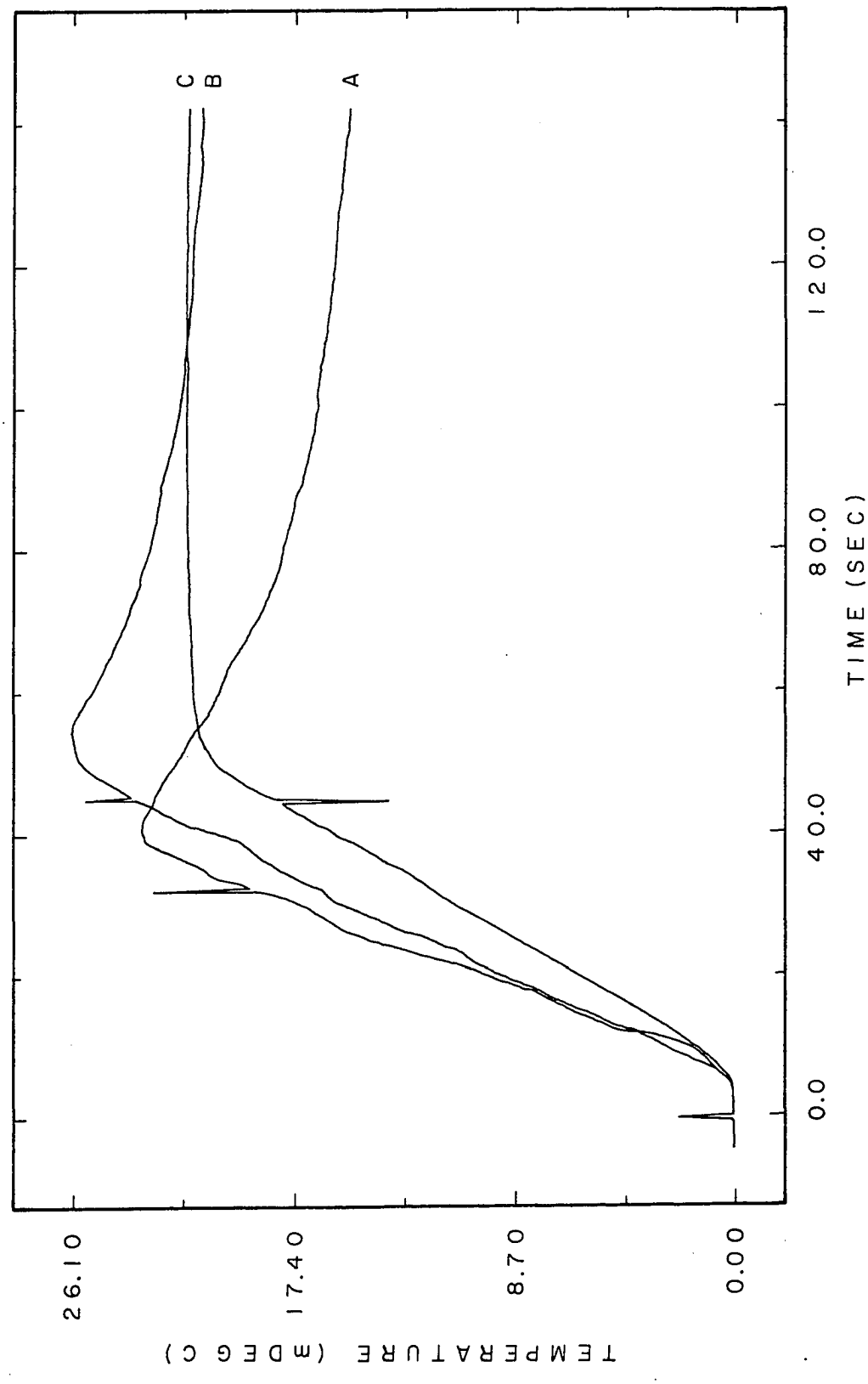
C
B
A
26.10
17.40
8.70
0.00
TEMPERATURE (mDEG C)
0.0
40.0
80.0
120.0
TIME (SEC)

Figure VI.5. Theoretical heating curves of the reference cell as a function of r_s

$e_+ = 1000.0$ mV

$e_- = 1000.2$ mV

$R_f = 1.056$ MΩ

$C_f = 0.047$ μfd

Radius (r_s): A 0.64 cm

B 1.27 cm

C 1.85 cm

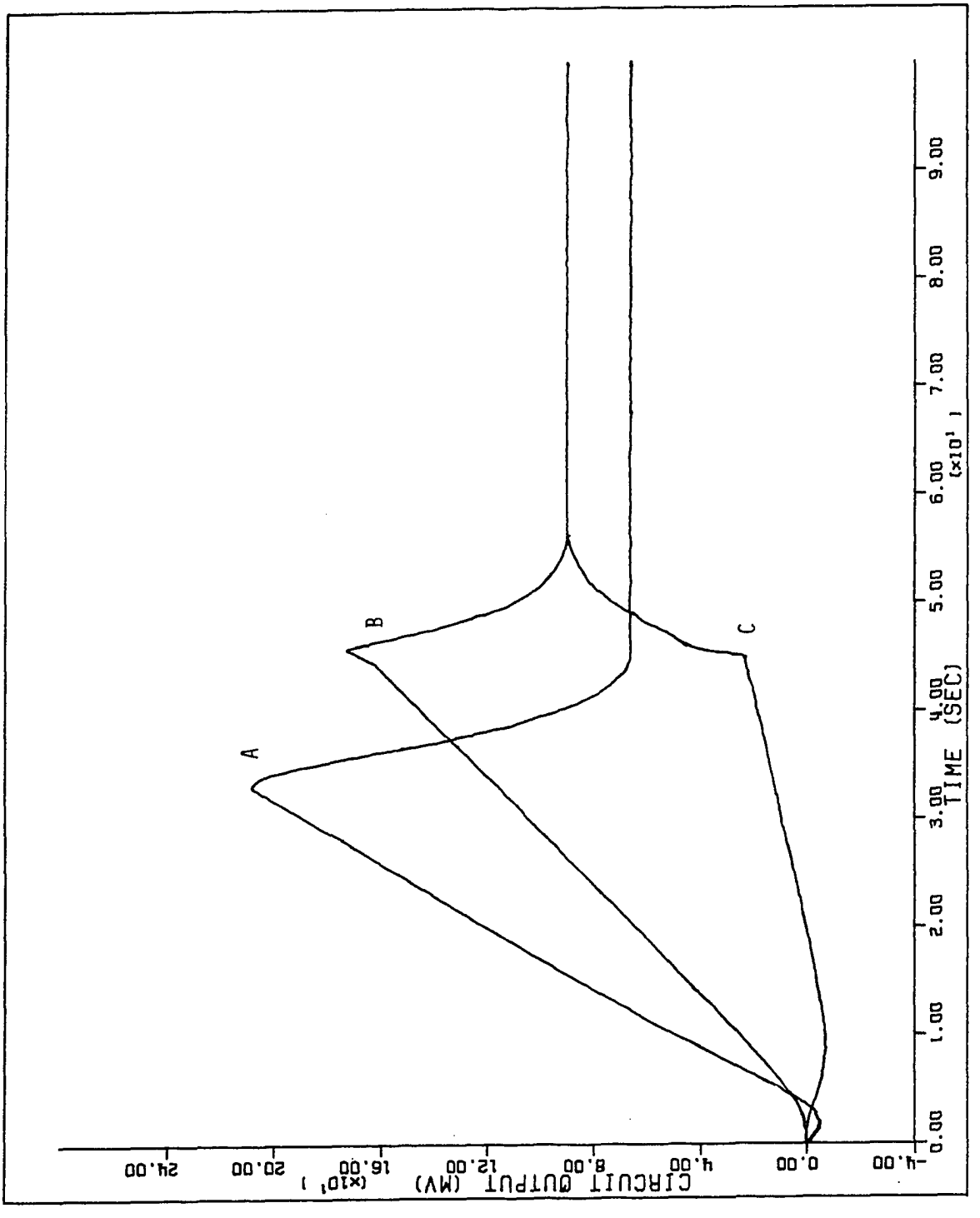
CIRCUIT OUTPUT (MV)
(x10¹)
-4.00
0.00
4.00
8.00
12.00
16.00
20.00
24.00
0.00
1.00
2.00
3.00
4.00
5.00
6.00
7.00
8.00
9.00
TIME (SEC)
(x10¹)
A
B
C

Figure VI.6. Experimental heating curves of the reference cell as a function of N_s

r_s = 1.63 cm

N_s: A 400 rev/min

B 800 rev/min

C 1000 rev/min

D 1980 rev/min

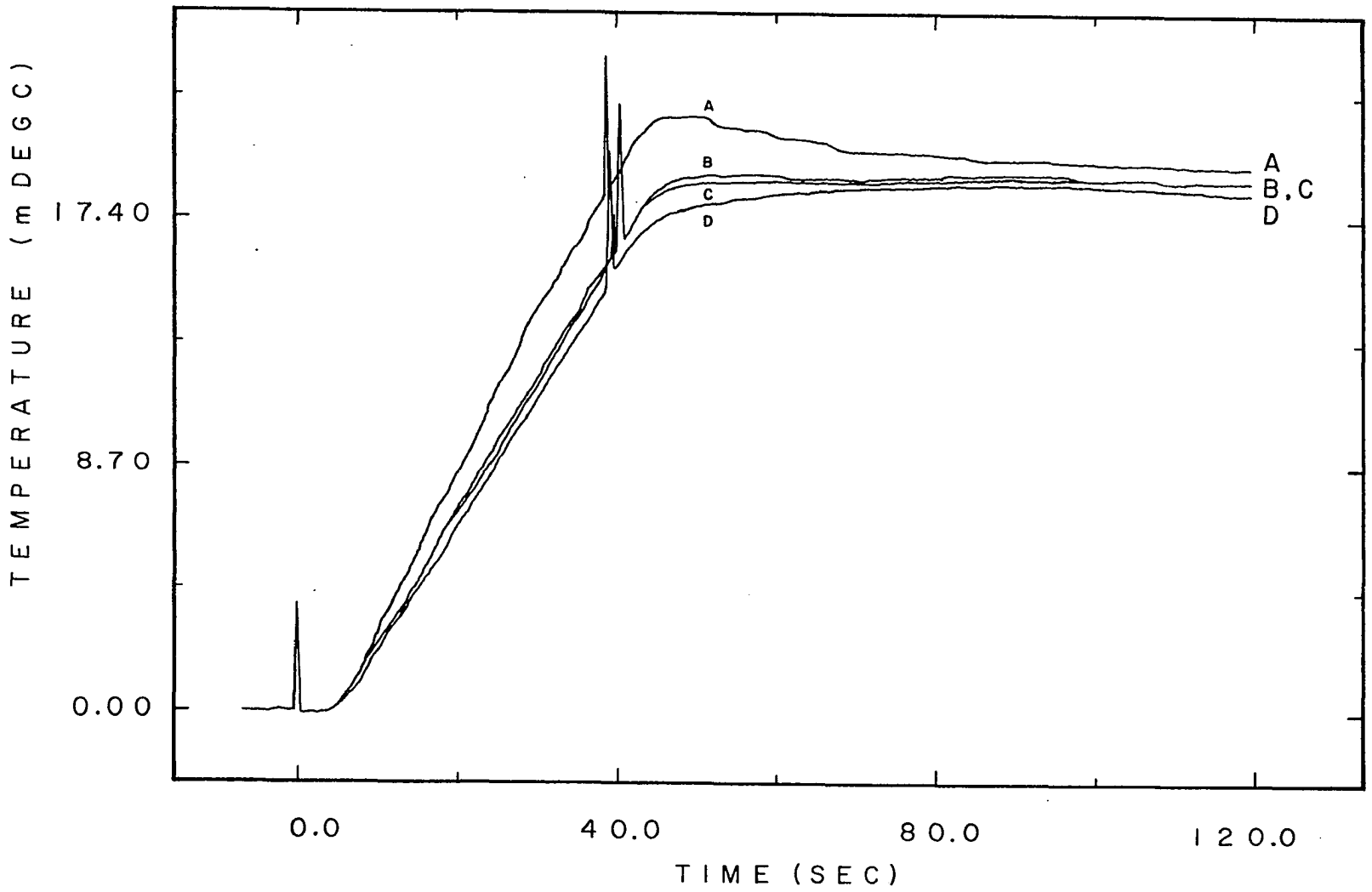
TEMPERATURE (mDEGC)
17.40
8.70
0.00
0.0
40.0
80.0
120.0
TIME (SEC)
A
B
C
D
A
B,C
D

Figure VI.7. Theoretical heating curve of the reference cell as a function of N_S

$r_S = 1.63$ cm

N_S: A 400 rev/min

B 800 rev/min

C 1200 rev/min

D 1600 rev/min

E 2000 rev/min

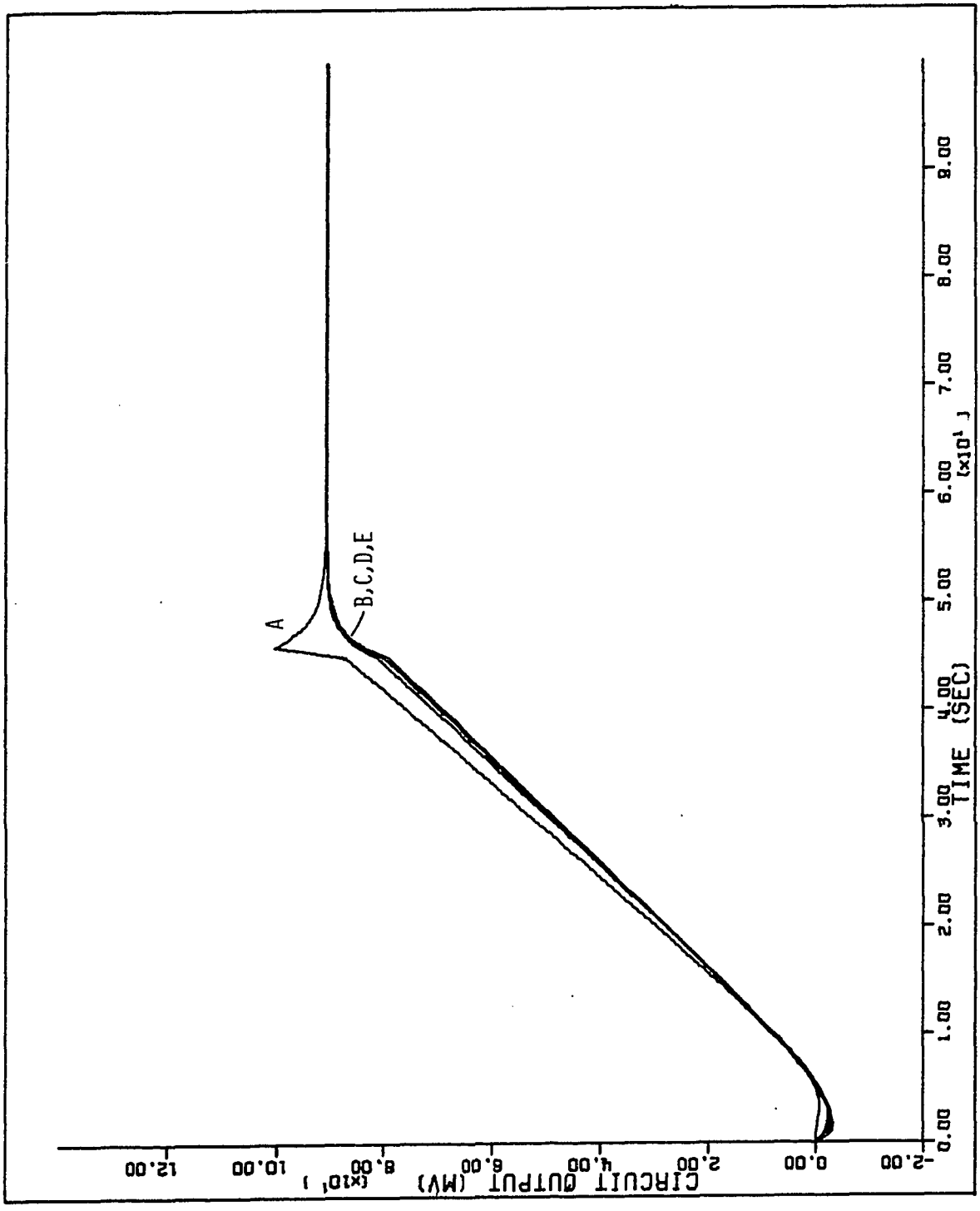
A
B,C,D,E
CIRCUIT OUTPUT (MV)
(x10¹)
-2.00
0.00
2.00
4.00
6.00
8.00
10.00
12.00
0.00
1.00
2.00
3.00
4.00
5.00
6.00
7.00
8.00
9.00
TIME (SEC)
(x10¹)

critical damping of a calorimeter can be achieved by proper choice of r_s and N_s. The conclusion of some workers that k becomes constant after 3 to 30 sec dependent only on calorimeter design is not supported by this result. Certainly, C_w influences the response but it does not have the overwhelming importance commonly thought.

The effect of changing solvent was investigated by substituting toluene for water. The heating curves are shown in Figure VI.8. The thermal conductivity and heat capacity of toluene are considerably different than those of water causing the extensive overshoot observed in Figure VI.8. The sudden downward plunge of e_o after the start of the heating probably results from discarding the T_{b1} term in the derivation. The error is on the order of 2 mdeg C. All results shown were corrected throughout this work for the offset error calculated at t=0. The complexity of the calorimetric system precludes an exact derivation including the T_{b1} term.

The theoretically calculated values of γ_b *vs.* t and temperature of the bulk solution in the region of the thermistor *vs.* t are given in Figures VI.9 and VI.10, respectively. Inspection of these figures reveals that in contrast to most differential variables, γ_b is relatively constant throughout whereas T_b undergoes considerable variation. The excess temperature of the bulk solution in the region of the thermistor is given in Figure VI.11. It

Figure VI.8. Theoretical heating curves of the reference cell with toluene as the bulk solvent as a function of N_s

r_s = 1.63 cm

N_s: A 400 rev/min

B 800 rev/min

C 1200 rev/min

D 1600 rev/min

E 2000 rev/min

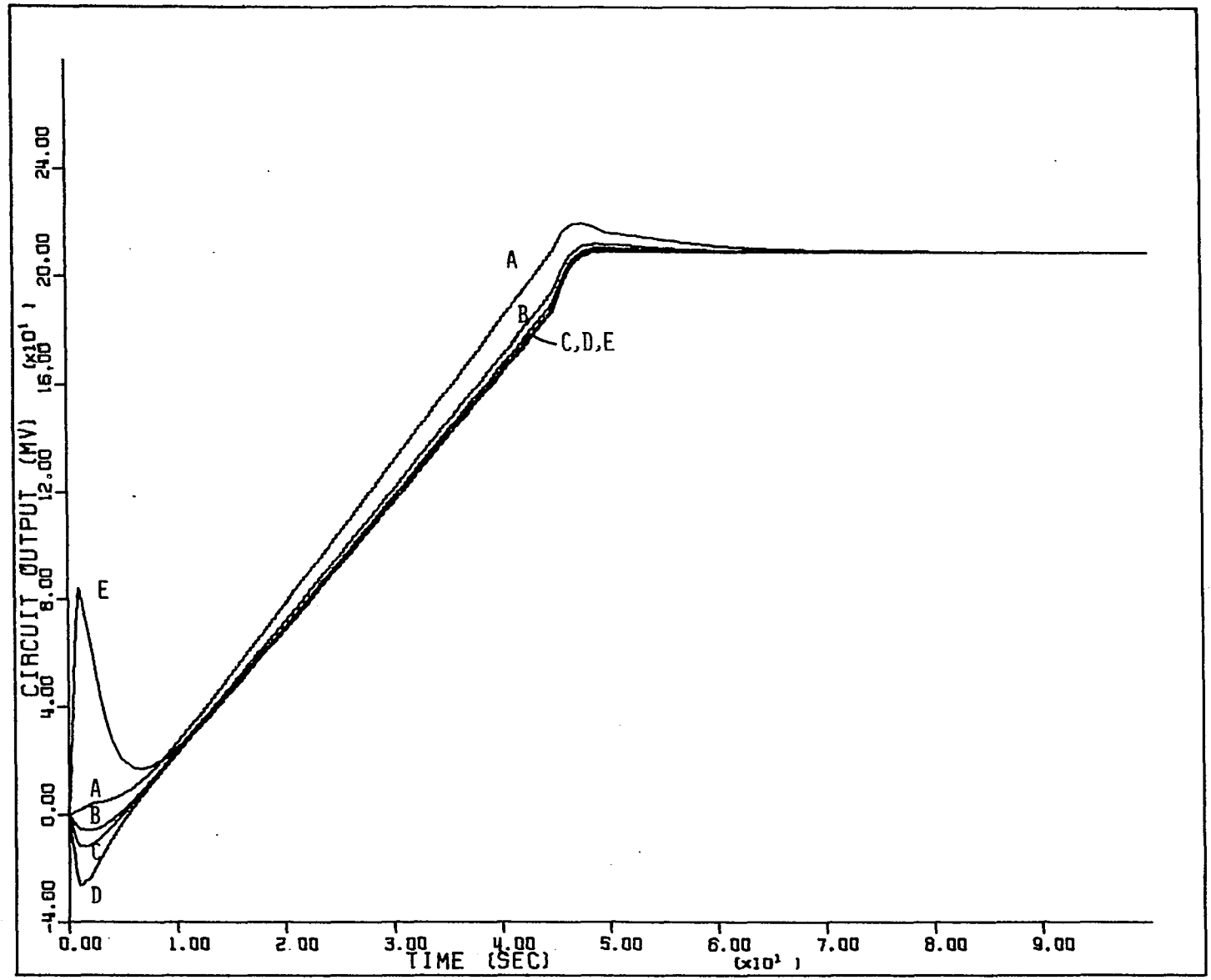
CIRCUIT OUTPUT (MV)
(x10¹)
24.00
20.00
16.00
12.00
8.00
4.00
0.00
-4.00
A
B
C,D,E
E
A
B
C
D
0.00
1.00
2.00
3.00
4.00
5.00
6.00
7.00
8.00
9.00
TIME (SEC)
(x10¹)

Figure VI.9. Theoretical heating rate of the reference cell as a function of N_s

r_s = 1.63 cm

N_s: A 400 rev/min

B 800 rev/min

C 1200 rev/min

D 1600 rev/min

E 2000 rev/min

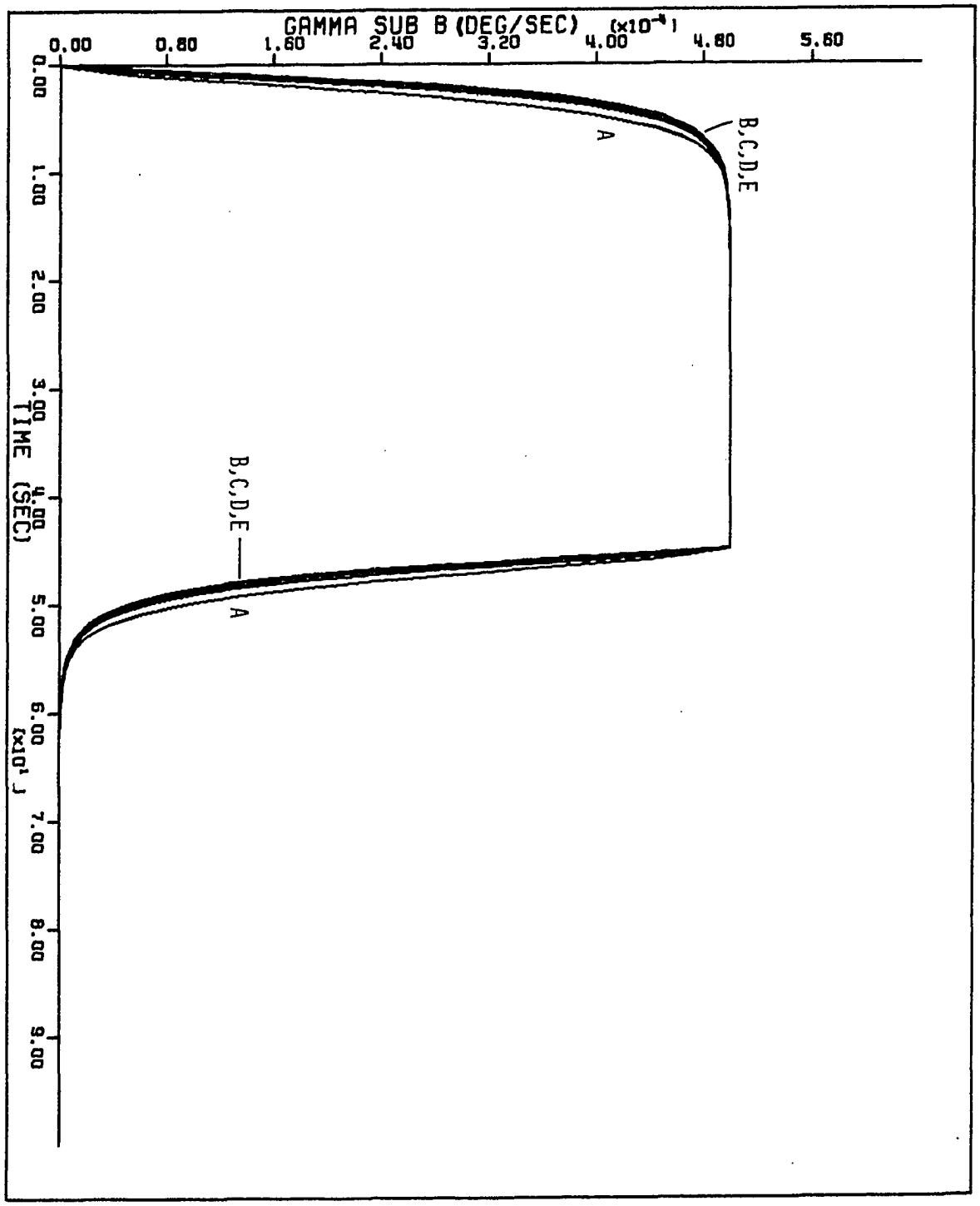
GAMMA SUB B (DEG/SEC) (x10⁻⁴)
0.00
0.80
1.60
2.40
3.20
4.00
4.80
5.60
TIME (SEC)
0.00
1.00
2.00
3.00
4.00
5.00
6.00
7.00
8.00
9.00
(x10¹)
A
B,C,D,E
B,C,D,E
A

Figure VI.10. Theoretical bulk solution temperature as a function of N_s

$r_s = 1.63$ cm

N_s: A 400 rev/min

B 800 rev/min

C 1200 rev/min

D 1600 rev/min

E 2000 rev/min

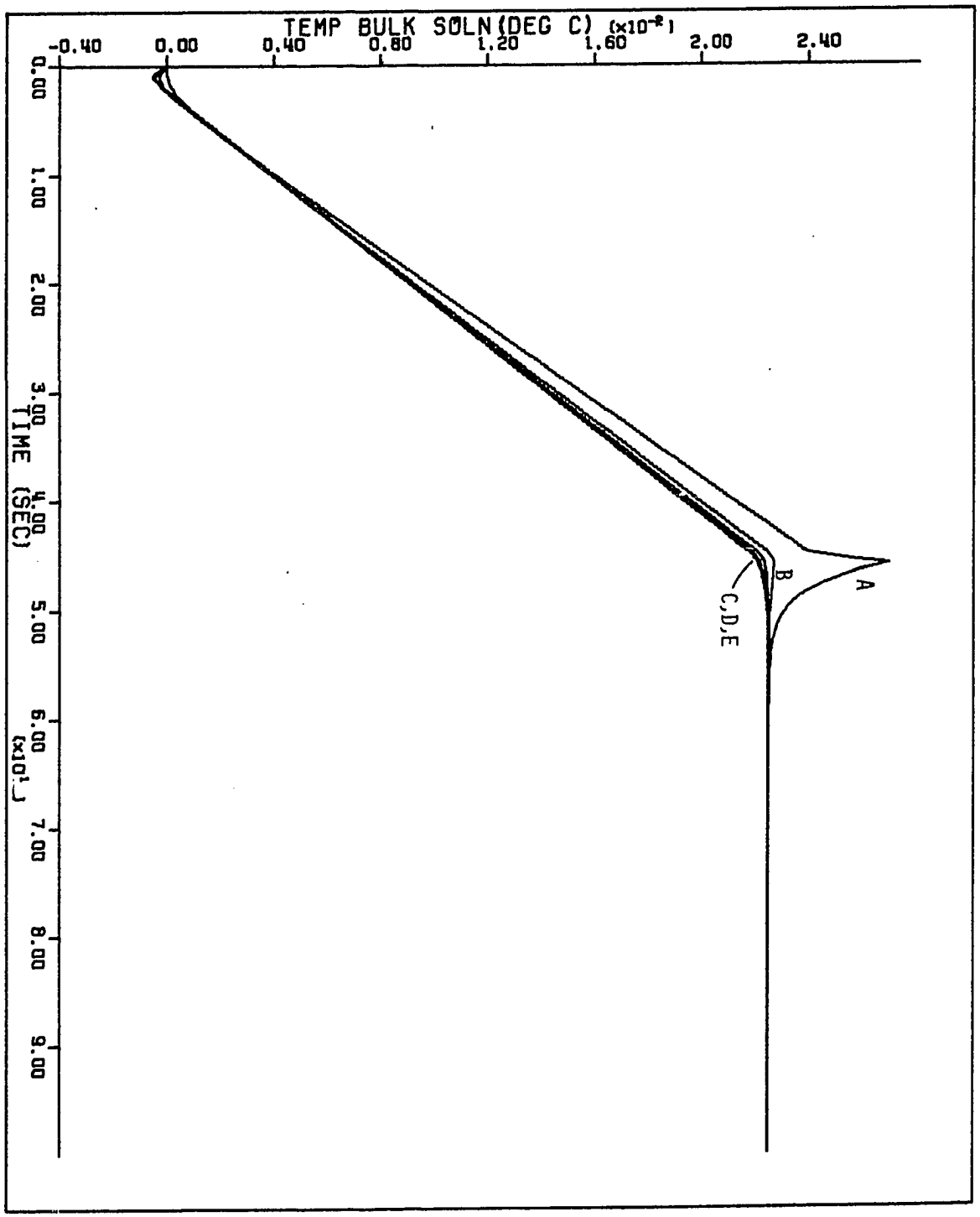
TEMP BULK SOLN (DEG C) (x10⁻²)
-0.40
0.00
0.40
0.80
1.20
1.60
2.00
2.40
0.00
1.00
2.00
3.00
4.00
5.00
6.00
7.00
8.00
9.00
TIME (SEC)
(x10¹)
A
B
C,D,E

Figure VI.11. Theoretical excess temperature of bulk solution at the thermistor position as a function of N_s

r_s = 1.63 cm

N_s: A 400 rev/min

B 800 rev/min

C 1200 rev/min

D 1600 rev/min

E 2000 rev/min

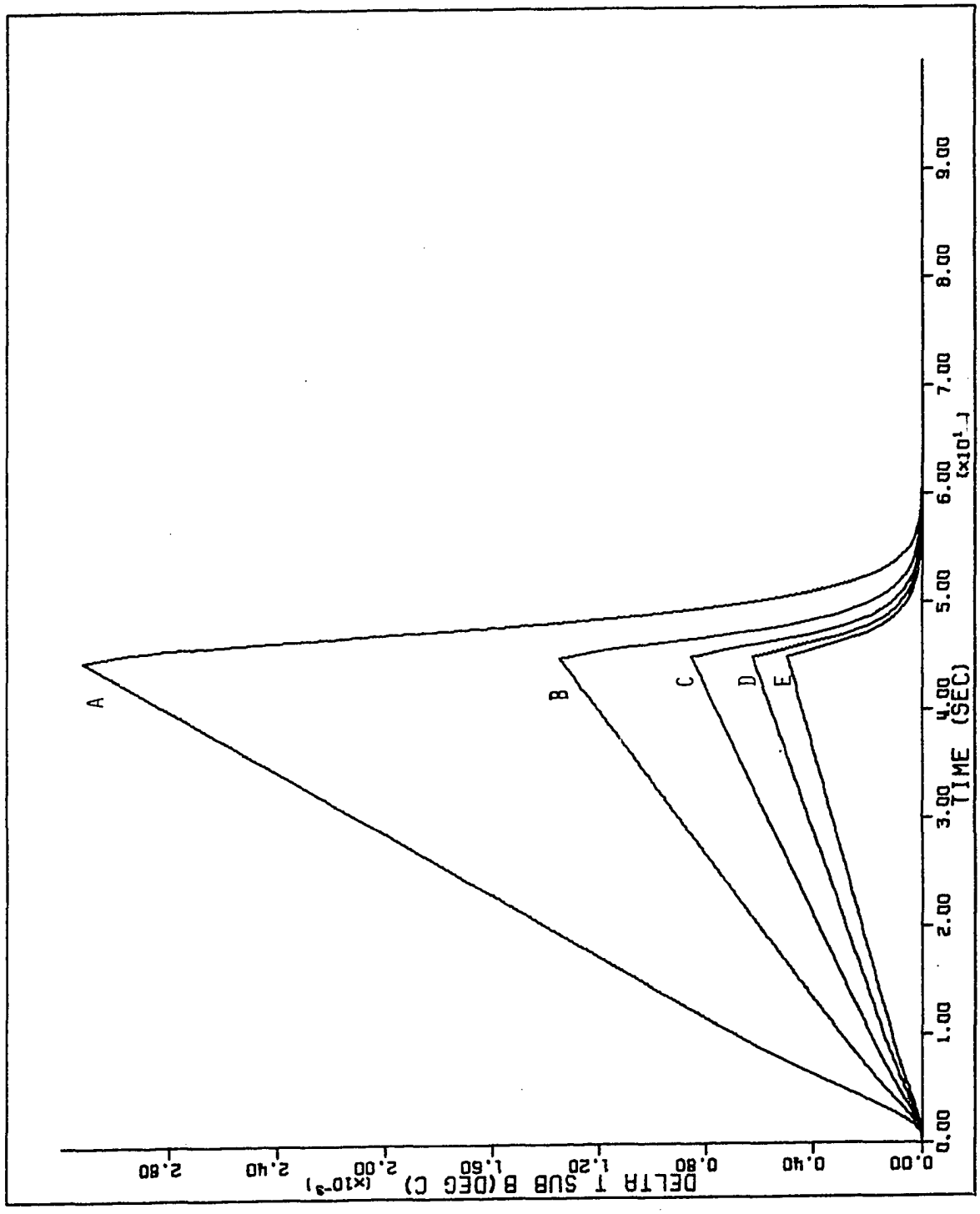
DELTA T SUB B(DEG C) (x10⁻³)
0.00
0.40
0.80
1.20
1.60
2.00
2.40
2.80
TIME (SEC)
1.00
2.00
3.00
4.00
5.00
6.00
7.00
8.00
9.00
(x10¹)
A
B
C
D
E

is apparent from Figure VI.11 that a considerable amount of the roughness in Figure VI.10 is a consequence of the lack of smoothness in the curve of ΔT_b *vs.* t. The value of T_{t-b} *vs.* t is much smoother as shown in Figure VI.12; however, at t_{co}, the plot is not as smooth as in the initial region. Perhaps, the linear approximations made in the derivation of the thermistor inner conductivity need to be modified (*cf.* Figure V.7).

Reynolds numbers for the bulk solution calculated at the edge of the stirrer disc, at the position of the electrical heater, and at the surface of the thermistor are given in Figure VI.13. Heat transfer coefficients for the calorimeter wall, calibration heater, calorimeter probes, and thermistor probes *vs.* N_s are given in Figure VI.14. The values of α^2 and $Z_1 Z_3(1 + C_w/C_b)$ in Figure VI.15 show that for r_s = 1.63-cm, the calorimeter system is critically damped when N_s > 600-rpm which is in agreement with experimental results given in Figure VI.6. As a compromise between heat of stirring, opening of the solid sample holder, and critical damping of the calorimeter system, a rotation speed of 1000 rpm and a disc of 1.63-cm radius were used for the remainder of the calorimetric work described in this thesis. Finally, all of the time constants of the calorimeter system are given in Figure VI.16.

Figure VI.12. Theoretical temperature difference across thermistor thermal boundary layer and thermistor bead as a function of N_s

r_s = 1.63 cm

N_s: A 400 rev/min

B 800 rev/min

C 1200 rev/min

D 1600 rev/min

E 2000 rev/min

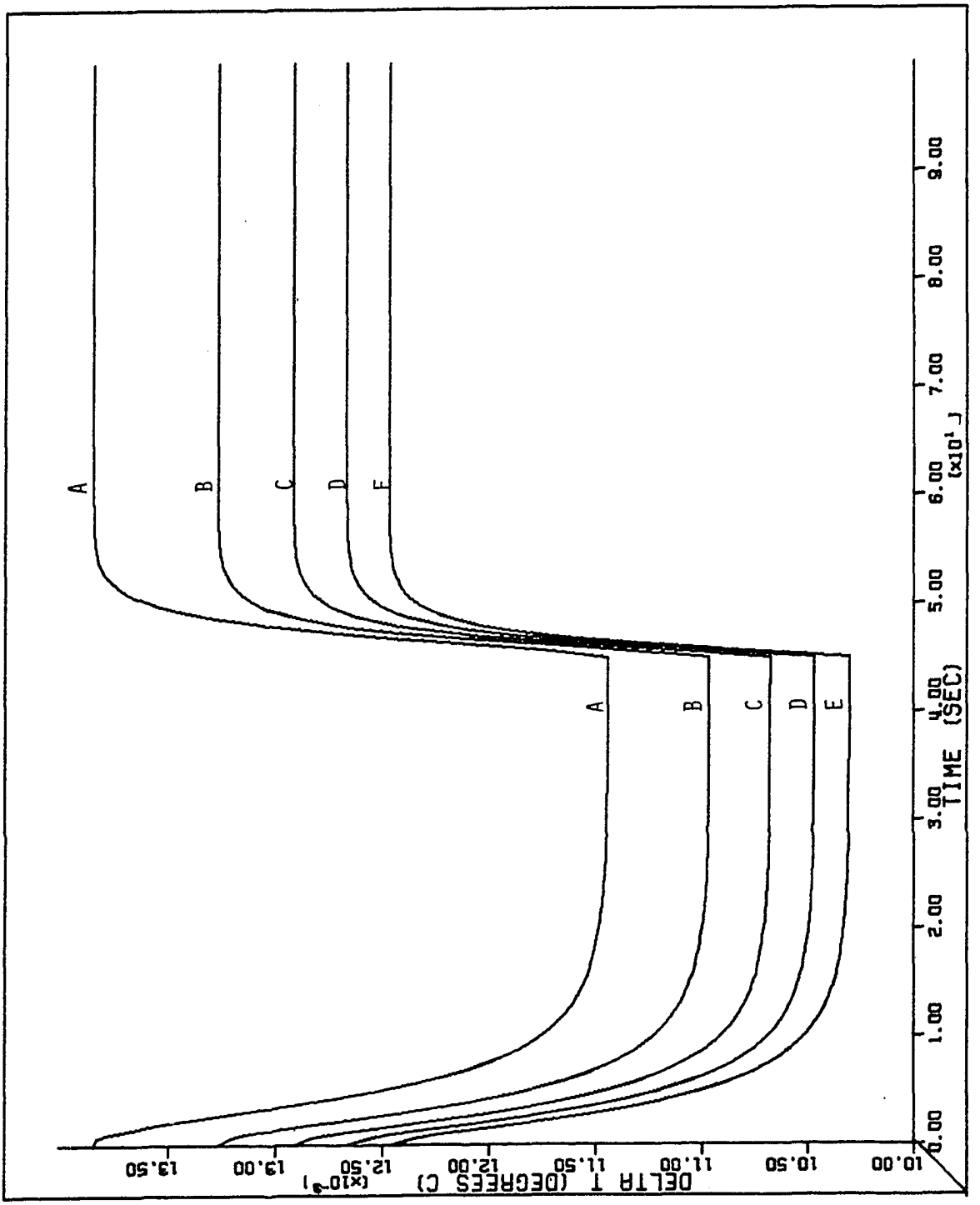
DELTA T (DEGREES C)
(x10⁻³)
10.00
10.50
11.00
11.50
12.00
12.50
13.00
13.50
TIME (SEC)
(x10¹)
0.00
1.00
2.00
3.00
4.00
5.00
6.00
7.00
8.00
9.00
A
B
C
D
E
A
B
C
D
E

Figure VI.13. Calculated Reynolds numbers for the bulk solution and thermistor as a function of N_s

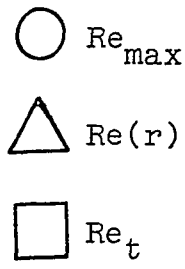

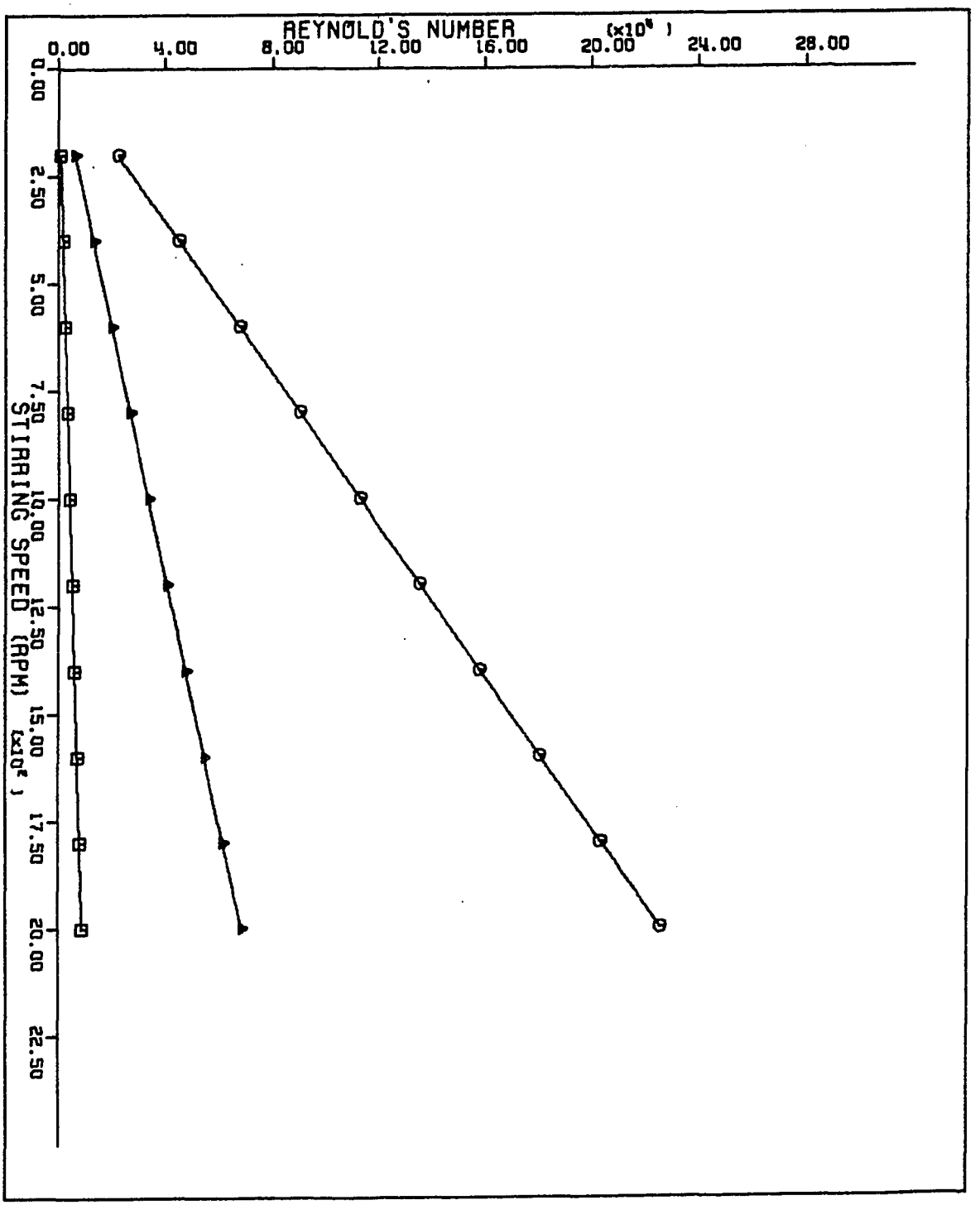
REYNOLD'S NUMBER (x10⁶)
0.00
4.00
8.00
12.00
16.00
20.00
24.00
28.00
STIRRING SPEED (RPM) (x10²)
0.00
2.50
5.00
7.50
10.00
12.50
15.00
17.50
20.00
22.50

Figure VI.14. Theoretical heat transfer coefficients of the calorimeter components as a function of N_s

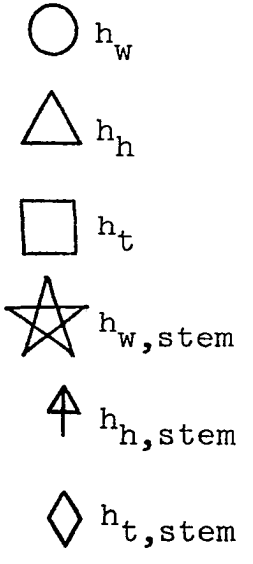

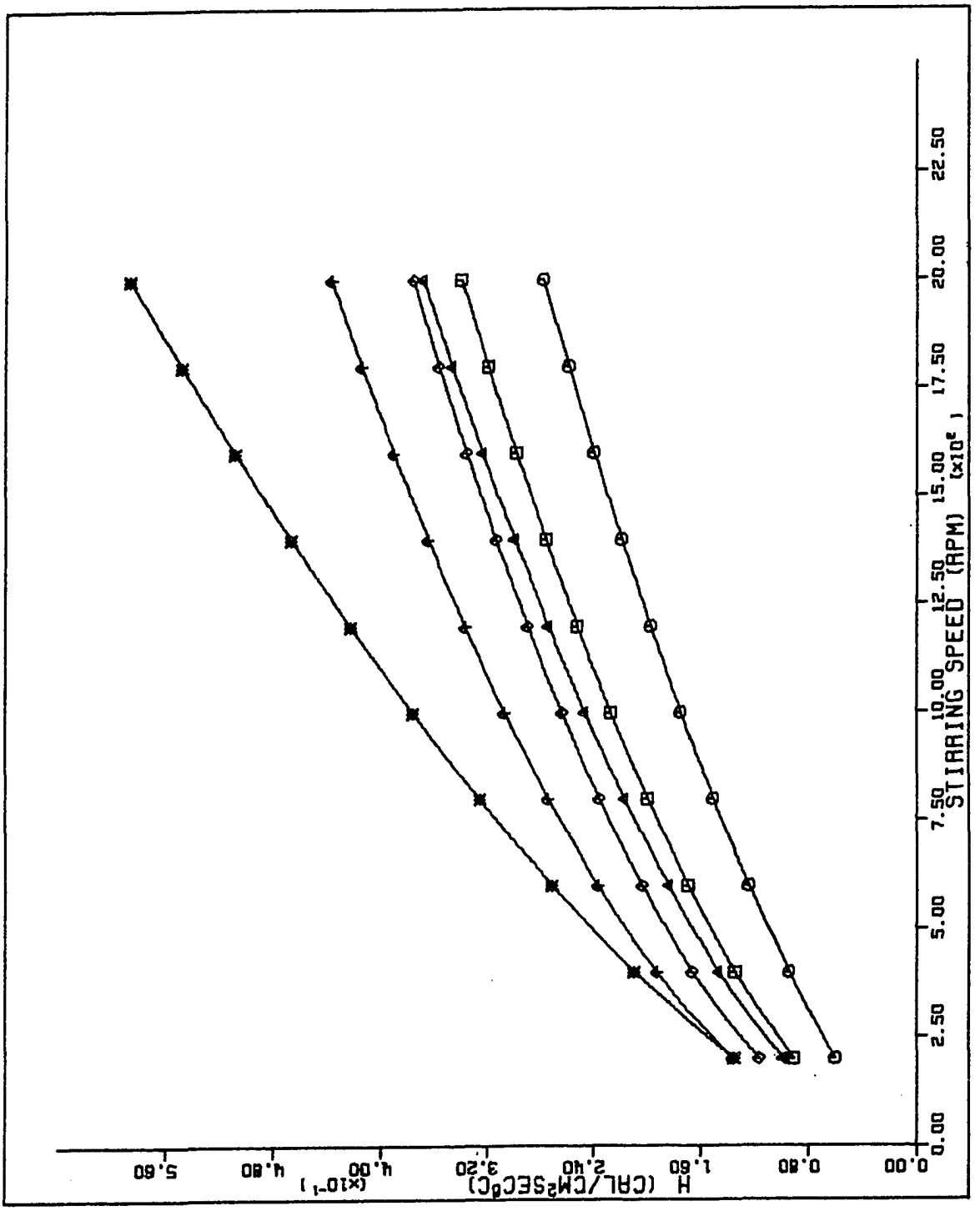
STIRRING SPEED (RPM) (x10²)
0.00
2.50
5.00
7.50
10.00
12.50
15.00
17.50
20.00
22.50
H (CAL/CM²SEC°C) (x10⁻¹)
0.00
0.80
1.60
2.40
3.20
4.00
4.80
5.60

Figure VI.15. Calculated values of alpha squared and product of inverse time constants as a function of N_s

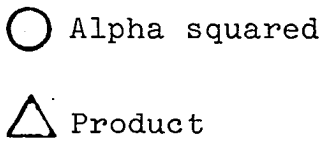

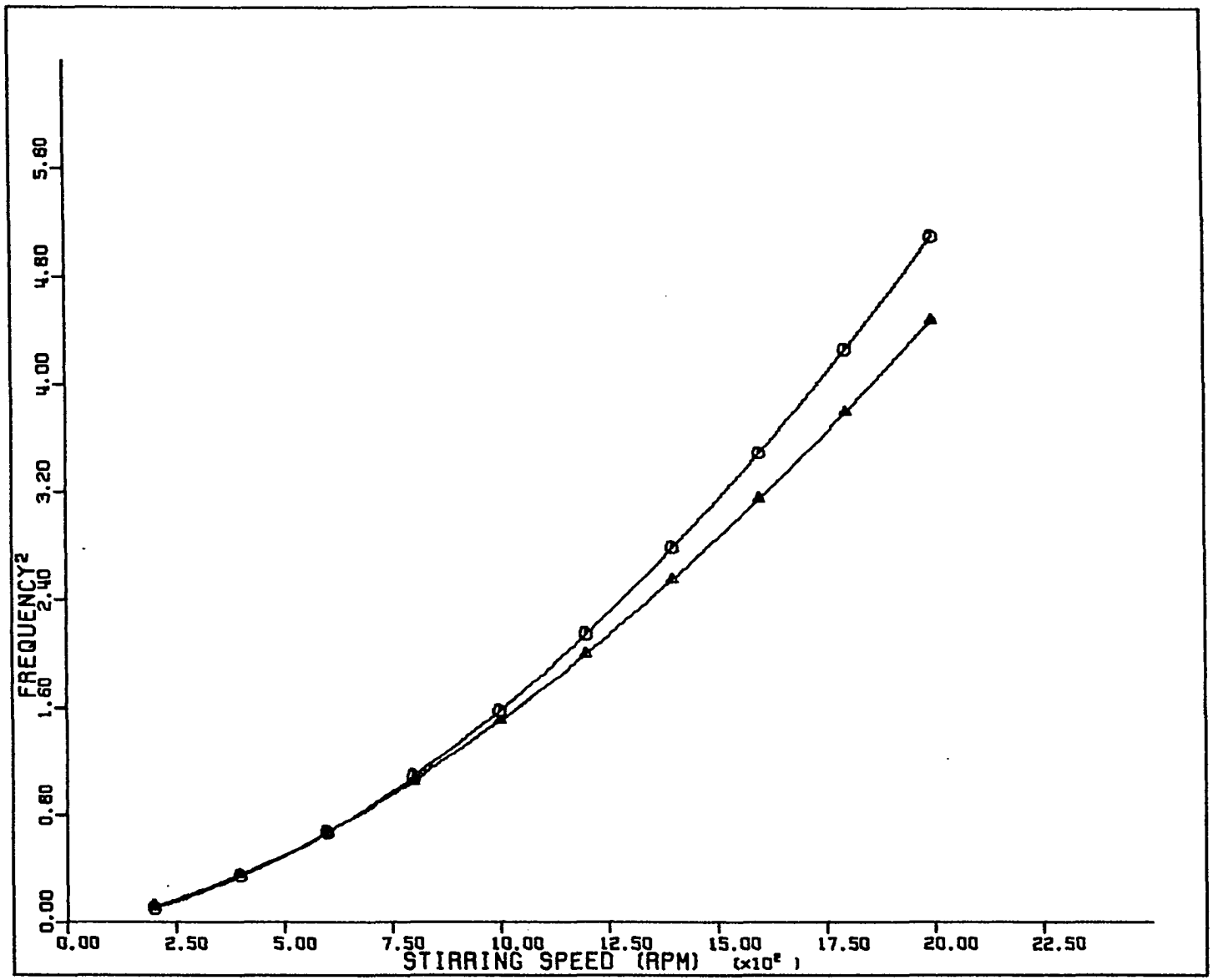
FREQUENCY²
0.00
0.80
1.60
2.40
3.20
4.00
4.80
5.60
0.00
2.50
5.00
7.50
10.00
12.50
15.00
17.50
20.00
22.50
STIRRING SPEED (RPM) (×10²)

Figure VI.16. Theoretical time constants of calorimeter as a function of N_s

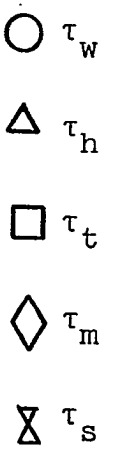

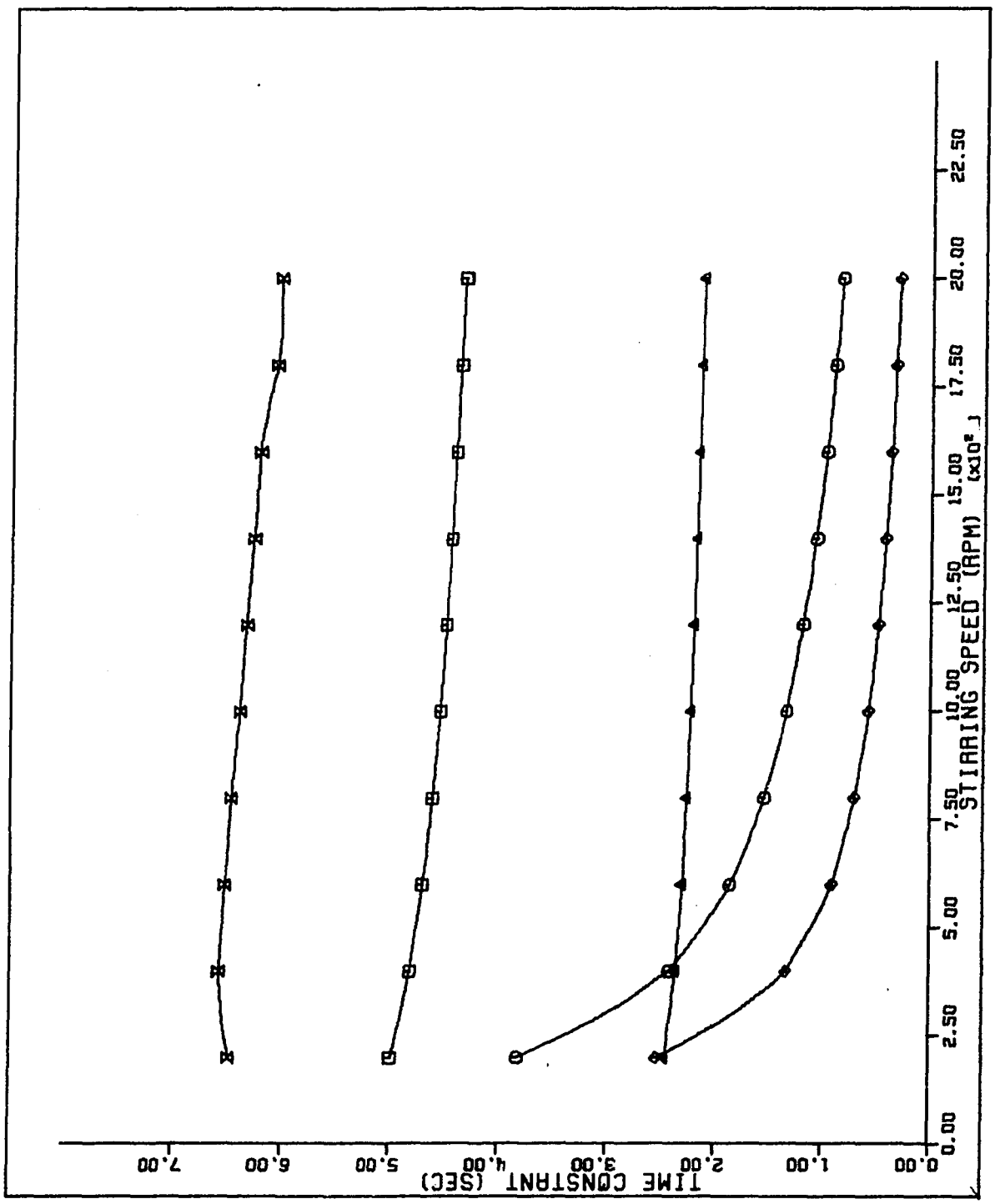
TIME CONSTANT (SEC)
0.00
1.00
2.00
3.00
4.00
5.00
6.00
7.00
STIRRING SPEED (RPM)
0.00
2.50
5.00
7.50
10.00
12.50
15.00
17.50
20.00
22.50
(x10³)

4. Time constant dependence on calorimeter cell operating parameters

This section will summarize time constant dependences as predicted by computer simulation and compare them with experimental results. As shown in Figure V.5, the experimental dependence of τ_s on γ_b for N_s = 430 rpm and r_s = 1.63 cm was small. Computer simulation predicted correctly that τ_s would increase as $1/\gamma_b$ increases. However, the predicted change was very small: τ_s = 6.57 sec at $\gamma_b = 4.92 \times 10^{-4}$ deg C/sec τ_s = 6.65 sec at a $\gamma_b = 2 \times 10^{-5}$ deg C/sec.

Experimental results indicated that at N_s = 1000 rpm, τ_s changes rapidly with $1/\gamma_b$. Simulation predicted a very small change: 6.38 sec going to 6.27 sec for the same range in γ_b cited above but in the wrong direction. Dependence of τ_s on N_s was predicted therefore in error at high stirrer velocities for r_s = 1.63 cm. Comparison of other experimental and simulation results for different values of r_s show qualitative agreement but not quantitative agreement. Experimental results are given in Figure VI.17 for a study with r_s = 0.64, 1.27 and 1.85 cm. Simulated values of τ_s were 2.85, 3.89 and 11.43 sec, respectively, at a $\gamma_b = 4.92 \times 10^{-4}$ deg C/sec. The lack of agreement is thought to proceed from the phenomenological equation derived for the excess temperature within the calorimeter cell. An exponent of two-thirds was assigned to the radius-ratio factor because the bulk solution was in a fully turbulent condition.

Figure VI.17. Experimental time constants of the calorimeter *vs* $1/\gamma_b$ as a function of r_s

$e_+ = e_- = 1000.0$ mV

r_s: ○ 0.64 cm

□ 1.27 cm

△ 1.85 cm

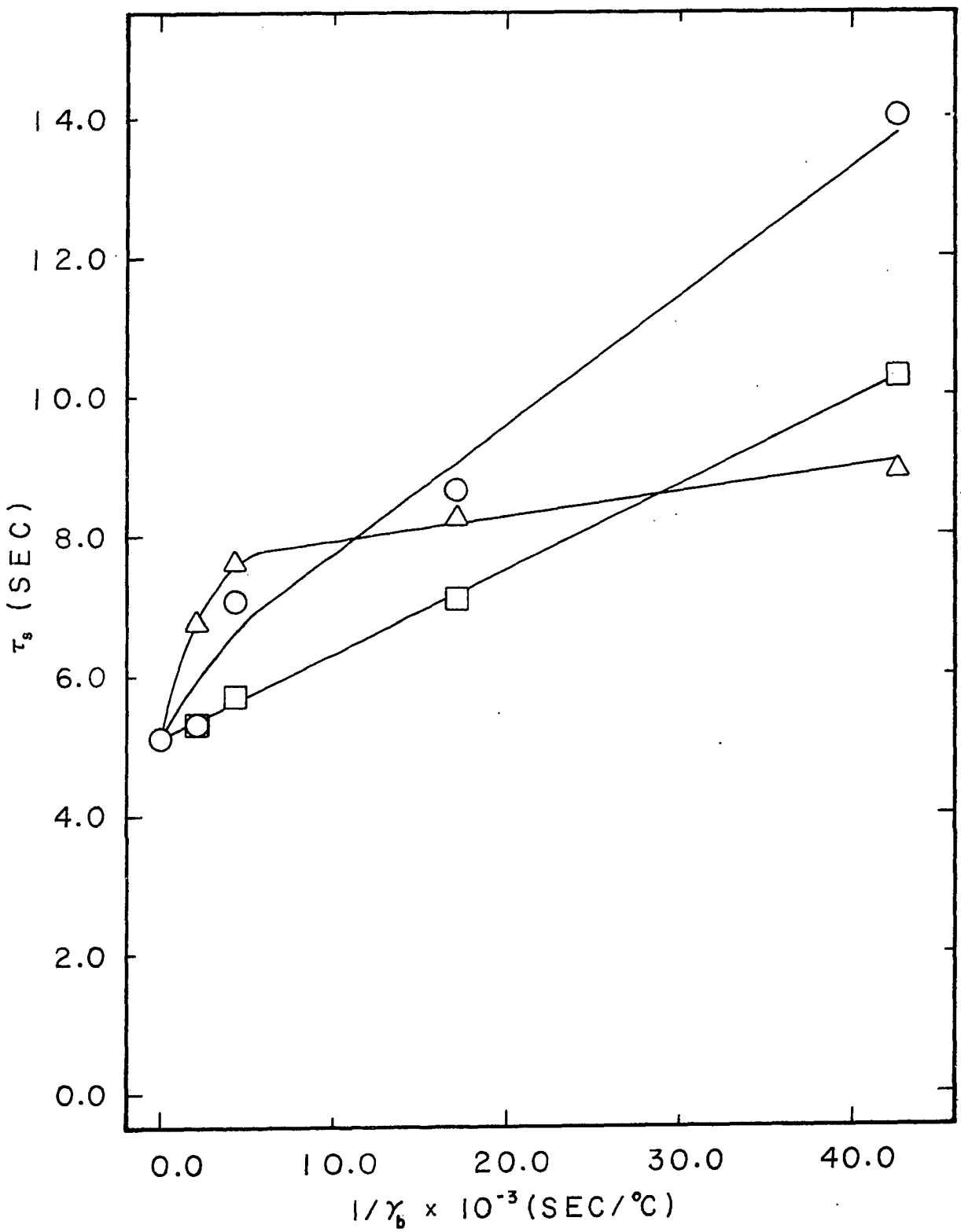
14.0
12.0
10.0
8.0
6.0
4.0
2.0
0.0
τ_s (SEC)
0.0
10.0
20.0
30.0
40.0
$1/\gamma_b \times 10^{-3}$ (SEC/°C)

Comparison of the exponents of Reynolds-number factors of heat transfer equations derived empirically for cylinders and spheres in fully turbulent flows suggests that the exponent should be decreased to ~ 0.6.

The dependence of τ_s on electrical heater placement was also shown in Figure V.5. Calculation of changes in τ_s as a function of χ and ε was not made. The first order theory pertaining to excess temperature regions within the calorimeter predicts that because of the oscillatory nature of the transcendental functions involved, when $\chi = 45°$ or $135°$ and $\varepsilon = 0°$, the excess temperature in the region of the temperature sensor should equal zero. What can be said at the present time from experimental data and development of the theoretical model is that an electrical heater should generally not be placed in the same horizontal plane as the temperature sensor. Although the equation predicts nodal regions, it was derived on the assumption that the design of the heater approximated a point source. If $\chi < 90°$, the bulk solution should flow away from the temperature sensor towards the electrical heater. This would allow three-quarters of a revolution for dissipation of heat through solution mixing.

In this work, the position of the calibration heaters was not chosen on the basis of the present theory since that portion of the general theory of electrical heating in calorimetry was developed after the calorimeter was

constructed. The effect of τ_h was examined by computer simulation in that the size of τ_h was doubled through a change in C_h. The predicted τ_s at 400 rpm was 9.6 sec and 9.0 sec at 1000 rpm. A similar effect on τ_s would be expected if τ_w were doubled in the present situation. As shown in Figure VI.16, the time constant of mixing was strongly dependent on N_s. This suggests that temperature-time characteristics of calorimeters are very strongly dependent on the time constant of mixing expecially at low rotational velocities.

The effect of P_t on τ_s which was briefly mentioned in Section V.B.3 was not examined by simulation. The effect as determined experimentally is seen by comparison of Figure VI.17 with Figure VI.18 where e_- was reduced to 500.00 mV.

5. Optimization of calorimetry system response

The discussion given in the preceeding sections to various parameters in the calorimetry system shows the complexity involved in optimization of response for calorimetry systems. A total of forty-two separate parameters are needed for the computer simulation described in Section VI.C.3. Designing a new calorimeter would seem to be a very difficult task and a priori optimization tedious.

Crude measurements of the time constant of mixing with the proposed stirring system is considered the most important to verify the model used in simulations. Rough estimates of the cell 'wall' parameters are next in importance followed by

Figure VI.18. Experimental time constants of the calorimeter vs $1/\gamma_b$ as a function of r_s

$e_+ = e_- = 500.0$ mV

r_s: ○ 0.64 cm

□ 1.27 cm

△ 1.85 cm

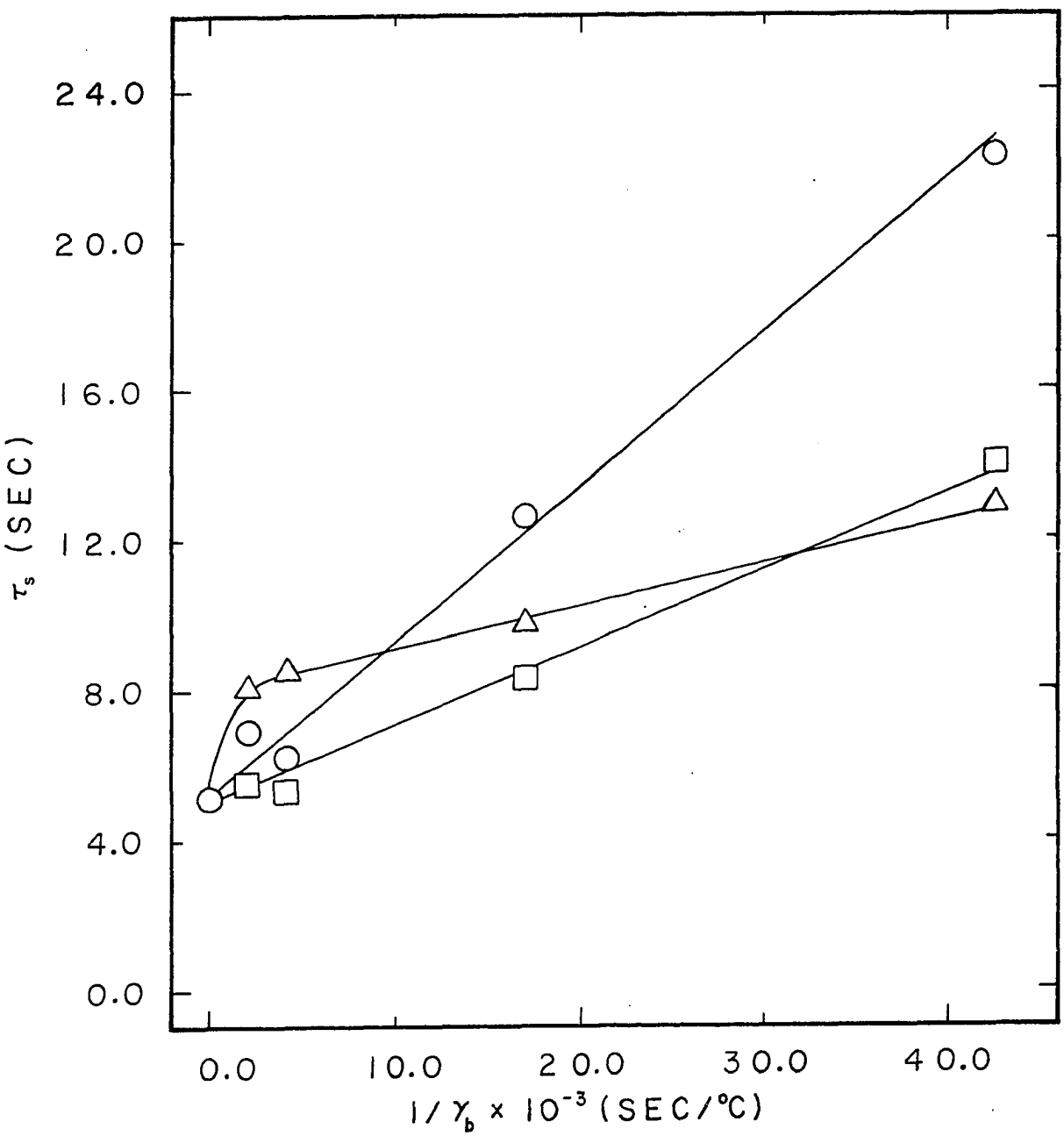
24.0
20.0
16.0
12.0
8.0
4.0
0.0
τ_s (SEC)
0.0
10.0
20.0
30.0
40.0
$1/\gamma_b \times 10^{-3}$ (SEC/°C)

the temperature sensor characteristics. Examination of these variables in the computer program will provide a reasonable first estimate as to the condition for critical damping. Optimization of calorimeter response was shown above to be strongly dependent on N_s and r_s. Another possible approach but one not used in this research is the adjustment of the thickness of the epoxy used to protect the thermistor. This is similar to the procedure suggested by Polaczek and Lisicki (137) who covered their thermocouple with polyethylene.

The use of perforations in the disc stirrers was shown to have the same effect as increasing N_s or r_s but cavitation occurred along the stirrer shaft and bulk solution sprayed onto the cell walls and lid. Both of these undesirable characteristics suggest that impeller and propeller stirrers should not be considered in future calorimeter designs.

VII. STANDARD CHEMICAL SYSTEMS FOR CALORIMETRY

A. Heat of Solution of KCl(s)

1. History

Cohen and Kooy (176) suggested in 1928 that KCl(s) be used as a reference material in solution calorimetry. Subsequent investigations, as summarized by Somsen, et al. (177), and by Parker (178), show a considerable variability of results. It is the opinion of Vasil'ev and Lobanov (179) that such variability is largely due to insufficient precautions in purification of KCl(s). The impurities in KCl(s) as prepared by recrystallization for use in calorimetry would be other alkali metal halides and occluded mother liquor. Most workers dried KCl(s) at 100-120 °C which they presumed was sufficient to remove volatile impurities. The literature of calorimetry is silent on the removal of anion and cation impurities from standard KCl(s) by chemical and physical methods.

The presently accepted value of the heat of solution of KCl(s), as calculated at infinite dilution by Parker from the best data, is

$$\Delta H_S^\circ(H_2O, S, 298.15\ K) = 4115 \pm 10\ cal/mole$$

2. Experimental

a. Preparation of KCl(s) The KCl(s) used in this work as a standard for solution calorimetry was prepared from Baker Analyzed Reagent grade potassium chloride, Lot #30182. The material as received was dissolved in a minimum amount of triply distilled water. The triply distilled water was prepared with a demineralization following the first distillation and with a second distillation from alkaline permanganate solution. The aqueous solution of KCl was passed through a fine fritted-glass filter under vacuum. The filter was cleaned prior to use by soaking in a hot 1:1 H_2SO_4-HNO_3 mixture followed by thorough washing with triply distilled water while under vacuum.

The clear filtrate was raised to the boiling point and treated with $Cl_2(g)$, according to the procedure of Bates (180), to remove Br^-, a principal impurity. Dispersed prepurified nitrogen was used as a sparge to remove $Cl_2(g)$ while the solution cooled to room temperature. The nitrogen used throughout this work was obtained from Air Products and Chemicals of Allentown, Pennsylvania. The solution was heated a second time and sparged with purified nitrogen while cooling. When the solution temperature dropped to approximately 40 °C, the nitrogen sparge was discontinued and the solution was cooled slowly to room temperature.

The large crystals from this purification step were recrystallized in a sufficient volume of triply distilled

water so that only one-third of the solid material dropped out of solution upon cooling. The small shiny white crystals from the second recrystallization were ground in an agate mortar and screened to 60 mesh and smaller size.

The solid was heated at approximately 200 °C at a pressure of 0.5 torr for 12 hours. At 160 °C, many crystals were seen to pop, indicating that occluded mother liquor is not easily removed from this size of crystal. The dried material was kept in a weighing bottle within a vacuum desiccator over Anhydrone obtained from G. F. Smith Chemical Company of Columbus, Ohio.

The purity of KCl(s) prepared as described above was determined by the standard gravimetric method (181) using $AgNO_3$.

b. Injection of KCl(s) into H_2O All trials except the first were carried out at 25.00 ± 0.01 °C by the following procedure. All samples were introduced into the sample chamber of the solid sample injector (described in Section IV.C.2) directly from the weighing bottle with a stainless steel microspatula. The sample chamber was kept closed with a Teflon plug at all times except during transfer of samples into it. The mass of KCl(s) was obtained by difference from the sample chamber mass before and after addition of a sample of KCl(s). Weighing of all solid samples used for calorimetric studies was performed on an Ainsworth FDJ

equal-arm microbalance to the nearest microgram. Weights of KCl(s) were corrected to weight in vacuum using the density of KCl(s), 1.98 g/cm^3. The closed sample chamber was carefully placed into the bottom of the solid sample injector and lifted upward into position. A silicone rubber disc was used to hold the sample chamber in place and seal the injector system.

Triply distilled water which was thermostated at 25.00 ± 0.01 deg C was transferred to both cells of the calorimeter by the procedure described in Section VI.B.2.

The Dewar cells were raised in place and stirring begun. Immediately after assembly, either of the containers was heated to within 0.0001 deg C of the other as determined by the recorded output of OA-3. For these experiments, $e_{o,3}$ was recorded at a sensitivity of 2.805 mV/in on a Heath EU-20W recorder at chart rate of 0.5 in/min. The initial temperature of the reference cell was ∿24.98 deg C and a thermal equilibration period of 30-60 minutes brought the temperature to ∿24.99 deg C. During the equilibration time, the trickle heater in the reference cell was used to reduce the temperature differential between the calorimeter cells to less than 5×10^{-5} deg C as determined by a constant near-zero value of $e_{o,3}$.

Electrical heating of the reaction cell was commenced at ∿24.99 deg C, the exact temperature being calculated beforehand for each run. Approximately one-half of the calculated heat

energy was added electrically before injection of the KCl(s) at 25.0 deg C and the remainder after injection to maintain the temperature differential between the cells at the smallest possible amount.

The calibration heater in the reaction cell was used to bring $e_{o,3}$ to within 0.3-in of the estimated null point from the foreslope at the first turn-off. Subsequent increments of energy reduced the divergence between the extrapolated foreslope and actual afterslope to ∿0.05-in which corresponded to an energy of ∿0.01 calorie. The remaining difference was calculated graphically using appropriate circuit and recorder calibrations.

Separate determinations were made of the energy blank of the solid sample injector due to mechanical heat from pushing the plunger down 0.12-in and heat of vaporization of the bulk solvent into the empty sample chamber.

An amplifier gain of 100 was used with Circuit A throughout these measurements.

3. Results and discussion

The solid sample injector energy blank was 1.30 ± 0.90 x 10^{-2} calorie on the basis of four determinations. The uncertainty given is deviation for 95% confidence. Since the energy blank determinations were made over short time intervals, 30-60 sec, the calculated uncertainties can be compared to calculated circuit noise for 0.1 - 20 Hz. The

uncertainty for circuit noise calculations expressed in calories for Circuit A is 0.34×10^{-2} cal. Since the blank is the difference between measurements over two intervals of time, the calculated uncertainty is 0.68×10^{-2} cal. Thus, there is good agreement between the theoretical uncertainty and the uncertainty of experimental results.

The purity as given by the manufacturer for this lot of KCl(s) was 99.3%. After repurification, a purity of 99.97 ± 0.20% was found based on three determinations.

The temperature at injection of the sample of KCl in the first trial was 25.250 deg C. The calculated value of ΔH_S for the first trial was corrected to 25.00 deg C using the empiric empirical correction given by Vasil'ev and Lobanov (179) of 33 cal/deg C.

Least-squares analysis of the plot of five determinations of H_S *vs* $\sqrt{m}_{KCl}$ for a concentration range of 3.0027×10^{-3} - 1.0650×10^{-2} m yielded

$$\Delta H_S = (4115.9 \pm 3.6) + (536.9 \pm 44.8)m^{\frac{1}{2}} \text{ cal}$$

Hence, the experimental value of ΔH_S° found is in excellent agreement with the value calculated by Parker (178).

The slope of 537 cal/mole $\sqrt{m}$ is in fair agreement with the theoretical value of ∿480 considering the uncertainties in the theoretical value which ranges from 458 - 491 (182).

B. Heat of Neutralization for Reaction of NaOH(aq) and $HClO_4$(aq)

1. History

The use of the NaOH(aq)-$HClO_4$(aq) neutralization reaction as a standard system in solution calorimetry has a very short history compared to the use of KCl(s).

In 1964 Hale and coworkers (183) studied ΔH_N over a concentration range of 4.72×10^{-3} - 1.62×10^{-2} M with HCl(aq) and $HClO_4$(aq). This was followed by the work of Vanderzee and Swanson (184) who used the NaOH(aq)-$HClO_4$(aq) system to determine ΔH_N° (H_2O, L, 298.15 K) through measurements of ΔH_N at ~0.015 M and application of heat of dilution corrections determined separately. Hale *et al.* (183) used a plot of ΔH_N *vs* $\sqrt{\mu}$ to calculate ΔH_N° as well as direct calculation of ΔH_N° at different concentration strengths using heat of dilution corrections.

The advantages of $HClO_4$(aq) over HCl(aq) are a much smaller heat of dilution and greater stability of titer.

2. Experimental

a. *Preparation of solution* Reagent grade $HClO_4$(aq), Lot #733257, was obtained from Fisher Scientific Co. The concentrated $HClO_4$(aq) as received was brought to the boiling point to oxidize any Cl^-(aq) present. Prepurified nitrogen was dispersed through the acid with a coarse fritted-glass

dispersion tube while the solution was being cooled to room temperature.

The nitrogen used for sparging $HClO_4$(aq) of Cl_2(g) and in subsequent work involving acid or bases was prepurified nitrogen passed through a purification train. The purification train consisted of a scrubber filled with Ascarite followed by solutions of the following: 1) vanadium(II) sulfate in 1 M sulfuric acid over amalgamated zinc; 2) alkaline permanganate and distilled water.

The cooled $HClO_4$(aq) was diluted to ∿1 m with boiled triply distilled water while under a blanket of purified nitrogen.

The NaOH(aq) solution was prepared from Baker Analyzed Reagent NaOH pellets, Lot #43188, dissolved in freshly boiled triply distilled water to make a saturated solution while hot. This solution was allowed to settle for one month and then filtered through a fine fritted-glass filter funnel under vacuum in an atmosphere of purified nitrogen within a glove bag. The resulting solution was transferred to the final receiving vessel and diluted with freshly boiled triply distilled water while in the glove bag. The final solution was adjusted under nitrogen after an approximate titration to ∿0.2 m.

Both reagents were stored in three-neck round bottom Pyrex flasks setting on cork rings. All glass connections

were made with Teflon stopcocks at the outlets for those solutions which flowed by gravity. The solutions were protected from carbon dioxide and evaporative losses by bubbler chambers containing nearly the same concentration as the primary solutions involved. The outlet of the NaOH(aq) solution projected into a small three-neck round bottom Pyrex flask which had a rubber septum covering one of the necks and a purified nitrogen inlet in the other neck. The $HClO_4$(aq) solution was tranferred to the titrant storage bottle used on the thermometric titration calorimeter by a nitrogen flushed polyethylene bottle. The titrant storage bottle was protected by a bubbler tube containing $HClO_4$(aq) of the same concentration as used in titrations.

b. Standardization of solutions The NaOH(aq) was standardized by weight titration against National Bureau of Standards primary standard potassium hydrogen phthalate sample 84f. Between 1.2 - 1.4 g samples of primary standard were used for weight titrations and were weighed with a precision of ± 0.1 mg. The potassium hydrogen phthalate was dissolved in 100 ml of boiled triply distilled water. The standard NaOH(aq) was placed in a 100-ml polyethylene bottle fitted with a drawn-out Teflon capillary tip and weighed by substitution on an Ainsworth 28N single pan balance. The increments of titrant, as small as 6-mg, could be added using the plastic bottle as the weight buret. The pH of the

solution was measured with a Beckman No. 40495 high alkalinity glass electrode vs a Beckman asbestos-fiber SCE filled with saturated NaCl(aq). The pH was read with a Corning Digital 112 pH meter to ± 0.001 pH unit. The pH meter was calibrated against two standard buffers originating from the National Bureau of Standards. These buffers were a phosphate buffer at pH 6.685 (25 deg C) and a borax buffer at pH 9.180 (25 deg C) (163).

The titration cell used was a 300-ml Berzelius beaker fitted with a Teflon top having openings for the monitoring electrodes, a nitrogen dispersion tube and the lead from a Pt mesh electrode used for solution grounding.

The concentration of $HClO_4$(aq) was determined by titrations in triplicate of the $HClO_4$(aq) solution against the standardized NaOH(aq). Approximately 10 g of $HClO_4$(aq) solution was diluted by 100 ml of boiled triply distilled water.

Densities of standard NaOH(aq) and standard $HClO_4$(aq) solutions were determined at ∿20 deg C and ∿25 deg C by the pycnometer method using triply distilled water as the reference liquid.

The concentration of carbonate in the standard NaOH(aq) was determined by nephelometry using the method of standard additions. Standard solutions used were 0.1024 M Na_2CO_3(aq) and 1 M $BaCl_2$(aq) prepared from Baker Analyzed grade chemicals.

Triply distilled water was used to prepare these solutions and as the blank. Nephelometric measurements were made with a Hach Clinical Nephelometer, Model #2424, on the 10 x scale. Cells supplied by the manufacturer were thoroughly cleaned with soap and water followed by rinsing with triply distilled water. A rubber septum was put loosely into the mouth of the glass tube and a hypodermic needle connected to a purified nitrogen line was inserted and used to sweep the nephelometry cell of $CO_2(g)$. The top of the rubber septum was then folded down over the lid of the cell to give a tight seal.

Approximately 19.9 g of standard NaOH(aq) were weighed out by difference using a glass 20-ml syringe fitted with a stainless steel needle. The standard NaOH(aq) was injected slowly into the cell followed by a 0.5-ml injection of $BaCl_2(aq)$ solution. The relative scale of the nephelometer was read after a 3-min waiting period. An injection of 5 - 25 µl standard $Na_2CO_3(aq)$ was made 1 min later and the shake-read cycle started. Separate measurements of the blank were made and all instrument readings were corrected for the blank.

c. Thermometric titration of NaOH(aq) with $HClO_4$

The mean temperature for all neutralization experiments was 25.00 ± 0.05 deg C.

The motor driven piston syringes described in Section IV.C.2 were filled from the titrant reservoir. The drive motor was operated briefly in the forward direction with the three-way stopcock turned to the inject position as a pre-titration check of the titrant injection system. The brake was used to stop the titrant syringe pistons at the desired position. The tips of the injection capillaries were wiped clean of acid with a Kimwipe taking care not to withdraw titrant by capillary action. The drive motor of syringe was then reversed to form an air bubble in the capillary tip to prevent pretitration diffusion of the acid into the base.

To reduce contamination by atmospheric $CO_2(g)$ of the triply distilled water added by pipet, the calorimeter cells were flushed before solvent addition with purified nitrogen and covered with watch glasses. These covers were pushed aside only as necessary to add solutions.

Triply distilled water which had been vigorously boiled in a 2-l Pyrex suction flask and cooled to room temperature under purified nitrogen was used for the bulk solution in all determinations of heat of neutralization. The suction flask had been cleaned prior to use with boiling 1:1 mixture of H_2SO_4 and $HClO_4$. The flask was then thoroughly rinsed with triply distilled water.

The initial temperature of the triply distilled water before pipeting was adjusted to 24.0 ± 0.1 deg C by partial

immersion of the suction flask into a cold water bath. The lower initial temperature of the triply distilled water for these experiments was necessary since the calorimeter cells were heated twice before a thermometric titration to determine heat capacity ratios.

Throughout temperature adjustment and pipeting, a strong flow of purified nitrogen was maintained over the triply distilled water. This was accomplished by connection of the side arm of the section flask with the flow of purified nitrogen.

The mass of triply distilled water added by the calibrated pipet was kept constant throughout this work. The apparent mass of samples of base ranged from 0.999 - 14.2 g. The masses of water and base were determined by difference to ± 0.1 mg.

Glass syringes equipped with stainless steel needles of equal size were used to add nearly equal masses of triply distilled water and standard NaOH(aq) to the reference cell and reaction cell of the calorimeter. The syringe needles were immersed about 1 cm into the bulk solution while the additional water or base were added.

Purified nitrogen was dispersed into the vapor volume of the calorimeter cells through 10 mm medium porosity fritted-glass sparging tubes while the calorimeter assembly was raised in place. The nitrogen sparge was continued approximately 5 min after solution stirring was begun.

After final assembly of the calorimeter, the containers were heated simultaneously to raise their temperatures to approximately 24.6 deg C and adjusted to within 0.0001 deg C of each other. For these experiments, $e_{o,3}$ was recorded at a sensitivity of 11.15 mV/in on a critically damped Heath EU-20W recorder at a chart rate of 0.5 in/min. Additionally, $e_{o,4}$ (see Section VI.B.2) was recorded manually on the recorder at one minute intervals. The time signal of WWV, Fort Collins, Colorado, was used as a time marker in the measurement of $e_{o,4}$.

A thermal equilibration period of 30 - 60 min brought the temperature to approximately 24.7 deg C. During the equilibration time, the trickle heater in the reference cell was used to reduce the temperature differential between the calorimeter cells to less than 5×10^{-5} deg C as determined by a constant near-zero value of $e_{o,3}$. The heat capacity ratio of the calorimeter cells was determined both before and after the thermometric titration. Thus, by extrapolation, the heat capacity ratio of the calorimeter cells was determined at the mean temperature of the thermometric titration (185).

In the initial experiments, 7.555-calories were added to each cell alternately to determine the respective heat capacities. In the second series and subsequent work, approximately 10 calories were added simultaneously to each cell to determine the heat capacity ratio. The heat capacities

of the reference cell and reaction cell were determined twice before thermometric titration and twice afterward.

Before titrations were commenced, the baseline was again adjusted to near-zero and a baseline equal in time to the time anticipated for the titration was run.

The temperature of the titrant was monitored versus the temperature of the titrand in the reference cell of the calorimeter. Thermometric titrations were begun when the temperature difference between the titrand and titrant was approximately one-half of the projected temperature rise due to the electrical heating needed to equal the chemical reaction heat in the reaction cell of the calorimeter. The sensitivity of the temperature bridge used for titrant-titrand temperature differences was 68.44 ± 0.08 mV/deg C. This temperature bridge output, $e_{o,5}$, was measured with a Corning Digital 112 pH meter in the mV mode. Since the resolution of the pH meter was ± 0.1 mV, the temperature resolution of the second temperature bridge was ± 1.5 mdeg C.

Approximately one-fourth of the calculated energy was added electrically to the reference cell before simultaneous addition of titrant to both cells was begun. Electrical heating of the reference cell continued during and after the thermometric titration until the recorded output of OA-3 approached the estimated baseline. The estimated baseline position was calculated by extrapolation of the foreslope.

Calculations were made with a hand calculator on the $e_{o,4}$ data. Thus, the temperature differential between the calorimeter cells was maintained at the smallest possible amount throughout the titration procedure.

An initial series of seven thermometric titrations of NaOH(aq) with $HClO_4$(aq) was performed varying the concentrations of base and keeping the quantity of acid constant. A second series of thermometric titrations was performed with a nearly stoichiometric ratio of acid to base throughout. That is, the base was added to the triply distilled water and its mass plus concentration were used to adjust the quantity of acid to be added so that the acid would be in excess by only approximately 1.5%. Titrant flow rates ranged from 0.00025 - 0.005 ml/sec.

Separate determinations were made of the energy blank of the titrant injection system caused by a slight temperature mismatch of the titrant thermostating reservoirs above each cell of the calorimeters.

An amplifier gain of 100 was used with Circuit B throughout these and subsequent calorimetric measurements.

3. Results and discussion

The concentrations of standard NaOH(aq) and $HClO_4$(aq) were calculated from titration data according to the procedure of Yan (186). The concentration of standard NaOH(aq) found was 0.21980 m with a relative standard deviation of 0.48 ppt.

The concentration of $HClO_4$(aq) was 0.96156 m with a relative standard deviation of 0.20 ppt.

The densities of standard NaOH(aq) and $HClO_4$(aq) at 19.5 deg C were 1.0081 g/cm^3 and 1.0557 g/cm^3, respectively. At 25.02 deg C, the respective densities were 1.0066 g/cm^3 and 1.0535 g/cm^3.

The mean concentration of $CO_3^=$(aq) in the standard NaOH(aq) solution from duplicate trials was 5.3×10^{-5} m. Therefore, the relative concentration of $CO_3^=$(aq) in the standard NaOH(aq) solution was 0.25 ppt. As discussed by Vanderzee and Swanson (184), such a concentration of $CO_3^=$(aq) would reduce the evolved heat for the titrations with NaOH(aq) as the limiting reagent by approximately 2 cal/mole.

The energy blank of the titrant injection system as determined from four trials with 2.000 ml of 0.96156 m $HClO_4$(aq) injected into 298.28 g of triply distilled water was in calories

$$q_{HClO_4} = (0.0371 \pm 0.0036) + (0.00411 \pm 0.00052)e_{o,5}(mV)$$

The energy blank was exothermic in the reaction cell which implied that the aluminum calorimeter head was warmer above the reaction cell. The friction of a tighter fitting bearing above the reaction cell was probably the source of heat. This conclusion was also in accord with the fact that the trickle heater in the reference cell had to be used continuously to

maintain a constant near-zero value of $e_{o,3}$. The temperature difference in the aluminum block as calculated from electrical energy input to the trickle heater and heat transfer coefficients of calorimeter cell probes was approximately 6.5 mdeg C.

Error due to mismatch of the amount of $HClO_4$(aq) injected into each calorimeter cell was also corrected for in q_{HClO_4}. Proportional amounts of q_{HClO_4} were applied to thermometric titrations where the volume of $HClO_4$(aq) titrant added was not equal to 2.000 ml.

The results of two initial sets of thermometric titrations of NaOH(aq) with $HClO_4$(aq) are given in Tables VII.1 and VII.2 and plotted in Figure VII.1 as a function of the initial concentration of NaOH(aq). The value of c_2/c_1 used to calculate the corrected reaction energy was obtained at the mean reaction temperature by a graphical fit of c_2/c_1 versus temperature data. The calculated final pH given in Table VII.1 for the reaction cell was not corrected for activity. Results given in Table VII.1 were obtained by using a constant amount of acid with varying amounts of base. The final ionic strength of the first series was nearly identical throughout with the exception of those trials with excess base. Results in Table VII.2 were obtained by maintaining a nearly stoichiometric ratio of acid to base. A maximum of 1.5% excess base was used in the second series

Table VII.1. Heat of neutralization of NaOH(aq)
(Constant amount of acid)

$n_{a,1} = 1.9937 \pm 0.0002 \times 10^{-4}$ moles

$n_{a,2} = 2.0055 \pm 0.0002 \times 10^{-3}$ moles

Trial #	$n_{NaOH} \times 10^3$ (moles)	$m_{NaOH} \times 10^3$ (moles/kg)	n_a/n_b
4	1.0979	4.4168	1.8267
5	0.88615	3.4983	2.2632
6	0.65825	2.6095	3.0467
7	1.7689	6.8743	1.1338
8	1.9868	7.6910	1.0094
9	0.44173	1.7582	4.5401
11	2.3772	9.1410	0.84364
12	1.4369	5.6176	1.3957
18	2.2095	8.5194	0.90767

Final reaction pH (calculated)	q_{HClO_4} (calories)	q (calories)	$-\Delta H_N$ (Kcal/mole)
2.447	0.0467	14.652	13.345
2.355	0.0392	11.874	13.400
2.272	0.0383	8.676	13.181
3.037	0.0309	23.402	13.230
4.143	0.0556	26.187	13.180
2.206	0.0360	5.705	12.915
11.155	0.0440	27.769	13.846
2.653	0.0371	19.196	13.360
10.309	0.0381	27.502	13.713

Table VII.2. Heat of neutralization of NaOH(aq)

Trial #	$n_{NaOH} \times 10^3$ (moles)	$m_{NaOH} \times 10^3$ (moles/kg)	n_a/n_b
8	1.9868	7.6910	1.0094
15	0.65540	2.5976	1.0150
16	1.1082	4.3576	1.0017
17	1.5375	5.9997	1.0109
19	2.21975	0.87795	1.0130
20	3.1320	11.884	1.0044
22	2.7315	10.438	1.0044

Final reaction pH (calculated)	q_{HClO_4} (calories)	q (calories)	$-\Delta H_N$ (Kcal/mole)
4.143	0.0556	26.187	13.180
5.194	0.0129	8.154	12.442
5.734	0.0254	14.162	12.780
4.775	0.0318	20.171	13.119
5.545	0.0047	2.694	12.260
4.486	0.0714	41.332	13.197
4.917	0.0707	36.013	13.185

Figure VII.1. Heat of neutralization of NaOH(aq) as a function of initial concentration

△ Acid concentration constant, base concentration varies

□ $n_a/n_b \simeq 1$

○ Reference 183

⬡ Reference 187

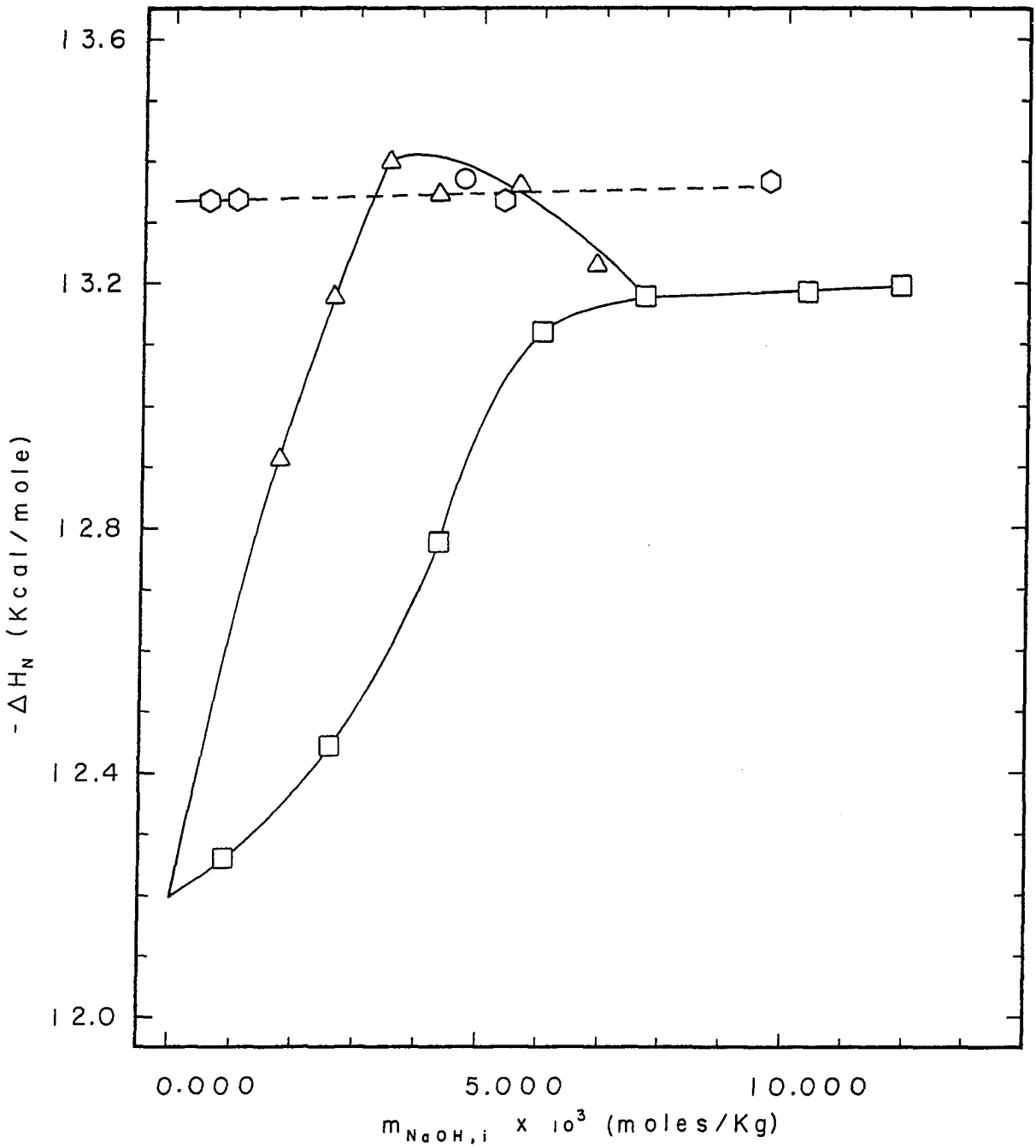
13.6
13.2
12.8
12.4
12.0
$-\Delta H_N$ (Kcal/mole)
0.000
5.000
10.000
$m_{NaOH,i}$ x 10^3 (moles/Kg)

to approximate the maximum excess acid used in the thermometric titrations of 4-aminopyridine(aq).

These results strongly diverge from all previously reported values of ΔH_N in this range of base concentration. The usual results are shown by the dashed line in Figure VII.1 from the data of Hale *et al.* (183) and Eatough *et al.* (187). The second reference is a very recent study of the NaOH-$HClO_4$ system in water with a greatly improved isothermal titration calorimeter. It is the only report of thermometric titrations of NaOH(aq) which achieved a precision comparable to the present experiments at a lower concentration of NaOH(aq).

Additional sets of data of ΔH_N were obtained for a nearly constant amount of base with varying amounts of acid, Table VII.3 and Figure VII.2, and ΔH_N as a function of [$NaClO_4$(aq)] in the reference cell of the calorimeter as given in Table VII.4 and Figure VII.3.

Although the data of Tables VII.1 and VII.2 can be used singly or combined to give many interesting plots, the most informative are produced in Figures VII.4 and VII.5. In Figure VII.4, the values of ΔH_N obtained for Table VII.1 were plotted *versus* n_a/n_b and in Figure VII.5 *versus* the final reaction cell pH corrected for activity. When n_a/n_b was less than one, the value of ΔH_N found was in considerable excess of the presently accepted value of ΔH_N at that ionic strength.

Table VII.3. Heat of neutralization of NaOH(aq)

(∿Constant amount of base)

Trial #	$n_{NaOH} \times 10^3$ (moles)	$m_{NaOH} \times 10^3$ (moles/kg)	$n_{HClO_4} \times 10^3$ (moles)	$m_{HClO_4} \times 10^3$ (moles/kg)
15	0.65540	2.5976	0.66179	2.6159
14	0.65200	2.5848	1.4740	5.8082
6	0.65825	2.6095	2.0055	7.8847

Final reaction pH (calculated)	q_{HClO_4} (calories)	q (calories)	$-\Delta H_N$ (Kcal/mole)
5.194	0.0129	8.154	12.442
3.085	0.0288	8.400	12.884
2.272	0.0383	8.676	13.181

Figure VII.2. Heat of neutralization of NaOH(aq) as a function of n_a/n_b (constant base concentration)

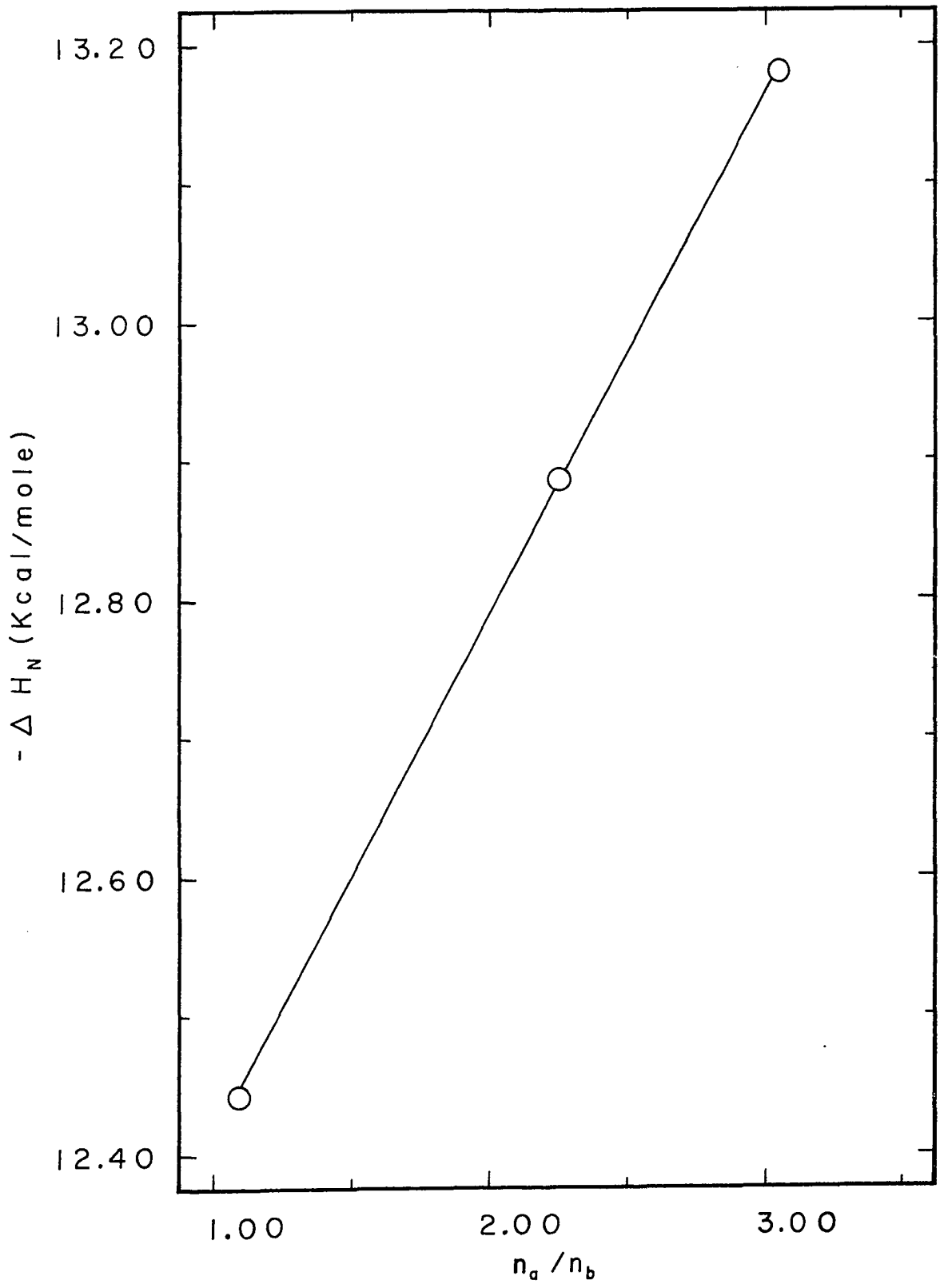
13.20
13.00
12.80
12.60
12.40
- Δ H_N (Kcal/mole)
1.00
2.00
3.00
n_a / n_b

Table VII.4. Heat of neutralization of NaOH(aq) when $NaClO_4$(aq) is present in reference cell of the calorimeter

$n_{a,2} = 1.1101 \times 10^{-3}$ moles

Trial #	$n_{NaOH} \times 10^3$ (moles)	$m_{NaOH} \times 10^3$ (moles/kg)	$n_{NaClO_4} \times 10^3$ (moles)	$m_{NaClO_4} \times 10^3$ (moles/kg)
16	1.1082	4.3576	0.0000	0.000
23	1.1049	4.4358	3.0904	12.161
24	1.1019	4.4236	1.0759	4.2341

q_{HClO_4} (calories)	q (calories)	$-\Delta H_N$ (Kcal/mole)
0.0254	14.162	12.780
0.0218	14.431	13.061
0.0217	14.330	13.005

Figure VII.3. Heat of neutralization of NaOH(aq) as a function of the concentration of $NaClO_4$ (constant base concentration)

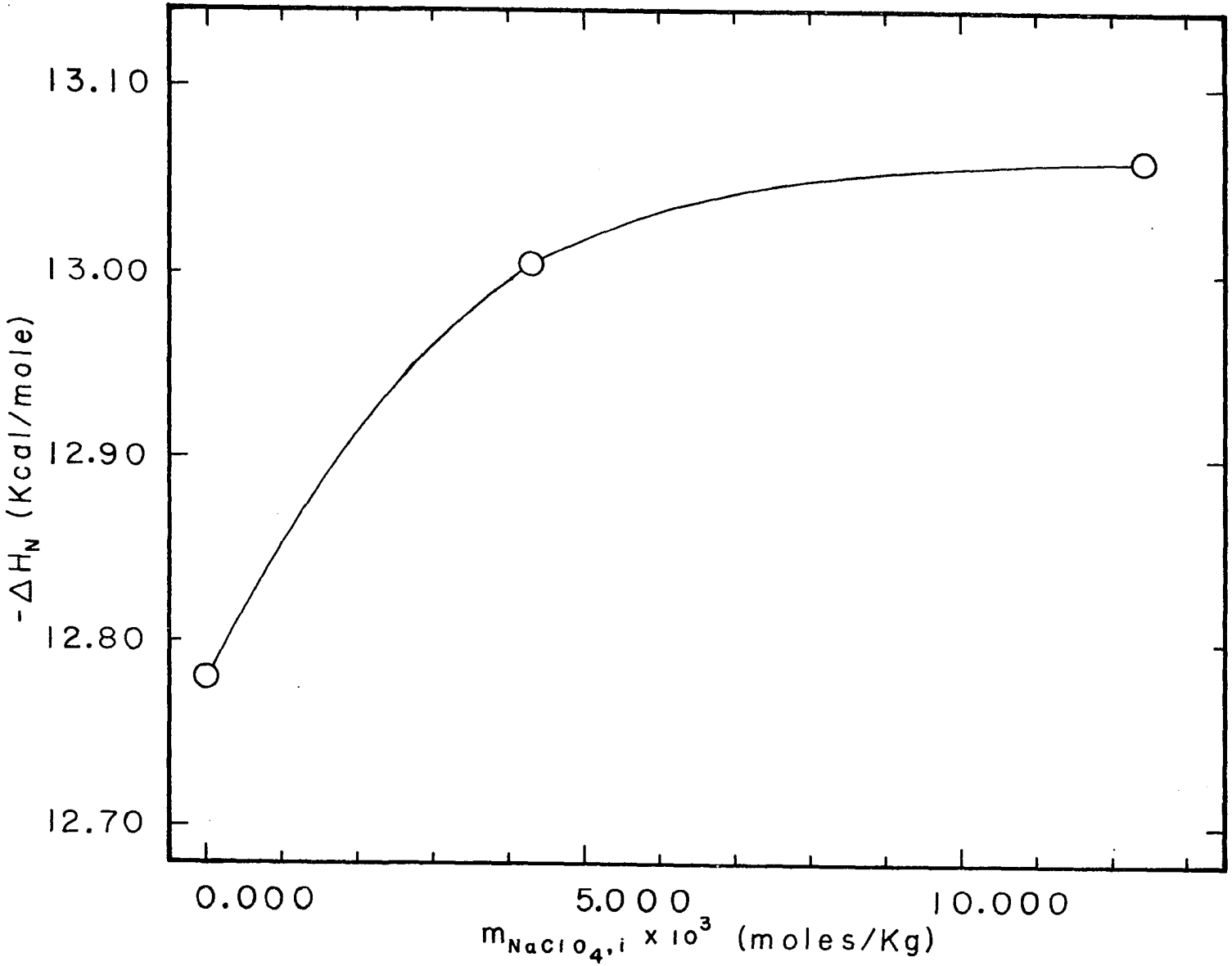
13.10
13.00
12.90
12.80
12.70
$-\Delta H_N$ (Kcal/mole)
0.000
5.000
10.000
$m_{NaClO_4,i} \times 10^3$ (moles/Kg)

Figure VII.4. Heat of neutralization of NaOH(aq) as a function of n_a/n_b (constant acid concentration)

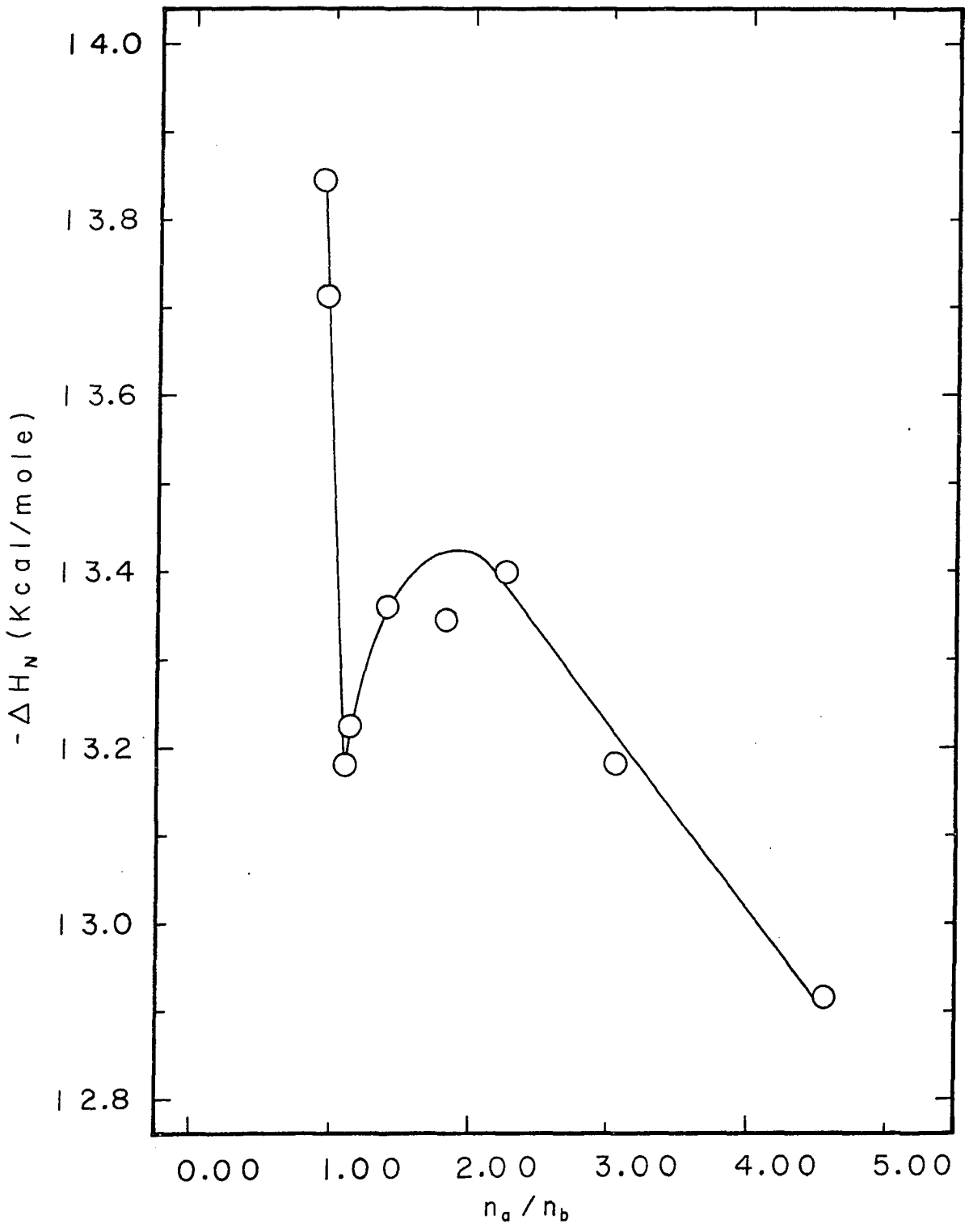
14.0
13.8
13.6
13.4
13.2
13.0
12.8
$-\Delta H_N$ (Kcal/mole)
0.00
1.00
2.00
3.00
4.00
5.00
n_a / n_b

Figure VII.5. Heat of neutralization of NaOH(aq) as a function of uncorrected endpoint pH ($n_a \simeq n_b$)

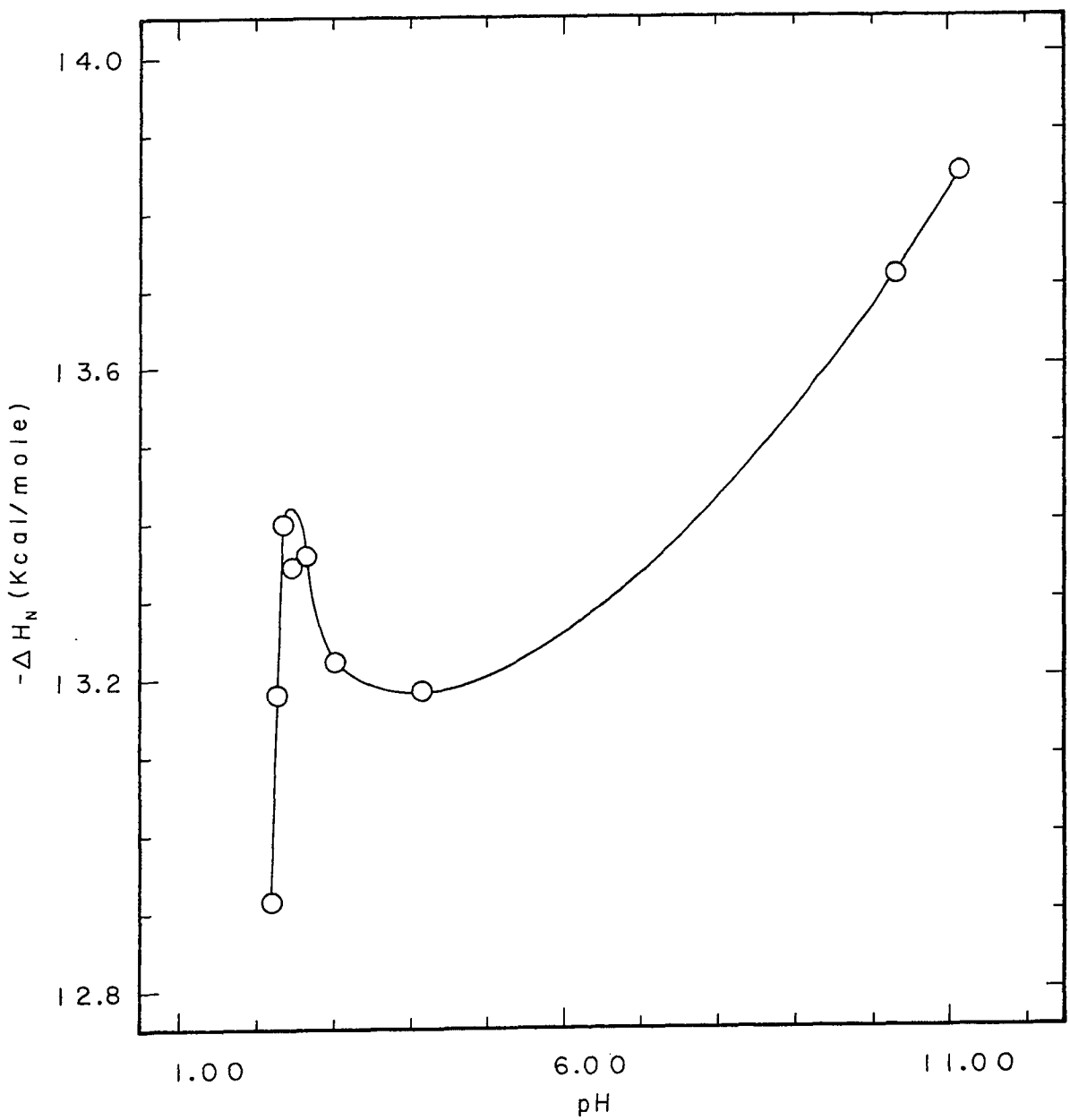
14.0
13.6
13.2
12.8
-ΔH_N (Kcal/mole)
1.00
6.00
11.00
pH

The value of ΔH_N° obtained with excess base by differential calorimetry would be larger than that at $n_a/n_b = 1$. The only other reported results of ΔH_N° using differential calorimetry was by Papee et al. (188) who used an unspecified acid to base ratio with base present in approximately four fold excess at all times. The reported value of - 13,500 cal/mole for ΔH_N° by Papee and coworkers is in agreement with the conclusion reached above in respect to the effect of excess base upon the value of ΔH_N obtained.

The surprising result from the present experiments is that ΔH_N° obtained from the original data of Tables VII.1 or VII.2 is nearly identical when compared graphically. The reason for the divergence of the present results from accepted results for ΔH_N obtained by single cell calorimetry was difficult to determine other than the readily discernible dependence of ΔH_N on endpoint pH. Unless the dependence of ΔH_N on endpoint pH is a very strong function of NaOH(aq) concentration, the reason must be sought elsewhere.

The thermometric titration data presented in Table VII.3 indicates that as excess acid was added to both cells of the calorimeter, the measured value of ΔH_N increased. Since the measured value of ΔH_N would increase either if the reaction was exothermic in the reaction cell or endothermic in the reference cell, an additional single trial was performed where $HClO_4$(aq) titrant was added as a slug to the reaction

cell with the solid sample injector as part of Trial #19. After the usual thermometric titration and determinations of the heat capacity were finished in Trial #19, additional $HClO_4(aq)$ titrant was added as a slug and since it was initially isothermal with the contents of the calorimeter, no corrections needed to be applied.

The reaction was exothermic with 0.252 calories of heat liberated from the addition of 0.6202 g of $HClO_4(aq)$ titrant. The measured reaction heat was therefore -423 cal/mole for this trial at a final concentration of $NaClO_4(aq)$ plus $HClO_4(aq)$ of 3.273×10^{-3} m. The addition of excess acid to $NaClO_4(aq)$ produced as the product of neutralization gives an exothermic reaction from the data obtained for Table VII.3.

The heat of dilution from excess acid added to each cell of the calorimeter should be equal since the ionic strengths were equal after neutralization of available base was finished. Hence, the exothermic reaction in the reaction cell was due to an additional chemical reaction.

The results given in Table VII.4 can be interpreted either that the heat of dilution of $HClO_4(aq)$ becomes increasingly exothermic as the initial ionic strength decreases or there is a heat of mixing between $HClO_4(aq)$ and $NaClO_4(aq)$. The results given in Table VII.4 are in accord with the results of Table VII.2 where the changes in the reaction energy per mole at higher ionic strengths (>10 mmol)

are relatively small. The possibility of a heat of mixing between $HClO_4$(aq) and $NaClO_4$(aq) was examined by Swanson and Vanderzee (184) but was dismissed on the basis of results obtained at $\mu = 1.0$ for 1-1 electrolytes by Young, et al. (189). If the heat of mixing for $HClO_4$(aq) added to $NaClO_4$(aq) at the concentrations employed in this work was truly zero, then the obvious conclusion is that the heat of dilution of $HClO_4$(aq) is quite exothermic at low ionic strengths.

Comparison with the results obtained for ΔH_N of 4-aminopyridine(aq) with $HClO_4$(aq) immediately shows that the rapid dropoff of ΔH_N with decreasing concentrations of NaOH(aq) is related to some characteristic of the NaOH-$HClO_4$ system and not some general characteristic of the calorimeter. The discrepancy between the present results for ΔH_N and accepted results for the NaOH-$HClO_4$ system was not a feature of experimental technique since a number of the results for the NaOH-$HClO_4$ system were obtained concurrently with thermometric titrations of 4-aminopyridine(aq) with $HClO_4$(aq).

Several attempts were made to formulate a quantitative model for the observed changes in ΔH_N as a function of pH, ionic strength, and acid base ratio. They were based on changes in ionic hydration. All were unsuccessful.

Fitting the results for ΔH_N obtained in Trials #8, 11, and 18 versus the final solution pH corrected for activity

yielded a value of ΔH_N = - 13.337 Kcal/mole at a pH of 7 and approximate molality of 8 x 10^{-3} m. This value corresponds very closely to the presently accepted value of ΔH_N^o = - 13.345 Kcal/mole (178) but differs by approximately 50 cal/mole from the value for ΔH_N as determined by single cell calorimetry at the same concentration.

VIII. INVESTIGATION OF 4-AMINOPYRIDINE AS A CALORIMETRIC STANDARD

A. Introduction

Besides the NaOH(aq)-$HClO_4$(aq) system, the use of tris(hydroxymethyl)aminomethane(aq) (THAM) has been proposed, together with $HClO_4$(aq), as a suitable calorimetric standard by Wilson and Smith (190).

The substitution of a base in solid form for NaOH(aq) which would be more resistant to reaction with components of the laboratory atmosphere is a very desirable goal. The potential of THAM(s) as a solution calorimetry standard has been examined by several workers (187, 191-194) whose conclusions are generally favorable for the proposal. Yet, the use of THAM(s) for acidimetry and calorimetry is not completely blissful. Recrystallization is the only present viable method of purification of THAM(s) with the attendant problem of occlusion of mother liquor. Additionally, decomposition of THAM(s) occurs upon the application of heat to remove the occluded volatile impurities. Variable purity of reagent grade THAM(s) was shown by Koch et al. (191) to preclude the consideration of THAM(s) as a primary standard for acidimetry.

What is needed then is a weak base having the same favorable handling characteristics as THAM(s) without

problems of purification. The successful use of 4-aminopyridine(s) as a titrimetric standard by Hoyle (91) led to the suggestion that 4-aminopyridine(s) should be examined carefully as a primary standard in solution calorimetry.

When this work was begun, consultation of the literature revealed no determinations of ΔH_N of 4-aminopyridine(aq) by calorimetry; only reports of studies of ΔH_N with potentiometry and electrochemical cells (14, 15) were found. Subsequently, ΔH_N of 4-aminopyridine(aq) was determined by Christensen *et al.* (16) using thermometric titrimetry as part of a general study of substituted pyridines. No special mention of 4-aminopyridine(aq) was made in that study although the agreement between electrochemical and calorimetric methods was reasonable. It then became the ultimate objective of this work to independently examine ΔH_N of 4-aminopyridine(aq) as a function of concentration (not done by Christensen, *et al.*) to determine the suitability of 4-aminopyridine(aq) as a primary standard for solution calorimetry.

B. Experimental

1. Purification of 4-aminopyridine(s)

The sample of 4-aminopyridine(s) used in this work was obtained as reject material from the purification procedure of Hoyle (91). This material was dark brown in color and

obviously much more impure than that usually obtainable from commercial sources.

The purification of the 4-aminopyridine(s) was accomplished in two steps. The crude material was dissolved in dry toluene, decolored with activated carbon and recrystallized. The second step in purification was sublimation at 110 °C. The sublimation temperature was determined from the results of differential thermal analysis of the semipurified material. The sublimation apparatus consisted of a 6-in diameter inverted Pyrex funnel ground to fit smoothly against a Pyrex cover glass of equal diameter. A Pyrex rod with 6-mm diameter and 10-in length was fused perpendicular to the center of the inside of the cut-off bottom from a 500-ml Erlenmeyer flask. This rod-dish device was suspended inside the inverted funnel above the crude 4-aminopyridine(s) which was spread over the concave surface of the cover glass.

The outer surface of the inverted funnel was cooled by a tightly wound coil of 0.125-in copper tubing molded in the form of a cone covering the entire funnel surface except for the neck. The coil was cooled by a stream of tap water. Crystals of 4-aminopyridine(s) formed on the underside of the funnel. Any crystals which became dislodged were caught by the rod-dish device. The rate of sublimation was ~0.2 g/day with this device. The rate of deposition was

purposely kept low to assure minimal vapor-phase transfer of impurities. The sublimed material was collected once a week from the sublimation apparatus and kept in closed weighing bottles over Anhydrone in a desiccator.

2. Determination of purity of 4-aminopyridine(s)

The purity of 4-aminopyridine(s) and several commercially available samples of reagent grade THAM(s) were determined by weight titration with a second set of standard NaOH(aq) and $HClO_4$(aq) solutions according to the procedure in Section VII.B.2.a for NaOH(aq). The sample size was 0.150-0.200 g weighed out by difference on an Ainsworth FDJ equal-arm microbalance to the nearest microgram. The samples of THAM(s) were ground in an agate mortar and pestle, sieved to 60-mesh or smaller and dried over Anhydrone for 12 hr at 1 torr.

All masses were corrected to vacuum using experimentally determined densities of NaOH(aq) and $HClO_4$(aq) and a density of 7.84 for all standard weights.

As described in Section II.B, 4-aminopyridine forms complexes with many transition elements. The volatility of these complexes is unreported. Hence, the presence of metallic impurities, notably iron, was checked by arc emission spectroscopy. Arc emission spectroscopic analyses were performed on an ARL Model 26000-1 Spectroscopic Analyzer and Comparator. Kodak Spectrum Analysis Film 5367 SA-1 was used

to record all spectra. Approximately 15 mg samples of 4-aminopyridine(s) were used in duplicate spectral analyses.

3. Thermometric titration of 4-aminopyridine(aq) with $HClO_4$(aq)

The procedures were a hybrid of those described in Section VII.A.2.b for KCl(s) and Section VII.B.2.c for NaOH(aq).

The temperature at which ΔH_S of 4-aminopyridine(s) was determined was 24.85 ± 0.02 deg C. All determinations of ΔH_N of 4-aminopyridine(aq) with $HClO_4$(aq) were made at 25.00 ± 0.05 deg C.

4. Preparation of 4-aminopyridine perchlorate(s)

The procedure of Barnes and Matuszko (195) was used to prepare 4-aminopyridine perchlorate(s). However, 4-aminopyridine(s) purified by sublimation was used instead of semipure 4-aminopyridine(s). This insured a pure product and reduced the possibility of explosion due to heavy metal contamination (196).

The concentrated $HClO_4$(aq) was boiled to oxidize Cl^-(aq) and sparged with purified nitrogen during cooling to remove the resulting Cl_2(g).

Plastic vessels were used to hold the mother liquor during preparation of 4-aminopyridine perchlorate(s). The filtrate from the initial preparation was discarded.

The dense white mass of 4-aminopyridine perchlorate(s) crystals was recrystallized in fresh EtOH. A final rinse of cold EtOH was used on the final recrystallized product which was then dried in a continuously pumped vacuum desiccator. The dried 4-aminopyridine perchlorate(s) was kept in weighing bottles in a desiccator over Anhydrone.

The density of 4-aminopyridine perchlorate(s) was determined by the pycnometer method using Dow Corning DC-550 silicone fluid as a standard.

Because of obvious safety considerations, considerable care was taken in testing the stability of 4-aminopyridine perchlorate(s). Mechanical and thermal shock tests were performed under a variety of conditions before calorimetric experiments were begun. A hammer was used to determine whether 4-aminopyridine perchlorate(s) would detonate under physical shock. Several crystals of 4-aminopyridine perchlorate(s) were placed on a hot spatula to check reaction to thermal shock.

Heats of solution of 4-aminopyridine perchlorate(s) were determined according to the procedure described in Section VII.A.2.b for KCl(s) at a mean temperature of 25.00 ± 0.01 deg C. 4-Aminopyridine perchlorate(s) used for calorimetry was not ground but was used in the finely crystalline form obtained from purification.

5. Spectral properties of 4-aminopyridine(s) and 4-aminopyridine perchlorate(s)

NMR spectra were obtained with a Varian Associates A-60 Nuclear Magnetic Resonance Spectrometer. Spectra were obtained of 4-aminopyridine and 4-aminopyridine perchlorate at ambient temperatures in reagent grade DMSO with TMS as an internal standard. UV spectra of 4-aminopyridine(aq) and 4-aminopyridine perchlorate(aq) were obtained with a Bausch and Lomb Spectronic 600 recording spectrometer. Quartz 1.00 cm cells were used with the supporting solution as the reference. The instrument was allowed to warm up for a minimum of 6 hrs before any measurements were taken.

6. Thermal properties of 4-aminopyridine(s) and 4-aminopyridine perchlorate(s)

DTA was performed either with the ADAM-8-DTA constructed at Iowa State University or a DuPont 900 Differential Thermal Analyzer. The heating rates used for DTA analyses were 2.5 deg C/min (ADAM-8-DTA) and 10 deg C/min (DuPont 900 DTA). TGA was performed with a DuPont 950 Thermogravimetric Analyzer at a heating rate of 5 deg C/min. Integrations of thermal peaks in DTA were made on the original recorded curves with a Keuffel and Esser Compensating Polar Planimeter. The requirement of loose and thinly spread samples in TGA and tightly packed samples for DTA was carefully observed.

DTA was used to determine adsorption of water over a 24 hr period by 4-aminopyridine(s) in an atmosphere of 50% and 100% relative humidity. The 50% relative humidity was obtained by using a saturated aqueous solution of $Mg(NO_3)_2$ in a desiccator equibrated at 25 ± 1 deg C for 1-week before use (194).

The 4-aminopyridine(s) used for water adsorption studies was the same material those purity was determined earlier. The finely ground 4-aminopyridine was placed at a depth of 1 mm in a weighing bottle cover for this experiment.

C. Results and Discussion

1. Purity and properties of 4-aminopyridine(s) and 4-aminopyridine perchlorate(s)

The purity of 4-aminopyridine(s) as determined by triplicate weight titrations of NaOH(aq) vs NBS 84f potassium acid phthlate(aq), $HClO_4$(aq) vs standard NaOH(aq), and 4-aminopyridine(aq) vs standard $HClO_4$(aq), was 99.983%. The absolute standard deviation determined according to the procedure of Blaedel and Meloche (197), was 0.034%. Weight

$$\sigma_r = [\delta^2_{NaOH} + \delta^2_{HClO_4} + \delta^2_{4\text{-}AP}]^{\frac{1}{2}}$$

$$\sigma_a = \text{Purity}_{\ 4\text{-}AP} \times \sigma_r$$

titrations of tris(hydroxymethyl)aminomethane (THAM) samples #1 (Fisher Primary Standard Grade, Lot #71253) and #2

(Mallinckrodt Reagent Grade) yielded 99.712 ± 0.038% and 99.842 ± 0.041%, respectively, for the purity. The variances cited were calculated as for 4-aminopyridine(s).

Thus, the purity of 4-aminopyridine(s) prepared by one recrystallization and one sublimation from crude material was judged to be considerably better than commercially available THAM(s) with exception of SRM THAM(s) available from NBS.

No metal impurities were detected by arc emission spectrographic analysis which implies individual metallic contaminants were < 100 ppm (198). The identity of any impurities present remained unknown; it is suspected that water adsorbed during the brief exposure to the room atmosphere during transfer operations was the largest impurity. These titrations and associated work were performed during periods of time when the relative humidity was approximately 80%. The finely ground material certainly presented a large area for adsorption.

NMR spectra of 4-aminopyridine in DMSO showed a AA'XX' spectra with the α-protons absorbing at δ7.92, β-protons at δ6.42 and exocyclic amino(γ-) protons at δ5.86. $J_{\alpha\beta}$ and $J_{\alpha'\beta'}$ were 6-Hz and $J_{\alpha'\beta}$ or $J_{\alpha\beta'}$ were 1-Hz.

NMR spectra of 4-aminopyridine perchlorate produced considerable downfield shifts of absorptions: α at δ8.04, β at δ6.76, and $-NH_2$ at δ7.86. The proton of $HClO_4$ bonded to the nitrogen of the pyridine ring gave a very broad

absorption at δ12.85 indicating that it is quite acidic. Addition of D_2O removed the absorptions at δ7.86 and δ12.85 confirming the identities of each absorption as due to $-NH_2$ and $-N^+H$, respectively.

Accurate integration ratios were difficult to obtain because of the broadness of the absorption peak at δ12.85 and the closeness of the absorptions for β-protons and amino protons. The experimental ratio obtained was 64:32:13 for the β + amino proton absorption peaks, proton absorption, and ring nitrogen proton. The values of $J_{\alpha\beta}$ and $J_{\alpha'\beta'}$ were 7 Hz and $J_{\alpha'\beta} = J_{\alpha\beta'}$ were approximately 1.5 Hz for 4-aminopyridine perchlorate, undeuterated.

The conclusions that can be made from these NMR analyses are as follows:

(1) Reactions of 4-aminopyridine with strong proton acids produce acidic salts in DMSO.

(2) The electron density decreases dramatically at the exocyclic amino nitrogen when the heterocyclic N is protonated as evidenced by the large downfield shift of its absorption.

(3) The proton donated by the acid is bonded to the heterocyclic ring N and not to the exocyclic amino N.

Although NMR is not accepted as a precise quantitative method for purity determination, the presence of significant amounts, > 1% w/w of decomposition products of 4-aminopyridine (EtOH) by $HClO_4$(aq) produced during the synthesis of 4-aminopyridine perchlorate(s), were not found. The salt, 4-aminopyridine

perchlorate(s), is definitely a monosalt since the disalt, 4-aminopyridine diperchlorate, can only be formed in strongly acid solutions (see Section II.B).

UV absorption spectra of the monoperchlorate salt in aqueous phosphate buffer at pH 6.685 and 0.1 M $HClO_4$(aq) at 4×10^{-5} M showed a single absorption maximum at 262-nm (α-band) whereas the diperchlorate salt at 1×10^{-4} M in 11.5 M $HClO_4$(aq) gave an absorption maxima at 256-nm and a shoulder at 275-nm. The UV absorption spectra of 4-aminopyridine(aq) in 0.1 M NaOH(aq) gave one absorption maximum at 245-nm (p-band). There also was an end absorption on all spectra at 208-nm, the so-called β band (10).

Because of resonance stabilization,

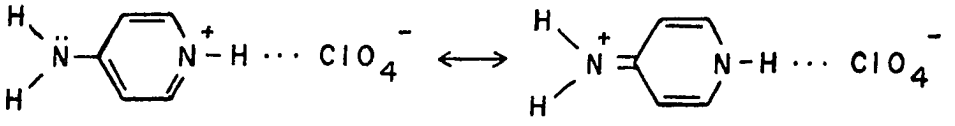

(I) (II)

structures (I) and (II) are equally probable in aqueous solution. The location of the perchlorate group is uncertain but the location shown is probably sterically favorable. The bathochromic shifts observed in the UV spectra and shifts in NMR absorption of the γ-protons (amino) would lead to a strong argument for a resonance structure resembling structure II.

DTA of a large sample (∿0.15 g) of 4-aminopyridine(s) showed a very large depression of the baseline due to thermal lag even with the slow heating rate used, 2.5 deg C/min. Integration of the areas of the sublimation endotherm and melting point was used to calculate an approximate value of the heat of sublimation for 4-aminopyridine(s). The heat of fusion (91) together with the ratio of areas yielded a value for ΔH_{sub} of 17 Kcal/mole.

Determination of water adsorbed by 60-mesh and finer particles of 4-aminopyridine(s) over a 24 hr period was performed with small samples (∿1 mg). Only a smoothly decreasing slope and melting point endotherm were observed in DTA of small samples with an observed melting point of 162 deg C for pure 4-aminopyridine(s).

The blank determined with dry 4-aminopyridine(s) corresponded to 0.03 mole percent impurity which is in excellent agreement with results from weight titrations. DTA showed that 4-aminopyridine(s) adsorbed 0.45 mole percent water in an atmosphere of 50% relative humidity and 0.75 mole percent in a water saturated atmosphere. DTA of THAM(s) sample #1 showed a large endotherm (three times the area of the melting point endotherm) at 135 deg C indicative of occluded mother liquor. The melting point of THAM(s) sample #1 as determined by DTA was 169 deg C.

TGA of dry 4-aminopyridine(s) was used to determine an energy of activation for sublimation by slope analysis for

weight loss below 150 deg C. Weight losses were very small for temperatures less than 120 deg C in agreement with qualitative results found in purification by sublimation of 4-aminopyridine(s). Fitting the TGA weight loss data to the Arrhenius equation yielded

$$-\frac{1}{w_s}\frac{dw}{dt} = 1.63 \times 10^9 \text{ min}^{-1} \exp\left(\frac{-9.97 \times 10^3}{T}\right)$$

with a correlation coefficient of 0.992. The pre-exponential frequency factor A is 1.63×10^9 min^{-1} and the energy of activation equals 19.7 ± 0.8 Kcal/mole for sublimation. The heat of sublimation in this case will be nearly equal to the apparent activation energy since the work of transporting the vapor from solid surface to surfaces of the cell enclosure will be small in TGA. The agreement between heat of sublimation determined by DTA and TGA is reasonable considering the present lack of agreement as to the validity of using the Arrhenius equation for nonisothermal methods (199).

DTA and TGA data for 4-aminopyridine perchlorate are shown in Figure VIII.1. The melting point of 4-aminopyridine perchlorate(s) determined from DTA is 275 deg C which is in good agreement with that reported by Barnes and Matuszko (195). The amount of volatile impurities on 4-aminopyridine perchlorate(s) was 0.04% as determined by TGA.

A slight upward swing of the TGA trace occurred when the 4-aminopyridine perchlorate(s) detonated at approximately

Figure VIII.1. DTA and TGA curves for 4-aminopyridine perchlorate(s)

DTA: Size 4 mm in microtube
Reference glass beads
Atmosphere air
Heating rate 10 deg C/min
Base line slope 0
Shift 0

TGA: Size 10.00 mg
Atmosphere air
Heating rate 10 deg C/min
Suppression 9.00 mg
Shift 0
Time constant 1 sec

Note: Temperature scales shown were not corrected for C/A thermocouple nonlinearity.

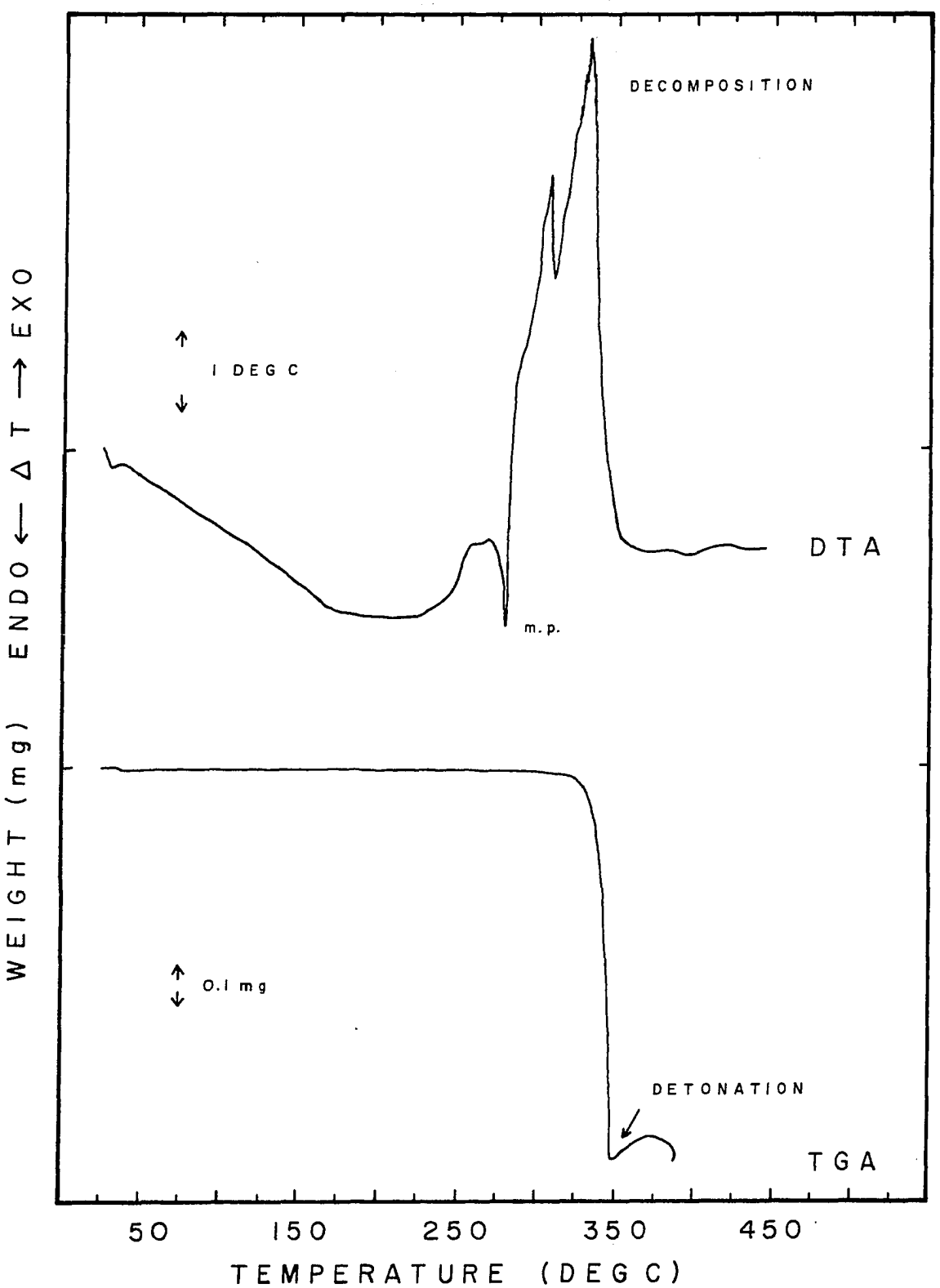
DECOMPOSITION
1 DEG C
DTA
m.p.
0.1 mg
DETONATION
TGA
WEIGHT (mg) ENDO ← ΔT → EXO
50
150
250
350
450
TEMPERATURE (DEG C)

340 deg C. This was nearly coincident with the second large exothermic decomposition peak. The cause of detonation is not certain. Aluminum pans were used for TGA and perhaps the 4-aminopyridine perchlorate(s) decomposed the usual surface protective coating of Al_2O_3(s) on the pans. Aluminum metal is very reactive with most oxidants once the protective Al_2O_3(s) is removed. Hence, care was exercised in handling 4-aminopyridine perchlorate(s) and in no case should future workers be careless in handling this compound.

The density of 4-aminopyridine perchlorate(s) found corrected to vacuum was 1.5470 g/cm^3.

2. Heat of solution of 4-aminopyridine(s)

Results of heat of solution measurements made when 4-aminopyridine(s) was added just prior to each thermometric titration are given in Table VIII.1 and are shown in Figure VIII.2. The shape of the experimental curve suggested that ΔH_S was a function of m^2. A simple quadratic, $a + bm + cm^2$, gave a reasonable fit; however, the best fit to the data was obtained when the data was fitted to

$$\Delta H_S = a + bm^{\frac{1}{2}} + cm + dm^{3/2} + dm^2$$

The parameters of this equation for ΔH_S (cal/mole) are

$$\Delta H_S = 3.896 \times 10^3 + 1.4130 \times 10^4\, m^{\frac{1}{2}} - 2.9987 \times 10^5\, m + 3.0683 \times 10^6\, m^{3/2} - 1.1823 \times 10^7\, m^2$$

Table VIII.1. Heat of solution of 4-aminopyridine(s)

Trial #	$n_{4\text{-AP}} \times 10^3$ (moles)	$m_{4\text{-AP}} \times 10^3$ (moles/kg)	$m_{4\text{-AP}}^{\frac{1}{2}} \times 10^2$ $(\text{moles/kg})^{\frac{1}{2}}$	q (calories)	ΔH_S (Kcal/mole) (Experimental)	ΔH_S (Kcal/mole) (Calculated)
1	1.97610	7.9268	8.9032	8.306	4.203	4.199
2	1.55419	6.2343	7.8957	6.520	4.195	4.193
3	1.11789	4.4844	6.6965	4.668	4.175	4.181
4	0.65132	2.6131	5.1118	2.713	4.166	4.163
5	0.22677	0.90972	3.0162	0.935	4.123	4.123
6	3.14541	12.617	11.233	13.108	4.167	4.165
7	2.62013	10.510	10.252	10.972	4.188	4.193

Figure VIII.2. Heat of solution of 4-aminopyridine(s) as a function of concentration

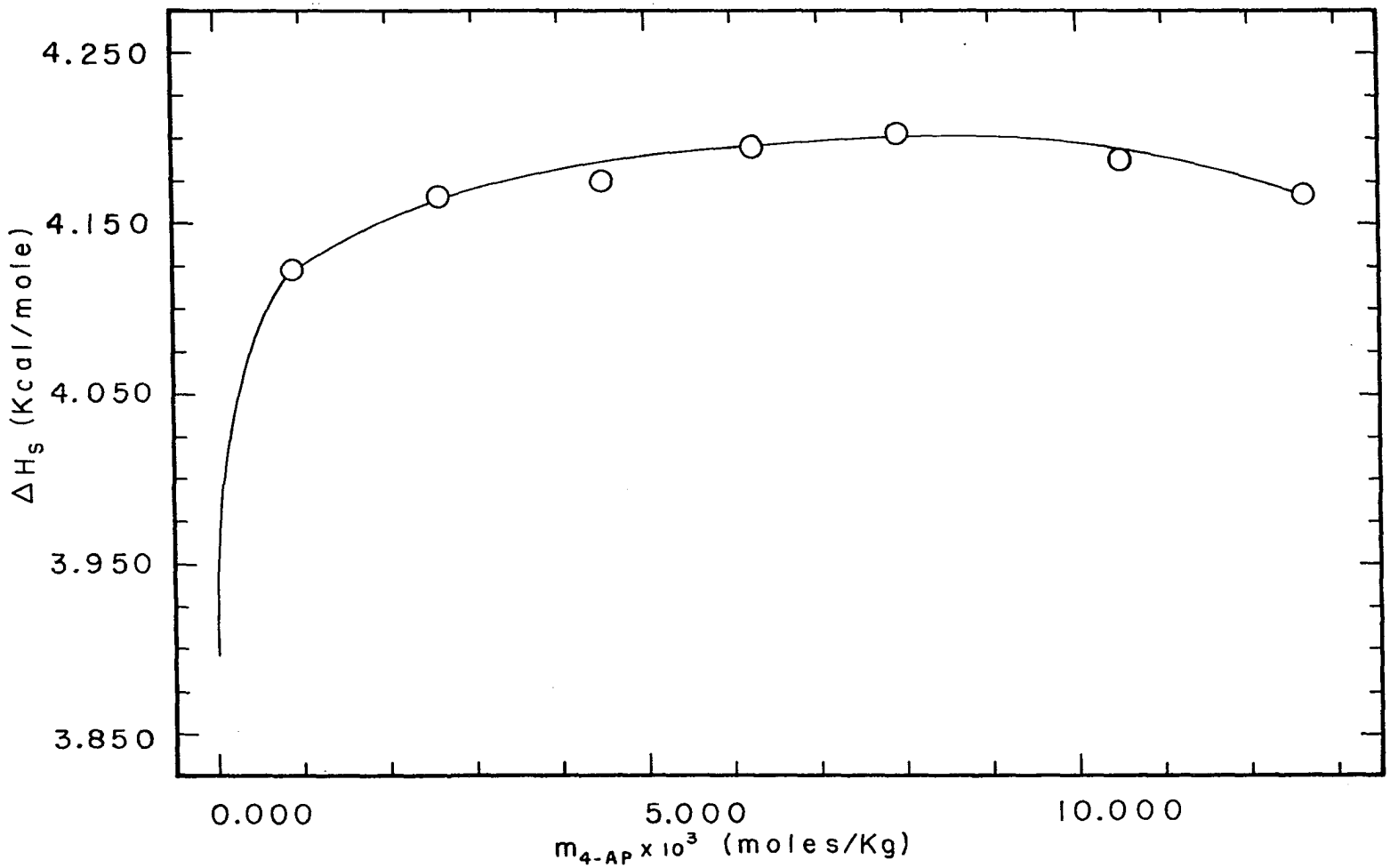
4.250
4.150
4.050
3.950
3.850
ΔH_s (Kcal/mole)
0.000
5.000
10.000
$m_{4\text{-}AP} \times 10^3$ (moles/Kg)

The average standard deviation between the least squares fit obtained above and the experimental data was 4 cal/mole. The value of the heat of solution for 4-AP(s) at infinite dilution

$$\Delta H_{S,a}{}^{\circ}(H_2O,\ S,\ 298.15\ K) = 3896 \pm 4\ \text{cal/mole}$$

with the standard deviation assigned being the average standard deviation as discussed above. Incomplete dissociation of 4-aminopyridine(aq) and solvent-base reactions are the reasons that a more complex relation must be used to relate the heat of solution to the solute concentration than the usual $m^{\frac{1}{2}}$ dependence of thermodynamic quantities. The relative error was 1 ppt in these determinations which was the same relative error as in the heat of solution determinations of KCl(s).

3. Heat of neutralization of 4-aminopyridine(aq) with $HClO_4$(aq)

Differential thermometric titration of 4-aminopyridine(aq) was in principle nearly ideal. The initial ionic strength of both calorimeter cells was nearly equal since 4-aminopyridine(aq) was only slightly dissociated. Hence, the problems found in the titration of NaOH(aq) with $HClO_4$(aq) were expected to be greatly reduced or absent in thermometric titrations of 4-aminopyridine(aq).

Approximately 1.5% excess $HClO_4$(aq) titrant was added after the calculated equivalence point was reached as was

also done in titrations of NaOH(aq). The reason the same amount of excess acid was added in both series of titrations (4-AP and NaOH) was to make their reaction patterns as similar as possible. More particularly, in the titration of 4-aminopyridine(aq), excess acid was added on the premise that since each reaction heat was calculated from the endpoint value only, suppression of salt hydrolysis was desirable. The excess acid lowered the concentration of free base from approximately 10^{-6} m to 10^{-8} m at a 4-aminopyridine perchlorate(aq) concentration of 10^{-3} m.

The values of K_b and K_{bh} for 4-aminopyridine(aq) were determined very precisely by Bates and Hetzer (15). From Table VIII.2, the final pH of each thermometric titration equaled approximately 4 and using the expression for K_{bh}, the concentration of free base was calculated. The maximum error in reaction heats by exclusion of heat of hydrolysis due to free base was then calculated. The error was on the order of 0.1 ppt and was therefore considered negligible. The concentration of 4-aminopyridine perchlorate(aq) was then essentially that calculated on the basis of total 4-aminopyridine(s) added to the calorimeter corrected for dilution by the titrant.

Before multiplication by the heat capacity ratio c_2/c_1 at the endpoint, heats of neutralization were corrected for the blank error of the HClO(aq) titrant discussed in

Table VIII.2. Parameters of thermometric titrations of 4-aminopyridine(aq)

Trial #	$m_{1,2}$ (grams)	$T_{b,1}$ (deg C) (mean reaction temperature)	Moles excess $HClO_4$ x 10^5
1	249.2955	25.029	2.760
2	249.2988	25.032	0.479
3	249.2952	25.007	0.416
4	249.2543	24.945	0.758
5	249.2790	24.986	0.074
6	249.3018	25.025	0.126
7	249.2986	24.987	0.906

Final solution pH	c_2/c_1 (Experimental)	c_2/c_1 (Calculated)
	1.0105	1.0108
3.948	1.0100	1.0099
3.998	1.0089	1.0089
4.010	1.0080	1.0080
4.057	1.0073	1.0073
3.673	1.0134	1.0136
3.562	1.0128	1.0124

Section VIII.B.3. The ratio of c_2/c_1 used to calculate the corrected reaction energy was obtained at the mean reaction temperature by a graphical fit of c_2/c_1 *versus* temperature data. The results of seven differential thermometric titrations of 4-aminopyridine(aq) with $HClO_4$(aq) are given in Table VIII.3 and produced in Figure VIII.3. The calculated fit to a quadratic equation of the form

$$y = a + bm^{\frac{1}{2}} + cm$$

corresponded best to the experimental results.

The calculated equation for ΔH_N (cal/mole) was

$$-\Delta H_N = 1.1164 \times 10^4 + 7.37740 \times 10^2\ m^{\frac{1}{2}} + 2.58834 \times 10^3\ m$$

with an average standard deviation of 11 cal/mole. The standard deviation in experimental results is in excellent agreement with the standard deviation predicted for this equipment in Section III.C.2. The heat of neutralization at infinite dilution

$$\Delta H_N^{\circ}(H_2O,\ 298.15\ K) = -\ 11164 \pm 11\ cal/mole$$

The assigned error at infinite dilution was taken as the average standard deviation obtained above.

A study of heat of neutralization *versus* endpoint pH was not made in the case of 4-aminopyridine(aq). Therefore, a judgment could not be made as to presence of endpoint pH

Table VIII.3. Heat of neutralization of 4-aminopyridine(aq)

Trial #	$n_{4\text{-AP}} \times 10^3$ (moles)	$m_{4\text{-APH}} \times 10^3$ (moles/kg)	$m^{\frac{1}{2}}_{4\text{-APH}} \times 10^2$ $(\text{moles/kg})^{\frac{1}{2}}$	n_a/n_b
1	1.97610	7.8673	8.8698	1.0149
2	1.55419	6.1978	7.8726	1.0039
3	1.11789	4.4655	6.6824	1.0047
4	0.65132	2.6067	5.1055	1.0033
5	0.22677	0.90892	3.0148	1.0041
6	3.14541	12.468	11.166	1.0049
7	2.62013	10.407	10.201	1.0044

q_{HClO_4} (calories)	q (calories)	$-\Delta H_N$ (Kcal/mole) (Experimental)	$-\Delta H_N$ (Kcal/mole) (Calculated)
0.0505	22.217	11.243	11.250
0.0349	17.483	11.249	11.238
0.0220	12.560	11.236	11.225
0.0112	7.290	11.192	11.208
0.0032	2.538	11.192	11.189
0.0656	35.492	11.284	11.279
0.0401	29.495	11.257	11.266

Figure VIII.3. Heat of neutralization of 4-aminopyridine(aq) as a function of concentration

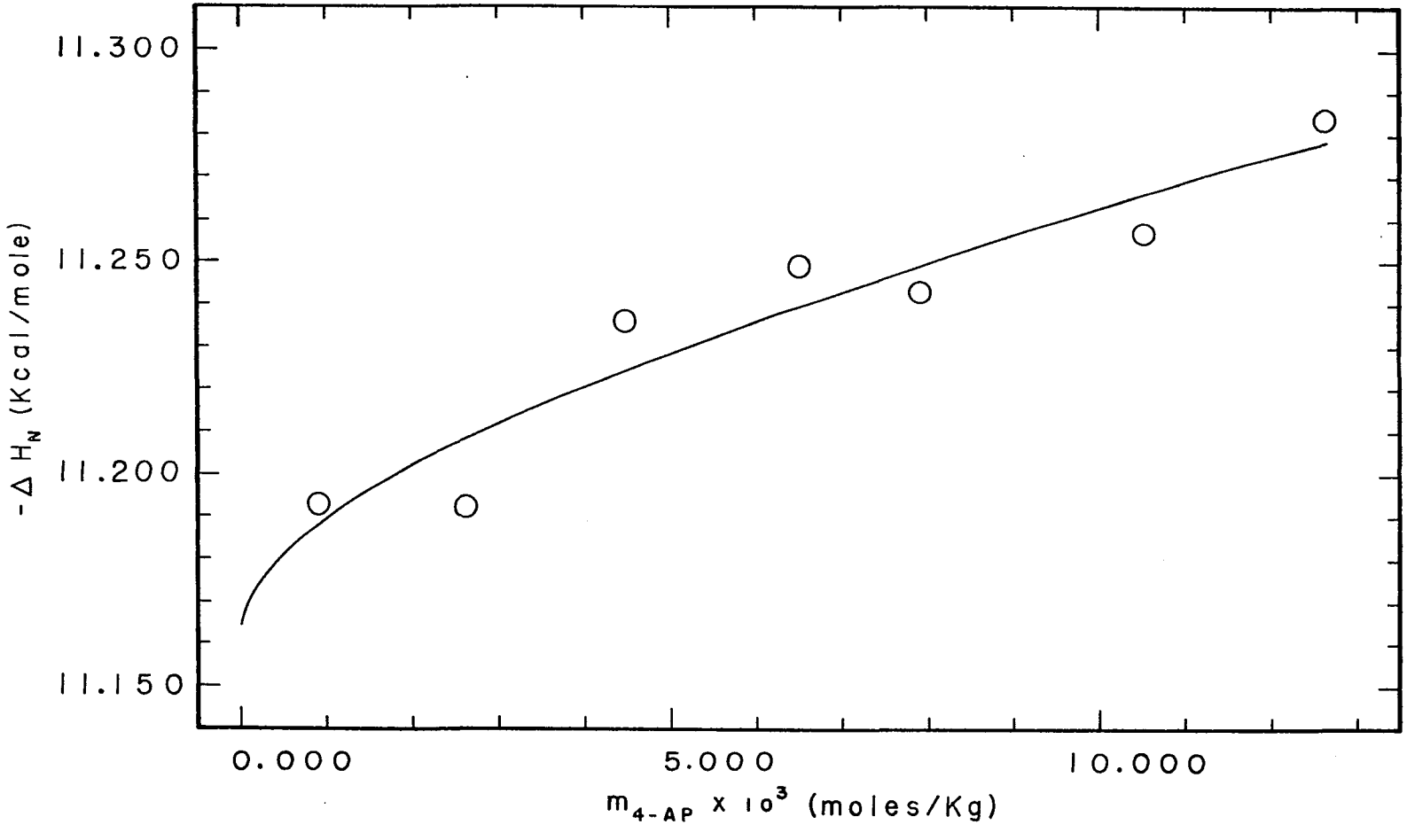
11.300
11.250
11.200
11.150
$-\Delta H_N$ (Kcal/mole)
0.000
5.000
10.000
$m_{4\text{-}AP} \times 10^3$ (moles/Kg)

sensitivity. However, sensitivity to the endpoint pH was judged to be far smaller for 4-aminopyridine(aq) than NaOH(aq) for the following reasons: The results for 4-aminopyridine(aq) obtained corresponded far more closely to previous work than the initial results of NaOH(aq) and the ΔH_N *versus* m relation is a reasonable one. The endpoint pH of the thermometric titrations of 4-aminopyridine(aq) differed from the equivalence point pH of 5.22 ([4-AP(aq)] $\sim 10^{-3}$ M) far less than that calculated in the thermometric titration of NaOH(aq). That is, Δ pH equaled approximately one in the titration of 4-aminopyridine(aq) and one to five in the titration of NaOH(aq).

The only other determination of ΔH_N° by calorimetry was also obtained by thermometric titrimetry. Christensen *et al.* (16) used a single cell calorimeter, correcting for mechanical and extraneous chemical heats from data obtained in separate experiments. Christensen and co-workers assumed on the basis of previous work (200) with weakly dissociated compounds titrated in the concentration range of 0.005 to 0.015 M that their experimental value of ΔH_N = - 11.31 Kcal/mole for 4-aminopyridine(aq) determined at an unspecified concentration within this concentration range was equal to ΔH_N°. That is, they found essentially no systematic variation in values of ΔH_N determined within this concentration range for other compounds and assumed therefore that 4-aminopyridine(aq)

could be treated similarly. Indeed, their calculated uncertainty for 4-aminopyridine(aq), 0.04 Kcal/mole, such a conclusion is very reasonable. The results given in Table VIII.3 show only a small change of ΔH_N in the concentration range of 0.005 - 0.013 m and deviations greater than ± 0.02 Kcal/mole would probably obscure any trend in the data.

The nonlinear relationship of ΔH_N to the concentration of 4-aminopyridine perchlorate(aq) found in this work presented a dilemma. The fact that ΔH_N decreased with decreasing concentration was expected on the basis of heats of neutralization of NaOH(aq), etc. However, the lack of agreement with conventional thermometric results indicated that probably either the heat of dilution of $HClO_4$(aq) was not fully compensated for in the differential titrations or the presence of a change in ΔH_N *versus* m was masked in previous thermometric titrimetry by an error in the heat of dilution of $HClO_4$(aq). Accurate measurements of heats of dilution are difficult particularly at the low concentrations used today in thermometric titrimetry. Cabani and Gianni (201) discussed at length the changes in calculated values of ΔH_D for HSO_4^-(aq) as determined by thermometric titrations of Na_2SO_4(aq) with $HClO_4$(aq) when slightly different heat of dilution *versus* m relations were assumed.

The value of ΔH_N° determined by Bates and Hetzer (15) from electromotive force measurements was -11.255 ± 0.025 Kcal/mole.

There is now a considerable divergence of available values for ΔH_N° for 4-aminopyridine(aq) as was the case for NaOH(aq) for many years as discussed by Hale et al. (183). Hence, an unequivocal recommendation of the correct value for ΔH_N° for 4-aminopyridine(aq) could not be given from the results of past and present work.

Taking into account the previous thermometric titration results and the present work, a value for ΔH_N of -11.28 ± 0.04 Kcal/mole is recommended for use when 4-aminopyridine(aq) is used as a calorimetric standard in the concentration range of 0.008 - 0.012 m.

The ratio of the calorimeter cell heat capacities was fitted to an equation of the same form as used to fit ΔH_N of 4-aminopyridine(aq). The experimental and calculated least squares fit from the following equation are given in Table VIII.2:

$$c_2/c_1 = 1.0074 - 2.6489 \times 10^{-2}\ m^{\frac{1}{2}} + 7.3274 \times 10^{-1}\ m$$

The closeness of the experimental and calculated values bears out the validity of the original assumptions used in derivations of heat capacity ratio determinations in Section III.C.2. The value of $(c_2/c_1)_{m=0}$ determined here differs only by 1.9 ppt from that determined after thermometric titrations of NaOH(aq) as discussed in Section VI.C.1.b. The agreement between the $(c_2/c_1)_{m=0}$ determined

here and the mean value of $(c_2/c_1)_{m=0}$ determined in the thermometric titrations of NaOH(aq) was not as close with a 2.3 ppt difference between the two values.

The agreement between the values of $(c_2/c_1)_{m=0}$ is excellent since the methods of determining the cell heat capacity ratio were entirely different. In the titrations of NaOH(aq), the calorimeter cell heat capacities were determined separately and sequentially. Here, the heat capacity ratio only was determined and calculated according to the procedure discussed in Section III.C.2.

4. Heat of solution of 4-aminopyridine perchlorate(s)

Determinations of heat of solution of 4-aminopyridine perchlorate(s) in water uncorrected for hydrolysis are given in Table VIII.4 along with the equation used for a least squares fit of the data. Reaction 1 defines the apparent heat of solution as measured experimentally.

$$4\text{-APHClO}_4(s) + H_2O(l) \rightarrow 4\text{-APHClO}_4(aq)\ (m_1);\ \Delta H_{s,a} \qquad [1]$$

Since 4-aminopyridine perchlorate is the product of the neutralization reaction of a weak base and a strong acid, extensive hydrolysis will occur at low concentrations of $4\text{-APHClO}_4(aq)$. Reaction 2 defines the hydrolysis of $4\text{-APHClO}_4(aq)$ and consequent changes in concentration of $4\text{-APHClO}_4(aq)$.

Table VIII.4. Heat of solution of 4-aminopyridine perchlorate(s)

Trial #	$n_{4\text{-APH}} \times 10^3$ (moles)	$m_{4\text{-APH}} \times 10^3$ (moles/kg)	$m^{\frac{1}{2}}_{4\text{-APH}} \times 10^2$ $(\text{moles/kg})^{\frac{1}{2}}$
1	1.41972	5.6952	7.5467
2	0.27037	1.0846	3.2933
3	0.83468	3.3484	5.7865
4	2.26780	9.0973	9.5380

q (calories)	$\Delta H_{S,2}$ (Kcal/mole) (Experimental)	$\Delta H_{S,2}$ (Kcal/mole) (Calculated)
12.608	8880	8880
2.485	9192	9192
7.504	8990	8990
19.932	8789	8789

$$\Delta H_{S,2} = 9.543 \times 10^3 - 1.2112 \times 10^4 \, m^{\frac{1}{2}} + 4.4085 \times 10^4 \, m$$

$$4\text{-APHClO}_4(aq) + H_2O(l) \rightleftharpoons 4\text{-AP}(aq)\ (m_3) + H_3O^+(aq)\ (m_3) + ClO_4^-(aq)\ (m_3) + 4\text{-APHClO}_4(aq)\ (m_2) \qquad [2]$$

The true concentration of $4\text{-APHClO}_4(aq)$ then is m_2 rather than m_1. The heat of hydrolysis was endothermic since the heat of neutralization was exothermic and accordingly $\Delta H_{S,a}$, the apparent heat of solution would be more endothermic than the true heat of solution $\Delta H_{S,2}$. The concentration of free 4-AP(aq) was calculated from the expression for K_{bh} by the method of successive approximations which in turn was used to calculate $n_{4\text{-AP}}$ and q_h the energy correction for hydrolysis. The corrected concentration for $4\text{-APHClO}_4(aq)$ (m_2), 4-AP(aq) (m_3), and q_h along with the corrected reaction heats are given in Table VIII.5. The corrected heats of solution are produced in Figure VIII.4. These measurements when fitted to a quadratic equation yielded

$$\Delta H_{S,2} = 9.520 \times 10^3 - 1.1620 \times 10^4\ m^{\frac{1}{2}} + 4.1028 \times 10^4\ m$$

with the calculated results being identical to the experimental results in each case. This type of agreement can only be considered fortuitous. The value of $\Delta H_{S,2}^{\circ}$ then is

$$\Delta H_{S,2}^{\circ}(H_2O,\ 298.15\ K) = 9520 \pm 10\ cal/mole$$

Table VIII.5. Heat of solution of 4-aminopyridine perchlorate(s) corrected for hydrolysis

Trial #	$m_{4\text{-APH}} \times 10^3$ (moles/kg)	$m^{\frac{1}{2}}_{4\text{-APH}} \times 10^2$ $(\text{moles/kg})^{\frac{1}{2}}$	$m_{4\text{-AP}} \times 10^6$ (moles/kg)
1	5.6931	7.5453	2.092
2	1.0837	3.2920	0.913
3	3.3468	5.7852	1.605
4	9.0947	9.5366	2.644

$q_h \times 10^3$ (calories)	q (calories)	$\Delta H_{S,2}$ (Kcal/mole) (Experimental)	$\Delta H_{S,2}$ (Kcal/mole) (Calculated)
5.86	12.602	8877	8877
2.55	2.482	9182	9182
4.49	7.500	8985	8985
7.43	19.925	8785	8785

Figure VIII.3. Heat of solution of 4-aminopyridine perchlorate(s) as a function of concentration

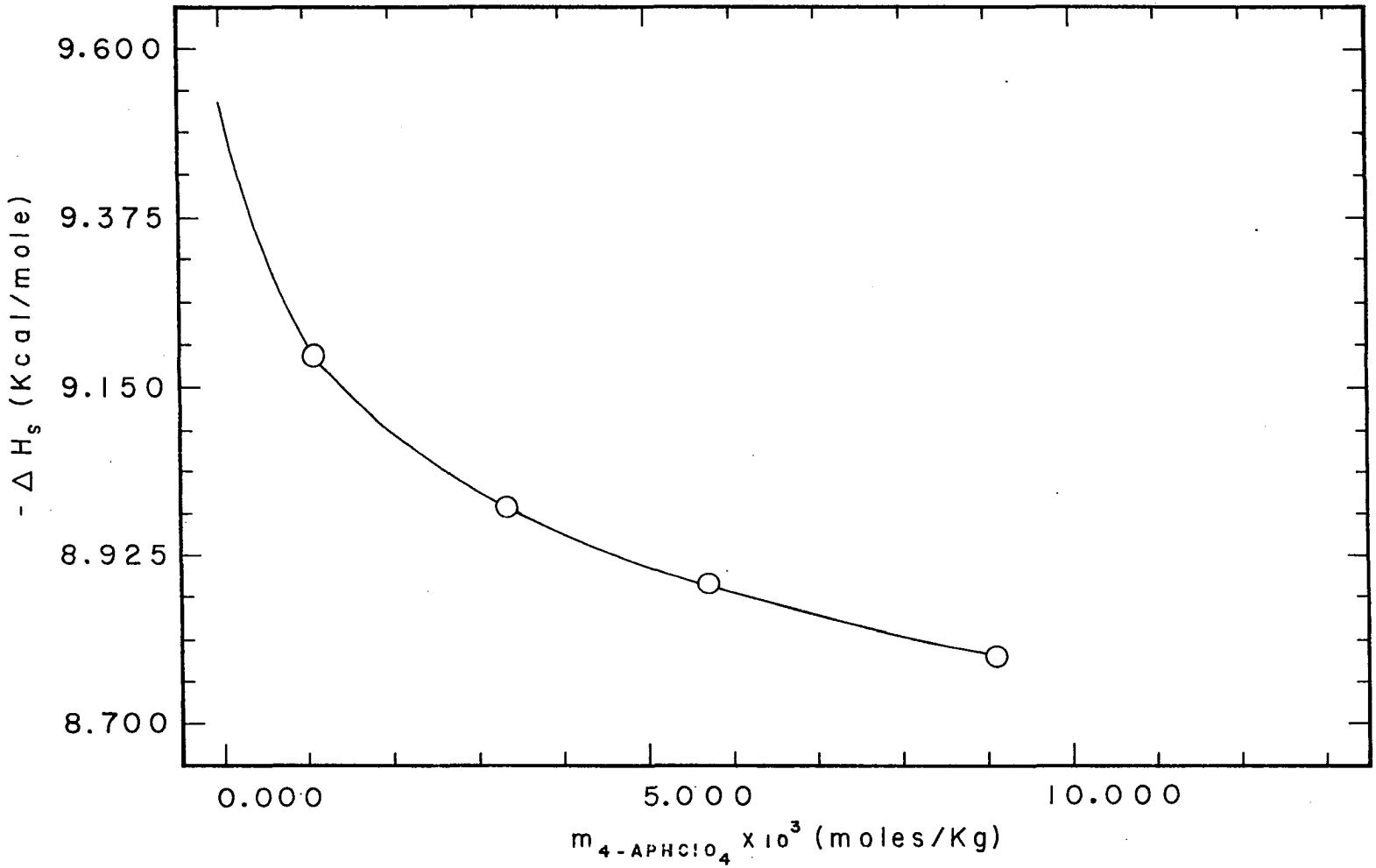
9.600
9.375
9.150
8.925
8.700
- Δ Hs (Kcal/mole)
0.000
5.000
10.000
m4-APHClO4 X 10³ (moles/Kg)

Although the calculated and experimental results agreed exactly, the error sum was assigned on the basis of other determinations of heats of solution made in this work.

The results from the work presented allowed the calculation of several other thermodynamic parameters. The reactions involved in heats of solution and neutralization

$$4\text{-AP(s)} + H_2O(l) \rightarrow 4\text{-AP(aq)}\ (m_4);\ \Delta H_{S,a} \qquad [3]$$

$$4\text{-AP(aq)}\ (m_4) + HClO_4(aq)\ (m_5) \rightleftharpoons 4\text{-APHClO}_4(aq)\ (m_6);\ \Delta H_N \qquad [4]$$

when added together yield the reaction of 4-AP(s) with $HClO_4(aq)$ (m_5). Such a reaction would then seem to be the compliment of reaction 1. That is,

$$\begin{aligned} &4\text{-AP(s)} + HClO_4(aq)\ (m_5) \longrightarrow 4\text{-APHClO}_4(aq)\ (m_6);\ \Delta H_{N,1} \\ &\quad 4\text{-APHClO}_4(s) + H_2O(l) \longrightarrow \nearrow \end{aligned} \qquad [5]$$

and $\Delta H_{S,a} + \Delta H_N = \Delta H_{N,1} = -\Delta H_{S,2}$

whence

$$\Delta H_{S,a}{}^{\circ} + \Delta H_N{}^{\circ} = \Delta H_{N,1}{}^{\circ}$$

Substitution of numerical data yields

$$\Delta H_{N,1}{}^{\circ}(H_2O,\ 298.15\ K) = -\ 7269 \pm 15\ \text{cal/mole}$$

The error sum for $\Delta H_{N,1}{}^{\circ}$ was taken as the sum of the assigned standard deviations calculated for $\Delta H_{S,a}$ of 4-AP(s) and $\Delta H_N{}^{\circ}$. Hence, it is evident that $H_{N,1} \neq -H_{S,2}$ and there

must be another reaction that was ignored in Reaction 5. This reaction sequence did not consider the equilibria

$$4\text{-AP(aq)}\ (m_4) + H_2O(l) \rightleftharpoons 4\text{-APH}^+\text{(aq)}\ (m_7) + OH^-\text{(aq)}\ (m_7) + 4\text{-AP(aq)}\ (m_8);\ \Delta H_i$$

which is the heat of ionization or dissocation of the free base. It should be readily apparent from Hess's Law of Heat Additivities that the true heat of solution for 4-AP(s) is given by

$$\Delta H_{S,1} = \Delta H_{S,a} + \Delta H_i$$

and

$$\Delta H_{S,a} + \Delta H_i + \Delta H_N = -\Delta H_{S,2}$$

whence

$$\Delta H_i^{\circ} = -\Delta H_{S,a}^{\circ} - \Delta H_N^{\circ} - \Delta H_{S,2}^{\circ}$$

and $\Delta H_i^{\circ}(H_2O,\ 298.15\ K) = -2252 \pm 24$ cal/mole. The error sum for ΔH_i° was taken as the sum of the assigned standard deviations of each molar heat of reaction. The value obtained for ΔH_i° is in good agreement with the value of $\Delta H_i^{\circ} = -2268$ cal/mole calculated by Bates and Hetzer (15) at 25 deg C from electromotive force measurements.

IX. SUMMARY

The voltage output of a new resistance bridge was derived theoretically and confirmed experimentally. A semi-rigorous theoretical solution to dynamic thermistor temperature response was developed in this work. Methods of obtaining critically damped dynamic response of a temperature sensor in a calorimeter were deduced from the theoretical derivations and confirmed experimentally.

Several calorimetric studies in aqueous solution of heats of solution and heats of neutralization verified the applicability of the new calorimeter designed and constructed for this work. The reaction of 4-aminopyridine and $HClO_4$ was proposed as a primary standard for solution calorimetry.

Finally, a solution to existing problems of dynamic temperature measurement was proposed.

X. SUGGESTIONS FOR FUTURE WORK

Optimization of calorimetry system response was discussed in Section VI.C.5. Although the system response can be readily optimized in one solvent by adjustment of N_s and r_s, changes in solvent composition will still present grave experimental problems.

Tsederberg (202) in his review on thermal conductivities of gases and liquids showed that for aqueous solutions of electrolytes, the thermal conductivity of the solutions is given by

$$\lambda_{b'} = \lambda_b \left(\frac{c_{p,b'}}{c_{p,b}}\right)\left(\frac{\rho_{b'}}{\rho_b}\right)^{4/3}\left(\frac{M_b}{M_{b'}}\right)^{1/3}$$

where $M_{b'} = 0.01\ (M_s g_s + M_b g_b)$,

M_s = molecular weight of solute,

g_s = mass of solute.

The changes in thermal conductivity for concentrations normally used in thermometric titrimetry (< 1 M) are negligible. For example, an aqueous solution 40% by weight of NaOH has a thermal conductivity 1.08 times that of water. The example cited for aqueous solutions is not unusual in magnitude but is unusual in direction. That is, an increase in concentration of electrolyte usually decreases thermal conductivity. It is therefore apparent that changes in ionic strength of aqueous solutions will have negligible effects on the dynamic characteristics of calorimeter systems.

The thermal conductivity does, however, change dramatically when the bulk solvent is changed from water to nonaqueous liquids.

Incorporation of the analog circuit proposed by Nakanishi and Fujieda (203) in future uses of the circuit described in this work is suggested to aid in optimization over a larger range of bulk solvent compositions.

The thrust of future work then should be aimed at further improvements in instrumentation. Temperature sensors should be particularly improved as to temperature resolution and versatility of application. Concurrently, methods of reducing the heat of stirring while maintaining efficient mixing should be investigated. Calculations using moments of inertia showed that the stirrer shaft contributed a larger amount of stirring heat than the disc in the present calorimeter. The shaft size in the present case was made as a compromise between stirring heat, structural strength requirements, chemical inertness and cost. The use of KEL-F would meet strength and inertness requirements for a smaller diameter shaft with very little loss in stirring efficiency.

The derivations of thermistor response and noise depends on empirical equations. Thus, a completely theoretical solution with the present system is considered impossible. The following design changes are expected to simplify the development of a rigorous mathematical solution and increase

system sensitivity without increasing system noise: A rotating disc thermistor thermometer should be constructed with a Teflon shroud to electrically and thermally insulate the sides of the thermistors from the bulk solution. An AC bridge operating at 100 Hz and constructed with operational amplifiers is proposed to amplify the thermistor signals. Laminar flow will, therefore, be insured throughout the entire rotational velocity range used in calorimetry and the present problem of nonuniform flow over the thermistor surface will be eliminated. A rigorous mathematical solution for this rotating disc thermometer has already been worked out by Liu and Stewart (204) making predictions of thermistor response straight forward.

Incorporation of electrochemical sensors either as a ring surrounding the thermistor disc or superimposed on top of the disc (205) should yield far reaching advantages in studies of adsorption isotherms and thermodynamics of heterogeneous catalysis. It is suggested that such a sensor combination use a thermistor disc made from one PTC thermistor and six NTC thermistors imbedded in thermally conductive epoxy within a brass ring and faced by a disc of platinum or gold.

XI. BIBLIOGRAPHY

1. H. J. V. Tyrrell and A. E. Beezer, "Thermometric Titrimetry," Chapman and Hall, London, 1968.

2. L. S. Bark and S. M. Bark, "Thermometric Titrimetry," Pergamon Press, London, 1969.

3. J. Jordan in "Treatise on Analytical Chemistry," Pt. 1, Vol. 8, I. M. Kolthoff and P. J. Elving, Eds., John Wiley and Sons, New York, N.Y., 1968.

4. P. W. Carr, Crit. Rev. Analyt. Chem., 2, 491 (1972).

5. J. J. Christensen, R. M. Izatt, L. D. Hansen, and J. A. Partridge, J. Phys. Chem., 19, 2003 (1966).

6. E. Ochai, J. Org. Chem., 18, 534 (1953).

7. H. J. den Hartog and J. Overhoff, Rec. Trav. Chim., 69, 468 (1950).

8. R. Camps, Arch. Pharm., 240, 354 (1902).

9. A. Albert, J. Chem. Soc., 1951, 1376.

10. A. Albert, J. Chem. Soc., 1948, 2240.

11. L. Sucha, Z. Urner, and M. Suchanek, Sb. Vys. Sk. Chem.-Technol. Praze, Anal. Chem., H7, 103 (1971).

12. I. R. Bellobono and G. Fevini, J. Chem. Soc., B-10, 2034 (1971).

13. I. G. Per'kov, P. E. Chaplanov, and I. T. Polkovnichenko, Zh. Fiz. Khim., 48, 1005 (1974).

14. J. J. Elliot and S. F. Mason, J. Chem. Soc., 1959, 2352.

15. R. G. Bates and H. B. Hetzer, J. Res. Nat. Bur. Stand., 64A, 427 (1960).

16. J. J. Christensen, D. E. Smith, M. D. Slade, and R. M. Izatt, Thermochimica Acta, 5, 35 (1972).

17. M. Paabo, R. A. Robinson, and R. G. Bates, Anal. Chem., 38, 1573 (1966).

18. H. Hirayama and T. Kubota, J. Pharm. Soc. Japan, 73, 140 (1953).

19. M. L. Bender and Y.-L. Chow, J. Amer. Chem. Soc., 81, 3929 (1959).

20. P. J. Brignell, C. D. Johnson, A. R. Katritzky, N. Shakir, H. O. Tarhan, and G. Walker, J. Chem. Soc., B-11, 1233 (1967).

21. W. Bruegel, Z. Elektrochem., 66, 159 (1962).

22. J. C. Craig, Jr., and D. E. Pearson, J. Heterocyl. Chem., 5, 631 (1968).

23. B. M. Lynch, B. C. Macdonald, and J. G. K. Webb, Tetrahedron, 24, 3595 (1968).

24. A. R. Katritzky and J. M. Lagowski, J. Chem. Soc., 1961, 43.

25. J. P. Dorie, S. Odiot, and M. L. Martin, Compt. Rend. H. Acad. Sci., 274, 2022 (1972).

26. J. J. Delpuech and G. Serratrice, Org. Magn. Resonance, 4, 667 (1972).

27. R. F. C. Brown, L. Radom, S. Sternhill, and I. D. Rae, Can. J. Chem., 46, 2577 (1968).

28. S. G. Schulman, A. C. Capomacchia, and M. S. Rietta, Anal. Chim. Acta, 91, 56 (1971).

29. E. W. Schafer, R. B. Brunton, and D. J. Cunningham, Toxicol. Appl. Pharmacol., 26, 532 (1973).

30. V. Sobek, Physiol. Bohemoslov., 19, 417 (1970).

31. N. E. Saade, J. Chanelet, and P. Lonchampt, C. R. Soc. Biol., 165, 1242 (1971).

32. M. Lemeignan, Therapie, 26, 927 (1971).

33. V. Mitsov, Farmatsiya(Sofia), 21, 42 (1971).

34. V. Mitsov and P. Uzunov, Eksp. Med. Morfol., 11, 162 (1972).

35. E. Knobloch, Coll. Czech. Chem. Comm., 12, 407 (1947).

36. A. G. Pozdeeva and E. G. Novikov, Zh. Prikl. Khim. (Leningrad), 42, 2626 (1969).

37. B. Emmert and W. Dorn, Ber. Dtsch. Chem. Ges., 48, 687 (1915).

38. G. V. Budu and L. V. Nazarova, Zh. Neorg. Khim., 18, 1531 (1973).

39. Y. Couturier and C. Petitfaux, C. R. Acad. Sci., Ser. C., 275, 953 (1972).

40. A. W. Addison, R. D. Gillard, and D. H. Vaughan, J. Chem. Soc., Dalton Trans., 1973, 1187.

41. J. J. R. Frausto da Silva and R. Wooton, J. Chem. Soc., D-8, 421 (1969).

42. M. R. Caira, J. M. Haigh, and L. R. Nassimbeni, J. Inorg. Nucl. Chem., 34, 3171 (1972).

43. R. P. Henry, P. C. H. Mitchell, and J. E. Prue, Inorg. Chim. Acta, 7, 125 (1973).

44. P. S. Relan, S. L. Chopra, and I. S. Bhatia, Proc. Chem. Symp., 1st, 2, 31 (1969).

45. T. Birchall and N. N. Greenwood, J. Chem. Soc., A-2, 286 (1969).

46. J. A. McCleverty, N. M. Atherton, N. G. Connelly, and C. J. Winscom, J. Chem. Soc., A-15, 2242 (1969).

47. D. G. Batyr and I. I. Bulgak, Isv. Akad. Nauk Mold. SSR, Ser. Biol. Khim. Nauk, 3, 71 (1971).

48. D. G. Batyr and I. I. Bulgak, Zh. Neorg. Khim., 17, 3364 (1972).

49. L. J. Boucher and J. C. Bailar, Jr., J. Inorg. Nucl. Chem., 27, 1093 (1965).

50. Y. Yamano, I. Masuda, and K. Shinra, Inorg. Nucl. Chem. Lett., 4, 581 (1968).

51. R. J. Bromfield, R. H. Dainty, R. D. Gillard, and B. T. Heaton, Nature (London), 223, 735 (1969).

52. A. L. Crumbliss and F. Basolo, Science, 164, 1168 (1969).

53. P. Bikartten and D. V. R. Rao, J. Inst. Chem. (Calcutta), 41, 223 (1969).

54. J. Cabral and M. F. Cabral, Rev. Port. Quim., 12, 85 (1970).

55. J. P. Fox, R. Banninger, R. T. Proffitt, and L. L. Ingraham, Inorg. Chem., 11, 2379 (1972).

56. P. C. Roy and D. V. R. Rao, Indian J. Chem., 11, 371 (1973).

57. L. E. Moore, R. B. Gerhart, and W. E. Bull., J. Inorg. Nucl. Chem., 26, 896 (1964).

58. W. E. Bull and L. E. Moore, J. Inorg. Nucl. Chem., 27, 1341 (1965).

59. J. L. Burmeister and T. P. O'Sullivan, Inorg. Chim. Acta, 3, 479 (1969).

60. M. K. Misra and D. V. R. Rao, Indian J. Chem., 8, 86 (1970).

61. S. J. Cole, G. C. Curthoys, E. A. Magnusson, and J. N. Phillips, Inorg. Chem., 11, 1024 (1972).

62. C. W. Frank and L. B. Rogers, Inorg. Chem., 5, 615 (1966).

63. P. B. Bowman and L. B. Rogers, J. Inorg. Nucl. Chem., 28, 2215 (1966).

64. G. W. Bushnell, Can. J. Chem., 49, 555 (1971).

65. H. D. Hardt and H. Gechnizdjani, Z. Anorg. Allg. Chem., 397, 23 (1973).

66. D. Craciuescu and A. H. J. Benbassat, Farm. Aikak., 81, 174 (1972).

67. C. H. Kirksey, P. Hambright, and C. B. Storm, Inorg. Chem., 8, 2141 (1969).

68. B. K. Mohapatra and D. V. R. Rao, Z. Anorg. Allg. Chem., 372, 332 (1970).

69. M. S. Novakovskii, V. N. Voinova, V. A. Starodub, and V. K. Yoshko, Zh. Neorg. Khim., 17, 72 (1972).

70. Ts. B. Konunova and M. F. Frunze, Poverkh. Yavleniya Adsorbtsiya, Koord. Vzaimodeistvie, 1972, 12.

71. Ts. B. Konunova and M. F. Frunze, Zh. Neorg. Khim., 18, 1800 (1973).

72. D. P. Johnson, J. Wilinski, and R. D. Bereman, J. Inorg. Nucl. Chem., 35, 2854 (1973).

73. W. Strohmeier and G. Schoenauer, Berichte, 95, 1767 (1962).

74. A. W. Addison, K. Dawson, R. D. Gillard, B. T. Heaton, and H. Shaw, J. Chem. Soc., Dalton Trans., 1972, 589.

75. J. L. Burmeister and H. J. Gysling, Inorg. Chim. Acta, 1, 110 (1967).

76. C. V. Melios, M. M. Ortega, and S. Tabak, An. Acad. Brasil. Cienc., 40, 143 (1968).

77. P. Bikarttan and D. V. R. Rao, J. Inst. Chem. (Calcutta), 41, 177 (1968).

78. C. H. Kirksey and P. Hambright, Inorg. Chem., 9, 958 (1970).

79. V. A. Starodub, M. S. Novakovskii, V. N. Voinova, and A. V. Belous, Zh. Neorg. Khim., 17, 2615 (1972).

80. N. A. Subbotina, V. V. Zelentsov, and V. I. Spitsyn, Vestn. Mosk. Univ., Khim., 24, 52 (1969).

81. H. P. Fritz and D. Sellmann, Z. Naturforsch., 22, 610 (1967).

82. K. Vrieze, H. C. Volger, M. Gronert, and A. P. Praat, J. Organometal. Chem., 16, 19 (1969).

83. B. E. North and M. Rosenblum, J. Organometal. Chem., 21, 445 (1970).

84. K. R. Bkaskar and S. Singh, Spectrochim. Acta, Part A., 33, 1155 (1967).

85. G. Aloisi, G. Cauzzo and U. Mazzucato, Trans. Faraday Soc. 63, 1858 (1967)

86. J. M. Daisey and A. J. Sonnesa, J. Phys. Chem., 76, 1895 (1972).

87. R. C. Poller and J. C. Spillman, J. Chem. Soc., A. Inorg. Phys., Theor., 1966, 1024.

88. J. Ulstrup, Acta Chem. Scand., 23, 3091 (1969).

89. Z. Waclawek and J. Hurwic, Rocz. Chem., 41, 1993 (1967).

90. C. E. Van Hall and K. G. Stone, Anal. Chem., 27, 1580 (1955).

91. W. C. Hoyle, Ph.D. Thesis, Iowa State University, 1973.

92. F. T. Wooten, Proc. IEEE, 55, 564 (1967).

93. H. W. Linde, L. B. Rogers, and D. N. Hume, Anal. Chem., 25, 404 (1953).

94. B. C. Tyson, W. H. McCurdy, and C. E. Bricker, Anal. Chem., 33, 1640 (1961).

95. S. N. Hajiev and M. J. Agarunov, "Temperature, Its Measurement and Control in Science and Industry," Reinhold Publishing Corp., New York, N.Y., 1972, Vol. 4, Part 2, pp. 1065-1069.

96. S. Johansson, Ark. Kemi, 24, 189 (1964).

97. H. J. V. Tyrrell and A. E. Beezer, "Thermometric Titrimetry," Chapman and Hall, London, 1968, pp. 46-68.

98. L. S. Bark and S. M. Bark, "Thermometric Titrimetry," Pergamon Press, London, 1969, pp. 21-41.

99. R. C. LaForce, S. F. Ravitz, and W. B. Kendall, Rev. Sci. Inst., 35, 729 (1964).

100. E. B. Smith, C. S. Barnes, and P. W. Parr, Anal. Chem., 44, 1663 (1972).

101. S. H. Ediz, M. van Swaay, and H. D. McBride, Chem. Instrum., 3, 299 (1972).

102. C. E. Vanderzee and J. A. Swanson, J. Phys. Chem., 67, 285 (1963).

103. K. J. Jahr, G. Weise, and G. Schluchardt, Z. Phys. Chem., 61, 73 (1968).

104. H. W. Trolander, D. A. Case, and R. W. Harruf, "Temperature, Its Measurement and Control in Science and Industry," Reinhold Publishing Corp., New York, N.Y., 1972, Vol. 4, part 2, p. 1002.

105. M. J. Bowman and F. H. Sagar, IEEE Trans., IM-21(1), 48 (1972).

106. D. Buhl, Anal. Chem., 40, 715 (1968).

107. N. E. Vanderborgh and W. D. Spall, Anal. Chem., 40, 256 (1968).

108. R.W.A. Scarr and R. A. Setterington, Proc. IEEE, 107B, 395 (1960).

109. M. Prudenziati, A. Taroni, and G. Zanarini, IEEE Trans., IECI-17(6), 407 (1971).

110. E. Andrich, Philips Tech. Rev., 30, 170 (1969).

111. H. A. Sauer and J. R. Fisher, J. Amer. Ceram. Soc., 43, 297 (1960).

112. G. N. Tekster-Proskuryakova and I. T. Sheftel, Radio Eng. and Electronic Phys., 5, 781 (1966).

113. "Applications Manual for Operational Amplifiers," Philbrick/Nexus Research, a Teledyne Company, Dedham, Mass., 1968, p. 102.

114. "Operational Amplifiers, Part IV," Analog Devices, Inc., Cambridge, Mass., 1968.

115. C. D. Motchenbacher and F. C. Fitchen, "Low-Noise Electronic Design," Wiley-Interscience, New York, N.Y., 1973, pp. 7-115.

116. H. S. Carslaw and J. C. Jaeger, "Conduction of Heat in Solids," Clarendon Press, Oxford, England, 1959, pp. 237-246.

117. R. A. Rasmussen, Rev. Sci. Inst., 33, 38 (1962).

118. Y. V. Kudryavtsev, et al., "Unsteady-State Heat Transfer," Iliffe Books Ltd., London, 1966, p. 86.

119. S. S. Kutateladze, "Fundamentals of Heat Transfer," Academic Press, New York, N.Y., 1963, pp. 242-244.

120. J. W. Murdock, C. J. Foltz, and C. Gregory, Trans. ASME, J. Eng. Power, 85, 27 (1963).

121. A. W. Rice, H. L. Toor, and F. S. Manning, A. I. Ch. E. J., 10, 125 (1964).

122. C. Papadopoulos, Chem. Ind. (London), 33, 932 (1971).

123. R. S. Brodkey, A. I. Ch. E. J., 9, 448 (1963).

124. M. Dutt and T. Stickney, ISA Trans., 9, 81 (1970).

125. R. P. Benedict, "Fundamentals of Temperature, Pressure, and Flow Measurements," Wiley, New York, N.Y., 1969, p. 162.

126. M. D. Scadron and I. Warshawsky, "Experimental Determination of Time Constants and Nusselt Numbers for Bare-Wire Thermocouples in High Velocity Air Streams and Analytic Approximation of Conduction and Radiation Errors," NACA, TN 2599, Jan., 1952, p. 1.

127. L. D. Bowers and P. W. Carr, Thermochimica Acta, 10, 129 (1974).

128. W. P. White, "The Modern Calorimeter," Chemical Catalog Co., New York, N.Y., 1928.

129. K. L. Churney, G. T. Armstrong, and E. D. West, "Status of Thermal Analysis," O. Menis, Ed., National Bureau of Standards Special Publication, 338, 23 (1970).

130. H. A. Skinner, J. M. Sturtevant, and S. Sunner, "Experimental Thermochemistry," H. A. Skinner, Ed., Interscience, New York, N.Y., 1962, p. 157.

131. S. Sunner and I. Wadsö, Acta Chem. Scand., 13, 97 (1959).

132. J. J. Christensen, R. M. Izatt, and L. D. Hansen, Rev. Sci. Instrum., 36, 779 (1965).

133. "Tronac Thermometric Titration Calorimeter," Tronac, Box 37, Orem, Utah 84057.

134. J. J. Christensen, H. D. Johnston, and R. M. Izatt, Rev. Sci. Instrum., 39, 1356 (1968).

135. C. E. Johansson, Talanta, 17, 739 (1970).

136. R. J. Davenport, private communication, Iowa State University, 1973.

137. J. Polaczek and Z. Lisicki, J. Thermal Anal., 3, 3 (1971).

138. R. S. Brodkey, "The Phenomena of Fluid Motions," Addison-Wesley, London, 1967, p. 327.

139. M. D. Scadron and I. Warshawsky, "Experimental Determination of Time Constants and Nusselt Numbers for Bare-Wire Thermocouples in High Velocity Air Streams and Analytic Approximation of Conduction and Radiation Errors," NACA, TN 2599, Jan., 1952, pp. 2-6.

140. W. R. Bratschun, A. J. Mountvala, and A. C. Pincus, "Uses of Ceramics in Nicroelectronics, A Survey," NASA SP-5097, 1971, pp. 16-19.

141. A. Žukauskas, "Advances in Heat Transfer," Academic Press, New York, N.Y., 1972, p. 144.

142. S. Nagata, M. Nishikawa, and T. Takimoto, Heat Transfer - Japanese Research, 1, April-June, 49 (1972).

143. S. Kopperl and J. Parascandola, J. Chem. Educ., 48, 237 (1971).

144. F. T. Gucker, Jr., H. B. Pickard, and R. W. Planck, J. Amer. Chem. Soc., 61, 459 (1939).

145. M. A. Mohs, Ph.D. thesis, Iowa State University, 1970.

146. M. L. McGlashan, J. Chem. Thermodynamics, 1, 118 (1969).

147. J. J. Christensen, H. D. Johnston, and R. M. Izatt, Rev. Sci. Inst., 39, 1356 (1968).

148. F. Becker, Chemie-Ing.-Techn., 41, 1060 (1969).

149. W. Köhler, O. Riedel, and H. Scherer, Chemie-Ing.-Techn., 44, 1216 (1972).

150. J. J. Christensen, J. W. Gardner, D. J. Eatough, R. M. Izatt, P. J. Watts, and R. M. Hart, Rev. Sci. Inst., 44, 481 (1973).

151. H. L. Friedman and Yung-Chi Wu, Rev. Sci. Inst., 36, 1236 (1965).

152. H. W. Trolander, D. A. Case, and R. W. Harruf, "Temperature, Its Measurement and Control in Science and Industry," Reinhold Publishing Corp., New York, N.Y., 1972, Vol. 4, part 2, p. 1002.

153. L. F. Ebell, Anal. Chem., 37, 446 (1965).

154. M. J. Stern, R. Withnell, and R. J. Raffa, Anal. Chem., 38, 1275 (1966).

155. "The Merck Index," P. G. Stecher, Ed., 8th ed., Merck, Rathway, N.J., 1968, p. 810.

156. J. F. Swindells, "Calibration of Liquid-in-Glass Thermometers," National Bureau of Standards Monograph 90, National Bureau of Standards, Washington, D.C., 1965, pp. 12-13.

157. L. C. Pharo, Rev. Sci. Inst., 36, 211 (1965).

158. D. P. Wrathall and W. L. Gardner, "Temperature, Its Measurement and Control in Science and Industry," Reinhold Publishing Corp., New York, N.Y., 1972, Vol. 4, part 3, p. 2223.

159. L. D. Hansen and E. A. Lewis, Anal. Chem., 43, 1393 (1971).

160. OM. N. Bhatnagar and A. N. Campbell, Chem. Instrum., 4, 179 (1973).

161. "Catalog MGP 681," Victory Engineering Corp., Springfield, N.J., 1967, p. 5.

162. D. W. Rogers and R. J. Sasiela, Talanta, 20, 232 (1972).

163. "Handbook of Chemistry and Physics," R. C. Weast, Ed., 47th ed., Chemical Rubber Co., Cleveland, Ohio, 1967.

164. Y. S. Touloukian, R. W. Powell, C. Y. Ho, and P. G. Klemens, "Thermophysical Properties of Matter, Thermal Conductivity, Nonmetallic Solids," Vol. 2, Plenum Press, New York, N.Y., 1970, p. 257.

165. Y. S. Touloukian and E. H. Buyco, "Thermophysical Properties of Matter, Specific Heat, Nonmetallic Solids," Vol. 5, Plenum Press, New York, N.Y., 1970, p. 1313.

166. H. Lee and K. Neville, "Handbook of Epoxy Resins," McGraw Hall Book Co., New York, N.Y., 1967, pp. 6-32.

167. I. M. Gottlieb, "Regulated Power Supplies," H. W. Sams and Co., Inc., Indianapolis, Indiana, 1971, p. 70.

168. S. Gunn, J. Chem. Thermodynamics, 3, 19 (1971).

169. W. Swietoslawski, "Microcalorimetry," Reinhold, New York, N.Y., 1946, p. 147.

170. H.J.V. Tyrrell and A. E. Beezer, "Thermometric Titrimetry," Chapman and Hall, London, 1968, p. 25.

171. "Thermal Conductivity," R. P. Tye, Ed., Academic Press, London, 1969, p. 146.

172. R. C. Weast, Ed., "Handbook of Chemistry and Physics," Chemical Rubber Publishing Co., 47th ed., 1966-67.

173. R. E. Treybal, "Mass-Transfer Operations," 2nd ed., McGraw-Hill, New York, N.Y., 1968, p. 33.

174. R. C. Reid and R. K. Sherwood, "The Properties of Gases and Liquids," 2nd ed., McGraw-Hill, New York, N.Y., 1966, p. 548.

175. Y. S. Touloukian and T. Makita, "Thermophysical Properties of Matter, Specific Heat, Nonmetallic Liquids and Gases," Vol. 6, Plenum, New York, N.Y., 1970, p. 285.

176. E. Cohen and J. Kooy, Z. Physik. Chem., A139, 271 (1928).

177. S. Somsen, J. Coops, and M. W. Tolk, Rec. Trav. Chim., 82, 231 (1963).

178. V. B. Parker, "Thermal Properties of Aqueous Uni-univalent Electrolytes," NSRDS-NBS2, U. S. Government Printing Office, Washington, D.C., 1965.

179. V. P. Vasil'ev and G. A. Lobanov, Russ. J. Inorg. Chem., 11, 383 (1966).

180. R. G. Bates, "Electrometic pH Determinations," Wiley, New York, N.Y., 1954, pp. 186-188.

181. H. Diehl, "Quantitative Analysis," Oakland Street Science Press, Ames, Iowa, 1970, p. 104.

182. P. W. Carr, "Analytical Aspects of Thermometric Titrations," in "Critical Reviews of Analytical Chemistry," L. Meites, Ed., Chemical Rubber Co., Cleveland, Ohio, Jan., 1972, p. 546.

183. J. D. Hale, R. M. Izatt, and J. J. Christensen, J. Phys. Chem., 67, 2605 (1963).

184. C. E. Vanderzee and J. A. Swanson, J. Phys. Chem., 67, 2608 (1963).

185. F. D. Rossini in "Experimental Thermochemistry," R. D. Rossini, Ed., Interscience, New York, N.Y., 1956, p. 16.

186. J. F. Yan, Anal. Chem., 37, 1855 (1965).

187. D. J. Eatough, J. J. Christensen, and R. M. Izatt, J. Chem. Thermodynamics, 7, 417 (1975).

188. H. M. Papee, W. J. Canady, and K. J. Laidler, Can. J. Chem., 34, 1677 (1956).

189. T. F. Young, Y. C. Wu, and A. A. Krawetz, Discussions Faraday Soc., 24, 37 (1957).

190. E. W. Wilson, Jr., and D. F. Smith, Anal. Chem., 41, 1903 (1969).

191. W. F. Koch, D. L. Briggs, and H. Diehl, Talanta, 22, 637 (1975).

192. J. J. Christensen, G. L. Kimball, and R. M. Izatt, Thermochimica Acta, 5, 293 (1973).

193. E. J. Prosen and M. V. Kilday, J. Res. Nat. Bur. Stand., 77A, 581 (1973).

194. A. P. Brunetti, E. J. Prosen, and R. N. Goldberg, J. Res. Nat. Bur. Stand., 77A, 599 (1973).

195. C. J. Barnes and A. J. Matuszko, J. Org. Chem., 27, 2239 (1962).

196. H. Diehl, private communication, Iowa State University, 1973.

197. W. J. Blaedel and V. W. Meloche, "Elementary Quantitative Analysis," Row, Peterson and Co., Evanston, Ill., 1957, pp. 574-576.

198. M. Slavin, "Emission Spectrochemical Analysis," Vol. 36 of "Chemical Analysis," P. J. Elving and I. M. Kolthoff, Eds., Wiley-Interscience, New York, N.Y., 1971, p. 157.

199. G. Gyulai and E. J. Greenhow, Talanta, 21, 131 (1974).

200. J. J. Christensen, R. M. Izatt, and L. D. Hansen, J. Amer. Chem. Soc., 89, 213 (1967).

201. S. Cabani and P. Gianni, Anal. Chem., 44, 253 (1972).

202. N. V. Tsederberg, "Thermal Conductivity of Gases and Liquids," M.I.T. Press, Cambridge, Mass., 1965, p. 230.

203. M. Nakanishi and S. Fujieda, Anal. Chem., 44, 574 (1972).

204. K-T Liu and W. E. Stewart, Int. J. Heat Mass Transfer, 15, 187 (1972).

205. B. B. Graves, Anal. Chem., 44, 993 (1972).

XII. ACKNOWLEDGEMENTS

The author wishes to thank Dr. Dennis C. Johnson for his direction of the research and assistance in preparation of the manuscript.

The author thanks the Department of Chemistry of Iowa State University for research funds and equipment used in this research.

Special thanks are given to Mr. Dale A. Fitzgibbons whose critical comments proved invaluable in development of the theoretical models proposed in this work. His thorough knowledge of the Fortran IV language saved many hours of labor in writing computer programs. He is also thanked for taking the photographs used in this thesis.

Finally, the author acknowledges the patience of his wife, Glennyce, and the skill of Sue Musselman who typed the manuscript.

XIII. APPENDIX A: LIST OF SYMBOLS

a, a_1, a_2, b, b_1, c, c_1, d, d_1, L, K, m, M, n, N, r, Z, α, β, δ, ε, ζ, η, θ, Λ, ξ, σ, ϕ, x, ψ coefficients

A_e Cross sectional area of epoxy filling plus Teflon tubing in thermistor mounting (cm^2)

A_h Surface area of electrical heater (cm^2)

A_{stem} Surface area of mounting tubes in contact with bulk solution (cm^2)

A_t Total surface area of thermistor (cm^2)

A_{ts} Total cross sectional area of thermistor stem (cm^2)

A_{tw} Cross sectional area of thermistor lead wires (cm^2)

A_w Surface area of calorimeter wall in contact with bulk solution (cm^2)

A_1 Area of thermistor used to calculate radial heat transfer through epoxy film to bulk solution (cm^2)

A_2 Area of thermistor used to calculate radial heat transfer into thermistor stem (cm^2)

C Correlation coefficient of circuit noises

c_b Volume heat capacity of bulk solution (cal/cm^3-deg C)

C_b Heat capacity of bulk solution (cal/deg C)

C_f Feedback capacitor for operational amplifier (μF)

c_{Cu} Mass heat capacity of copper metal (cal/g-deg C)

C_h Heat capacity of electrical heater (cal/deg C)

c_p Mass heat capacity of bulk solution (cal/g-deg C)

c_r Mass heat capacity of resistive element (cal/g-deg C)

c_{rl} Concentration of limiting reactant (mole/g)

c_t Volume heat capacity of thermistor material (cal/cm^3-deg C)

c_t' Mass heat capacity of thermistor material (cal/g-deg C)

C_t Heat capacity of thermistor (cal/deg C)

C_w Heat capacity of calorimeter wall (cal/deg C)

c_1 Heat capacity of reference cell of calorimeter cell (cal/deg C)

c_2 Heat capacity of reaction cell of calorimeter cell (cal/deg C)

D_b Thermal diffusivity of bulk solution (cm^2/sec)

D_t Thermal diffusivity of thermistor material (cm^2/sec)

E_g Gap energy of semiconductor (eV)

e_n Short term electronic noise which is random in nature (V)

$e_{o,3}$ Output voltage of Operational Amplifier 3 (V)

Δe_{os} Long term electronic drift of amplifier offsets (V)

e_{rms} rms noise voltage (V)

E_{std} Potential difference measured across standard resistor (V)

e_+, e_- Positive and negative voltages applied to thermistors t_2 and t, respectively (V)

E_1 Potential difference measured across R_{ch_1} (V)

E_2 Potential difference measured across R_{ch_2} (V)

f Frequency (Hz)

f_1 Fraction of total surface area of thermistor in A_1

f_2 Fraction of total surface area of thermistor in A_2

g_1 Dimensionless function determined for conductive heat transport through composite solid for A_1

g_2 Dimensionless function determined for conductive heat transport through composite solid for A_2

h h_t/λ_{eq} (1/cm)

h_h Heat transfer coefficient of cylindrically shaped electrical heater (cal/cm^2-sec-deg C)

h_{hs} Heat transfer coefficient of heater stem (cal/cm^2-sec-deg C)

h_s Convective heat transfer coefficient of thermistor stem (cal/cm^2-sec-deg C)

h_{stem} Heat transfer coefficient of heater, thermistor, mounting tubes, etc. (cal/cm^2-sec-deg C)

h_t Convective heat transfer coefficient of thermistor bead (cal/cm^2-sec-deg C)

h_w Heat transfer coefficient of calorimeter wall (cal/cm^2-sec-deg C)

ΔH_r Heat of reaction/mole of limiting reactant (cal/mole)

$I_{o,n}$ Output noise of circuit expressed as current noise at output of summing amplifier (amp)

I_{th}	Thevenin current
J	Mechanical equivalent of heat
k_B	Boltzmann constant
k	Heat loss modulus
l_b	Depth of bulk solution (cm)
l_1	Height of stirrer disc above the bottom of the calorimeter (cm)
l_2	Depth of immersion of stirrer disc in bulk solution (cm)
m	Molality of reactant
M	Molarity of reactant
m_{Cu}	Mass of copper sheath of electrical heater resistive element (g)
m_r	Mass of electrical heater resistive element (g)
m_{rl}	Mass of limiting reactant (g)
m_1	Mass of bulk solvent added to reference cell of calorimeter (g)
m_2	Mass of bulk solvent added to reaction cell of calorimeter (g)
N_s	Rotation speed of stirrer (rev/min)
Nu	Nusselt number
P_h	Electrical energy supplied for heating per unit time (cal/sec)
P_t	Electrical power applied to thermistor (cal/sec)
Pr	Prandtl number

Q_h	Heat supplied electrically to the calorimeter (cal)
r_c	Radius of calorimeter cell (cm)
r_h	Radius of electrical heater (cm)
r_s	Radius of stirrer disk (cm)
r_{sh}	Radius of stirrer shaft (cm)
r_{st}	Radius of thermistor stem (cm)
r_{stem}	Average radius of mounting tubes (cm)
r_t	Radius of thermistor bead (cm)
R_{ch_1}	Calibration resistor in calorimeter reference cell (Ω)
R_{ch_2}	Calibration resistor in calorimeter reaction cell (Ω)
R_f	Feedback resistance of operational amplifier (Ω)
R_{std}	Standard resistor (Ω)
R_t	Resistance of thermistor at its geometric center (Ω)
R_{th}	Thevenin resistance
Re	Reynolds number
s	Laplacian operator
S	Standard deviation
Sc	Schmidt number
t	Time (sec)
t_1, t_2	Thermistors in bridge circuit
T_a	Ambient temperature of bridge amplifier enclosure (deg C)
T_b	Temperature of bulk solution (deg K)

T_{bl} Temperature of bulk solution at the interface of the bulk solution and electrical heater boundary layer (deg K)

T_h Temperature of electrical heater (deg K)

T_i Calorimeter internal temperature (deg C)

T_j Calorimeter jacket temperature (deg C)

T_s Temperature of thermistor stem at interface of Teflon tubing and glass mount (deg K)

T_t Thermistor temperature at the geometric center (deg K)

$T_{t,r}$ Temperature of epoxy-thermistor interface (deg K)

$T_{t,w}$ Temperature of epoxy covered thermistor-bulk solution interface (deg K)

T_w Temperature of calorimeter wall (deg K)

U Fluid velocity (cm/sec)

$U_s(r)$ Radial velocity of bulk fluid at distance r due only to stirrer disc (cm/sec)

$U_{sh}(r)$ Radial velocity of bulk fluid at distance r due only to stirrer shaft (cm/sec)

V_{th} Thevenin voltage

x_{Cu} Thickness of copper tubing surrounding metal film resistor (cm)

x_e Thickness of epoxy film on thermistor (cm)

$x_{e,h}$ Thickness of epoxy coating an electrical heater (cm)

x_s Thickness of stirrer disc (cm)

x_{ts} Length of thermistor stem (cm)

Z_t Pre-exponential term in thermistor resistance functions (Ω)

α Temperature coefficient of resistance of bridge resistor (ohm/deg C)

α_n Roots of the transcendental equation

$$r_t \alpha_n \cot r_t \alpha_n + r_t h - 1 = 0$$

α_t Material coefficient of thermistor with positive temperature coefficient (1/deg K)

β_t Material coefficient of thermistor with negative temperature coefficient (deg K)

γ_b Bulk solution heating rate (deg C/sec)

γ_{bkg} Heating rate of bulk solution by heat transferred through calorimeter wall from environment (deg C/sec)

γ_{str} Heating rate of bulk solution by stirring (deg C/sec)

γ_t Heating rate of thermistor by electrical power (deg C/sec)

γ_{th} Heating rate of bulk solution by thermistor (deg C/sec)

δ_b Dissipation constant of epoxy plus stem and boundary layer (cal/sec-deg C)

δ_o Dissipation constant of thermistor bead (cal/sec-deg C)

δ_t Dissipation constant of thermistor assembly (cal/sec-deg C)

λ_b Thermal conductivity of bulk solution (cal/cm-sec-deg C)

λ_{Cu} Thermal conductivity of copper metal (cal/cm-sec-deg C)

λ_e Thermal conductivity of epoxy (cal/cm-sec-deg C)

λ_{eq} Equivalent thermal conductivity of thermistor material plus epoxy and stem (cal/cm-sec-deg C)

λ_h Thermal conductivity of electrical heater (cal/cm-sec-deg C)

λ_i Inner thermal conductivity of thermistor material corrected for epoxy and stem effects (cal/cm-sec-deg C)

λ_r Thermal conductivity of metal film resistor (cal/cm-sec-deg C)

λ_s Equivalent thermal conductivity of thermistor stem (cal/cm-sec-deg C)

λ_t Thermal conductivity of thermistor material (cal/cm-sec-deg C)

λ_w Thermal conductivity of thermistor lead wires (cal/cm-sec-deg C)

μ Ionic strength

ν_b Kinematic viscosity of bulk solution (cm^2/sec)

ρ $h_t r_t$ (cal/cm-sec-deg C)

ρ_t Mass density of thermistor material (g/cm^3)

σ_s Dimensionless shielding parameter

τ_b Time constant of epoxy plus stem and boundary layer (sec)

τ_h Time constant of electrical heater (sec)

τ_m Time constant of mixing (sec)

$\tau_{m,disc}$ Time constant of mixing for stirrer disc (sec)

$\tau_{m,shaft}$ Time constant of mixing for stirrer shaft (sec)

τ_o Time constant of thermistor bead (sec)

τ_t Time constant of thermistor assembly (sec)

τ_w Time constant of calorimeter wall (sec)

ω $2\pi f$, angular frequency (rads/sec)

ω_s Angular velocity of stirrer (rad/sec)

XIV. APPENDIX B: DERIVATION OF THERMISTOR THERMAL CONDUCTIVITIES

A. Transient Equivalent Conductivity

Using the algebraic form of Fourier's law of conduction

$$Q = \frac{A}{x} \lambda \Delta T \qquad [1]$$

where Q = heat energy flowing through material (cal)

x = thickness of material (cm)

A = area through which thermal flux is conducted (cm^2)

The energy leaving region L_1 by conductive heat transport to the surface A_1 in the theoretical model shown in Figure B.1 is

$$Q_{r,1} = f_1 \frac{A_t}{r_t} \lambda_t g_1 \Delta T_{t-w} \qquad [2]$$

$$\text{where } f_1 \frac{A_t}{r_t} \lambda_t g_1 = (\tfrac{1}{2}) \frac{4\pi r_t^2}{r_t} \lambda_t \left(\frac{r_t \lambda_e}{r_t \lambda_e + x_e r_t}\right) \qquad [3]$$

Refer to Appendix A for explanation of symbols.

Equations 2 and 3 are derived as follows: For region L_1, there are two materials forming a composite solid, epoxy and thermistor bead material. Negligible contact resistance is assumed between the two since they are in excellent mechanical contact with each other. Hence, there are two temperature differences to consider

$$\Delta T_1 = T_t - T_{t,r_t}$$

$$\Delta T_2 = T_{t,r_t} - T_{t,w}$$

Figure B.1. Model of thermistor used for theoretical calculations

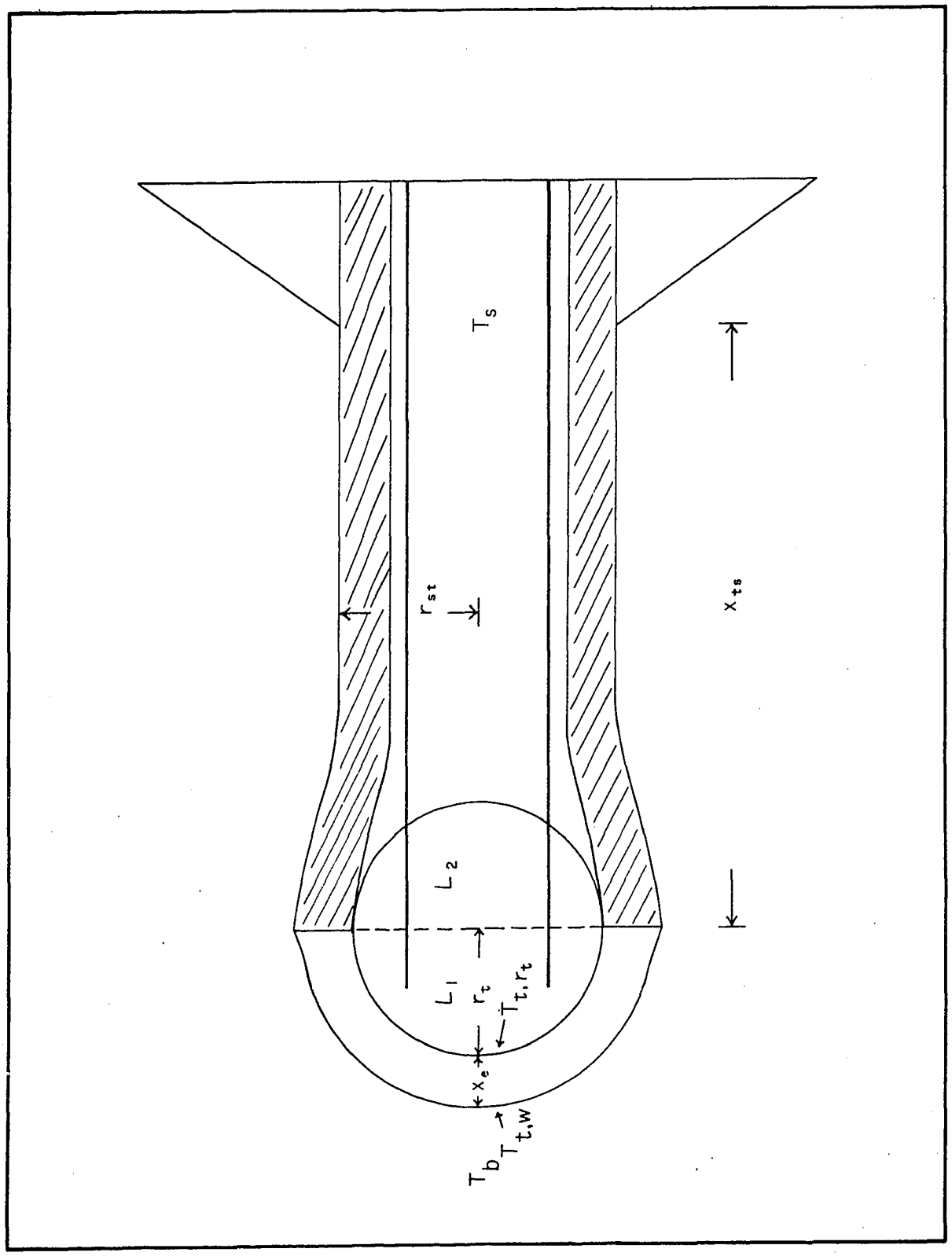
T_s
r_{st}
x_{ts}
L_2
L_1
r_t
T_t, r_t
x_e
T_b
$T_{t,w}$

$$Q_{r,1} = 2\pi \frac{r_t^2}{r_t} \lambda_t \Delta T_1 \quad \text{and}$$

$$Q_{r,2} = 2\pi \frac{r_t^2}{x_e} \lambda_e \Delta T_2$$

$$\Delta T_1 + \Delta T_2 = \Delta T_{t-w} = T_t - T_{t,w}$$

$$\Delta T_{t-w} = \frac{Q_{r,1}\, r_t}{2\pi\, r_t^2\, \lambda_t} + \frac{Q_{r,2}\, x_e}{2\pi\, r_t^2\, \lambda_e}$$

assuming no lateral heat losses, $Q_{r,1} = Q_{r,2}$, and

$$Q_{r,1} = 2\pi\, r_t\, \lambda_t \left(\frac{r_t\, \lambda_e}{r_t\, \lambda_e + x_e\, \lambda_t}\right)(T_t - T_{t,w}) \qquad [4]$$

which is equivalent to Equation 2 and 3.

Similarly, for the heat flow out of the thermistor into the thermistor stem (longitudinal heat flow)

$$Q_{r,3} = f_2 \frac{A_t}{r_t} \lambda_t\, g_2\, \Delta T_{t-s} \qquad [5]$$

$$\text{where } f_2 \frac{A_t}{r_t} g_2 = \left(\frac{1}{2}\right) \frac{4\pi r_t^2}{r_t} \lambda_t \left(\frac{r_t \lambda_s}{r_t \lambda_s + x_{ts} \lambda_t}\right) \qquad [6]$$

Equations 5 and 6 are derived in a manner similar to Equation 4.

Fourier's law in heat transfer is analogous to Ohm's law in electrical current theory. Hence, equivalent resistances and conductivities can be calculated by linear

combinations. The thermistor electrical leads, epoxy, and Teflon provide parallel heat conduction pathways from the thermistor bead.

From the analogy of parallel resistances, it can be readily shown that

$$\lambda_s = \frac{A_e \lambda_e + A_{tw} \lambda_w}{A_{ts}} \qquad [7]$$

In like manner, regions L_1 and L_2 are acting in parallel to conduct heat to the bulk solution. The total energy is defined as

$$Q_{r,t} = (f_1 + f_2) \frac{A_t}{r_t} \lambda_{eq} \Delta T_{\overline{tws}}$$

where $\overline{tws}$ indicates the average temperature difference to the bulk solution interface with the thermistor assembly. Then,

$$(f_1 + f_2) \lambda_{eq} \frac{A_t}{r_t} = \frac{Q_{r,t}}{\Delta T_{\overline{tws}}} = \frac{Q_{r,1}}{\Delta T_{t-w}} + \frac{Q_{r,3}}{\Delta T_{t-s}} \qquad [8]$$

and since $f_1 + f_2 = 1$

$$\lambda_{eq} = f_1 \lambda_t g_1 + f_2 \lambda_t g_2 \qquad [9]$$

in this work, $f_1 = f_2 = 0.5$, hence,

$$\lambda_{eq} = 0.5\left[\lambda_t\left(\frac{r_t \lambda_e}{r_t \lambda_e + x_e \lambda_t}\right) + \lambda_t\left(\frac{r_t \lambda_s}{r_t \lambda_s + x_{ts} \lambda_t}\right)\right] \qquad [10]$$

Finally, Equation 10 needs to be corrected for convective heat loss from the thermistor stem. Convective heat loss from the area A_1 is calculated as part of the equations for a sphere from Carslaw and Jaeger (116). At the stem-bulk solution interface, the energy conducted radially as the result of longitudinal heat conduction is given by

$$Q_x = \frac{2\pi r_{st} x_{ts}}{r_{st}} \lambda_s \Delta T_{s-w}$$

and an equal amount of energy, Q_r, is dissipated into the bulk solution

$$Q_r = 2\pi r_{st} x_{ts} h_s \Delta T_{w-b}$$

Hence,

$$\frac{\Delta T_{s-w}}{\Delta T_{w-b}} = \frac{h_s r_{st}}{\lambda_s} \qquad [11]$$

Multiplying the second part of Equation 10 with Equation 11 yields the final equation

$$\lambda_{eq} = 0.5\left[\lambda_t\left(\frac{r_t \lambda_e}{r_t \lambda_e + x_e \lambda_t}\right) + \lambda_t\left(\frac{r_t r_{st} h_s}{r_t \lambda_s + x_{ts} \lambda_t}\right)\right] \qquad [12]$$

Equation 12 is then the equivalent conductivity, used in the transient part of the Equation B.5 and B.6 derived in section III.

B. Steady-State Inner Conductivity

The problem of heat flow must be reduced to that of a sphere, the thermistor, connected by a vanishingly small connection to a half sphere attached to an insulated base. The half sphere has a thermal conductivity of λ_s and radius of r_s. From Equations 3 and 5, the ratio of $1/\lambda_t'/1/\lambda_s'$ can be derived where λ_t' is λ_t corrected to half-sphere geometry with epoxy coating and λ_s' is λ_s corrected to a thin rod having heat flow into one end and the other end insulated. The value of λ_s' is directly proportional to h_s. Hence, Equation 11 is used to include the effect of h_s on λ_s'.

$$1/\lambda_t' = \frac{\Delta T_{t-w}}{Q_{r,1}} = \frac{1}{2\pi\, r_t\, \lambda_t} \left(\frac{r_t\, \lambda_e + x_e\, \lambda_t}{r_t\, \lambda_e}\right) \qquad [13]$$

$$1/\lambda_s' = \frac{\Delta T_{t-s}}{Q_{r,3}} = \frac{1}{2\pi\, r_t\, \lambda_t} \left(\frac{r_t\, \lambda_s + x_{ts}\, \lambda_t}{r_t\, \lambda_s}\right) \qquad [14]$$

and including Equation 11

$$1/\lambda_s' = \frac{\Delta T_{t-s}}{Q_{r,3}} \frac{\Delta T_{w-b}}{\Delta T_{s-w}} = \frac{1}{2\pi\, r_t\, \lambda_t} \cdot \left(\frac{\lambda_s}{h_s\, r_{st}}\right)\left(\frac{r_t\, \lambda_s + x_{ts}\, \lambda_t}{r_t\, \lambda_s}\right) \qquad [15]$$

accordingly,

$$Q_{r,\text{total}} = \frac{4\pi\, r_t^2}{r_t} \lambda_t\, \Delta T_{t,r_t} \qquad [16]$$

and

$$Q_x = Q_{r,s} = \frac{2\pi r_{st}^2}{r_{st}} \lambda_s \Delta T_{t,r_s} \quad [17]$$

which becomes

$$\frac{Q_{r,total}}{\Delta T_{t,r_t}} = 4\pi r_t \lambda_t \quad [18]$$

and

$$\frac{Q_{r,s}}{\Delta T_{t,r_s}} = 2\pi r_s \lambda_s \quad [19]$$

Multiplying Equation 13 by 18 and 15 by 19, the ratio

$$\frac{1/\lambda_t' \lambda_t}{1/\lambda_s' \lambda_s'} = \frac{\lambda_s' \lambda_t}{\lambda_t' \lambda_s} = \frac{\frac{\Delta T_{t-w}}{Q_{r,1}} \frac{Q_{r,total}}{\Delta T_{t,r_t}}}{\frac{\Delta T_{t-s}}{Q_{r,3}} \frac{Q_{r,s}}{\Delta T_{t,r_s}} \frac{\Delta T_{w-b}}{\Delta T_{s-w}}}$$

$$= \left(\frac{\Delta T_{t-w}}{\Delta T_{t-s}}\right)\left(\frac{Q_{r,total}}{Q_{r,1}}\right)\left(\frac{Q_{r,3}}{Q_{r,s}}\right)\left(\frac{\Delta T_{t,r_s}}{\Delta T_{t,r_t}}\right)\left(\frac{\Delta T_{s-w}}{\Delta T_{w-b}}\right)$$

$$= 2 \frac{\lambda_t}{\lambda_e}\left(\frac{h_s r_{st}}{\lambda_s}\right)\left(\frac{r_t \lambda_e + x_e \lambda_t}{r_t \lambda_s + x_{ts} \lambda_t}\right) \quad [20]$$

is written.

Equation 20 yields a dimensionless number which is used to multiply λ_t to obtain λ_i. That this is a reasonable result is seen that as x_e increases the temperature difference across the epoxy and boundary layer will increase. Analysis of other parameters of Equation 20 is equally straightforward except for h_s. The changes of h_s are meaningless until λ_i is divided

by $h_t r_t$. The ratio h_s/h_t is nearly unity throughout the fluid velocity range used in this study.

XV. APPENDIX C: DERIVATION OF BULK SOLUTION HEATING RATE

A. Main Period

The setup and solution of the bulk solution temperature, T_b, with respect to time was described in Section III.B.3 of this thesis. The same method of solution and initial conditions apply to dT_b/dt versus time. Reference to the original equations in Section III.B.3 will be made throughout so that the source of each equation can be readily traced.

Starting from Equation B.76, the partial fraction expansion of the coefficient of P_h may be written for Case I (underdamping) as

$$\frac{M_1}{s} + \frac{M_2}{(s + Z_2)} + \frac{M_3}{(s + \alpha + \beta j)} + \frac{M_4}{(s + \alpha - \beta j)} \qquad [1]$$

working the algebra and taking the inverse transform yields

$$\frac{dT_b}{dt}(t) = \frac{P_h}{(C_b + C_w)} + \frac{P_h Z_3 (Z_2 - Z_1)}{(Z_2^2 - Z_2(Z_1 + Z_3))C_b + Z_1 Z_3 (C_b + C_w)} \cdot$$

$$\exp\{-Z_2 t\} - \frac{2P_h\, r_{11}}{(C_b + C_w)} \exp\{-\alpha t\} \cdot$$

$$\cos(\beta t - \theta_{11}) - \gamma_{bkg} \frac{C_w}{C_b} \frac{Z_3}{\beta} \exp\{-\alpha t\} \cdot$$

$$\sin \beta t \qquad [2]$$

where $\theta_{11} = \text{arc sin}\{b_{11}/r_{11}\}$

and $$r_{11} = [(a_{11})^2 + (b_{11})^2]^{\frac{1}{2}}$$

$$a_{11} = \frac{Z_2\beta[\phi - \alpha(Z_1 - Z_2)]}{\psi} \qquad [3]$$

$$b_{11} = \frac{Z_2[\alpha\phi + \beta^2(Z_1 - Z_2)]}{\psi} \qquad [4]$$

Proceeding to Case II (critical damping) as stated in Equation B.101, the coefficient of P_h is given by

$$\frac{M_5}{s} + \frac{M_6}{(s + Z_2)} + \frac{M_7}{(s + \alpha)^2} + \frac{M_8}{(s + \alpha)} \qquad [5]$$

and the final solution by

$$\frac{dT_b}{dt}(t) = \frac{P_h Z_1 Z_3}{C_b \alpha^2} + \frac{P_h}{C_b}\left[\frac{Z_3(Z_2 - Z_1)}{(\alpha - Z_2)^2}\right] \cdot$$

$$\exp\{-Z_2 t\} + \frac{P_h}{C_b}\left[\frac{Z_2 Z_3(Z_1 - \alpha)}{\alpha(\alpha - Z_2)}\right] \cdot$$

$$t \exp\{-\alpha t\} +$$

$$\frac{P_h}{C_b}\left[\frac{Z_2 Z_3 \alpha(\alpha - Z_2) - (Z_1 - \alpha)(Z_2 - 2\alpha)}{\alpha^2(Z_2 - \alpha)^2}\right] \cdot$$

$$\exp\{-\alpha t\} - \gamma_{bkg} \frac{C_w}{C_b} Z_3 t \exp\{-\alpha t\} \qquad [6]$$

Case III (overdamping) derived from the condition described in Equation B.112 yields for the coefficient of P_h

$$\frac{M_9}{s} + \frac{M_{10}}{(s + Z_2)} + \frac{M_{11}}{(s + \alpha + \sigma)} + \frac{M_{12}}{(s + \alpha - \sigma)} \qquad [7]$$

and the final solution

$$\frac{dT_b}{dt}(t) = \frac{P_h Z_1 Z_3}{C_b(\alpha + \sigma)(\alpha - \sigma)} + \frac{P_h Z_3 (Z_2 - Z_1)}{C_b(\alpha + \sigma - Z_2)(\alpha - \sigma - Z_2)} \cdot$$

$$\exp\{-Z_2 t\} + \frac{P_h Z_2 Z_3 (Z_1 - \alpha - \sigma)}{2C_b \sigma(\alpha + \sigma)(Z_2 - \alpha - \sigma)} \cdot$$

$$\exp\{-(\alpha + \sigma)t\} -$$

$$\frac{P_h Z_2 Z_3 (Z_1 - \alpha + \sigma)}{2C_b \sigma(\alpha - \sigma)(Z_2 - \alpha + \sigma)} \exp\{-(\alpha - \sigma)t\} -$$

$$\gamma_{bkg} \frac{C_w Z_3}{C_b \sigma} \exp\{-t\} \sinh \sigma t \qquad [8]$$

B. Anterior Period

The treatment of Case I proceeds from Equation B.123 with the coefficient of $T_h(0)$ given by

$$\frac{N_1}{(s + Z_2)} + \frac{N_2}{(s + \alpha + \beta j)} + \frac{N_3}{(s + \alpha - \beta j)} \qquad [9]$$

and the final solution by

$$\frac{dT_b}{dt}(t) = \left[\frac{C_w Z_3}{C_b \beta} \exp\{-\alpha t\} \sin \beta t\right] \cdot$$

$$\left[\gamma_{bkg} - \frac{P_h}{C_b + C_w}\right] +$$

$$[2\, r_{12} \exp\{-\alpha t\} \cos(\beta t - \theta_{12})] \cdot$$

$$\left[\frac{P_h}{C_b + C_w}\right] +$$

$$\left[\left(\frac{C_h Z_2 Z_3 (Z_1 - Z_2)}{C_b (Z_2^2 - (Z_1 + Z_3) Z_2 + Z_1 Z_3 (1 + C_w/C_b))}\right)\right] \cdot$$

$$\exp\{-Z_2 t\} + \frac{2 C_h Z_2 r_{13}}{C_b} \exp\{-\alpha t\} \cdot$$

$$\cos(\beta t - \theta_{13})\left]\left[\frac{P_h}{h_h A_h} + \frac{P_h \tau_m}{C_b + C_w} + \frac{P_h t_{co}}{C_b + C_w}\right]\right. \qquad [10]$$

where $\theta_{12} = \text{arc sin}\{b_{12}/r_{12}\}$

and $r_{12} = [(a_{12})^2 + (b_{12})^2]^{1/2}$

$$a_{12} = 1/2 \qquad [11]$$

$$b_{12} = \left(\frac{Z_1 - \alpha}{2\beta}\right) \qquad [12]$$

$$\theta_{13} = \text{arc sin}\{b_{13}/r_{13}\}$$

$$r_{13} = [(a_{13})^2 + (b_{13})^2]^{1/2}$$

$$a_{13} = \frac{Z_3 (Z_2 - Z_1)\beta}{\Lambda} \qquad [13]$$

$$b_{13} = \frac{Z_1 Z_2 Z_3 - Z_3 (Z_1 + Z_2)\alpha + Z_1 Z_3^2 (1 + C_w/C_b)}{\Lambda} \qquad [14]$$

where $\Lambda = 2\beta[Z_2^2 - 2Z_2\alpha + Z_1 Z_3 (1 + C_w/C_b)]$ [15]

In Case II, the coefficient of $T_h(0)$ is divided into partial fractions starting from Equation B.150 as

$$\frac{N_4}{(s + Z_2)} + \frac{N_5}{(s + \alpha)^2} + \frac{N_6}{(s + \alpha)} \qquad [16]$$

and the final solution becomes

$$\frac{dT_b}{dt}(t) = \left[\frac{C_w Z_3}{C_b} t \exp\{-\alpha t\}\right]\left[\gamma_{bkg} - \frac{P_h}{C_b f C_w}\right] +$$

$$[(Z_1 - \alpha)t \exp\{-\alpha t\} + \exp\{-\alpha t\}] \cdot$$

$$\left[\frac{P_h}{C_b + C_w}\right] +$$

$$\left[\frac{C_h Z_2 Z_3 (Z_1 - Z_2)}{C_b(\alpha - Z_2)^2} \exp\{-Z_2 t\} +\right.$$

$$\frac{C_h Z_2 Z_3 (Z_1 - \alpha)}{C_b(Z_2 - \alpha)} t \exp\{-\alpha t\} +$$

$$\left.\frac{C_h Z_2 Z_3 (Z_2 - Z_1)}{C_b(Z_2 - \alpha)^2} \exp\{-\alpha t\}\right] \cdot$$

$$\left[\frac{P_h}{h_h A_h} + \frac{P_h \tau_m}{C_b + C_w} + \frac{P_h t_{co}}{C_b + C_w}\right]$$

Finally, the partial fraction expansion of the coefficient of $T_h(0)$ given in Equation B.170 is

$$\frac{N_7}{(s + Z_2} + \frac{N_8}{(s + \alpha + \sigma)} + \frac{N_9}{(s + \alpha - \sigma)}$$

which leads to the solution

$$\frac{dT_b}{dt}(t) = \left[\frac{C_w Z_3}{C_b \sigma} \exp\{-\alpha t\} \sinh \sigma t\right] \cdot$$

$$\left[\gamma_{bkg} - \frac{P_h}{C_b + C_w}\right] +$$

$$\left[\frac{(Z_1 - \alpha + \sigma)}{2\sigma} \exp\{-(\alpha - \sigma)t\} -\right.$$

$$\left.\frac{(Z_1 - \alpha - \sigma)}{2\sigma} \exp\{-(\alpha + \sigma)t\}\right] \cdot$$

$$\left[\frac{P_h}{C_b + C_w}\right] +$$

$$\left[\frac{C_h Z_2 Z_3 (Z_1 - Z_2)}{C_b(\alpha + \sigma - Z_2)(\alpha - \sigma - Z_2)} \exp\{-Z_2 t\} -\right.$$

$$\frac{C_h Z_2 Z_3 (Z_1 - \alpha - \sigma)}{2C_b\sigma(Z_2 - \alpha - \sigma)} \exp\{-(\alpha + \sigma)t\} +$$

$$\left.\frac{C_h Z_2 Z_3 (Z_1 - \alpha + \sigma)}{2C_b\sigma(Z_2 - \alpha + \sigma)} \exp\{-(\alpha - \sigma)t\}\right] \cdot$$

$$\left[\frac{P_h}{h_h A_h} + \frac{P_h \tau_m}{C_b + C_w} + \frac{P_h t_{co}}{C_b + C_w}\right] \qquad [17]$$

XVI. APPENDIX D: COMPUTER PROGRAM LISTINGS

A. Thermistor Time Constant, Dissipation Constant, and Average Time Constant of Mixing

The program developed to calculate thermistor time constants, dissipation constants and time of mixing at a radius of 0.5 r_c was coded in the FORTRAN IV language and is intended to be used with the IBM OS/360 WATFIV compiler. Table D.1 lists the program identifiers with their names and corresponding symbols if used in the text.

Table D.1. Definitions of identifiers used in program #1

Identifier	Definition	Symbol
ALSTEM	Length of thermistor stem	x_{st}
AMBAB	Thermal conductivity of bulk solution	λ_b
AMBAE	Thermal conductivity of epoxy	λ_e
AMBAT	Thermal conductivity of thermistor material	λ_t
AMBATL	Thermal conductivity of thermistor lead wires	λ_w
AREAW	Cross sectional area of thermistor lead wires	A_{tw}
CSUBT	Volume heat capacity of thermistor material	c_t
DISIT	Dissipation constant of thermistor assembly	δ_t

Table D.1 (Continued)

Identifier	Definition	Symbol
HSUBT	Convective heat transfer coefficient of thermistor bead	h_t
NSUBS	Rotation speed of stirrer	N_s
PR	Prandtl number of bulk solution	Pr
R	Distance thermistor is from center of calorimetry cell	r
RE	Reynolds number of bulk solution at r	Re
REMAX	Reynolds number of bulk solution at edge of stirrer disk	Re_{max}
RET	Reynolds number of bulk solution at surface of thermistor	Re_t
REYN	Reynolds number of bulk solution at 0.5 r_c	
RLSUBE	Thickness of epoxy film on thermistor	x_e
RSM	Radius used to calculate an average mixing time constant, 0.5 r_c	
RSUBC	Radius of calorimeter cell	r_c
RSUBST	Radius of thermistor stem	r_{st}
RSUBS	Radius of stirrer disk	r_s
RSUBT	Radius of thermistor bead	r_t
SC	Schmidt number of bulk solution	Sc
TAUM	Time constant of mixing	m
TAUT	Time constant of thermistor assembly	t

Figure D.1. Thermistor time constant, dissipation constant, and average time constant of mixing

```
C
C      THIS PROGRAM IS DESIGNED TO CALCULATE THE TIME CONSTANT OF MIXING
C      FOR THE DEWAR CELLS USED IN CALORIMETRY.  THE RELATION OF OMEGA
C      AND THE TIME CONSTANT OF MIXING IS OBTAINED BY ITERATIVE CALCULATIONS.
C      THE TIME CONSTANT OF MIXING IS CALCULATED ASSUMING ONLY A DISC
C      CONTRIBUTION TO STIRRING.  TIME OF MIXING IS CALCULATED AT 1/2
C      R SUB C TO GIVE AN AVERAGE VALUE.
C      REYNOLDS # IS CALCULATED AT R, THE DISTANCE THAT THE THERMISTOR
C      IS FROM THE CENTER OF THE DEWAR CELL.  REYN# IS CALCULATED FOR
C      R=1/2 OF R SUB C, OR R SUB MIXING.
C      ALL PARAMETERS USED ARE THOSE FOR 25.0 DEGREE C.
C
C      THIS RUN IS USED TO CALCULATE THE TIME CONSTANT AND DISSIPATION
C      CONSTANT FOR R PTC.
C
       DIMENSION WSUBS(40),NSUBS(40),REMAX(40),RE(40),TAUM(40),RET(40),
      &TNU(40),HSUBT(40),TAUT(40),DISIT(40),NAME(20),RSUBT(2),URDIVU(40),
      &REYN(40)
       READ(5,100) R,RSUBC,RSUBS,RLSUBE,RSM,ALSTEM,RSUBST,AREAW
  100  FORMAT(F4.2,2X,F4.2,2X,F4.2,2X,E13.3,2X,F4.2,2X,F4.2,2X,F5.3,
      &2X,E13.3)
       READ(5,105) AMBAB,AMBAE,AMBAT,CSUBT,AMBATL
  105  FORMAT(E13.3,2X,E13.3,2X,E13.3,2X,F5.3,2X,F5.3)
       READ(5,110) PR,SC,VISB
  110  FORMAT(F4.2,2X,F6.1,2X,E13.4)
       READ(5,115)(NAME(I),I=1,20)
  115  FORMAT(20A4)
       WRITE(6,200)(NAME(I),I=1,20)
  200  FORMAT('1',20A4)
       WRITE(6,205) R,RSUBC,RSUBS,RLSUBE,RSM
  205  FORMAT(1X,'R=',E13.3,2X,'R SUB C=',E13.3,2X,'R SUB S=',E13.3,2X,
      &'RL SUB E=',F5.3,2X,'R SUB MIXING=',F4.2)
       WRITE(6,210) PR,SC,VISB
  210  FORMAT(1X,'PRANDTL#=',F4.2,2X,'SCHMIDT#=',F6.1,2X,'VISB=',E13.4)
       DO 500 I=1,40
```

Figure D.1. (Continued)

```
      NSUBS(I) = 50*I
      WSUBS(I) = 0.1047*NSUBS(I)
      REMAX(I)=(2*RSUBC*RSUBS*WSUBS(I))/VISB
      VALM= -0.617 +8.211E-3*(REMAX(I))**0.786
      VALS=0.585 +3.172E-3*(REMAX(I))**0.833
      ASUB1=(VALS - VALM)/(VALM - 1)
      ASUB2=(1 - VALS)/(VALM - 1)
      URDIVU(I)=1+ASUB1*(R/RSUBC)**2+ASUB2*(R/RSUBC)**(2*VALM)
      RE(I)=URDIVU(I)*RSUBS*WSUBS(I)*R/VISB
      URDIV=1+ASUB1*(RSM/RSUBC)**2+ASUB2*(RSM/RSUBC)**(2*VALM)
      REYN(I)=URDIV*RSUBS*WSUBS(I)*RSM/VISB
      F=0.0791*REYN(I)**(-0.25)
      YSUBO=SQRT(F/8)*REYN(I)
      U=YSUBO/RSUBC
      USTAR=U*VISB
      USUBX=1.3*USTAR
      S=0.341*RSUBC/USUBX
      E=1.49*USUBX**3
      TAUM(I)=0.5*(3*S+SQRT(VISB/E)*ALOG(SC))
500   CONTINUE
      WRITE(6,215)(I,NSUBS(I),WSUBS(I),REMAX(I),RE(I),TAUM(I),REYN(I),
     &I=1,40)
215   FORMAT(1X,'I=',I2,2X,'RPM=',I4,3X,'OMEGA=',F5.1,3X,'REMAX=',F8.1,
     &3X,'REYNOLDS #=',F7.1,2X,'TAU MIX (SEC)=',F6.3,2X,'REYN#=',F7.1)
      READ(5,120) NTHERS
120   FORMAT(I2)
      DO 510 J=1,NTHERS
      READ(5,125)(NAME(I),I=1,20)
125   FORMAT(20A4)
      WRITE(6,220)(NAME(I),I=1,20)
220   FORMAT('1',20A4)
      K=0
300   K=K+1
      READ(5,135) RSUBT(K)
135   FORMAT(E13.3)
```

Figure D.1. (Continued)

```
      IF(RSUBT(K).GT.1.0) GO TO 310
      GO TO 300
310   CONTINUE
      K=1
      DO 520 I=1,40,1
      RET(I)=(URDIVU(I)*RSUBS*RSUBT(K)*WSUBS(I)*2)/VISB
      TNU(I)=0.50+0.0875*RET(I)**0.58*PR**0.356
      HSUBT(I)=(TNU(I)*AMBAB)/RSUBT(K)
      HSUBST=0.239*(URDIVU(I)*WSUBS(I)*RSUBS*2*RSUBST/VIS3)**0.50*
     &PR**0.30*AMBAB/RSUBST
      AREAT=3.14*RSUBST**2
      AMBAST=(AREAT*AMBAE+AREAW*AMBATL)/AREAT
      DSUBT=AMBAT/CSUBT
      AMBAI=4*AMBAT*HSUBST*RSUBST*(RSUBT(K)*AMBAE+RLSUBE*AMBAT)/
     &(AMBAE*AMBAST*(RSUBT(K)*AMBAST+ALSTEM*AMBAT))
      TAUT(I)=RSUBT(K)**2/(6*DSUBT)*(1+AMBAT*AMBAI/(HSUBT(I)*RSUBT(K)))
      DISIT(I)=25.1*RSUBT(K)*AMBAT*(1/(1+AMBAT*AMBAI/(HSUBT(I)*RSUBT(K)
     &)))
520   CONTINUE
      WRITE(6,230)(I,NSUBS(I),RET(I),TNJ(I),HSUBT(I),I=1,40)
230   FORMAT(1X,'I=',I2,2X,'RPM=',I4,3X,'REYNOLDS#,T=',F7.1,3X,
     &'NUSSELT#,T=',F5.2,3X,'HSUBT=',E13.4)
      WRITE(6,235) RSUBT(K),AMBAT,AMBAE,CSUBT,AMBAB
235   FORMAT('1',1X,'RSUBT=',E13.3,2X,'LAMBDA,T=',E13.3,2X,'LAMBDA,E=',
     &E13.3,2X,'HEAT CAP,T=',F5.3,2X,'LAMBDA,BULK SOLN=',E13.3)
      WRITE(6,240)(I,NSUBS(I),TAUT(I),DISIT(I),I=1,40)
240   FORMAT(1X,'I=',I2,2X,'RPM=',I4,3X,'THERM TAU (SEC)=',F5.2,3X,
     &'THERM DELTA (CAL/SEC C)=',E13.3)
510   CONTINUE
      STOP
      END
```

Table D.1 (Continued)

Identifier	Definition	Symbol
TNU	Nusselt number of bulk solution at thermistor surface	Nu
URDIVU	Ratio of bulk solution velocity at r to bulk	$U(r)/U_{max}$
VISB	Kinematic viscosity of bulk solution	ν_b
WSUBS	Angular velocity of stirrer	ω_s

B. Time Constant of Mixing

This program was written to include all stirrer contributions in calculation of the time constant of mixing. Provision for inclusion of experimentally determined time constants of mixing is made in this program. The program was coded in the FORTRAN IV language and is intended to be used with the IBM OS/360 WATFIV compiler. Table D.2 lists only those identifiers not already cited in Table D.1.

Table D.2 Definitions of identifiers used in program #2

Identifier	Definition	Symbol
RPM	Experimental rotation speed of stirrer	
RSUBSS	Radius of stirrer shaft	r_{sh}

Figure D.2. Time constant of mixing

```
C
C      THIS PROGRAM IS DESIGNED TO CALCULATE THE TIME CONSTANT OF MIXING
C      FOR THE DEWAR CELLS USED IN CALORIMETRY.  THE RELATION OF OMEGA
C      AND THE TIME CONSTANT OF MIXING IS OBTAINED BY ITERATIVE CALCULATIONS.
C      R EQUAL TO THE DISTANCE THAT THE CELL HEATER AND THERMISTOR SENSOR
C      ARE FROM THE GEOMETRIC CENTER OF THE CELL.
C      ALL PARAMETERS JSED ARE THOSE FOR 25.0 DEGREE C.
C
       DIMENSION WSUBS(10),NSUBS(10),REMAX(10),RE(10,5),TAUM(10,5),
      &NAME(20),RPM(20),TAUMEP(20),ANSUBS(10),TM(10),URDIVU(10,5),
      &UXMAX(10,5),XL(5),YL(5)
       READ(5,100) R,RSUBC,RSUBS,RSUBSS
100    FORMAT(F4.2,2X,F4.2,2X,F4.2,2X,F4.2)
       READ(5,110) PR,SC,VISB
110    FORMAT(F4.2,2X,F6.1,2X,E13.4)
       READ(5,115)(NAME(I),I=1,20)
115    FORMAT(20A4)
       WRITE(6,117)(NAME(I),I=1,20)
117    FORMAT('1',20A4)
       WRITE(6,140) R,RSUBC,RSUBS,RSUBSS
140    FORMAT(1X,'R=',E13.3,2X,'R SUB CELL=',E13.3,2X,'R SUB STIRRER=',
      &E13.3,2X,'R SUB SHAFT=',E13.3)
       WRITE(6,141) PR,SC,VISB
141    FORMAT(1X,'PRANDTL#=',F4.2,2X,'SCHMIDT#=',F6.1,2X,'VISB=',E13.4)
       DO 501 II=1,5
       DO 500 I=1,10
       NSUBS(I)=200*I
       WSUBS(I) = 0.1047*NSUBS(I)
       REMAX(I)=(2*RSUBC*RSUBS*WSUBS(I))/VISB
       VALM= -0.617 +8.211E-3*(REMAX(I))**0.786
       VALS=0.585 +3.172E-3*(REMAX(I))**0.833
       ASUB1=(VALS - VALM)/(VALM - 1)
       ASUB2=(1 - VALS)/(VALM - 1)
       URDIVU(I,II)=1 +ASUB1*(R/RSUBC)**2+ASUB2*(R/RSUBC)**(2*VA_M)
       RE(I,II)=URDIVU(I,II)*RSUBS*WSUBS(I)*R/VISB
```

Figure D.2. (Continued)

```
      F=0.0791*RE(I,II)**(-0.25)
      YSUBO=SQRT(F/8)*RE(I,II)
      UX=YSUBO/RSUBC
      USTAR=UX*VISB
      UXMAX(I,II)=(SQRT(2/F)+3.75)*USTAR
      USUBX=(0.6+1.102*R/RSUBC)*USTAR
      S=0.341*RSUBC/USUBX
      E=1.49*USUBX**3
      TAUMDS=0.5*(3*S+SQRT(VISB/E)*ALOG(SC))
      REMSS=(2*RSUBC*RSUBSS*WSUBS(I))/VISB
      VALMSS=-0.617+8.211E-3*REMSS**0.786
      VALSSS=0.585+3.172E-3*REMSS**0.833
      ASUB11=(VALSSS-VALMSS)/(VALMSS-1)
      ASUB22=(1-VALSSS)/(VALMSS-1)
      URDIVS=1+ASUB11*(R/RSUBC)**2+ASUB22*(R/RSUBC)**(2*VALMSS)
      REYSS=URDIVS*RSUBSS*WSUBS(I)*R/VISB
      FF=0.0791*REYSS**(-0.25)
      YSUBOS=SQRT(FF/8)*REYSS
      UXS=YSUBOS/RSUBC
      USTARS=UXS*VISB
      USUBRS=(0.8+0.413*R/RSUBC)*USTARS
      SS=0.341*RSUBC/USUBRS
      EE=1.49*USUBRS**3
      TAUMSS=0.5*(3*SS+SQRT(VISB/EE)*ALOG(SC))
      TAUM(I,II)=1/((1/TAUMDS+1/TAUMSS)/2)
500   CONTINUE
      WRITE(6,145) R
145   FORMAT('0','THE TIME CONSTANTS OF MIXING CALCULATED AT R=',F4.2,
     &1X,'FOR N SUBS S=200 TO 2000 RPM, ARE')
      WRITE(6,150)(I,NSUBS(I),WSUBS(I),REMAX(I),RE(I,II),URDIVU(I,II),
     &UXMAX(I,II),TAUM(I,II),I=1,10)
150   FORMAT(1X,'I=',I2,2X,'RPM=',I4,2X,'OMEGA=',F5.1,2X,'RE MAX=',F8.1,
     &2X,'REY=',F7.1,2X,'U(R)/U=',F5.3,2X,'U SUB X MAX=',F5.1,2X,'TAU
     &MIX (SEC)=',F6.3)
      R=R+0.30
```

Figure D.2. (Continued)

```
501     CONTINUE
        READ(5,134) XL,YL
134     FORMAT(10A4)
        READ(5,138) NPTS
138     FORMAT(I2)
        READ(5,160)(RPM(J),TAUMEP(J),J=1,NPTS)
160     FORMAT(F6.1,2X,F4.2)
        DO 660   II=1,5
        DO 670 I=1,10
        ANSUBS(I)=NSUBS(I)
670     TM(I)=TAUM(I,II)
        IF(II.GT.1) GO TO 675
        CALL GRAPH(10,ANSUBS,TM,3,1,10.0,8.0,250.0,0.0,0.0,0.0,0.0,XL,YL,
       &';',';')
        GO TO 660
 675    CONTINUE
        IF(II.EQ.5) GO TO 700
690     CALL GRAPHS(10,ANSUBS,TM,0,2,';')
        GO TO 660
700     CALL GRAPHS(10,ANSUBS,TM,3,1,';')
660     CONTINUE
        CALL GRAPHS(NPTS,RPM,TAUMEP,4,7,';')
        STOP
        END
```

Table D.2 (Continued)

Identifier	Definition	Symbol
TAUMEP	Experimental time constant of mixing	
UXMAX	Ratio of bulk solution velocity at r to bulk solution velocity at r_{sh}	

C. Approximate Temperature Response of the Stirred Fluid in a Cylindrical Calorimeter During Electrical Heating

The program developed to calculate the bulk solution temperature, T_b, with respect to time, the value of dT_b/dt with respect to time, and the thermistor circuit output voltage, e_o, with respect to time was coded in the FORTRAN IV language. The program can be used either with the IBM OS/360 FORTRAN G compiler or WATFIV compiler. Table C.3 lists only those identifiers not already cited in Tables D.1 and D.2.

Table D.3 Definitions of identifiers used in program #3

Identifier	Definition	Symbol
ALP	Alpha squared	
ALPHA	$(Z_1 + Z_3)/2$	
ALPRI	Roots of transcendental equation	α_n

Table D.3 (Continued)

Identifier	Definition	Symbol
AMBAH	Thermal conductivity of electrical heater	λ_h
ASUBH	Surface area of electrical heater	A_h
ASUBST	Surface area of mounting tubes in contact with bulk solution	A_{stem}
ASUBW	Surface area of calorimeter wall in contact with bulk solution	A_w
BETA	Material coefficient of thermistor with negative temperature coefficieint	β_t
C	Constant used along with ALPRI	
CHI	Trignometric angle	
CONST	Calculated value of C for thermistor studied	
CPSOL	Mass heat capacity of bulk solution	c_p
CSUBB1	Heat capacity of bulk solution	C_b
CSUBH	Heat capacity of electrical heater	C_h
CSUBW	Heat capacity of calorimeter wall	C_w
DELTAT	Calculated value of temperature difference, $T_t - T_b$	
DELTTB	Excess bulk solution temperature	

Table D.3 (Continued)

Identifier	Definition	Symbol
DRDT	Change of thermistor resistance with respect to temperature at initial temperature of the bulk solution	dR/dT
EOOA3	Output voltage of Operational Amplifier 3	$e_{o,3}$
EPSIL	Trignometric angle	
ESUBIN	Negative voltage applied to thermistor t_1	e_-
GAM	Bulk solution heating rate	γ_b
GAMBKG	Heating rate of bulk solution by heat transferred through calorimeter wall from environment	γ_{bkg}
GAMSTR	Heating rate of bulk solution by stirring	γ_{str}
HSTEM	Heat transfer coefficient of heater, thermistor, mounting tubes, etc.	h_{stem}
HSUB1	Height of stirrer disc above the bottom of the calorimeter	l_1
HSUB2	Depth of immersion of stirrer disc in bulk solution	l_2
HSUBH	Heat transfer coefficient of cylindrical shaped electrical heater	h_h
HSUBHS	Heat transfer coefficient of heater stem	h_{hs}
HSUBST	Heat transfer coefficient of thermistor stem	h_s
HSUBW	Heat transfer coefficient of calorimeter wall	h_w

Table D.3 (Continued)

Identifier	Definition	Symbol
NHT	Value of time of heating	
NT	Value of t	
PSUBT	Electrical power applied to thermistor	P_t
RESRF	Feedback resistance of Operational Amplifier 3	R_f
RESRT	Resistance of thermistor at its geometric center	R_t
RSTEM	Average radius of mounting tubes	r_{stem}
RSUBH	Radius of electrical heater	r_h
TAU	Calculated time constant of calorimetry system	
TAUH	Time constant of electrical heater	τ_h
TAUHAR	Calculated time constant of calorimeter + contents	
TAUW	Time constant of calorimeter wall	τ_w
TEMBUK	Temperature of bulk solution	T_b
TEMPBI	Temperature error in T_b at t = 0 due to approximate solution of equations	
TEMPI	Initialization temperature used in calculations	
URATIO	Ratio of bulk solution velocity due stirrer shaft at r to bulk solution velocity due to stirrer disc	

Table D.3 (Continued)

Identifier	Definition	Symbol
XSUBD	Thickness of stirrer disc	x_s
XSUBE	Thickness of epoxy film on thermistor	x_e
XSUBS	Length of thermistor stem	x_{ts}
ZAM	$Z_1 Z_3 (1 + C_w/C_b)$	

Figure D.3. Approximate temperature response of the stirred fluid in a cylindrical calorimeter during electrical heating

```
C
C     THIS PROGRAM IS DESIGNED TO CALCULATE THE EFFECT OF STIRRING RATE
C     UPON THERMISTOR RESPONSE.  A CONSTANT HEATING RATE IS ASSUMED.
C     REYNOLDS # IS CALCULATED AT R, THE DISTANCE THAT THE THERMISTOR
C     IS FROM THE CENTER OF THE DEWAR CELL.
C     INITIAL TEMPERATURE= 25.000 DEG C.  ALL PARAMETERS USED ARE THOSE
C     GIVEN OR CALCULATED AT 25.0 DEG C.
C     PARAMETERS USED ARE THOSE OF NTC THERMISTORS.
C     GAMMA SUB B IS CORRECTED FOR THE CELL TIME CONSTANT, HEATER TIME
C     CONSTANT, AND TIME OF MIXING.
C     A STEADY STATE ELECTRICAL POWER IS ASSUMED IN THIS PROGRAM.
C
      DIMENSION WSJBS(10),NSUBS(10),NAME(20),C(50),ALPHA(50,6),NT(101),
     &CONST(10),ALPRI(10,6),DELTAT(101,10),DELTTB(101,10),URDIVU(10),
     &REMAX(10),RE(10),TAUM(10),RET(10),TNU(10),HSUBT(10),TAUW(10),
     &GAM(101,10),EDDA3(101,10),HSUBH(10),HSUBW(10),TAUH(10),TAU(10),
     &UXMAX(10),ALP(10),ZAM(10),TAUHAR(10),TEMBUK(101,10),TEMPBI(1,10),
     &XL(5),YL(5),U(101),V(101),W(101),X(101),Y(101),Z(101),TAUT(10)
      DIMENSION HSUBST(10),HSUBHS(10),HSTEM(10),INITAU(10),ANSUBS(10),
     &URATIO(10)
C
C     ****FORMATS FOR DATA INPUT STATEMENTS****
      READ(5,100) ESUBIN,PSUBT,RESRF,RESRT,BETA,DRDT,RSUBT,XSUBE
  100 FORMAT(F7.5,2X,E10.3,2X,E13.5,2X,E13.5,2X,F5.1,2X,F6.2,2X,F5.3,2X,
     &F4.2)
      READ(5,102) XSUBS,RSUBST,AREAW,AMBAT,CSUBT,AMBAE,AMBAW
  102 FORMAT(F4.2,2X,F5.3,2X,E10.3,2X,E10.3,2X,F5.3,2X,E10.3,2X,F5.3)
      READ(5,104) PSUBH,GAMBKG,GAMSTR,RSUBH,ASUBH,CSUBH,AMBAH
  104 FORMAT(E10.3,2X,E10.3,2X,E10.3,2X,F4.2,2X,F4.2,2X,F4.2,2X,E10.3)
      READ(5,106) RSUBS,RSUBSS,XSUBD,HSJB1,HSUB2,CHI,EPSIL,R,RSUBC,RSTEM
     &,ASUBST,ASUBW
  106 FORMAT(F4.2,2X,F4.2,2X,F4.2,2X,F3.1,2X,F5.2,2X,F6.4,2X,F6.4,2X,
     &F4.2,2X,F4.2,2X,F4.2,2X,F5.1,2X,F5.1)
      READ(5,108) CSUBW,CSUBB1,CPSOL,AMBAB,PR,SC,VISB,TEMPI,NHT
  108 FORMAT(F4.1,2X,F5.1,2X,F5.3,2X,E10.3,2X,F4.2,2X,F5.1,2X,E11.4,2X,
```

Figure D.3. (Continued)

```
     &F6.2,2X,I3)
      READ(5,110)(C(I),(ALPHA(I,J),J=1,6),I=1,50)
 110  FORMAT(F7.3,2X,F7.4,3X,F7.4,3X,F7.4,3X,F7.4,3X,F7.4,3X,F7.4)
C
C     ....FORMATS FOR DATA PRINT STATEMENTS....
      READ(5,112)(NAME(I),I=1,20)
 112  FORMAT(20A4)
      WRITE(6,225)(NAME(I),I=1,20)
 225  FORMAT('1',20A4)
      WRITE(6,200) ESUBIN,PSUBT,RESRF,RESRT,BETA,DRDT
 200  FORMAT('0','E SUB IN=',F7.5,2X,'P SUB T=',E10.3,2X,'R SUB F=',
     &E13.5,2X,'RES OF THERM=',E13.5,2X,'BETA=',F6.1,2X,'DR/DT=',F6.2)
      WRITE(6,202) RSUBT,XSUBE,XSUBS,RSUBST,AREAW
 202  FORMAT('0','R SUB T=',F5.3,2X,'X SUB E=',F4.2,2X,'LENGTH OF THERM
     &STEM=',F4.2,2X,'R SUB THERM STEM=',F5.3,2X,'AREA THERM LEADS=',
     &E10.3)
      AREAT=3.14*RSUBST**2
      AMBAST=(AREAT*AMBAE+AREAW*AMBAW)/AREAT
      DSUBT=AMBAT/CSUBT
      WRITE(6,204) AMBAT,CSUBT,DSUBT,AMBAE,AMBAW,AMBAST
 204  FORMAT('0','LAMBDA SUB T=',F6.4,2X,'C SUB T=',F5.3,2X,'D SUB T=',
     &F6.4,2X,'LAMBDA SUB E=',E10.3,2X,'LAMBDA SUB W=',F5.3,2X,
     &'LAMBDA STEM=',E10.3)
      WRITE(6,206) PSUBH,GAMBKG,GAMSTR,RSUBH,ASUBH,CSUBH,AMBAH
 206  FORMAT('0','P SUB H=',F7.5,2X,'GAM SUB BKG=',F7.5,2X,'GAM SUB STIR
     &=',F7.5,2X,'R SUB H=',F4.2,2X,'A SUB H=',F4.2,2X,'C SUB H=',F4.2,
     &2X,'LAMBDA SUB H=',F7.5)
      WRITE(6,208) RSUBS,RSUBSS,XSUBD,HSUB1,HSUB2,CHI,EPSIL
 208  FORMAT('0','R SUB S=',F4.2,2X,'R SUB SHAFT=',F4.2,2X,'X SUB D=',
     &F4.2,2X,'H SUB 1=',F3.1,2X,'H SUB 2=',F5.2,2X,'ANGLES:',1X,
     &'CHI (RADS)=',F6.4,2X,'EPSILON (RADS)=',F6.4)
      WRITE(6,210) R,RSUBC,RSTEM,ASUBST,ASUBW,CSUBW,CSUBB1,CPSIL
 210  FORMAT('0','R=',F4.2,2X,'R SUB C=',F4.2,2X,'R SUB STEMS=',F4.2,2X,
     &'AREA OF STEMS=',F5.1,2X,'AREA OF WALL=',F5.1,2X,'C SUB W=',F4.1,
     &2X,'C SUB B=',F5.1,2X,'C SUB P=',F5.3)
```

Figure D.3. (Continued)

```
      WRITE(6,212) AMBAB,PR,SC,VISB,TEMPI,NHT
212   FORMAT('0','LAMBDA SUB B=',E10.3,2X,'PRANDTL #=',F4.2,2X,
     &'SCHMIDT #=',F6.1,2X,'VIS B=',E11.4,2X,'INITIAL TEMP,DEG K=',F6.2,
     &2X,'HEATING TIME=',I3)
C
C     CALCULATION OF THE TIME CONSTANT OF MIXING AT R:
C
      DO 500 I=1,10
      NSUBS(I)=200*I
      WSUBS(I)=0.1047*NSUBS(I)
      REMAX(I)=(2*RSUBC*RSUBS*WSUBS(I))/VISB
      VALM=-0.617+8.211E-3*REMAX(I)**0.786
      VALS=0.585+3.172E-3*REMAX(I)**0.833
      ASUB1=(VALS-VALM)/(VALM-1)
      ASUB2=(1-VALS)/(VALM-1)
      URDIVJ(I)=1+ASUB1*(R/RSUBC)**2+ASUB2*(R/RSUBC)**(2*VALM)
      RE(I)=URDIVJ(I)*RSUBS*WSUBS(I)*R/VISB
      F=0.0791*RE(I)**(-0.25)
      YSUBO=SQRT(F/8)*RE(I)
      UX=YSUBO/RSUBC
      USTAR=UX*VISB
      UXMAX(I)=(SQRT(2/F)+3.75)*USTAR
      USUBX=(0.8+1.102*R/RSUBC)*USTAR
      S=0.341*RSUBC/USUBX
      E=1.49*USUBX**3
      TAUMDS=0.5*(3*S+SQRT(VISB/E)*ALOG(SC))
      REMSS=(2*RSUBC*RSUBSS*WSUBS(I))/VISB
      VALMSS=-0.617+8.211E-3*REMSS**0.786
      VALSSS=0.585+3.172E-3*REMSS**0.833
      ASUB11=(VALSSS-VALMSS)/(VALMSS-1)
      ASUB22=(1-VALSSS)/(VALMSS-1)
      URDIVS=1+ASUB11*(R/RSUBC)**2+ASUB22*(R/RSUBC)**(2*VALMSS)
      REYSS=URDIVS*RSUBSS*WSUBS(I)*R/VISB
      FF=0.0791*REYSS**(-0.25)
      YSUBOS=SQRT(FF/8)*REYSS
```

Figure D.3. (Continued)

```
      UXS=YSUBOS/RSUBC
      USTARS=UXS*VISB
      USUBRS=(0.8+0.413*R/RSUBC)*USTARS
      SS=0.341*RSUBC/JSUBRS
      EE=1.49*USUBRS**3
      TAUMSS=0.5*(3*SS+SQRT(VISB/EE)*ALOG(SC))
      TAUM(I)=1/((1/TAUMDS+1/TAUMSS)/2)
      URATIO(I)=URDIVU(I)/URDIVS
  500 CONTINUE
C
C     ....FORMATS FOR PRINTING OF HYDRODYNAMIC PARAMETERS FOR
C     CALORIMETER CELL....
      READ(5,112)(NAME(I),I=1,20)
      WRITE(6,214)(NAME(I),I=1,20)
  214 FORMAT('0',20A4)
      WRITE(6,216)(I,NSUBS(I),WSUBS(I),JRDIVU(I),REMAX(I),RE(I),
     &UXMAX(I),TAUM(I),I=1,10)
  216 FORMAT(1X,'I=',I2,2X,'RPM=',I4,3X,'OMEGA=',F5.1,3X,'U(R)/U=',
     &F5.3,3X,'RE MAX=',F8.1,3X,'REYNOLDS#=',F7.1,2X,'U SUB X MAX=',
     &F5.1,2X,'TAU MIX (SEC)='F6.3)
C
C     THE DO LOOP 502 CALCULATES THE CALORIMETER RESPONSE TO A RAMP
C     CHANGE IN BULK SOLUTION TEMPERATURE BY ELECTRICAL HEATING.
C
      DO 502 I=1,10
C
C     CALCULATION OF THERMAL CHARACTERISTICS AND HYDRODYNAMIC PARAMETERS
C     FOR THERMISTOR SENSOR:
C
      HSUBST(I)=0.239*(URDIVU(I)*WSUBS(I)*RSUBS*2*RSUBST/VISB)**0.50*
     &PR**0.30*AMBAB/RSUBST
      AMBAI=2*AMBAT*HSUBST(I)*RSUBST*(RSUBT*AMBAE+XSUBE*AMBAT)/
     &(AMBAE*AMBAST*(RSUBT*AMBAST+XSUBS*AMBAT))
      AMBAEQ=0.5*(AMBAT*RSUBT*AMBAE/(RSUBT*AMBAE+XSUBE*AMBAT)+AMBAT*
     &RSUBST*RSUBT*HSUBST(I)/(RSUBT*AMBAST+XSUBS*AMBAT))
```

Figure D.3. (Continued)

```
      RET(I)=(URDIVU(I)*RSUBS*RSUBT*WSUBS(I)*2)/VISB
      TNU(I)=0.50+0.0875*RET(I)**0.58*PR**0.356
      HSUBT(I)=(TNU(I)*AMBAB)/RSUBT
      CONST(I)=RSUBT*HSUBT(I)/AMBAEQ-1
      H=HSUBT(I)/AMBAEQ
      HX=HSUBT(I)/(AMBAI*AMBAT)
      TAUT(I)=RSUBT**2/(5*DSUBT)*(1+2/(HX*RSUBT))
      M=1
 301  CONTINUE
      IF(CONST(I).GT.C(M)) GO TO 310
      IF(CONST(I).LT.C(M)) GO TO 311
 310  M=M+1
      GO TO 301
 311  CORRC=(CONST(I)-C(M-1))/(C(M)-C(M-1))
      DELTA=PSUBT/(25.1*RSUBT*AMBAT)*(1+2/(HX*RSUBT))
      RESTH=RESRT-DRDT*DELTA
      RESRX=RESTH
      TEMPB=TEMPI
C
C     CALCULATION OF THERMAL CHARACTERISTICS FOR ELECTRICAL HEATER,
C     SOLUTION PROBES, AND CALORIMETER WALL:
C
      HSUBH(I)=(0.50+0.0875*(URDIVU(I)*WSUBS(I)*RSUBS*2*RSUBH/VISB)**
     &0.58*PR**0.355)*AMBAB/RSUBH
      HSUBHS(I)=0.239*(URDIVU(I)*WSUBS(I)*RSUBS*2*RSUBH/VISB)**0.50*PR**
     &0.30*AMBAB/RSUBH
      TAUH(I)=CSUBH*HSUBHS(I)*RSUBH/(HSUBH(I)*ASUBH*AMBAH)
      HSUBW(I)=0.128*(0.637*RSUBS**2*WSUBS(I)/VISB)**0.667*PR**0.33*
     &(RSUBS/RSUBC)**(-0.25)*(HSUB1/HSUB2)**0.15*HSUB2/(RSUBC**2)*
     &(XSUBD/(2*RSUBC))**0.15*AMBAB
      HSTEMD=0.135*(URDIVU(I)*WSUBS(I)*RSUBS*2*RSTEM/VISB)**0.63*PR**
     &0.36*AMBAB/RSTEM
      HSTEMS=0.135*(URDIVU(I)*WSUBS(I)*RSUBSS*2*RSTEM/VISB)**0.63*PR**
     &0.36*AMBAB/RSTEM
      HSTEM(I)=(RSUBSS/(RSUBSS+RSUBS))**0.67*HSTEMS+(RSUBS/(RSUBSS+
```

Figure D.3. (Continued)

```
      Z1=1/TAUW(I)
      Z2=1/TAUH(I)
      Z3=1/TAUM(I)
      TAUHAR(I)=1/((Z1+Z2+Z3)/3)
      ALPHAA=(Z1+Z3)/2
      ALP(I)=ALPHAA**2
      ZAM(I)=Z1*Z3*(1+CSUBW/CSUBB1)
      DIF=ALP(I)-ZAM(I)
      AK1=1/(CSUBB1+CSUBW)
      GAMAB=GAMBKG*RSUBS**2*WSUBS(I)**2/(2.913E4*CPSOL)
      DO 504 L=1,101
      LL=1
      NT(L)=L-1
      IF(NT(L).GT.NHT) GO TO 318
      Z11=Z2*NT(L)
      Z12=ALPHAA*NT(L)
C
C     CALCULATION OF THE INTEGRAL OF THE BULK SOLUTION TEMPERATURE
C     AND ITS DERIVATIVE WITH RESPECT TO TIME FOR THE MAIN PERIOD:
      IF(DIF) 400,410,420
C
C     ....UNDERDAMPED RESPONSE....
 400  AK2=Z3*(Z2-Z1)/((Z2**2-Z2*(Z1+Z3))*CSUBB1+Z1*Z3*(CSUBB1+CSUBW))
      PHI=Z1*Z2-(Z1+Z2)*ALPHAA+ZAM(I)
      BETAA=SQRT(-DIF)
      PSI=2*Z1*(Z2**2-Z2*(Z1+Z3)+ZAM(I))*BETAA
      ZETA=PSI/Z1
      A=Z2*BETAA*(PHI-ALPHAA*(Z1-Z2))/PSI
      B=Z2*(ALPHAA*PHI+(Z1-Z2)*BETAA**2)/PSI
      RR=SQRT(A**2+B**2)
      THETA=ARSIN(B/RR)
      AK3=-Z3*CSUBW/(BETAA*CSUBB1)
      AK4=-AK2/Z2
      AP=Z2*BETAA*CSUBB1*(2*ALPHAA*PHI+(BETAA**2-ALPHAA**2)*(Z1-Z2))/
     &(Z1*Z3*PSI*(CSUBB1+CSUBW)**2)
```

Figure D.3. (Continued)

```
      BP=Z2*CSUBB1*(ALPHAA**2*PHI+2*ALPHAA*BETAA**2*(Z1-Z2)-BETAA**2*
     &PHI)/(Z1*Z3*PSI*(CSUBB1+CSUBW)**2)
      RP=SQRT(AP**2+BP**2)
      THETAP=ARSIN(BP/RP)
      APP=-0.5*CSUBW*AK1
      BPP=-0.5*ALPHAA*CSUBW*AK1/BETAA
      RPP=SQRT(APP**2+BPP**2)
      THETPP=ARSIN(BPP/RPP)
      IF(Z11.GT.50..OR.Z12.GT.50.) GO TO 409
      TEMBUK(L,I)=PSUBH*(AK1*NT(L)+AK4*EXP(-Z11)+2*RP*EXP(-Z12)*
     &COS(BETAA*NT(L)-THETAP))+2*GAMAB/Z1*EXP(-Z12)*COS(BETAA*NT(L)-
     &THETPP)
      IF(L.NE.1) GO TO 401
      TEMPBI(LL,I)=TEMBUK(L,I)
401   GAM(L,I)=PSUBH*(AK1+AK2*EXP(-Z11)-2*RR*AK1*EXP(-Z12)*COS(BETAA*
     &NT(L)-THETA))+AK3*EXP(-Z12)*SIN(BETAA*NT(L))*GAMAB
      GO TO 315
409   GAM(L,I)=PSUBH*AK1
      TEMBUK(L,I)=PSUBH*AK1*NT(L)
      GO TO 316
C
C     ....CRITICAL DAMPED RESPONSE....
410   AK21=4*Z1*Z3/(CSUBB1*(Z1**2+2*Z1*Z3+Z3**2))
      AK22=4*Z3*(Z2-Z1)/(CSUBB1*(Z1+Z3-2*Z2)**2)
      AK23=2*Z2*Z3*(Z1-Z3)/(CSUBB1*(Z1+Z3)*(Z1+Z3-2*Z2))
      AK24=4*Z2*Z3*((Z1+Z3)*(Z1+Z3-2*Z2)+2*(Z1-Z3)*(Z1+Z3-Z2))/(CSUBB1*
     &(Z1+Z3)**2*(2*Z2-Z1-Z3)**2)
      AK25=-Z3*CSUBW/CSUBB1
      AK26=-AK23/ALPHAA
      AK27=Z3*CSUBW/(ALPHAA**2*CSUBB1)
      AK28=-AK27*ALPHAA
      IF(Z11.GT.50..OR.Z12.GT.50.) GO TO 419
      TEMBUK(L,I)=PSUBH*(AK21*NT(L)+AK22/Z2*EXP(-Z11)+AK26*NT(L)*
     &EXP(-Z12))+GAMAB*(AK27*(1-EXP(-Z12))+AK28*NT(L)*EXP(-Z12))
      IF(L.NE.1) GO TO 411
```

Figure D.3. (Continued)

```
      TEMPBI(LL,I)=TEMBUK(L,I)
411   GAM(L,I)=PSUBH*(AK21+AK22*EXP(-Z11)+AK23*EXP(-Z12)*NT(L)+
     &AK24*EXP(-Z12))+AK25*NT(L)*EXP(-Z12)*GAMAB
      GO TO 315
419   GAM(L,I)=PSUBH*AK21
      TEMBUK(L,I)=PSUBH*AK21*NT(L)+GAMAB*AK27
      GO TO 316
C
C     ....OVERDAMPED RESPONSE....
420   SIGMA=SQRT(DIF)
      AK31=Z1*Z3/(CSUBB1*(ALPHAA+SIGMA)*(ALPHAA-SIGMA))
      AK32=Z3*(Z2-Z1)/(CSUBB1*(ALPHAA+SIGMA-Z2)*(ALPHAA-SIGMA-Z2))
      AK33=Z2*Z3*(Z1-ALPHAA-SIGMA)/(2*CSUBB1*SIGMA*(ALPHAA+SIGMA)*(Z2-
     &ALPHAA-SIGMA))
      AK34=-Z2*Z3*(Z1-ALPHAA+SIGMA)/(2*CSUBB1*SIGMA*(ALPHAA-SIGMA)*(Z2-
     &ALPHAA+SIGMA))
      AK35=-Z3*CSJBW/(SIGMA*CSUBB1)
      Z13=(ALPHAA+SIGMA)*NT(L)
      Z14=(ALPHAA-SIGMA)*NT(L)
      AK36=-AK32/Z2
      AK37=-AK33/(ALPHAA+SIGMA)
      AK38=-AK34/(ALPHAA-SIGMA)
      AK39=AK31*CSUBW/Z1
      AK40=Z3*CSUBW/(2*SIGMA*CSUBB1*(ALPHAA-SIGMA))
      IF(Z11.GT.50..OR.Z12.GT.50.) GO TO 429
      TEMBUK(L,I)=PSUBH*(AK31*NT(L)+AK35*EXP(-Z12)+AK37*EXP(-Z13)+AK38*
     &EXP(-Z14))+GAMAB*(AK39+AK40*EXP(-Z13)-AK40*EXP(-Z14))
      IF(L.NE.1) GO TO 421
      TEMPBI(LL,I)=TEMBUK(L,I)
421   GAM(L,I)=PSUBH*(AK31+AK32*EXP(-Z11)+AK33*EXP(-Z13)+AK34*EXP
     &(-Z14))+AK35*EXP(-Z12)*SINH(SIGMA*NT(L))*GAMAB
      GO TO 315
429   GAM(L,I)=PSUBH*AK31
      TEMBUK(L,I)=PSUBH*AK31*NT(L)+GAMAB*AK39
      GO TO 316
```

Figure D.3. (Continued)

```
      TEMBUK(L,I)=PSUBH*AK31*NT(L)+GAMAB*AK39
      GO TO 316
 315  IF(NT(L).EQ.0.) GAM(L,I)=0.0
C
C     CALCULATION OF BULK EXCESS TEMPERATURE FOR POSITION OF THERMISTOR
C     WITHIN THE CALORIMETER:
C
 316  SIGMAS=RSUBS**0.667*(R*RSUBC)**(-0.33)*URATIO(I)
      DELTTB(L,I)=3.14*GAM(L,I)*NT(L)*TAUM(I)/TAUH(I)*HSUB2/RSUBC*
     &COS(SIGMAS*CHI)*SIN(SIGMAS*EPSIL)
      TEMBUK(L,I)=TEMBUK(L,I)-TEMPBI(LL,I)+DELTTB(L,I)
      SUM=0
      DO 506 N=1,6
      ALPRI(I,N)=(ALPHA(M,N)-ALPHA(M-1,N))*CORRC+ALPHA(M-1,N)
      T=DSUBT*ALPRI(I,N)**2*NT(L)
      IF(T.GT.50.0) GO TO 506
      SUMG=EXP(-T)/(ALPRI(I,N)*(RSUBT**2*
     &ALPRI(I,N)**2+RSUBT*H*(RSUBT*H-1))*SIN(RSUBT*ALPRI(I,N)))
      SUM=SUMG+SUM
 506  CONTINUE
      DELTAT(L,I)=PSUBT/(25.1*RSUBT*AMBAT)*(1+2/(HX*RSUBT))-
     &GAM(L,I)*RSUBT**2/(6*DSUBT)*(1+2/(HX*RSUBT)-24*H*SUM)
C
C     CALCULATION OF OUTPUT VOLTAGE OF OA3 AS DETERMINED BY THERMISTOR
C     RESPONSE TO THE SUM OF FORCED AND NATURAL RESPONSES OF THE
C     CALORIMETER SYSTEM FOR THE MAIN PERIOD:
C
      RESTHE=RESRT-DRDT*(TEMBUK(L,I)+DELTAT(L,I))
      EOOA3(L,I)=(RESRF*ESUBIN/RESTHE-RESRF*ESUBIN/RESTH)*1.0E3
      NTT=0
      GO TO 504
 318  NTT=NTT+1
      N=1
      T=DSUBT*ALPRI(I,N)**2*NTT
      IF(T.GT.50.0) GO TO 319
```

Figure D.3. (Continued)

```
 319   SUMP=0
 320   Z11=Z2*NTT
       Z12=ALPHAA*NTT
C
C      CALCULATION OF THE INTEGRAL OF THE BULK SOLUTION TEMPERATURE
C      AND ITS DERIVATIVE WITH RESPECT TO TIME FOR THE ANTERIOR PERIOD:
       IF(DIF) 430,440,450
C
C      ....UNDERDAMPED RESPONSE....
 430   AKK1 =-AK2
       A=Z3*BETAA*(Z2-Z1)/ZETA
       B=Z3*PHI/ZETA
       RRP=SQRT(A**2+B**2)
       AKK2=2*RRP/CSUBB1
       THETAP=ARSIN(B/RRP)
       AKK3=CSUBW*Z3/(CSUBB1*BETAA)
       AP=0.5
       BP=0.5*(Z1-ALPHAA)/BETAA
       RRPP=SQRT(AP**2+BP**2)
       THETPP=ARSIN(BP/RRPP)
       AP2=-CSUBB1*(Z1*Z3-ALPHAA**2-BETAA**2)/(2*Z1*Z3*(CSUBB1+CSUBW))
       BP2=-CSUBB1*(2*ALPHAA*BETAA**2+ALPHAA**3-ALPHAA*BETAA**2-(ALPHAA
      &**2+BETAA**2)*(Z1+Z3)+ALPHAA*Z1*Z3)/(2*Z1*Z3*BETAA*(CSUBB1+CSUBW))
       RP2=SQRT(AP2**2+BP2**2)
       THETA2=ARSIN(BP2/RP2)
       AP3=CSUBB1*AK1/(2*Z3)
       BP3=CSUBB1*(ALPHAA*Z1-ALPHAA**2-BETAA**2)*AK1/(2*Z1*Z3*BETAA)
       RP3=SQRT(AP3**2+BP3**2)
       THETA3=ARSIN(BP3/RP3)
       AP4=-0.5*CSUBW*AK1
       BP4=-0.5*CSUBW*AK1*ALPHAA/BETAA
       RP4=SQRT(AP4**2+BP4**2)
       THETA4=ARSIN(BP4/RP4)
       IF(Z11.GT.50..OR.Z12.GT.50.) GO TO 439
       TEMBUK(L,I)=(PSUBH/Z2+PSUBH*CSUBH*AK1*(NHT+TAUM(I)))*
```

Figure D.3. (Continued)

```
     &(AK1+AK2*EXP(-Z11)-2*RR*AK1*EXP(-Z12)*COS(BETAA*NTT-THETA))+
     &PSUBH*NHT*AK1*(CSUBB1*AK1+2*RP2*EXP(-Z12)*COS(BETAA*NTT-THETA2))+
     &PSUBH*AK1*(CSUBB1*AK1/Z3-2*RP3*EXP(-Z12)*COS(BETAA*NTT-THETA3))+
     &(PSUBH*NHT*AK1+(GAMAB-PSUBH*AK1)/Z1)*(CSUBW*AK1+2*RP4*EXP(-Z12)*
     &COS(BETAA*NTT-THETA4))
      GAM(L,I)=(PSUBH+PSUBH*CSUBH*Z2*AK1*(NHT+TAUM(I)))*
     &(AKK1*EXP(-Z11)+AKK2*EXP(-Z12)*COS(BETAA*NTT-THETAP))+
     &(GAMAB-PSUBH*AK1)*AKK3*EXP(-Z12)*SIN(BETAA*NTT)+PSUBH*AK1*2*RRPP*
     &EXP(-Z12)*COS(BETAA*NTT-THETPP)
      GO TO 321
 439  TEMBUK(L,I)=(PSUBH/Z2+PSUBH*CSUBH*AK1*(NHT+TAUM(I)))*
     &AK1+PSUBH*NHT*AK1**2*CSUBB1+PSUBH*AK1**2*CSUBB1/Z3+
     &(PSUBH*NHT*AK1+(GAMAB-PSUBH*AK1)/Z1)*CSUBW*AK1
      GO TO 322
C
C     ****CRITICAL DAMPED RESPONSE****
 440  AKK21=Z3*(Z1-Z2)/(CSUBB1*(ALPHAA-Z2)**2)
      AKK22=Z3*(Z1-ALPHAA)/(CSUBB1*(Z2-ALPHAA))
      AKK23=Z3*(Z2-Z1)/(CSUBB1*(Z2-ALPHAA)**2)
      AKK24=CSUBW*Z3/CSUBB1
      AKK25=Z1-ALPHAA
      AKK01=Z1*Z3/(ALPHAA**2*CSUBB1)
      AKK02=Z3*(Z2-Z1)/((ALPHAA-Z2)**2*CSUBB1)
      AKK03=Z2*Z3*(Z1-ALPHAA)/(ALPHAA*(ALPHAA-Z2)*CSUBB1)
      AKK04=Z2*Z3*((ALPHAA*(ALPHAA-Z2)-(Z2-ALPHAA)*(Z2-2*ALPHAA))/
     &(ALPHAA**2*(Z2-ALPHAA)**2*CSUBB1))
      AKK05=-(Z1-ALPHAA)*(Z3-ALPHAA)/ALPHAA
      AKK06=(ALPHAA*(Z1+Z3-2*ALPHAA)-(Z1-ALPHAA)*(Z3-ALPHAA))/
     &(ALPHAA**2)
      AKK07=Z1/(ALPHAA**2)
      AKK08=(ALPHAA-Z1)/ALPHAA
      AKK09=-Z1*Z3*CSUBW/(ALPHAA*CSUBB1)
      IF(Z11.GT.50..OR.Z12.GT.50.) GO TO 449
      TEMBUK(L,I)=(PSUBH/Z2+PSUBH*CSUBH*AK1*(NHT+TAUM(I)))*
     &(AKK01+AKK02*EXP(-Z11)+AKK03*NTT*EXP(-Z12)+AKK04*EXP(-Z12))+
```

Figure D.3. (Continued)

```
     &PSUBH*NHT*AK1*(AKK01*CSUBB1+AKK05*EXP(-Z12)+AKK06*EXP(-Z12))+
     &PSUBH*AK1*(AKK07*(1-EXP(-Z12))+AKK08*NTT*EXP(-Z12))+
     &(PSUBH*NHT*AK1+(GAMAB-PSUBH*AK1)/Z1)*(AKK01*CSUBW*(1+EXP(-Z12))+
     &AKK09*NTT*EXP(-Z12))
      GAM(L,I)=(PSUBH+PSUBH*CSUBH*Z2*AK1*(NHT+TAUM(I)))*
     &(AKK21*EXP(-Z11)+AKK22*NTT*EXP(-Z12)+AKK23*EXP(-Z12))+
     &(GAMAB-PSUBH*AK1)*AKK24*NTT*EXP(-Z12)+PSUBH*AK1*(AKK25*NTT+1)*
     &EXP(-Z12)
      GO TO 321
 449  TEMBUK(L,I)=(PSUBH/Z2+PSUBH*CSUBH*AK1*(NHT+TAUM(I)))*
     &AKK01+PSUBH*NHT*AK1*AKK01*CSUBB1+PSUBH*AK1*AKK07+
     &(PSUBH*NHT*AK1+(GAMAB-PSUBH*AK1)/Z1)*AKK01*CSUBW
      GO TO 322
C
C     ....OVERDAMPED RESPONSE....
 450  AKK31=-AK32
      AKK32=-0.5*Z3*(Z1-ALPHAA-SIGMA)/(CSUBB1*SIGMA*(Z2-ALPHAA-SIGMA))
      AKK33=0.5*Z3*(Z1-ALPHAA+SIGMA)/(CSUBB1*SIGMA*(Z2-ALPHAA+SIGMA))
      AKK34=CSUBW*Z3/(CSUBB1*SIGMA)
      AKK35=(Z1-ALPHAA+SIGMA)/(2*SIGMA)
      AKK36=-(Z1-ALPHAA-SIGMA)/(2*SIGMA)
      Z13=(ALPHAA+SIGMA)*NTT
      Z14=(ALPHAA-SIGMA)*NTT
      AKK311=(Z1-ALPHAA-SIGMA)*(Z3-ALPHAA-SIGMA)/(2*SIGMA*(ALPHAA+SIGMA)
     &)
      AKK312=(Z1-ALPHAA+SIGMA)*(Z3-ALPHAA+SIGMA)/(2*SIGMA*(SIGMA-ALPHAA)
     &)
      AKK313=(Z1-ALPHAA-SIGMA)/(2*SIGMA*(ALPHAA+SIGMA))
      AKK314=(Z1-ALPHAA+SIGMA)/(2*SIGMA*(SIGMA-ALPHAA))
      AKK315=Z1*Z3*CSUBW/(2*SIGMA*CSUBB1*(ALPHAA+SIGMA))
      AKK316=Z1*Z3*CSUBW/(2*SIGMA*CSUBB1*(SIGMA-ALPHAA))
      IF(Z11.GT.50..OR.Z12.GT.50..OR.Z13.GT.50..OR.Z14.GT.50.) GO TO 459
      TEMBUK(L,I)=(PSUBH/Z2+PSUBH*CSUBH*AK1*(NHT+TAUM(I)))*
     &(AK31+AK32*EXP(-Z11)+AK33*EXP(-Z13)+AK34*EXP(-Z14))+
     &PSUBH*NHT*AK1*(AK31*CSUBB1+AKK311*EXP(-Z13)+AKK312*EXP(-Z14))+
```

Figure D.3. (Continued)

```
     &PSUBH*AK1*(AK31*CSUBB1/Z3+AKK313*EXP(-Z13)+AKK314*EXP(-Z14))+
     &(PSUBH*NHT*AK1+(GAMAB-PSUBH*AK1)/Z1)*(AK31*CSUBW+AKK315*EXP(-Z13)+
     &AKK316*EXP(-Z14))
      GAM(L,I)=(PSUBH+PSUBH*CSUBH*Z2*AK1*(NHT+TAUM(I)))*
     &(AKK31*EXP(-Z11)+AKK32*EXP(-Z13)+AKK33*EXP(-Z14))+
     &(GAMAB-PSUBH*AK1)*AKK34*EXP(-Z12)*SINH(SIGMA*NTT)+PSUBH*AK1*
     &(AKK35*EXP(-Z14)+AKK36*EXP(-Z13))
      GO TO 321
 459  TEMBUK(L,I)=(PSUBH/Z2+PSUBH*CSUBH*AK1*(NHT+TAUM(I)))*
     &AK31+PSUBH*NHT*AK1*AK31*CSUBB1+PSUBH*AK1*AK31*CSUBB1/Z3+
     &(PSUBH*NHT*AK1+(GAMAB-PSUBH*AK1)/Z1)*AK31*CSUBW
      GO TO 322
 321  IF(GAM(L,I).LT.0.) GAM(L,I)=0.0
      GO TO 323
 322  GAM(L,I)=0.0
C
C     CALCULATION OF BULK EXCESS TEMPERATURE FOR POSITION OF THERMISTOR
C     WITHIN THE CALORIMETER:
C
 323  DELTTB(L,I)=3.14*GAM(L,I)*NT(L)*TAUM(I)/TAJH(I)*HSUB2/RSUBC*
     &COS(SIGMAS*CHI)*SIN(SIGMAS*EPSIL)
      TEMBUK(L,I)=TEMBUK(L,I)-TEMPBI(LL,I)+DELTTB(L,I)
      DELTAT(L,I)=PSUBT/(25.1*RSUBT*AMBAT)*(1+2/(HX*RSUBT))-
     &GAM(L,I)*RSUBT**2/(6*DSUBT)*(1+2/(HX*RSUBT))*SUMP
C
C     CALCULATION OF OUTPUT VOLTAGE OF OA3 AS DETERMINED BY THERMISTOR
C     RESPONSE TO THE NATURAL RESPONSE OF THE
C     CALORIMETER SYSTEM FOR THE ANTERIOR PERIOD:
C
      RESTHE=RESRT-DRDT*(TEMBUK(L,I)+DELTAT(L,I))
      EOOA3(L,I)=(RESRF*ESUBIN/RESTHE-RESRF*ESUBIN/RESTH)*1.0E3
 504  CONTINUE
      K=NHT+1
      J=0
 324  J=J+1
```

Figure D.3. (Continued)

```
      TESGAM=ABS((GAM(J,I)-GAM(K,I))/GAM(K,I))
      IF(TESGAM.LT.0.01) GO TO 325
      GO TO 324
  325 A1=(NT(K)-NT(J))/(EOOA3(K,I)-EOOA3(J,I))
      TAU(I)=NT(J)-A1*EOOA3(J,I)
      INITAJ(I)=J
  502 CONTINUE
C
C     ....FORMAT FOR HYDRODYNAMIC PARAMETERS FOR CALORIMETER THERMISTOR
C     SENSOR,CALORIMETER HEATER, AND CALORIMETER WALL....
      READ(5,112)(NAME(I),I=1,20)
      WRITE(6,214)(NAME(I),I=1,20)
      WRITE(6,220)(I,NSUBS(I),RET(I),TNU(I),HSUBT(I),HSUBST(I),I=1,10)
  220 FORMAT(1X,'I=',I2,2X,'RPM=',I4,3X,'REYNOLDS#,THERM=',F7.1,3X,
     &'NUSSELT#,THERM=',F5.2,3X,'H SUB THERM=',F6.4,2X,'H SUB THERM STEM
     &=',F6.4)
      READ(5,112)(NAME(I),I=1,20)
      WRITE(6,214)(NAME(I),I=1,20)
      WRITE(6,222)(I,CONST(I),(N,ALPRI(I,N),N=1,5),TAUT(I),I=1,10)
  222 FORMAT(1X,'I=',I2,2X,'CONST=',F7.3,2X,'A(',I1,')=',F7.4,1X,
     &'A(',I1,')=',F7.4,1X,'A(',I1,')=',F7.4,1X,'A(',I1,')=',F7.4,1X,
     &'A(',I1,')=',F7.4,1X,'A(',I1,')=',F7.4,2X,'TAU THERM (SEC)=',F5.2)
      READ(5,112)(NAME(I),I=1,20)
      WRITE(6,214)(NAME(I),I=1,20)
      WRITE(6,224)(I,NSUBS(I),HSUBH(I),HSUBHS(I),TAUH(I),I=1,10)
  224 FORMAT(1X,'I=',I2,2X,'RPM=',I4,3X,'H SUB HEATER=',F6.4,2X,'H SUB
     &HEATER STEM=',F6.4,2X,'TAU HEATER (SEC)=',F5.2)
      READ(5,112)(NAME(I),I=1,20)
      WRITE(6,225)(NAME(I),I=1,20)
      WRITE(6,226)(I,NSUBS(I),ALP(I),ZAM(I),HSUBW(I),HSTEM(I),TAUW(I),
     &I=1,10)
  226 FORMAT(1X,'I=',I2,2X,'RPM=',I4,2X,'ALPHA SQUARED=',F6.3,2X,
     &'FREQUENCY SQUARED=',F5.3,2X,'H SUB WALL=',F6.4,2X,'H SUB STEMS=',
     &F6.4,2X,'TAU WALL (SEC)=',F5.2)
      READ(5,112)(NAME(I),I=1,20)
```

Figure D.3. (Continued)

```
      WRITE(6,214)(NAME(I),I=1,20)
      WRITE(6,228)(I,NSUBS(I),TEMPBI(LL,I),TAUHAR(I),INITAU(I),TAU(I),
     &I=1,10)
228   FORMAT(1X,'I=',I2,2X,'RPM=',I4,2X,'INITIAL TEMP BULK SOLN, 1ST APP
     &ROX=',E13.4,2X,'TAJ HARMONIC (SEC)=',F5.2,2X,'J=',I3,2X,'TAU (SEC)
     &=',F5.2)
      READ(5,112)(NAME(I),I=1,20)
      WRITE(6,225)(NAME(I),I=1,20)
      WRITE(6,230)(C(I),(J,ALPHA(I,J),J=1,6),I=1,50)
230   FORMAT(1X,'CONST =',F7.3,2X,'A(',I1,')=',F7.4,1X,'A(',I1,')=',
     &F7.4,1X,'A(',I1,')=',F7.4,1X,'A(',I1,')=',F7.4,1X,'A(',I1,')=',
     &F7.4,1X,'A(',I1,')=',F7.4)
C
C     ....FORMATS FOR CALCULATED PARAMETERS: DELTA T, TEMP BULK SOLN,
C     GAMMA SUB B, DELTA TEMP BULK SOLN, & EQ GA3....
      READ(5,112)(NAME(I),I=1,20)
      WRITE(6,225)(NAME(I),I=1,20)
      WRITE(6,231)(NSUBS(I),I=1,5)
231   FORMAT(14X,'RPM=',I4,10X,'RPM=',I4,10X,'RPM=',I4,10X,'RPM=',I4,
     &10X,'RPM=',I4)
      WRITE(6,242)(NT(L),(DELTAT(L,I),I=1,5),L=1,101)
242   FORMAT(1X,'T (SEC)=',I3,2X,'DT=',E13.4,2X,'DT=',E13.4,2X,'DT=',
     &E13.4,2X,'DT=',E13.4,2X,'DT=',E13.4)
      READ(5,112)(NAME(I),I=1,20)
      WRITE(6,225)(NAME(I),I=1,20)
      WRITE(6,231)(NSUBS(I),I=6,10)
      WRITE(6,242)(NT(L),(DELTAT(L,I),I=6,10),L=1,101)
      READ(5,112)(NAME(I),I=1,20)
      WRITE(6,225)(NAME(I),I=1,20)
      WRITE(6,231)(NSUBS(I),I=1,5)
      WRITE(6,244)(NT(L),(TEMBUK(L,I),I=1,5),L=1,101)
244   FORMAT(1X,'T (SEC)=',I3,2X,'TB=',E13.4,2X,'TB=',E13.4,2X,'TB=',
     &E13.4,2X,'TB=',E13.4,2X,'TB=',E13.4)
      READ(5,112)(NAME(I),I=1,20)
      WRITE(6,225)(NAME(I),I=1,20)
```

Figure D.3. (Continued)

```
      WRITE(6,231)(NSUBS(I),I=6,10)
      WRITE(6,244)(NT(L),(TEMBUK(L,I),I=6,10),L=1,101)
      READ(5,112)(NAME(I),I=1,20)
      WRITE(6,225)(NAME(I),I=1,20)
      WRITE(6,231)(NSJBS(I),I=1,5)
      WRITE(6,246)(NT(L),(GAM(L,I),I=1,5),L=1,101)
246   FORMAT(1X,'T (SEC)=',I3,2X,'GAMA=',E13.4,2X,'GAMA=',E13.4,2X,
     &'GAMA=',E13.4,2X,'GAMA=',E13.4,2X,'GAMA=',E13.4)
      READ(5,112)(NAME(I),I=1,20)
      WRITE(6,225)(NAME(I),I=1,20)
      WRITE(6,231)(NSUBS(I),I=6,10)
      WRITE(6,246)(NT(L),(GAM(L,I),I=6,10),L=1,101)
      READ(5,112)(NAME(I),I=1,20)
      WRITE(6,225)(NAME(I),I=1,20)
      WRITE(6,231)(NSUBS(I),I=1,5)
      WRITE(6,248)(NT(L),(DELTTB(L,I),I=1,5),L=1,101)
248   FORMAT(1X,'T (SEC)=',I3,2X,'DT=',E13.4,2X,'DT=',E13.4,2X,'DT=',
     &E13.4,2X,'DT=',E13.4,2X,'DT=',E13.4)
      READ(5,112)(NAME(I),I=1,20)
      WRITE(6,225)(NAME(I),I=1,20)
      WRITE(6,231)(NSUBS(I),I=6,10)
      WRITE(6,248)(NT(L),(DELTTB(L,I),I=6,10),L=1,101)
      READ(5,112)(NAME(I),I=1,20)
      WRITE(6,225)(NAME(I),I=1,20)
      WRITE(6,231)(NSJBS(I),I=1,5)
      WRITE(6,250)(NT(L),(EOOA3(L,I),I=1,5),L=1,101)
250   FORMAT(1X,'T (SEC)=',I3,2X,'EO=',E13.5,2X,'EO=',E13.5,2X,'EO=',
     &E13.5,2X,'EO=',E13.5,2X,'EO=',E13.5)
      READ(5,112)(NAME(I),I=1,20)
      WRITE(6,225)(NAME(I),I=1,20)
      WRITE(6,231)(NSUBS(I),I=6,10)
      WRITE(6,250)(NT(L),(EOOA3(L,I),I=6,10),L=1,101)
C
C     ....ISU SIMPLOTTER SUBROUTINE CALL STATEMENTS....
      READ(5,134) XL,YL
```

Figure D.3. (Continued)

```
134   FORMAT(10A4)
      DO 508 I=1,10,2
      DO 510 II=1,101
      X(II)=NT(II)
510   Y(II)=E00A3(II,I)
      IF(I.NE.1) GO TO 330
      CALL GRAPH(101,X,Y,0,2,10.0,8.0,0.0,0.0,0.0,0.0,0.0,XL,YL,
     &';',';')
      GO TO 508
330   CALL GRAPHS(101,X,Y,0,2,';')
508   CONTINUE
      READ(5,134) XL,YL
      DO 512 I=1,10,2
      DO 514 II=1,101
514   U(II)=GAM(II,I)
      IF(I.NE.1) GO TO 340
      CALL GRAPH(101,X,U,0,2,10.0,8.0,0.0,0.0,0.0,0.0,0.0,XL,YL,
     &';',';')
      GO TO 512
340   CALL GRAPHS(101,X,U,0,2,';')
512   CONTINUE
      READ(5,134) XL,YL
      DO 516 I=1,10,2
      DO 518 II=1,101
518   V(II)=DELTAT(II,I)
      IF(I.NE.1) GO TO 350
      CALL GRAPH(101,X,V,0,2,10.0,8.0,0.0,0.0,0.0,0.0,0.0,XL,YL,
     &';',';')
      GO TO 516
350   CALL GRAPHS(101,X,V,0,2,';')
516   CONTINUE
      READ(5,134) XL,YL
      DO 520 I=1,10,2
      DO 522 II=1,101
522   W(II)=TEMBUK(II,I)
```

Figure D.3. (Continued)

```
      IF(I.NE.1) GO TO 360
      CALL GRAPH(101,X,W,0,2,10.0,8.0,0.0,0.0,0.0,0.0,0.0,XL,YL,
     &';',';')
      GO TO 520
360   CALL GRAPHS(101,X,W,0,2,';')
520   CONTINUE
      READ(5,134) XL,YL
      DO 524 I=1,10,2
      DO 526 II=1,101
526   Z(II)=DELTTB(II,I)
      IF(I.NE.1) GO TO 370
      CALL GRAPH(101,X,Z,0,2,10.0,8.0,0.0,0.0,0.0,0.0,0.0,XL,YL,
     &';',';')
      GO TO 524
370   CALL GRAPHS(101,X,Z,0,2,';')
524   CONTINUE
      READ(5,134) XL,YL
      DO 608 I=2,10,2
      DO 610 II=1,101
      X(II)=NT(II)
610   Y(II)=E00A3(II,I)
      IF(I.NE.2) GO TO 730
      CALL GRAPH(101,X,Y,0,2,10.0,8.0,0.0,0.0,0.0,0.0,0.0,XL,YL,
     &';',';')
      GO TO 608
730   CALL GRAPHS(101,X,Y,0,2,';')
608   CONTINUE
      READ(5,134) XL,YL
      DO 612 I=2,10,2
      DO 614 II=1,101
614   U(II)=GAM(II,I)
      IF(I.NE.2) GO TO 740
      CALL GRAPH(101,X,U,0,2,10.0,8.0,0.0,0.0,0.0,0.0,0.0,XL,YL,
     &';',';')
      GO TO 612
```

Figure D.3. (Continued)

```
740   CALL GRAPHS(101,X,U,0,2,';')
612   CONTINUE
      READ(5,134) XL,YL
      DO 616 I=2,10,2
      DO 618 II=1,101
618   V(II)=DELTAT(II,I)
      IF(I.NE.2) GO TO 750
      CALL GRAPH(101,X,V,0,2,10.0,8.0,0.0,0.0,0.0,0.0,0.0,XL,YL,
     &';',';')
      GO TO 616
750   CALL GRAPHS(101,X,V,0,2,';')
616   CONTINUE
      READ(5,134) XL,YL
      DO 620 I=2,10,2
      DO 622 II=1,101
622   W(II)=TEMBUK(II,I)
      IF(I.NE.2) GO TO 760
      CALL GRAPH(101,X,W,C,2,10.0,8.0,0.0,0.0,0.0,0.0,0.0,XL,YL,
     &';',';')
      GO TO 620
760   CALL GRAPHS(101,X,W,0,2,';')
620   CONTINUE
      READ(5,134) XL,YL
      DO 624 I=2,10,2
      DO 626 II=1,101
626   Z(II)=DELTTB(II,I)
      IF(I.NE.2) GO TO 770
      CALL GRAPH(101,X,Z,0,2,10.0,8.0,0.0,0.0,0.0,0.0,0.0,XL,YL,
     &';',';')
      GO TO 624
770   CALL GRAPHS(101,X,Z,0,2,';')
624   CONTINUE
      DO 628 I=1,10
628   ANSUBS(I)=NSUBS(I)
      READ(5,134) XL,YL
```

Figure D.3. (Continued)

```
C
C      DATA POINT SYMBOLS: REYNOLD'S NUMBER PLOT
C      CIRCLE:RE SUB MAX; TRIANGLE:RE SUB R; SQUARE:R SUB T
C
       CALL GRAPH(10,ANSUBS,REMAX,1,1,10.0,8.0,250.0,0.0,0.0,0.0,0.0,XL,YL,
      &';',';')
       CALL GRAPHS(10,ANSUBS,RE,2,1,';')
       CALL GRAPHS(10,ANSUBS,RET,10,1,';')
       READ(5,134) XL,YL
C
C      DATA POINT SYMBOLS: TIME CONSTANT PLOT
C      CIRCLE:TAU SUB W; TRIANGLE:TAU SUB H; SQUARE:TAU SUB T;
C      RHOMBUS: TAU SUB MIX; X BAR: TAU SUB R
C
       CALL GRAPH(10,ANSUBS,TAUW,1,1,10.0,8.0,250.0,0.0,0.0,0.0,0.0,XL,YL,
      &';',';')
       CALL GRAPHS(10,ANSUBS,TAUH,2,1,';')
       CALL GRAPHS(10,ANSUBS,TAUM,5,1,';')
       CALL GRAPHS(10,ANSUBS,TAUT,10,1,';')
       CALL GRAPHS(10,ANSUBS,TAU,12,1,';')
       READ(5,134) XL,YL
C
C      DATA POINT SYMBOLS: HEAT TRANSFER COEFFICIENT PLOT
C      CIRCLE:H SUB W; TRIANGLE:H SUB H; SQUARE:H SUB T
C      STAR:H SUB W,STEM; TREE:H SUB H,STEM; RHOMBUS:H SUB T,STEM
C
       CALL GRAPH(10,ANSUBS,HSUBW,1,1,10.0,8.0,250.0,0.0,0.0,0.0,0.0,XL,YL,
      &';',';')
       CALL GRAPHS(10,ANSUBS,HSTEM,11,1,';')
       CALL GRAPHS(10,ANSUBS,HSUBH,2,1,';')
       CALL GRAPHS(10,ANSUBS,HSUBHS,6,1,';')
       CALL GRAPHS(10,ANSUBS,HSUBT,10,1,';')
       CALL GRAPHS(10,ANSUBS,HSUBST,5,1,';')
       READ(5,134) XL,YL
C
```

Figure D.3. (Continued)

```
C       DATA POINT SYMBOLS: ALPHA SQUARED & ZAM PLOT
C       CIRCLE:ALPHA SQUARED; TRIANGLE:ZAM
C
        CALL GRAPH(10,ANSUBS,ALP,1,1,10.0,8.0,250.0,0.0,0.0,0.0,0.0,XL,YL,
       &';',';')
        CALL GRAPHS(10,ANSUBS,ZAM,2,1,';')
        STOP
        END
```